

**Politecnico di Milano**

---

SCHOOL OF INDUSTRIAL AND INFORMATION ENGINEERING

Master of Science Degree in Aeronautical Engineering



**POLITECNICO**  
**MILANO 1863**

**Derivation of the Ginzburg-Landau equation and its  
application to the Taylor-Couette flow**

Candidate:

**Emanuele Zuccoli**  
**883616**

Supervisor:

**Prof. Franco Auteri**



# Contents

<b>1</b>	<b>Introduction</b>	<b>15</b>
1.0.1	Linear stability . . . . .	15
1.0.2	Nonlinear stability . . . . .	16
1.0.3	Generation of the instabilities . . . . .	17
1.0.4	The instability of the Taylor-Couette flow . . . . .	18
<b>2</b>	<b>Dimensionless Navier–Stokes equations</b>	<b>21</b>
2.1	General governing equations . . . . .	21
2.2	Dimensionless equations: first formulation . . . . .	22
2.3	Dimensionless equations: second formulation . . . . .	24
<b>3</b>	<b>Taylor–Couette steady flow</b>	<b>25</b>
3.1	Exact solutions of the Navier-Stokes equations in cylindrical coordinates . . . . .	25
3.2	Derivation of the Taylor-Couette solution . . . . .	26
<b>4</b>	<b>Linear stability</b>	<b>29</b>
4.1	Linearized Navier-Stokes equations . . . . .	29
4.2	Numerical method for the linear stability . . . . .	32
4.3	Linear stability analysis of an inviscid flow . . . . .	35
4.3.1	Rayleigh's criterion: a necessary and sufficient condition for the stability of a circular inviscid flow . . . . .	35
4.3.2	Derivation of Rayleigh's criterion and analysis of some particular disturbances . . . . .	37
4.3.3	Axisymmetric disturbances . . . . .	37
4.3.4	Generic disturbances . . . . .	41
4.4	Linear stability analysis of a viscous flow . . . . .	45
4.4.1	Taylor vortices . . . . .	45
4.4.2	Spiral vortices . . . . .	56
<b>5</b>	<b>Nonlinear stability</b>	<b>59</b>
5.1	Van der Pol oscillator: modulation of the amplitude in time . . . . .	60
5.2	Duffing oscillator: the shift in the frequency . . . . .	66
5.3	Nonlinear dynamics for PDE . . . . .	70
5.3.1	Weakly nonlinear dynamics: from the evolution equation of a wave packet to the Ginzburg–Landau equation . . . . .	70
5.3.2	A model problem: the Swift–Hohenberg equation . . . . .	77
5.4	Weakly nonlinear expansion of the Navier-Stokes equations . . . . .	82
5.4.1	Resolution of the systems at the different orders . . . . .	84
5.5	Alternative derivation of the Ginzburg-Landau equation . . . . .	91
5.6	High-order approximation . . . . .	95
5.7	Solutions of the Ginzburg-Landau equation . . . . .	100
5.7.1	Stationary periodic solution . . . . .	101
5.7.2	Stationary non-periodic solution . . . . .	104
5.7.3	Unsteady periodic solution . . . . .	111
5.7.4	Unsteady non-periodic solution . . . . .	115

5.8	The Ginzburg-Landau equation with a forcing term . . . . .	125
5.8.1	Axial forcing term . . . . .	125
5.8.2	Radial forcing term . . . . .	128
5.8.3	Uniform and steady forcing term . . . . .	130
5.8.4	Evolution of a steady state subject to an impulsive forcing term . . . . .	135
<b>6</b>	<b>Conclusions and future developments</b>	<b>137</b>
<b>A</b>	<b>Estratto in italiano</b>	<b>139</b>
A.1	Capitolo 1: introduzione . . . . .	139
A.1.1	Stabilità lineare . . . . .	139
A.1.2	Stabilità non lineare . . . . .	139
A.2	Capitolo 2: equazioni di Navier–Stokes adimensionali . . . . .	140
A.3	Capitolo 3: corrente stazionaria di Taylor–Couette . . . . .	140
A.4	Stabilità lineare . . . . .	141
A.5	Stabilità non lineare . . . . .	144
A.6	Capitolo 6: conclusioni e sviluppi futuri . . . . .	145
<b>Bibliography</b>		<b>147</b>

# List of Figures

1.1	Taylor vortex flow ([14], [13]): streamline and cell pattern visualization around the cylinder . . . . .	18
1.2	Wavy vortex flow ([14], [13]): streamline and cell pattern visualization around the cylinder . . . . .	19
1.3	Modulated wavy vortex ([14]): streamlines visualization along a transversal section	19
1.4	Complete bifurcation diagram for the Taylor–Couette flow [8]. The curves are plotted against two Reynolds numbers: on the abscissa we have the Reynolds number related to the external cylinder; on the ordinate we have the Reynolds number related to the inner cylinder . . . . .	20
4.1	Rayleigh’s line . . . . .	36
4.2	Dispersion relation $\sigma(\beta)$ for $\alpha = 0$ , $\eta = 0.95$ and $\omega = -1$ . . . . .	38
4.3	Dispersion relation $\sigma(\beta, \omega)$ as a function of the axial wavenumber and of the ratio between the angular velocities, computed for $\alpha = 0$ , $\eta = 0.95$ . . . . .	39
4.4	Dispersion relation $\sigma(\beta)$ for $\alpha = 0$ , $\eta = 0.3$ and $\omega = -1$ . . . . .	40
4.5	Dispersion relation $\sigma(\beta, \omega)$ as a function of the axial wavenumber and of the ratio between the angular velocities, computed for $\alpha = 0$ , $\eta = 0.3$ . . . . .	40
4.6	Dispersion relation $\sigma(\beta)$ for $\alpha = 1$ , $\eta = 0.95$ and $\omega = -1$ . . . . .	41
4.7	Dispersion relation $\sigma(\beta, \omega)$ as a function of the axial wavenumber and of the ratio between the angular velocities, computed for $\alpha = 1$ , $\eta = 0.95$ . . . . .	42
4.8	Dispersion relation $\sigma(\beta)$ for $\alpha = 1$ , $\eta = 0.3$ and $\omega = -1$ . . . . .	43
4.9	Dispersion relation $\sigma(\beta, \omega)$ as a function of the axial wavenumber and of the ratio between the angular velocities, computed for $\alpha = 1$ , $\eta = 0.3$ . . . . .	44
4.10	Complete bifurcation diagram for the basic Taylor–Couette flow [8]. . . . .	46
4.11	Neutral curves in the plane $Re - \beta$ computed for $\alpha = 0$ , $\omega = 0$ and for two different values of $\eta$ . The red curve shows the neutral curve for $\eta = 0.95$ . The black curve shows the neutral curve for $\eta = 0.3$ . The critical points in the two cases are shown with a blue dot. . . . .	47
4.12	Neutral curve $Re(\beta)$ for $\alpha = 0$ , $\omega = 0$ , $\eta = 0.95$ . . . . .	48
4.13	Dispersion surface $\sigma(\beta, Re)$ for $\alpha = 0$ , $\omega = 0$ , $\eta = 0.95$ . The figure also emphasizes the character of the dispersion relation close to the critical point. . . . .	48
4.14	Dispersion relation curve $\sigma(Re)$ computed at $\beta = \beta_c$ , $\alpha = 0$ , $\omega = 0$ , $\eta = 0.95$ . . . . .	49
4.15	Dispersion relation curves $\sigma(\beta)$ for different values of the Reynolds number. The curves are computed for $\alpha = 0$ , $\omega = 0$ , $\eta = 0.95$ . . . . .	49
4.16	Neutral curve in the plane $Re - Re_o$ computed at the critical value of the axial wavenumber $\beta = \beta_c = 3.13$ and for $\alpha = 0$ , $\eta = 0.95$ . . . . .	50
4.17	Structure of the Taylor vortices in the case $\alpha = 0$ , $\omega = 0$ , $\eta = 0.95$ , $Re = Re_c = 185$ , $\beta = \beta_c = 3.13$ . . . . .	51
4.18	Neutral curve $Re(\beta)$ for $\alpha = 0$ , $\omega = 0$ , $\eta = 0.3$ . . . . .	52
4.19	Neutral curve in the plane $Re_o - Re$ computed at the critical axial wavenumber $\beta = \beta_c = 3.24$ and for $\alpha = 0$ , $\eta = 0.3$ . . . . .	53
4.20	Dispersion relation curves in the wide gap case $\eta = 0.3$ . The curves are computed also for $\alpha = 0$ , $\omega = 0$ . . . . .	53

4.21 Dispersion surface $\sigma(\beta, Re)$ computed for $\alpha = 0$ , $\omega = 0$ and $\eta = 0.3$ . The figure emphasizes the character of the dispersion relation in the neighbourhood of the critical point. . . . .	54
4.22 Structure of the Taylor vortices in the case $\alpha = 0$ , $\omega = 0$ , $\eta = 0.3$ , $Re = Re_c = 73.24$ , $\beta = \beta_c = 3.24$ . . . . .	55
4.23 Visualization of the patterns around the Cylinders: Spiral vortices 4.23a; Taylor vortices 4.23b . . . . .	56
4.24 Bifurcations of the Taylor–Couette basic flow. The chart shows the bifurcations that occur for negative values of $\omega$ , 4.24a, and the bifurcations that occur for positive values of $\omega$ , 4.24b. . . . .	57
4.25 Comparison of neutral curves in the plane $\beta - Re$ at $\eta = 0.95$ and $\omega = -0.8$ for different values of $\alpha$ . . . . .	57
4.26 Structure of Spiral vortices for $\alpha = 3$ , $\omega = -0.8$ , $\eta = 0.95$ , $Re_c = 266.3$ , $\beta_c = 3.56$ . . . . .	58
 5.1 Behaviour of the exact solution $u$ and of its temporal derivative $\frac{du}{dt}$ for the Van der Pol problem with $\epsilon = 0.01$ , $u(0) = 0.1$ , $\frac{du(0)}{dt} = 0$ . . . . .	62
5.2 Van der Pol exact solution for $\epsilon = 0.01$ , $u(0) = 0.1$ , $\frac{du(0)}{dt} = 0$ . The red point shows the starting point of the trajectory. The green point the final one. . . . .	63
5.3 Comparison between the exact solution (black curve) and the one obtained by using the Landau equation (red dot-curve) for $\epsilon = 0.01$ , $u(0) = 0.1$ . . . . .	63
5.4 Behaviour of the exact solution $u$ and of its temporal derivative $\frac{du}{dt}$ for the Van der Pol problem with $\epsilon = 1$ , $u(0) = 0.1$ , $\frac{du(0)}{dt} = 0$ . . . . .	64
5.5 Van der Pol exact solution for $\epsilon = 1$ , $u(0) = 0.1$ , $\frac{du(0)}{dt} = 0$ . The red point shows the starting point of the trajectory. The green point the final one. . . . .	64
5.6 Comparison between the exact solution (black curve) and the one obtained by using the Landau equation (red dot-curve) for $\epsilon = 1$ , $u(0) = 0.1$ . . . . .	65
5.7 Behaviour of the exact solution $u$ and of its temporal derivative $\frac{du}{dt}$ for the Duffing problem with $\epsilon = 0.01$ , $u(0) = 0.1$ , $\frac{du(0)}{dt} = 0$ . . . . .	67
5.8 Duffing exact solution computed for $\epsilon = 0.01$ , $u(0) = 0.1$ , $\frac{du(0)}{dt} = 0$ . The red point shows the starting point of the trajectory. The green point the final one. . . . .	67
5.9 Comparison between the exact solution (black curve) and the one obtained by using the Landau equation (red dot-curve) for $\epsilon = 0.01$ , $u(0) = 0.1$ . . . . .	68
5.10 Behaviour of the exact solution $u$ and of its temporal derivative $\frac{du}{dt}$ for the Duffing problem with $\epsilon = 1$ , $u(0) = 0.1$ , $\frac{du(0)}{dt} = 0$ . . . . .	68
5.11 Duffing exact solution computed for $\epsilon = 1$ , $u(0) = 0.1$ , $\frac{du(0)}{dt} = 0$ . The red point shows the starting point of the trajectory. The green point the final one. . . . .	69
5.12 Comparison between the exact solution (black curve) and the one obtained by using the Landau equation (red dot-curve) for $\epsilon = 1$ , $u(0) = 0.1$ . . . . .	69
5.13 Approximation of the dispersion relation in the neighbourhood of the non-hyperbolic point in the plane $\beta - \mathcal{R}$ . . . . .	71
5.14 Dispersion surface $\sigma(\mathcal{R}, \alpha)$ and neutral curve $\mathcal{R}(\alpha)$ . . . . .	78
5.15 Approximated behaviour of the dispersion relation close to the critical point. Figure shows the approximated dispersion surface $\sigma_{app}(\mathcal{R}, \beta)$ in the neighbourhood of the critical point $(\beta_c, \mathcal{R}_c) = (1, 2)$ . Figure shows the approximated neutral curve $\sigma_{app}(\mathcal{R}, \beta) = 0$ . . . . .	79
5.16 Behaviour of the function $f(z) = \mathcal{A}(z)e^{i\beta_c z}$ for two different values of the axial wavenumber and with $\epsilon^2 = 0.01$ . The critical wavenumber is $\beta_c = 3.13$ . . . . .	102
5.17 Comparison of the amplitude $\mathcal{A}(z)$ for two different values of the axial wavenumber and with $\epsilon^2 = 0.01$ . The critical wavenumber is $\beta_c = 3.13$ . . . . .	102
5.18 Streamline of the vortices for the two values of $\beta$ and with $\epsilon^2 = 0.01$ , both in the linear and nonlinear case. . . . .	102
5.19 Behaviour of the function $f(z) = \mathcal{A}(z)e^{i\beta_c z}$ for two different values of the axial wavenumber and with $\epsilon^2 = 0.1$ . The critical wavenumber is $\beta_c = 3.13$ . . . . .	103

5.20	Comparison of the amplitude $\mathcal{A}(z)$ for two different values of the axial wavenumber and with $\epsilon^2 = 0.1$ . The critical wavenumber is $\beta_c = 3.13$ . . . . .	103
5.21	Computational domain used for the DNS . . . . .	104
5.22	Representation of the behaviour of the Taylor vortices in the steady case for $\mathcal{R} = 109.40$ . . . . .	106
5.23	Comparison of the cell pattern formed both in the nonlinear and in the linear case. . . . .	107
5.24	Representation of the behaviour of the Taylor vortices in the steady case for $\mathcal{R} = 119.15$ . . . . .	109
5.25	Comparison of the cell pattern formed both in the nonlinear and in the linear case . . . . .	110
5.26	Behaviour of the solution $\mathcal{A}(z, t)$ for $\beta = \beta_c = 3.13$ . . . . .	112
5.27	Behaviour of the solution $\mathcal{A}(z, t)$ for $\beta = (1 + 0.05)\beta_c$ and $\beta_c = 3.13$ . . . . .	113
5.28	Comparison of the structure of the Taylor vortices at $t = 4000$ between the linear and the nonlinear case. . . . .	114
5.29	Structure of the Taylor vortices for $t = t_{fin} = 4000$ in the case $\epsilon^2 = 0.01$ . . . . .	116
5.30	Complete solution $\mathcal{A}(z, t)$ of the G–L equation with homogeneous Dirichlet boundary conditions at $z = \pm L$ and with $\epsilon^2 = 0.01$ . . . . .	117
5.31	Complete solution $\mathcal{A}(z, t)$ of the G–L equation with homogeneous Dirichlet boundary conditions at $z = \pm L$ and with $\epsilon^2 = 0.1$ . . . . .	119
5.32	Structure of the Taylor vortices for $t = t_{fin} = 1000$ in the case $\epsilon^2 = 0.1$ , with $\mathcal{A}(z, 0) = 1.e - 02$ and with homogeneous boundary conditions at $z = \pm L$ . . . . .	120
5.33	Complete solution $\mathcal{A}(z, t)$ of the G–L equation with homogeneous Dirichlet boundary conditions at $z = \pm L$ , $\epsilon^2 = 0.1$ and with a random initial condition $\mathcal{A}(z, 0) = (1.e - 04)rand(z)$ . . . . .	122
5.34	Structure of the Taylor vortices for $t = t_{fin} = 800$ in the case $\epsilon^2 = 0.1$ , $\mathcal{A}(z, 0) = (1.e - 04)rand(z)$ and with second order terms in the expansion of the solution. . . . .	123
5.35	Complete solution $\mathcal{A}(z, t)$ of the G–L equation with homogeneous Dirichlet boundary conditions at $z = \pm L$ , $\epsilon^2 = 0.1$ , with a random initial condition $\mathcal{A}(z, 0) = (1.e - 04)rand(z)$ . . . . .	124
5.36	Structure of the Taylor vortices for $t = t_{fin} = 6000$ in the case $\epsilon^2 = 0.01$ , $\mathcal{A}(z, 0) = (1.e - 04)rand(z)$ , subject to a sinusoidal forcing term along the axial direction and with second order terms in the expansion of the solution. . . . .	126
5.37	Complete solution $\mathcal{A}(z, t)$ of the G–L equation with homogeneous Dirichlet boundary conditions at $z = \pm L$ , $\epsilon^2 = 0.1$ , with a random initial condition $\mathcal{A}(z, 0) = (1.e - 04)rand(z)$ and subject to a sinusoidal forcing term. . . . .	127
5.38	Structure of the Taylor vortices for $t = t_{fin} = 6000$ in the case $\epsilon^2 = 0.01$ , $\mathcal{A}(z, 0) = (1.e - 04)rand(z)$ , subject to a sinusoidal forcing term along the radial direction and with second order terms in the expansion of the solution. . . . .	128
5.39	Complete solution $\mathcal{A}(z, t)$ of the G–L equation with homogeneous Dirichlet boundary conditions at $z = \pm L$ , $\epsilon^2 = 0.1$ , with a random initial condition $\mathcal{A}(z, 0) = (1.e - 04)rand(z)$ and subject to a sinusoidal forcing term. . . . .	129
5.40	Structure of the Taylor vortices for $t = t_{fin} = 6000$ in the case $\epsilon^2 = 0.01$ , $\mathcal{A}(z, 0) = (1.e - 04)rand(z)$ and with forcing term $\mathbf{f} = \mathbf{f}_1$ . . . . .	131
5.41	Complete solution $\mathcal{A}(z, t)$ of the G–L equation with homogeneous Dirichlet boundary conditions at $z = \pm L$ , $\epsilon^2 = 0.1$ , with a random initial condition $\mathcal{A}(z, 0) = (1.e - 04)rand(z)$ and subject to a uniform forcing term $\bar{g}_1$ . . . . .	132
5.42	Structure of the Taylor vortices for $t = t_{fin} = 6000$ in the case $\epsilon^2 = 0.01$ , $\mathcal{A}(z, 0) = (1.e - 04)rand(z)$ and with forcing term $\mathbf{f} = \mathbf{f}_2$ . . . . .	133
5.43	Complete solution $\mathcal{A}(z, t)$ of the G–L equation with homogeneous Dirichlet boundary conditions at $z = \pm L$ , $\epsilon^2 = 0.1$ , with a random initial condition $\mathcal{A}(z, 0) = (1.e - 04)rand(z)$ and subject to a uniform forcing term $\bar{g}_2$ . . . . .	134
5.44	Structure of the Taylor vortices for $t = t_{fin} = 4000$ in the case $\epsilon^2 = 0.01$ . The pattern formed is the steady condition given by a perturbation of the steady Taylor vortices with an impulse forcing term. . . . .	135
5.45	Solution of the complete G–L problem with $\delta(t)$ as a forcing term and $\mathcal{A}_{steady}^{GL}(z)$ as an initial condition. . . . .	136

A.1	Curve neutre per $\eta = 0.95$	141
A.2	Linee di corrente e andamento componenti di velocità relative ai vortici di Taylor per $\eta = 0.95$	142
A.3	Visualizzazione dei pattern caratteristici attorno ai cilindri: vortici a spirale A.3a; vortici di Taylor A.3b	142
A.4	Linee di corrente e componenti di velocità per i vortici a spirale generati ad $\alpha = 3, \omega = -0.8, \eta = 0.95, Re_c = 266.1, \beta_c = 3.08$	143
A.5	Comparazione della struttura dei vortici ottenuti con una simulazione DNS A.5a e con il modello di Ginzburg–Landau A.5b.	145

# List of Tables

- 5.1 Coefficients of the G–L equation for  $\alpha = 0$  and in the case the outer cylinder is fixed. The coefficients are also computed for three different values of  $\eta$ . . . . . 100
- 5.2 Comparison of the coefficients of the linear terms in the G–L equation for  $\eta = 0.95100$



# Abstract

In this thesis work, we studied the fluid dynamic stability of flows that are invariant, i.e. homogeneous, in one direction or more. The developed theory was then applied to the particular flow that develops between two rotating concentric cylinders, the Taylor–Couette flow. This stationary base flow in fact has two homogeneous directions along which it is symmetric by translation and reflection—the axial direction—and by rotation—the azimuthal direction.

This work is divided in two major parts: the first part is a preparatory study of the linear stability, both inviscid and viscous, of the 2D Taylor–Couette flow. The second part is the main contribution of this work and deals with the nonlinear stability of the aformentioned base flow. As regards the first part, a parametric analysis of the linear stability of the Taylor–Couette flow was carried out including all the parameters that play a role in the governing equations, fluid dynamic parameters, geometric parameters and kinematic parameters. In this context, the Taylor–Couette flow was obtained as an exact solution starting from the Navier–Stokes equations and then the equations describing the perturbations of the velocity and pressure fields were obtained and analysed under the hypothesis of validity of the linear theory. Coming to the second part of this work, we first explained the theory used to investigate the nonlinear stability of a generic dynamical system, and then we applied it to the Navier–Stokes equations considering the Taylor–Couette flow as a fixed point of the system. The need to investigate the nonlinear stability of our system lies in the fact that the Taylor–Couette solution can give rise to non-hyperbolic equilibrium states, for which there exists at least one eigenvalue of the associated linearised system, with null real part. In this case the linear stability is not able, alone, to predict the stability of the fixed point, and the only way to ascertain its stability is to apply methods that take into account the nonlinearities that are present in the governing equations. In particular, the method we used lies in the class of the perturbation methods and consists in carrying out an asymptotic expansion of the solution around a critical point of the linearised system. Using the multiple-scale method, it is possible to derive an equation—known as Ginzburg–Landau equation—which describes the nonlinear dynamics of the system right in the neighbourhood of the considered critical point. This equation has been applied to the first instability of the Taylor–Couette flow to axisymmetric disturbances and it has been solved under several conditions. Finally these solutions have been used to test the accuracy of the Ginzburg–Landau model to predict the complete solutions of particular Navier–Stokes problems.

**Keywords:** Taylor–Couette flow, Linear stability, Nonlinear stability, Weakly nonlinear analysis, Multiple-scale method, Ginzburg–Landau equation.



# Sommario

In questo lavoro di tesi, si è studiata la stabilità di correnti fluide con determinate proprietà di simmetria. Tali proprietà sono l'invarianza rispetto a traslazioni e rotazioni lungo due direzioni specifiche. La teoria sviluppata è stata poi applicata alla corrente che si sviluppa tra due cilindri concentrici rotanti, nota come corrente di Taylor–Couette. Questa corrente base stazionaria possiede infatti due direzioni omogenee lungo le quali la corrente è simmetrica per traslazione e riflessione—la direzione assiale—e per rotazione—la direzione azimutale.

Il seguente elaborato è diviso in due parti principali: la prima riguarda lo studio della stabilità lineare, inviscida e viscosa, della corrente di Taylor–Couette. La seconda parte tratta invece la stabilità non lineare e rappresenta il maggior contributo di questo lavoro. Per quanto riguarda la prima parte, si è impostato e risolto il problema relativo alla stabilità lineare della corrente di Taylor–Couette conducendo un'analisi parametrica che coinvolgesse tutti i parametri in gioco, fluidodinamici, geometrici e cinematici. Nella fattispecie è stata ricavata la soluzione esatta di Taylor–Couette a partire dalle equazioni di Navier–Stokes per poi ricavare e analizzare le equazioni che descrivono le perturbazioni del campo di velocità e del campo di pressione sotto le ipotesi di validità della teoria lineare. Proseguendo con la seconda parte dell'elaborato, si è passati a spiegare la teoria basata sullo studio della stabilità non lineare di un generico sistema dinamico, per poi applicare la trattazione alle equazioni di Navier–Stokes considerando come punto fisso del sistema la corrente di Taylor–Couette. La necessità di dover indagare la stabilità non lineare del nostro sistema risiede nel fatto che la soluzione base di Taylor–Couette può dar luogo a stati di equilibrio non iperbolicci, ossia tali per cui esiste almeno un autovalore del sistema linearizzato associato che ha parte reale nulla. In questo caso la sola stabilità lineare non è in grado di predire la stabilità del punto fisso in questione, la quale va accertata mediante l'applicazione di metodi che facciano intervenire i termini non lineari presenti nelle equazioni di governo. In particolare, il metodo che si è utilizzato si colloca tra i metodi perturbativi e consiste nell'effettuare un'espansione asintotica della soluzione nell'intorno di un punto critico del sistema linearizzato. Abbinando all'espansione asintotica il metodo delle scale multiple, è stato possibile derivare un'equazione—nota come equazione di Ginzburg–Landau—che descrive la dinamica non lineare del nostro sistema proprio nell'intorno del punto critico considerato. Questa equazione è stata applicata all'instabilità del flusso di Taylor–Couette rispetto a disturbi assialsimmetrici ed è stata risolta in diverse condizioni. Ciò ha permesso in ultimo di valutare l'accuratezza del modello di Ginzburg–Landau nel predire la soluzione completa di particolari problemi di Navier–Stokes.

**Parole chiave:** Corrente di Taylor–Couette, Stabilità lineare, Stabilità non lineare, Analisi debolmente non lineare, Metodo delle scale multiple, Equazione di Ginzburg–Landau.



# Chapter 1

## Introduction

The study of stability in fluid dynamics is of great importance as it can help to understand the triggering of complex physical mechanisms that lead the flow to totally change nature, passing from being laminar to being turbulent. This change in the flow structure, due to the transition, is possible if and only if the laminar flow is unstable.

The stability can be studied according to a linear and a nonlinear approach. As I will show later, the nonlinear stability approach, when it is framed in a weakly nonlinear setting, is based on the linear stability. We now proceed by analysing these two approaches more in depth.

### 1.0.1 Linear stability

Studying the linear stability of a generic dynamic system consists in evaluating the stability of its equilibrium state, under the hypothesis that the amplitude of the perturbations remains sufficiently small. In other words, the linear stability approach leads to results that agree with experiments only if the perturbations are not amplified to a point that causes the validity of the linear theory to cease.

A dynamic system can possess one or more states of equilibrium, also called fixed points of the system. Stability investigates how the perturbations of these fixed points evolve. In the context of linear stability, the eigenvalues of the system linearized around the equilibrium condition are computed. Based on the sign of the real part of the eigenvalues, three possible cases may emerge:

- If all the eigenvalues have strictly negative real part, then the fixed point is asymptotically stable.
- If there is at least an eigenvalue with positive real part, then the fixed point is unstable.
- If the system has all eigenvalues with negative real part, except at least one eigenvalue with zero real part, then the fixed point is called "non-hyperbolic" and its stability cannot be ascertained through a linear stability analysis.

Regarding this last possible case, the stability of the system must be ascertained by studying the nonlinear stability, hence by trying to take into account the weak nonlinearities of the system that emerge in a neighbourhood of the non-hyperbolic fixed point.

### 1.0.2 Nonlinear stability

It has been said in the previous paragraph that in order to study the stability of a non-hyperbolic state, one must necessarily study its nonlinear stability. Indeed, contrary to the linear stability theory which predicts a zero growth rate of the perturbations, the nonlinear stability analysis permits to establish in which way the nonlinear terms inside the governing equations emerge so that to give a negative or positive growth rate; hence to help the system to return to the initial equilibrium condition, to move towards another equilibrium condition, or to move away from it definitely. In this sense, the nonlinear terms, in the case of non-hyperbolic fixed points, play a decisive role in stabilizing or not the system.

The inclusion of the nonlinearities in this approach, is made possible by performing a weakly nonlinear expansion of the solution. This is an expansion in Taylor series of the amplitude of the perturbations in the vicinity of the neutral state. The amplitude is supposed to vary in a weakly manner with some slow scales—both time and spatial scales—in the sense that the variation of the amplitude depends on these slow variables, which are the physical variables rescaled by a control parameter that is supposed to be small. By a physical point of view, the introduction of new slow variables, permits to identify the time scales and the spatial scales at which the nonlinear effects become relevant. As it will be shown more in depth in this thesis, the method cited above refers to the multiple-scale method.

By applying the previous procedure, a partial differential equation, namely the Ginzburg–Landau equation, can be obtained. This equation describes the nonlinear dynamics of the whole initial system in the vicinity of the critical point for which the system loses its hyperbolicity characteristics.

The weakly nonlinear expansion approach, together with the multiple-scale approach, is the method usually employed to study the nonlinear stability. Other methods are even possible. One of this, is based on the centre manifold theorem, for which it is possible to construct a manifold in the neighbourhood of the fixed point and to reduce the dynamics of the entire starting system to the dynamics of a reduced order system on the manifold itself. Anyway, in this thesis, only the former method will be used.

### 1.0.3 Generation of the instabilities

The instability of a flow is generally caused by the presence of a disturbance to a state of equilibrium which can bring the whole solution of the problem, away from the equilibrium state as time increases. A perturbation to that state of equilibrium, can be generated in different ways. In the following, some of them are cited. The first way so that a flow becomes unstable may be given by the variation in the fluid properties, such as, for instance its density. This is the case of the Rayleigh–Bénard flow. Another possible cause is the presence of a particular forcing term in the Navier–Stokes equations or even the change in the boundary conditions of the problem. This latter case, is the one for which the Taylor–Couette instability sets in. The Taylor–Couette instability is also known as centrifugal instability because a variation in the boundary conditions of the steady Taylor–Couette problem, might let the pressure gradient not to be capable of balancing the centrifugal force acting on the fluid particles. As a matter of fact, in that situation, the centrifugal force acting on a fluid element, tends to pull the element towards the outer cylinder, so that the pressure gradient is not able to compensate this action. This kind of instability may easily be studied on the Taylor–Couette system, however it can occur in flows that are confined between curved boundaries, and it is called Dean instability in this case.

A further mechanism of instability concerns the effects of the viscosity. Viscosity in fact acts in two ways: on one hand it dissipates energy and therefore tends to stabilize the flow; on the other hand, it diffuses momentum and this characteristic may generate a viscous flow that is more unstable than the corresponding inviscid flow. For example, this second effect is largely evident in shear flows, such as the Poiseuille flow.

The mechanisms described above are the main sources of instability for a flow. They might also act simultaneously, leading to the formation of more complex bifurcated flows. In this thesis we will discuss only the Taylor–Couette instability, that originates from a centrifugal instability as explained before.

### 1.0.4 The instability of the Taylor-Couette flow

The flow that develops between two rotating cylinders is one of the most studied flows in the history of fluid dynamics. The first scientist to deal with it was Maurice Couette, who tried to obtain the viscosity of fluids by measuring the torque exerted by the fluid on the inner cylinder. He built a test rig consisting of two coaxial cylinders containing fluid and such that, through the rotation of the external cylinder only, with an angular velocity  $\Omega_b$ , he could measure the torque exerted on the inner wall. Based on his experiments, he discovered that, as long as the angular velocity of the cylinder remained below a threshold value, the torque was proportional to the product  $\nu\Omega_b$ . In contrast, if the angular velocity exceeded the limit value, the torque grew much faster and the flow became turbulent.

A few years later, Arnulph Mallock resumed Couette's experiments, but that time he allowed the rotation of the inner cylinder only, while the outer one was at rest. By rotating the cylinder with angular velocity  $\Omega_a$ , he observed that, depending on the intensity of the rotation, he couldn't reproduce the laminar flow found by Couette, as it became unstable earlier. The problem was solved definitively by Geoffrey Ingram Taylor, who discovered that the critical angular velocity of the inner cylinder beyond which the Couette flow becomes unstable, was much lower than the values used by Mallock in his experiments. Taylor built his experimental device allowing the rotation of both cylinders. This fact allowed the discovery of a wide series of secondary flows that were themselves the result of successive instabilities of the Couette base flow. Based on the assumption of considering cylinders with an infinite length, Taylor found that the first instability that arises in the Couette flow is a stationary and axisymmetric disturbance known as "Taylor vortex flow"—figure 1.1.

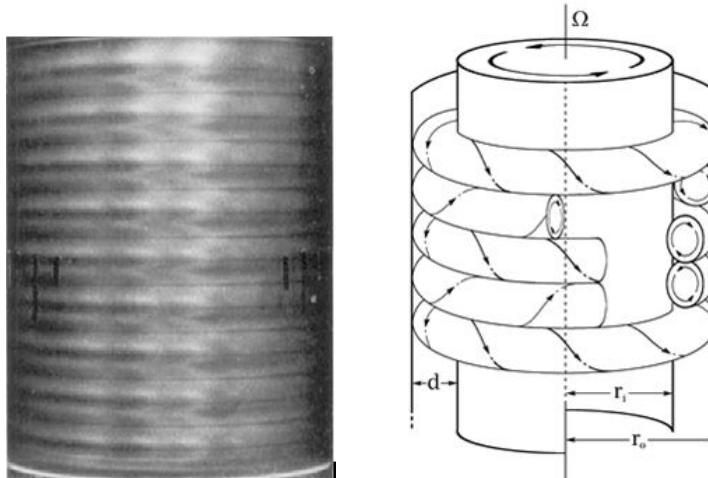


Figure 1.1: Taylor vortex flow ([14], [13]): streamline and cell pattern visualization around the cylinder

This type of motion is organized according to a well defined superposition of symmetrical structures composed of toroidal vortices, whose length is equal to half of the axial wavelength. Going further and increasing the angular velocity of the inner cylinder, the flow undergoes successive bifurcations, forming more and more complicated spatial structures and losing at the same time the peculiar characteristics of symmetry of Taylor vortices. It is to underline the fact that the comparison between the theoretical and experimental results obtained by Taylor are well in agreement because of the hypothesis to consider infinite-length-cylinders, or at least that the axial length of the cylinders is much greater than the difference between the radii.

The discoveries carried out by Taylor have paved the way for a possible explanation of the transition from the laminar regime to the turbulent one; particularly, in the case of the Taylor–Couette flow, this phase is observable through a wide series of new flows that emerge from new bifurcations. The type of pattern that is created starting from the first bifurcation of the base flow depends on the direction and the intensity of the angular velocity of the two cylinders. For example, using counter-rotating cylinders, spiral vortices arise, followed by wavy spirals or interpenetrating spirals, and via via more complex bifurcated flows, until turbulence sets in. Figure 1.2 shows some of these characteristic patterns. Another type of bifurcation

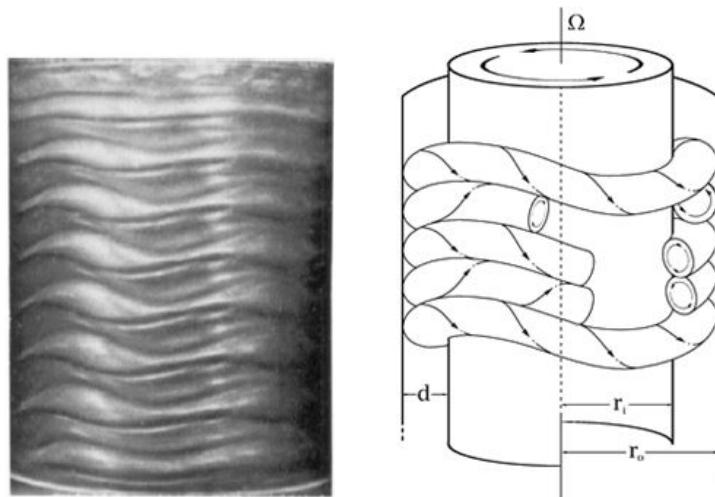


Figure 1.2: Wavy vortex flow ([14], [13]): streamline and cell pattern visualization around the cylinder

for example, leads to the generation of the so-called "modulated wavy vortex flow", i.e. Taylor vortices whose amplitude varies along the azimuthal direction, figure 1.3.

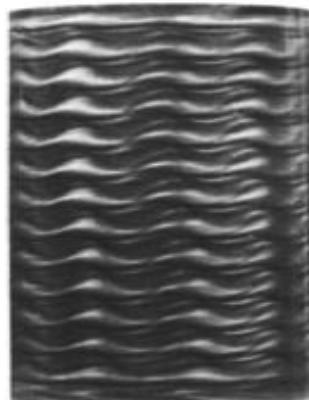


Figure 1.3: Modulated wavy vortex ([14]): streamlines visualization along a transversal section

As it is seen from figure 1.4, a lot of flows arise from successive bifurcations starting from the Taylor–Couette base flow and their character is more and more difficult to predict as the number of bifurcations increases. The next figure is taken from the works made by Andereck, Liu and Swinney [8], who, considering different angular velocity values for both the internal and the external cylinders, succeeded in obtaining a rich diagram which contains all the bifurcated solutions known so far.

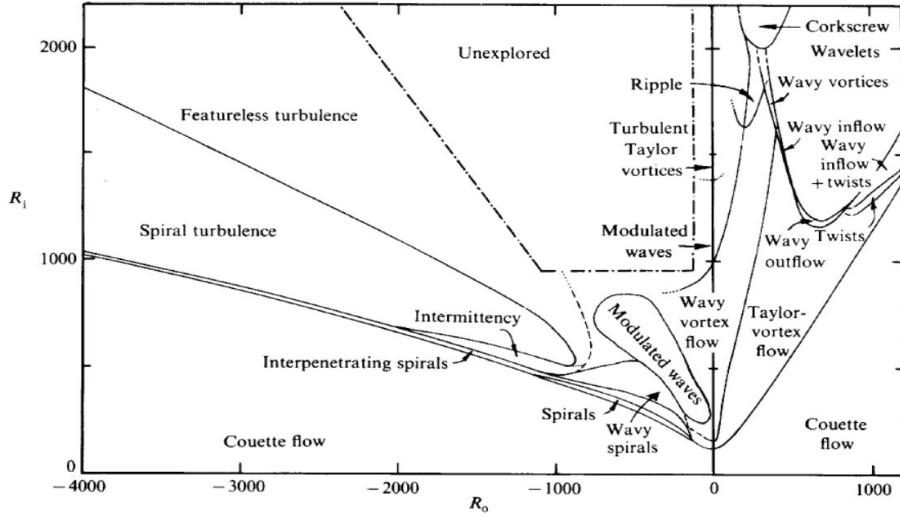


Figure 1.4: Complete bifurcation diagram for the Taylor–Couette flow [8]. The curves are plotted against two Reynolds numbers: on the abscissa we have the Reynolds number related to the external cylinder; on the ordinate we have the Reynolds number related to the inner cylinder

# Chapter 2

## Dimensionless Navier–Stokes equations

In this section we obtain the equations that govern the motion of an incompressible and viscous fluid in dimensionless form. The advantage of working with equations in dimensionless form is that we get rid of the physical properties of the particular fluid we are analysing, which in general will vary from fluid to fluid, to concentrate the attention on fewer dimensionless groups. In the dimensionless version, as we will show, the only parameter that has relevance in the equations is the Reynolds number; such a parameter can be calculated for any flow and does not depend on the specific fluid considered. There are two methods for making dimensionless the Navier–Stokes equations that lead to different positions of the Reynolds number. In particular, in the first procedure the Reynolds number eventually multiplies the viscous term  $\nabla^2 \mathbf{u}$ . In the second procedure instead, it stands in front of the nonlinear term  $(\mathbf{u} \cdot \nabla) \mathbf{u}$ .

### 2.1 General governing equations

The equations that govern the motion of fluids come directly from the principle of conservation of mass, the balance of momentum and the principle of conservation of energy. These three principles can be applied to the motion of compressible, viscous and heat conducting fluids. These equations, which are the "complete Navier–Stokes equations", can be gradually simplified assuming that the effects associated to the compressibility, the viscosity and the conductivity of the fluid are not relevant for the description of its motion. In particular, in this thesis work, we will always assume that the fluid is incompressible. We will also assume a uniform density and temperature field. Sometimes we will assume that the viscosity of the fluid will be neglected but this case will be specified when necessary. Assuming that the fluid does not exhibit its compressibility and thermal conductivity, the equations describing the fluid motion are reduced to the so-called "incompressible Navier–Stokes equations". From now on, since these equations are the only ones that we are going to use, they will simply be denoted as "Navier–Stokes Equations", referring implicitly to their incompressible form. These equations read

$$\begin{cases} \rho \frac{\partial \mathbf{u}}{\partial t} + \rho(\mathbf{u} \cdot \nabla) \mathbf{u} + \nabla p - \mu \nabla^2 \mathbf{u} = 0, \\ \nabla \cdot \mathbf{u} = 0, \end{cases} \quad (2.1)$$

where the fluid density  $\rho$  is supposed to be constant and equal to a known value. The viscosity will be assumed constant too. The equations (2.1), in order to admit a unique solution, must be supplemented with suitable boundary conditions and an initial condition. There are two kinds of boundary conditions that can be imposed: Dirichlet boundary conditions and Neumann boundary conditions. As regards the first type, they prescribe the value of the velocity on the whole—or at least on a part of the—boundary of the fluid domain. They are expressed by a relation like

$$\mathbf{u} = \mathbf{g}, \quad \text{on} \quad \Gamma_D \quad (2.2)$$

where  $\Gamma_D$  is the part of the boundary where Dirichlet boundary conditions are applied. Similar considerations can be made for Neumann boundary conditions, through which the total stress is imposed on the boundary. These conditions take the form:

$$\nu \frac{\partial \mathbf{u}}{\partial \hat{\mathbf{n}}} - p\hat{\mathbf{n}} = \mathbf{h}, \quad \text{on } \Gamma_N \quad (2.3)$$

where the symbol  $\frac{\partial}{\partial \hat{\mathbf{n}}}$  indicates the directional derivative at the boundary  $\Gamma_N$  of the normal unit vector. Finally the imposition of the initial condition takes the form

$$\mathbf{u}(\mathbf{r}, 0) = \mathbf{u}_0(\mathbf{r}). \quad (2.4)$$

The union of the governing equations with the boundary conditions and the initial condition, give rise to the complete Navier–Stokes problem (2.5) which describes the motion of a viscous incompressible fluid

$$\begin{cases} \rho \frac{\partial \mathbf{u}}{\partial t} + \rho(\mathbf{u} \cdot \nabla) \mathbf{u} + \nabla p - \mu \nabla^2 \mathbf{u} = 0, \\ \nabla \cdot \mathbf{u} = 0, \\ \mathbf{u} = \mathbf{g}, & \text{on } \Gamma_D, \\ \nu \frac{\partial \mathbf{u}}{\partial \hat{\mathbf{n}}} - p\hat{\mathbf{n}} = \mathbf{h}, & \text{on } \Gamma_N \equiv \partial V / \Gamma_D, \\ \mathbf{u}(\mathbf{r}, 0) = \mathbf{u}_0(\mathbf{r}). \end{cases} \quad (2.5)$$

As it can be seen, this is a nonlinear differential problem, where the unknowns are the velocity field of the fluid, which is a vector field, and the pressure, which instead is a scalar field. The unknowns of the problem will generally depend on four variables: three linked to space and one linked to time.

## 2.2 Dimensionless equations: first formulation

Let us consider an incompressible flow describing the motion of a fluid having a characteristic velocity magnitude  $U$  and such that it flows around a body of known shape, whose reference length is  $L$ . Let me suppose the density  $\rho$  and the dynamic viscosity  $\mu$  of the fluid are known. Thus, four parameters appear in the governing equations:  $L, U, \mu, \rho$ . These four parameters can be reduced to a single parameter only by means of Buckingham's theorem. In this way, the solutions to the equations that govern the motion of an incompressible and viscous fluid represent a family of solutions with a single variable parameter. Buckingham's theorem states that given a physical problem described by  $n$  physical variables and  $k$  fundamental units, it can be described with  $(n - k)$  dimensionless groups. In mathematical terms we have that the number of dimensionless parameters on which the problem depends are  $m = n - k$ .

In our case, the motion of an incompressible, viscous fluid, can be described by means of four physical variables

- the vector  $\mathbf{R}$ , which describes the position in the flow field,
- the velocity field  $\mathbf{w}$ ,
- the pressure  $P$ ,
- the density of the fluid  $\rho$ .

The fundamental units are instead a reference length  $L$ , a reference time scale  $T$  and the density  $\rho$ . By virtue of Buckingham's theorem, the number of parameters needed to describe the Navier–Stokes equations are  $m = 4 - 3 = 1$ . Hence just one parameter is sufficient in order to get the dimensionless N–S equations. This parameter, as we will show, is the Reynolds number. Having introduced the characteristic magnitudes of the problem, we now begin the derivation

of the dimensionless equations. We start by writing the equations of motion in dimensional form:

$$\begin{cases} \rho \frac{\partial \mathbf{w}}{\partial T} + \rho(\mathbf{w} \cdot \nabla) \mathbf{w} + \nabla P - \mu \nabla^2 \mathbf{w} = 0, \\ \nabla \cdot \mathbf{w} = 0. \end{cases} \quad (2.6)$$

By the introduction of the previous parameters, we now define the following dimensionless quantities:

- $\mathbf{r} = \frac{\mathbf{R}}{L}$ ,
- $\mathbf{u} = \frac{\mathbf{w}}{U}$ ,
- $t = \frac{U}{L} T$ ,
- $p = \frac{P - P_\infty}{\rho U^2}$ ,

where  $P_\infty$  is a reference value of the pressure. Having made this change of variables that bring us from the space of physical variables  $(\mathbf{w}, \mathbf{R}, T)$  to the set of corresponding dimensionless variables  $(\mathbf{u}, \mathbf{r}, t)$ , we express the differential operator who appear in the Navier–Stokes equations in the following way:

- $\frac{\partial}{\partial T} = \frac{U}{L} \frac{\partial}{\partial t}$ ,
- $\nabla = \frac{1}{L} \nabla$ ,
- $\nabla^2 = \frac{1}{L^2} \nabla^2$ .

We now have all the ingredients to write the Navier–Stokes equations in dimensionless form. We first start from the continuity equation. By applying the new differential operators to the dimensionless quantities, we obtain:

$$\nabla \cdot \mathbf{u} = 0. \quad (2.7)$$

Therefore, the shape of the equations has not changed. However, about the momentum equation we have:

$$\frac{U^2}{L} \frac{\partial \mathbf{u}}{\partial t} + \frac{U^2}{L} (\mathbf{u} \cdot \nabla) \mathbf{u} + \frac{1}{\rho L} \rho U^2 \nabla p - \frac{U \nu}{L^2} \nabla^2 \mathbf{u} = 0, \quad (2.8)$$

and by multiplying all the terms by  $\frac{L}{U^2}$ , we get

$$\frac{\partial \mathbf{u}}{\partial t} + (\mathbf{u} \cdot \nabla) \mathbf{u} + \nabla p - \frac{\nu}{LU} \nabla^2 \mathbf{u} = 0. \quad (2.9)$$

We define the Reynolds number  $Re$ , the dimensionless number such that  $Re = \frac{UL}{\nu}$ . Hence the momentum equation can be rewritten as

$$\frac{\partial \mathbf{u}}{\partial t} + (\mathbf{u} \cdot \nabla) \mathbf{u} + \nabla p - \frac{1}{Re} \nabla^2 \mathbf{u} = 0. \quad (2.10)$$

Finally, putting together both the continuity and the momentum equation, the first formulation of the dimensionless Navier–Stokes equations for an incompressible and viscous fluid, reads as

$$\begin{cases} \frac{\partial \mathbf{u}}{\partial t} + (\mathbf{u} \cdot \nabla) \mathbf{u} + \nabla p - \frac{1}{Re} \nabla^2 \mathbf{u} = 0, \\ \nabla \cdot \mathbf{u} = 0. \end{cases} \quad (2.11)$$

## 2.3 Dimensionless equations: second formulation

In this paragraph, we deal instead with a second possible formulation of the dimensionless N–S equations, which aims at highlighting the nonlinear term and the effects that the Reynolds number has on it. As we will show, this form is more convenient when dealing with low Reynolds number flows.

In order to get this second formulation, we build different dimensionless variables

- $\mathbf{r} = \frac{\mathbf{R}}{L}$ ,

- $\mathbf{u} = \frac{\mathbf{w}}{U}$ ,

- $t = \frac{\nu}{L^2} T$ ,

- $p = \frac{P - P_\infty}{\rho \nu U}$ ,

and concerning the differential operators we have:

- $\frac{\partial}{\partial t} = \frac{\nu}{L^2} \frac{\partial}{\partial t}$ ,

- $\nabla = \frac{1}{L} \nabla$ ,

- $\nabla^2 = \frac{1}{L^2} \nabla^2$ .

Inserting the new variables in the governing equations and performing the new derivatives, we again get that the continuity equations remains the same, whereas the momentum equation is modified as follows

$$\frac{\nu U}{L^2} \frac{\partial \mathbf{u}}{\partial t} + \frac{U^2}{L} (\mathbf{u} \cdot \nabla) \mathbf{u} + \frac{\nu U}{L^2} \nabla p - \frac{U \nu}{L^2} \nabla^2 \mathbf{u} = 0. \quad (2.12)$$

By multiplying the equation (2.12) by  $\frac{L^2}{\nu U}$ , we obtain the second formulation for the dimensionless Navier–Stokes equations:

$$\begin{cases} \frac{\partial \mathbf{u}}{\partial t} + Re(\mathbf{u} \cdot \nabla) \mathbf{u} + \nabla p - \nabla^2 \mathbf{u} = 0, \\ \nabla \cdot \mathbf{u} = 0. \end{cases} \quad (2.13)$$

Now, it is clear that if the Reynolds number is very low, the nonlinear term can be neglected and the equations reduce to the generalised "Stokes equations"

$$\begin{cases} \frac{\partial \mathbf{u}}{\partial t} + \nabla p - \nabla^2 \mathbf{u} = 0, \\ \nabla \cdot \mathbf{u} = 0. \end{cases} \quad (2.14)$$

# Chapter 3

## Taylor-Couette steady flow

The Taylor-Couette steady flow, often called just Taylor-Couette flow, constitutes an exact solution of the Navier-Stokes equations in cylindrical geometry. This flow is two-dimensional and invariant along the azimuthal and axial directions. The equations that describe this flow are derived below.

### 3.1 Exact solutions of the Navier-Stokes equations in cylindrical coordinates

The Navier-Stokes equations in cylindrical geometry admit exact solutions that can be described in closed form. One of these solutions describes the motion of a fluid between two infinitely long coaxial cylinders, which can rotate around a common axis. Since the cylinders are supposed to have a much greater axial extent with respect to the radial one, and the boundary condition is planar, the velocity field can be considered two-dimensional. We will also assume that, given the geometry and the symmetry properties of the flow, the velocity field is invariant under arbitrary translations along the axial direction, described respectively by the coordinate  $z$ , and under rotations along the angular direction, described by the coordinate  $\theta$ . Under such hypotheses the velocity and pressure fields can be expressed in general form as

$$\begin{aligned}\mathbf{u}(\mathbf{r}, t) &= u_r(r, t)\hat{\mathbf{r}} + u_\theta(r, t)\hat{\boldsymbol{\theta}}, \\ p(\mathbf{r}, t) &= p(r, t).\end{aligned}\tag{3.1}$$

For notational convenience, the unknowns have already been expressed in dimensionless form so that the governing equations will also be written in dimensionless form. In particular, according to the first of the two formulations described in paragraph 2.2, they are given by

$$\begin{cases} \frac{\partial \mathbf{u}}{\partial t} + (\mathbf{u} \cdot \nabla) \mathbf{u} + \nabla p - \frac{1}{Re} \nabla^2 \mathbf{u} = 0, \\ \nabla \cdot \mathbf{u} = 0. \end{cases}\tag{3.2}$$

Firstly, we analyze the continuity equation; so we have

$$\nabla \cdot \mathbf{u} = 0 \rightarrow \frac{1}{r} \frac{\partial}{\partial r} [ru_r(r, t)] + \frac{1}{r} \frac{\partial u_\theta(r, t)}{\partial \theta} = 0.\tag{3.3}$$

Now, as the flow does not depend on  $\theta$ , the equation above reduces to

$$\frac{1}{r} \frac{\partial}{\partial r} [ru_r(r, t)] = 0 \rightarrow u_r(r, t) = \frac{A(t)}{r}.\tag{3.4}$$

where the function  $A(t)$  is an arbitrary function of time only. In order to determine it, we have to impose the boundary conditions; a first condition can be imposed assuming that the normal

component is zero at the walls. This implies that  $A(t) = 0, \forall t > 0$ . Hence, we can deduce that the flow is purely azimuthal, namely

$$\mathbf{u}(\mathbf{r}, t) = u_\theta(r, t)\hat{\theta}. \quad (3.5)$$

We analyse now the momentum balance equation. For what concerns the nonlinear term, the only contribution that survives is

$$(\mathbf{u} \cdot \nabla) \mathbf{u} = -\frac{[u_\theta(r, t)]^2}{r} \hat{\mathbf{r}}. \quad (3.6)$$

The Laplacian instead will read as

$$\nabla^2 \mathbf{u} = \left[ \frac{1}{r} \frac{\partial}{\partial r} \left( r \frac{\partial u_\theta(r, t)}{\partial r} \right) - \frac{u_\theta(r, t)}{r^2} \right] \hat{\theta}. \quad (3.7)$$

Finally putting everything together, the momentum equation will read as

$$\frac{\partial u_\theta(r, t)}{\partial t} \hat{\theta} - \frac{[u_\theta(r, t)]^2}{r} \hat{\mathbf{r}} + \frac{\partial p(r, t)}{\partial r} \hat{\mathbf{r}} - \frac{1}{Re} \left[ \frac{1}{r} \frac{\partial}{\partial r} \left( r \frac{\partial u_\theta(r, t)}{\partial r} \right) - \frac{u_\theta(r, t)}{r^2} \right] \hat{\theta} = 0. \quad (3.8)$$

By decomposing the equation in the two directions  $\hat{\mathbf{r}}$  and  $\hat{\theta}$ , we get the following system of equations

$$\begin{cases} -\frac{[u_\theta(r, t)]^2}{r} + \frac{\partial p(r, t)}{\partial r} = 0, \\ \frac{\partial u_\theta(r, t)}{\partial t} - \frac{1}{Re} \left[ \frac{1}{r} \frac{\partial}{\partial r} \left( r \frac{\partial u_\theta(r, t)}{\partial r} \right) - \frac{u_\theta(r, t)}{r^2} \right] = 0. \end{cases} \quad (3.9)$$

The second equation of the system is decoupled from the first one and can be solved first. Once the solution of the second equation is found, the function  $u_\theta(r, t)$  can be used to determine the behaviour of the pressure. By simply integrating, the pressure is determined by the following relation

$$p(r, t) = \int \frac{[u_\theta(r, t)]^2}{r} dr + C(t), \quad (3.10)$$

where the function  $C(t)$  is a time-dependent function that can be chosen basing on a pressure reference condition.

It can be noticed that the momentum equation along the radial direction is analogous to the fundamental law of dynamics—appropriately scaled—in the form  $\mathbf{a} = \frac{\mathbf{f}}{m}$ . In fact, taking the pressure gradient to the right-hand side, we recognize the two contributions which appear in the previous expression: on the left-hand side the term  $-u_\theta^2/r$  represents the centripetal acceleration for a fluid particle; whereas on the right-hand side, the pressure gradient represents the centripetal force acting on the fluid particle.

## 3.2 Derivation of the Taylor-Couette solution

The Taylor-Couette flow represents a particular case of the solutions for the equations presented in the previous paragraph. It is in fact the stationary solution of the preceding equations, in which the fluid, after an initial transient, reaches a stationary state and just flows between two concentric cylinders which rotate in general at different angular velocities. We model this problem in the following way: we define  $R_a$  and  $R_b$  the radii of the inner and outer cylinder, respectively. We call  $\Omega_a$  and  $\Omega_b$  the angular velocities of the two cylinders. Then, we proceed as follows: we first write the governing equation in dimensional form and only in a second step we will make it dimensionless, highlighting the scaling quantities.

The equation that describes our problem is the following

$$\frac{d}{dR} \left( \frac{1}{R} \frac{d}{dR} (Ru_\theta) \right), \quad R_a < R < R_b \quad (3.11)$$

with boundary conditions

$$\begin{aligned} u_\theta(R_a) &= R_a \Omega_a, \\ u_\theta(R_b) &= R_b \Omega_b. \end{aligned} \quad (3.12)$$

To make the problem dimensionless, we define the following dimensionless parameters

$$\begin{aligned} \eta &= \frac{R_a}{R_b}, \\ d &= R_b - R_a, \\ \omega &= \frac{\Omega_b}{\Omega_a}. \end{aligned} \quad (3.13)$$

We assume a reference velocity  $U_{ref} = R_a \Omega_a$  and we write the dimensionless velocity component, the radial coordinate and the Reynolds number as

$$\begin{aligned} r &= \frac{R}{d}, \\ U(r) &= \frac{u_\theta(r)}{U_{ref}}, \\ Re &= \frac{R_a \Omega_a d}{\nu}. \end{aligned} \quad (3.14)$$

By adopting the change of variables above, the governing equation becomes

$$\frac{d}{dr} \left( \frac{1}{r} \frac{d}{dr} (rU) \right), \quad a < r < b, \quad (3.15)$$

where  $a = R_a/d$  and  $b = R_b/d$ . The form of the differential equation (3.15) has not been modified. About the boundary conditions instead, we get

$$\begin{aligned} u_\theta(R_a) &= R_a \Omega_a \rightarrow U(a) = 1, \\ u_\theta(R_b) &= R_b \Omega_b \rightarrow U(b) = \frac{\omega}{\eta}. \end{aligned} \quad (3.16)$$

By integrating a first time, we get

$$\frac{1}{r} \frac{d}{dr} (rU) = A \rightarrow \frac{d}{dr} (rU) = Ar, \quad (3.17)$$

and integrating a second time, we obtain

$$rU = \frac{A}{2} r^2 + B. \quad (3.18)$$

By rewriting with a notation abuse, the coefficient  $\frac{A}{2}$  as  $A$ , the general solution is found to be

$$U(r) = Ar + \frac{B}{r}. \quad (3.19)$$

As the aim is to find the unique solution of the differential problem, the boundary conditions have to be imposed. By doing so, we get the following linear system of two equations in the two unknowns  $A$  and  $B$

$$\begin{aligned} Aa + \frac{B}{a} &= 1, \\ Ab + \frac{B}{b} &= \frac{\omega}{\eta}. \end{aligned} \quad (3.20)$$

Hence, the final solution for the velocity is

$$U(r) = \frac{\omega - \eta^2}{\eta(1 + \eta)} r + \frac{\eta(1 - \omega)}{(1 - \eta)(1 - \eta^2)} \frac{1}{r}. \quad (3.21)$$

Once the velocity field has been obtained, we use this function to determine the pressure field. By making use of the radial component of the momentum equation, we have the following equation for the pressure only

$$\frac{dP(r)}{dr} = \frac{U^2(r)}{r}. \quad (3.22)$$

Integrating once we get

$$P(r) = \left( \frac{C^2}{2} r^2 + 2CD \ln(r) - \frac{D^2}{2r^2} + const \right). \quad (3.23)$$

where  $C$  and  $D$  are constants which depend on the parameters  $\eta$  and  $\omega$ , while the term *const* indicates an arbitrary dimensionless constant that can be chosen once the pressure has been fixed in a precise point.

We can now make some comments on the results obtained in this paragraph. A first comment concerns the form of the velocity: it can be seen as the sum of a rigid rotational motion and a rectilinear vortex.

A second observation, that will be useful in the development of the linear inviscid stability theory, is the definition of an angular velocity field of the fluid, which is defined as the scalar field  $\Omega(r)$  such that

$$\Omega(r) = \frac{U(r)}{r}. \quad (3.24)$$

In our particular case, it assumes the form

$$\Omega(r) = \frac{\omega - \eta^2}{\eta(1 + \eta)} + \frac{\eta(1 - \omega)}{(1 - \eta)(1 - \eta^2)} \frac{1}{r^2}, \quad (3.25)$$

with values at the limit of the radial domain, given by  $\Omega = \frac{1}{a}$  in  $r = a$  and  $\Omega = \frac{\omega}{\eta b}$  in  $r = b$ .

## Chapter 4

# Linear stability and its application to the Taylor–Couette flow

As it was mentioned in the introduction, the linear stability permits to study how the perturbations of a state of equilibrium, represented in our case by a steady basic flow, evolve in time until their amplitude remains infinitesimal. The equations that describe the linear stability in fluid dynamics are the Navier–Stokes equations linearized around the equilibrium solution. In this section, we will briefly introduce the Navier–Stokes equations written as a dynamical system, after that we will derive the linearized equations in a dimensionless form making use of the first formulation introduced in the paragraph 2.2. Then we will apply the theory of linear stability to the particular case of the Taylor–Couette stationary flow, considering firstly the inviscid case, and then extending it to the more general viscous case.

### 4.1 Linearized Navier-Stokes equations around a stationary basic solution

The Navier–Stokes equations described in paragraph 2.1 can be written as a continuum dynamical system that describes how an incompressible and viscous fluid moves. The writing of the governing equations in the typical form of dynamical systems can be done by introducing the following differential operators:

$$\mathcal{L} = \begin{pmatrix} -\frac{1}{Re} \nabla^2, & \nabla \\ \nabla \cdot, & 0 \end{pmatrix}, \quad (4.1)$$

$$\mathcal{N} = \begin{pmatrix} (\mathbf{u} \cdot \nabla), & 0 \\ 0, & 0 \end{pmatrix}, \quad (4.2)$$

$$\mathcal{B} = \begin{pmatrix} 1, & 0 \\ 0, & 0 \end{pmatrix}, \quad (4.3)$$

$$\mathbf{w} = \begin{pmatrix} \mathbf{u} \\ p \end{pmatrix}. \quad (4.4)$$

The operator  $\mathcal{L}$  represents the linear part of the whole Navier–Stokes spatial operator; on the other hand, the operator  $\mathcal{N}$  describes the nonlinear part of the Navier–Stokes operator. In this way, the equations can be written as

$$\mathcal{B} \frac{\partial \mathbf{w}}{\partial t} = \mathcal{L} \mathbf{w} + \mathcal{N} \mathbf{w}. \quad (4.5)$$

The search for a stationary equilibrium solution  $(\mathbf{U}(\mathbf{r}), P(\mathbf{r}))$  of the system (4.5), is performed by cancelling the temporal derivative term. This implies that the velocity field and the pressure field, are solutions of the following complete problem

$$\begin{cases} (\mathbf{U} \cdot \nabla) \mathbf{U} = \nabla P - \frac{1}{Re} \nabla^2 \mathbf{U}, \\ \nabla \cdot \mathbf{U}, \\ \mathbf{U} = \mathbf{g}, \\ \nu \frac{\partial \mathbf{U}}{\partial \hat{n}} - P \hat{\mathbf{n}} = \mathbf{h}, \end{cases} \quad \begin{array}{ll} & \text{on } \Gamma_D, \\ & \text{on } \Gamma_N \equiv \partial V / \Gamma_D, \end{array} \quad (4.6)$$

where  $\mathbf{g}$  and  $\mathbf{h}$  represent the boundary data.

We can now express the velocity field  $\mathbf{u}$  and the pressure field  $p$  as the sum of two terms: the first one given by the equilibrium state, the second one given by a perturbation term, whose amplitude is modulated by a small parameter  $\epsilon \ll 1$ :

$$\begin{aligned} \mathbf{u} &= \mathbf{U}(\mathbf{r}) + \epsilon \mathbf{u}', \\ p &= p_0(\mathbf{r}) + \epsilon p'. \end{aligned} \quad (4.7)$$

Substituting these expressions in the Navier–Stokes equations, at order one in  $\epsilon$ , we get the following equations for the unknowns  $(\mathbf{u}', p')$

$$\begin{cases} \epsilon \frac{\partial \mathbf{u}'}{\partial t} + \epsilon (\mathbf{u}' \cdot \nabla) \mathbf{U}(\mathbf{r}) + \epsilon (\mathbf{U}(\mathbf{r}) \cdot \nabla) \mathbf{u}' + \epsilon \nabla p' - \epsilon \frac{1}{Re} \nabla^2 \mathbf{u}' = 0, \\ \epsilon \nabla \cdot \mathbf{u}' = 0. \end{cases} \quad (4.8)$$

By simplifying the factor  $\epsilon$  in the system of equations and by imposing the boundary conditions, we obtain the following complete problem:

$$\begin{cases} \frac{\partial \mathbf{u}'}{\partial t} + (\mathbf{u}' \cdot \nabla) \mathbf{U}(\mathbf{r}) + (\mathbf{U}(\mathbf{r}) \cdot \nabla) \mathbf{u}' + \nabla p' - \frac{1}{Re} \nabla^2 \mathbf{u}' = 0, \\ \nabla \cdot \mathbf{u}' = 0, \\ \mathbf{u}'|_S = 0. \end{cases} \quad (4.9)$$

where the boundary of the whole domain has been indicated with  $S$ . This problem represents the differential problem for the study of the linear stability. Note that in the perturbed problem, the only boundary conditions that have to be imposed concerns the velocity components and are Dirichlet boundary conditions. The reason stands in the fact that, if in the original problem there are non-homogeneous boundary data, they are already prescribed for the stationary solution, as described in the problem (4.6).

The problem described by the system (4.9) is valid for any stationary state and can be described in any coordinate system. Regarding the work discussed in this paper, we will express the problems (4.6) and (4.9) in a cylindrical reference system. In particular, reminding we operate with non-dimensional equations whose unknowns are also functions of non-dimensional variables, we will have that  $\mathbf{r} = \frac{\mathbf{R}}{L} = (\frac{R}{L}, \theta, \frac{Z}{L})$ . By calling  $r = \frac{R}{L}$  and  $z = \frac{Z}{L}$  we get  $\mathbf{r} = (r, \theta, z)$ . The problem domain is thus defined by the set  $V = [(r, \theta, z) \in \mathbb{R}^3 : r \in (a, b), \theta \in (0, 2\pi), z \in (-\infty, +\infty)]$  where  $(a, b) = (\frac{R_a}{L}, \frac{R_b}{L})$ . The reference length  $L$  can be taken in different ways; in our case we assume  $L = d = R_b - R_a$ . After having exploited the dependence of the unknowns with respect to the dimensionless variables, we have

$$\mathbf{u}' = \mathbf{u}'(t, r, \theta, z), \quad p' = p'(t, r, \theta, z). \quad (4.10)$$

We now explicitly derive the linearized equations written in a cylindrical reference system

$(r, \theta, z)$ . They take the form

$$\begin{aligned} \frac{\partial u'_r}{\partial t} + \frac{U}{r} \left( \frac{\partial u'_r}{\partial \theta} - 2u'_\theta \right) + \frac{\partial p'}{\partial r} &= \frac{1}{Re} \left( \nabla^2 u'_r - \frac{u'_r}{r^2} - \frac{2}{r^2} \frac{\partial u'_\theta}{\partial \theta} \right), \\ \frac{\partial u'_\theta}{\partial t} + \frac{U}{r} \left( \frac{\partial u'_\theta}{\partial \theta} + u'_r \right) + u'_r \frac{dU}{dr} + \frac{1}{r} \frac{\partial p'}{\partial \theta} &= \frac{1}{Re} \left( \nabla^2 u'_\theta - \frac{u'_\theta}{r^2} + \frac{2}{r^2} \frac{\partial u'_R}{\partial \theta} \right), \\ \frac{\partial u'_z}{\partial t} + \frac{U}{R} \frac{\partial u'_z}{\partial \theta} + \frac{\partial p'}{\partial z} &= \frac{1}{Re} \nabla^2 u'_z, \\ \frac{1}{r} \frac{\partial}{\partial r} (ru'_r) + \frac{1}{r} \frac{\partial u'_\theta}{\partial \theta} + \frac{\partial u'_z}{\partial z} &= 0. \end{aligned} \quad (4.11)$$

where, for brevity of notation, the Laplacian operator related to a generic scalar function  $f$  has been introduced and takes the form

$$\nabla^2 f = \frac{1}{r} \frac{\partial}{\partial r} \left( r \frac{\partial f}{\partial r} \right) + \frac{1}{r^2} \frac{\partial^2 f}{\partial \theta^2} + \frac{\partial^2 f}{\partial z^2}. \quad (4.12)$$

At this point we express the unknowns of the equation (4.11) in the form of normal modes; this means we are allowed to express the velocity components and the pressure as travelling waves, whose amplitude is modulated in the non-homogeneous direction, in our case the radial direction  $r$ .

We will therefore have the relations

$$\begin{aligned} u'_r(r, \theta, z, t) &= \tilde{u}_r(r) e^{i\alpha\theta+i\beta z+st}, \\ u'_\theta(r, \theta, z, t) &= \tilde{u}_\theta(r) e^{i\alpha\theta+i\beta z+st}, \\ u'_z(r, \theta, z, t) &= \tilde{u}_z(r) e^{i\alpha\theta+i\beta z+st}, \\ p'(r, \theta, z, t) &= \tilde{p}(r) e^{i\alpha\theta+i\beta z+st}, \end{aligned} \quad (4.13)$$

with  $\alpha \in \mathbb{Z}$ ,  $\beta \in \mathbb{R}$ , while  $s \in \mathbb{C}$ .

We write here the Laplacian applied to a generic scalar function  $f$  that is supposed to be a travelling wave as defined before

$$\nabla^2 f = \left( \frac{1}{r} \frac{d}{dr} \left( r \frac{d\tilde{f}}{dr} \right) - \left( \frac{\alpha^2}{r^2} + \beta^2 \right) \tilde{f} \right) e^{i\alpha\theta+i\beta z+st}. \quad (4.14)$$

In an analogous way, we express the Laplacian (4.14) for  $u'_r, u'_\theta, u'_z, p'$ . By substituting the derivatives into the equations (4.11) and by simplifying the exponential term, we get

$$\begin{aligned} s\tilde{u}_r + \frac{U}{r} (i\alpha\tilde{u}_r - 2\tilde{u}_\theta) + \frac{d\tilde{p}}{dr} &= \frac{1}{Re} \left[ \frac{1}{r} \frac{d}{dr} \left( r \frac{d\tilde{u}_r}{dr} \right) - \left( \frac{\alpha^2}{r^2} + \beta^2 \right) \tilde{u}_r - \frac{\tilde{u}_r}{r^2} - \frac{2i\alpha}{r^2} \tilde{u}_\theta \right], \\ s\tilde{u}_\theta + \frac{U}{r} (\tilde{u}_r + i\alpha\tilde{u}_\theta) + \tilde{u}_r U' + \frac{i\alpha}{r} \tilde{p} &= \frac{1}{Re} \left[ \frac{1}{r} \frac{d}{dr} \left( r \frac{d\tilde{u}_\theta}{dr} \right) - \left( \frac{\alpha^2}{r^2} + \beta^2 \right) \tilde{u}_\theta - \frac{\tilde{u}_\theta}{r^2} + \frac{2i\alpha}{r^2} \tilde{u}_r \right], \\ s\tilde{u}_z + i\alpha \frac{U}{r} \tilde{u}_z + \beta \tilde{p} &= \frac{1}{Re} \left[ \frac{1}{r} \frac{d}{dr} \left( r \frac{d\tilde{u}_z}{dr} \right) - \left( \frac{\alpha^2}{r^2} + \beta^2 \right) \tilde{u}_z \right], \\ \frac{1}{r} \frac{d}{dr} (r\tilde{u}_r) + \frac{i\alpha}{r} \tilde{u}_\theta + i\beta \tilde{u}_z &= 0. \end{aligned} \quad (4.15)$$

We now define the differential operators:

$$\begin{aligned} \mathcal{D}^2 &= \frac{1}{r} \frac{d}{dr} \left( r \frac{d}{dr} \right) - \left( \frac{\alpha^2}{r^2} + \beta^2 \right), \\ \mathcal{D} &= \frac{1}{r} + \frac{d}{dr}, \end{aligned} \quad (4.16)$$

and using the notation  $U'$  for the derivative of  $U$  with respect to  $r$ , the system (4.15) can be written in the final form

$$\begin{aligned} & \left[ s + i\alpha \frac{U}{r} - \frac{1}{Re} \left( \mathcal{D}^2 - \frac{1}{r^2} \right) \right] \tilde{u}_r + \left( \frac{2i\alpha}{Rer^2} - 2\frac{U}{r} \right) \tilde{u}_\theta + \frac{d\tilde{p}}{dr} = 0, \\ & \left( \frac{U}{r} + U' - \frac{2i\alpha}{Rer^2} \right) \tilde{u}_r + \left[ s + i\alpha \frac{U}{r} - \frac{1}{Re} \left( \mathcal{D}^2 - \frac{1}{r^2} \right) \right] \tilde{u}_\theta + \frac{i\alpha}{r} \tilde{p} = 0, \\ & \left( s + i\alpha \frac{U}{r} - \frac{\mathcal{D}^2}{Re} \right) \tilde{u}_z + i\beta \tilde{p} = 0, \\ & \mathcal{D}\tilde{u}_r + \frac{i\alpha}{r} \tilde{u}_\theta + i\beta \tilde{u}_z = 0. \end{aligned} \quad (4.17)$$

The system 4.17 defines a generalized eigenvalue problem. By introducing the vector state  $\mathbf{w} = (\tilde{u}_r, \tilde{u}_\theta, \tilde{u}_z, \tilde{p})$ , the problem can be rearranged as

$$\mathbf{A}(Re, \alpha, \beta)\mathbf{w} = s\mathbf{B}(Re, \alpha, \beta)\mathbf{w} \quad (4.18)$$

where, on the right-hand side, the eigenvalue  $s$  has been pointed out. Note that  $s$  is in general a complex eigenvalue, therefore, if its real part is negative then the corresponding mode is asymptotically stable. If the real part is positive, the corresponding mode is unstable, whereas if the real part is null, the corresponding mode is "critical" in the sense that the system loses its hyperbolicity and the stability of the system must necessarily be examined using nonlinear techniques. We will analyse this situation in detail by studying the nonlinear stability of our system.

## 4.2 Numerical formulation of the problem of the linear stability

In this section we show how the problem can be treated numerically. The weak formulation of the linear problem is derived and then discretized using proper basis functions [40] (p. 227-240). In particular, we will discretize the unknowns using a spectral method with Legendre polynomials as base for the construction of the unknowns  $\tilde{u}_r(r), \tilde{u}_\theta(r), \tilde{u}_z(r), \tilde{p}(r)$ . We begin by deriving the weak formulation of the problem written in the form (4.17). We first multiply the equations by  $r$  to obtain

$$\begin{aligned} & \left[ sr + i\alpha U - \frac{1}{Re} \left( \frac{d}{dr} \left( r \frac{d}{dr} \right) - \left( \frac{\alpha^2}{r} + \beta^2 r \right) \right) \right] \tilde{u}_r + \frac{1}{Re} \frac{\tilde{u}_r}{r} + \left( \frac{1}{Re} \frac{2i\alpha}{r} - 2U \right) \tilde{u}_\theta + r \frac{d\tilde{p}}{dr} = 0, \\ & \left( \frac{d}{dr} (rU) - \frac{1}{Re} \frac{2i\alpha}{r} \right) \tilde{u}_r + \left[ sr + i\alpha U - \frac{1}{re} \left( \frac{d}{dr} \left( r \frac{d}{dr} \right) - \left( \frac{\alpha^2}{r} + \beta^2 r \right) \right) \right] \tilde{u}_\theta + \frac{1}{Re} \frac{1}{r} \tilde{u}_\theta + i\alpha \tilde{p} = 0, \\ & \left[ sr + i\alpha U - \frac{1}{Re} \left( \frac{d}{dr} \left( r \frac{d}{dr} \right) - \left( \frac{\alpha^2}{r} + \beta^2 r \right) \right) \right] \tilde{u}_z + i\beta r \tilde{p} = 0, \\ & \frac{d}{dr} (r \tilde{u}_r) + i\alpha \tilde{u}_\theta + i\beta r \tilde{u}_z = 0. \end{aligned} \quad (4.19)$$

Following the procedure shown in [27], we now apply a change of variables  $r \rightarrow x$  such that  $[a, b] \rightarrow [-1, 1]$  with

$$r = E(x + c), \quad (4.20)$$

and  $c = \frac{b+a}{b-a}$ ,  $E = \frac{b-a}{2}$ . Therefore the system (4.19) becomes

$$\begin{aligned}
& -\frac{1}{Re} \frac{1}{E} \frac{d}{dx} \left( (x+c) \frac{d\tilde{u}_r}{dx} \right) + \frac{1}{Re} \left( \frac{\alpha^2+1}{E(x+c)} + \beta^2 E(x+c) \right) \tilde{u}_r + i\alpha U(x) \tilde{u}_r \\
& \quad + \left( \frac{2i\alpha}{Re E(x+c)} - 2U(x) \right) \tilde{u}_\theta + (x+c) \frac{d\tilde{p}}{dx} = -sE(x+c)\tilde{u}_r, \\
& \left( \frac{d}{dx} [(x+c)U(x)] - \frac{1}{Re} \frac{2i\alpha}{E(x+c)} \right) \tilde{u}_r - \frac{1}{Re} \frac{1}{E} \frac{d}{dx} \left( (x+c) \frac{d\tilde{u}_\theta}{dx} \right) \\
& \quad + \frac{1}{Re} \left( \frac{\alpha^2+1}{E(x+c)} + \beta^2 E(x+c) \right) \tilde{u}_\theta + i\alpha U(x) \tilde{u}_\theta + i\alpha \tilde{p} = -sE(x+c)\tilde{u}_\theta, \quad (4.21) \\
& -\frac{1}{Re} \frac{1}{E} \frac{d}{dx} \left( (x+c) \frac{d\tilde{u}_z}{dx} \right) + \frac{1}{Re} \left( \frac{\alpha^2}{E(x+c)} + \beta^2 E(x+c) \right) \tilde{u}_z \\
& \quad + i\alpha U(x) \tilde{u}_z + i\beta E(x+c) \tilde{p} = -sE(x+c)\tilde{u}_z, \\
& \frac{d}{dx} [(x+c)\tilde{u}_r] + i\alpha \tilde{u}_\theta + i\beta E(x+c) \tilde{u}_z = 0.
\end{aligned}$$

At this point, we multiply the momentum equation by a vector test function  $\tilde{\mathbf{v}}(x) = (\tilde{v}_r(x), \tilde{v}_\theta(x), \tilde{v}_z(x)) \in H_0^1([-1, 1])$  and the continuity equation by a test function  $\tilde{q}(x) \in L^2([-1, 1])$ . Then we integrate the equations along  $x$ . By applying the boundary conditions, we obtain the following system of equations

$$\begin{aligned}
& \int_{-1}^1 \frac{x+c}{Re} \frac{d\tilde{u}_r}{dx} \frac{d\tilde{v}_r}{dx} + \frac{\tilde{v}_r}{Re} \left( \frac{\alpha^2+1}{(x+c)} + \beta^2 E^2(x+c) \right) \tilde{u}_r + \tilde{v}_r i\alpha EU \tilde{u}_r \\
& \quad + \int_{-1}^1 \tilde{v}_r \left( \frac{2i\alpha}{Re(x+c)} - 2EU(x) \right) \tilde{u}_\theta - E\tilde{p} \frac{d}{dx} [(x+c)\tilde{v}_r] = - \int_{-1}^1 \tilde{v}_r sE^2(x+c) \tilde{u}_r, \\
& \tilde{v}_\theta \left[ \frac{d}{dx} [(x+c)U(x)] E - \frac{2i\alpha}{Re(x+c)} \right] \tilde{u}_r + \int_{-1}^1 \frac{x+c}{Re} \frac{d\tilde{u}_\theta}{dx} \frac{d\tilde{v}_\theta}{dx} \\
& \quad + \frac{\tilde{v}_\theta}{Re} \left( \frac{\alpha^2+1}{(x+c)} + \beta^2 E^2(x+c) \right) \tilde{u}_\theta + \int_{-1}^1 \tilde{v}_\theta i\alpha UE \tilde{u}_\theta + \int_{-1}^1 \tilde{v}_\theta i\alpha E \tilde{p} = - \int_{-1}^1 \tilde{v}_\theta sE^2(x+c) \tilde{u}_\theta, \\
& \int_{-1}^1 \frac{x+c}{Re} \frac{d\tilde{u}_z}{dx} \frac{d\tilde{v}_z}{dx} + \frac{\tilde{v}_z}{Re} \left( \frac{\alpha^2}{(x+c)} + \beta^2 E^2(x+c) \right) \tilde{u}_z + \tilde{v}_z i\alpha U E \tilde{u}_z \\
& \quad + \int_{-1}^1 \tilde{v}_z i\beta E^2(x+c) \tilde{p} = - \int_{-1}^1 \tilde{v}_z sE^2(x+c) \tilde{u}_z, \\
& \int_{-1}^1 \tilde{q} \frac{d}{dx} [(x+c)\tilde{u}_r] + \tilde{q} i\alpha \tilde{u}_\theta + \tilde{q} i\beta E(x+c) \tilde{u}_z = 0. \quad (4.22)
\end{aligned}$$

Equations (4.22) express the weak formulation of the problem related to the linear stability. In order to solve it numerically, we introduce the discrete unknowns by means of the Legendre

polynomials [28], [29]. In particular, we express the velocity components and the pressure as

$$\begin{aligned}\tilde{u}_r(x) &= \sum_{n=2}^N \hat{u}_n L_n^*(x), \\ \tilde{u}_\theta(x) &= \sum_{n=2}^N \hat{v}_n L_n^*(x), \\ \tilde{u}_z(x) &= \sum_{n=2}^N \hat{w}_n L_n^*(x), \\ \tilde{p}(x) &= \sum_{k=0}^{M=N-2} \hat{p}_k L_k^\diamond(x),\end{aligned}\tag{4.23}$$

with  $L_k^\diamond(x) = \sqrt{k + \frac{1}{2}} L_k(x)$ ,  $k \geq 0$  and

$$\begin{aligned}L_0^*(x) &= 1, \\ L_1^*(x) &= \frac{x}{\sqrt{2}}, \\ L_n^*(x) &= \frac{L_{n-2}(x) - L_n(x)}{\sqrt{2(2n-1)}}, \quad n \geq 2,\end{aligned}\tag{4.24}$$

where  $L_n(x)$ ,  $n \geq 0$  are the Legendre polynomials. In this way, as  $L_n^*(\pm 1) = 0$ ,  $n \geq 2$ , the boundary conditions of the problem are automatically satisfied. Now by substituting the expressions (4.23) into the weak formulation (4.22), the following discrete eigenvalue problem can be found

$$\mathbf{A}_d(Re, \alpha, \beta, \eta, \omega) \mathbf{w}_d = s_d \mathbf{B}_d(Re, \alpha, \beta, \eta, \omega),\tag{4.25}$$

where  $\mathbf{w}_d = (\hat{\mathbf{u}}, \hat{\mathbf{v}}, \hat{\mathbf{w}}, \hat{\mathbf{p}})$  is the eigenvector associated to the velocity modes and the pressure modes.  $s_d$  is the corresponding eigenvalue. Notice that in the discrete case, the eigenvalue problem (4.25) returns a set of discrete eigenvalues as well as discrete eigenmodes for each value of the parameters  $Re, \alpha, \beta, \eta, \omega$ . For instance  $\hat{\mathbf{u}} = (\hat{u}_2, \hat{u}_3, \dots, \hat{u}_N)$  and  $\hat{\mathbf{p}} = (\hat{p}_0, \hat{p}_1, \dots, \hat{p}_M)$ . In the same problem  $\mathbf{A}_d$  and  $\mathbf{B}_d$  represent the discrete form of the operators  $\mathcal{A}$  and  $\mathcal{B}$  referred to the continuous eigenvalue problem (4.18). As a matter of fact  $\mathbf{A}_d$  and  $\mathbf{B}_d$  are matrices whose components are given by evaluating the integrals in the weak form (4.22) for any discrete mode.

### 4.3 Linear stability analysis of an inviscid flow

We begin the study of the linear stability of the flow that develops between two rotating coaxial cylinders, under the hypothesis that the effects associated to the viscosity are negligible. From this point of view, the viscous term in the Navier-Stokes equations disappears and, as the equation (3.8) shows, the shape of the azimuthal component of the velocity can be any arbitrary function of the distance  $r$ . By neglecting the viscous term, the system of equations (3.8) reduces to

$$\begin{cases} \frac{\partial P(r,t)}{\partial r} = \frac{[u_\theta(r,t)]^2}{r}, \\ \frac{\partial u_\theta(r,t)}{\partial t} = 0. \end{cases} \quad (4.26)$$

From the second equation of the system above, we obtain that  $u_\theta = u_\theta(r)$  is a function of the radial coordinate only and the dependence on time disappears. However, we observe about the first equation that there are two unknowns in just one equation. As a consequence, the velocity field, or similarly the angular velocity field  $\Omega = u_\theta/r$ , can be arbitrarily chosen. This being said, we first present Rayleigh's criterion as a necessary and sufficient condition for the stability of a non-viscous flow. Then we apply it to the Taylor-Couette solution. Finally we show some results about the stability of an inviscid flow subject to axisymmetric and non-axisymmetric disturbances.

#### 4.3.1 Rayleigh's criterion: a necessary and sufficient condition for the stability of a circular inviscid flow

John William Rayleigh was the first who wondered if there is a condition that establishes when the flow between two rotating cylinders becomes unstable. He postulated a criterion which states that by neglecting the viscosity of the fluid, a necessary and sufficient condition for a basic flow described by an angular velocity field  $\Omega(r)$ , to be stable, is that the following inequality must be satisfied in the whole domain where the fluid is confined [4](p. 273)

$$\frac{d}{dr}(r^2\Omega(r))^2 > 0. \quad (4.27)$$

Moreover, if the quantity  $(r^2\Omega(r))^2$  decreases everywhere in its domain, then the basic flow is unstable.

This criterion however, is valid only when the disturbances are axysymmetric. In order to analyse Rayleigh's criterion, we introduce a scalar function  $\Phi$ , the "Rayleigh's discriminant", defined as

$$\Phi(r) = \frac{1}{r^3} \frac{d}{dr}(r^2\Omega(r))^2 = \frac{2}{r}\Omega(r) \frac{d}{dr}(r^2\Omega(r)). \quad (4.28)$$

Rayleigh's criterion states that  $\Phi(r) > 0, \forall r \in I$  is required for stability, where  $I$  is the interval where the radial coordinate  $r$  can vary. By applying Rayleigh's discriminant to the Taylor-Couette flow, we obtain the following function

$$\begin{aligned} \Phi(r) &= 4A \left( A + \frac{B}{r^2} \right) = \\ &4 \frac{\omega - \eta^2}{\eta(1 + \eta)} \left( \frac{\omega - \eta^2}{\eta(1 + \eta)} + \frac{\eta(1 - \omega)}{(1 - \eta)(1 - \eta^2)} \frac{1}{r^2} \right), \end{aligned} \quad (4.29)$$

where  $A$  is the constant proportional to the linear part of the T-C solution (3.19),  $B$  is the constant that multiplies the term  $\frac{1}{r}$  in equation (3.19),  $\eta = \frac{R_a}{R_b}$  is the ratio between the radii and  $\omega = \frac{\Omega_b}{\Omega_a}$  is the ratio between the angular velocities of the cylinders. Now, enforcing  $\Phi$  to be positive in the whole radial domain  $I$ , several cases can arise depending on the sign of  $\omega$ :

- for  $\omega > 0$ 
  - if  $\omega > \eta^2 \Rightarrow \Phi(r) > 0 \quad \forall r \in I$  and the flow is stable.
  - if  $\omega < \eta^2 \Rightarrow \Phi(r) < 0 \quad \forall r \in I$  and the flow is unstable.

- for  $\omega < 0$ 
  - $\Phi(r) < 0$  for  $a < r < r_0$  and the flow is unstable in this subinterval.
  - $\Phi(r) > 0$  for  $r_0 < r < b$  and the flow is stable in this subinterval.

In the case  $\omega < 0$ , the point  $r_0$  has been introduced. It defines the so called "nodal surface", that is the point which separates the stable region from the unstable region. In particular it is the point inside  $I$  such that the angular velocity field vanishes. For the Taylor–Couette flow, it is expressed as

$$r_0 = \frac{\eta}{1-\eta} \left( \frac{\omega - 1}{\omega - \eta^2} \right)^{\frac{1}{2}}, \quad \omega < 0. \quad (4.30)$$

As mentioned before, the instability is confined in the subinterval  $a < r < r_0$ , which is the region close to the inner cylinder. In the limiting case for which  $\omega \rightarrow -\infty$ , we get that  $r_0 \rightarrow \frac{\eta}{1-\eta} = a$ . Hence the unstable region becomes thinner and thinner.

For  $\omega \geq 0$ , the stable region is separated from the unstable region through the Rayleigh's line, that is represented in figure 4.1.

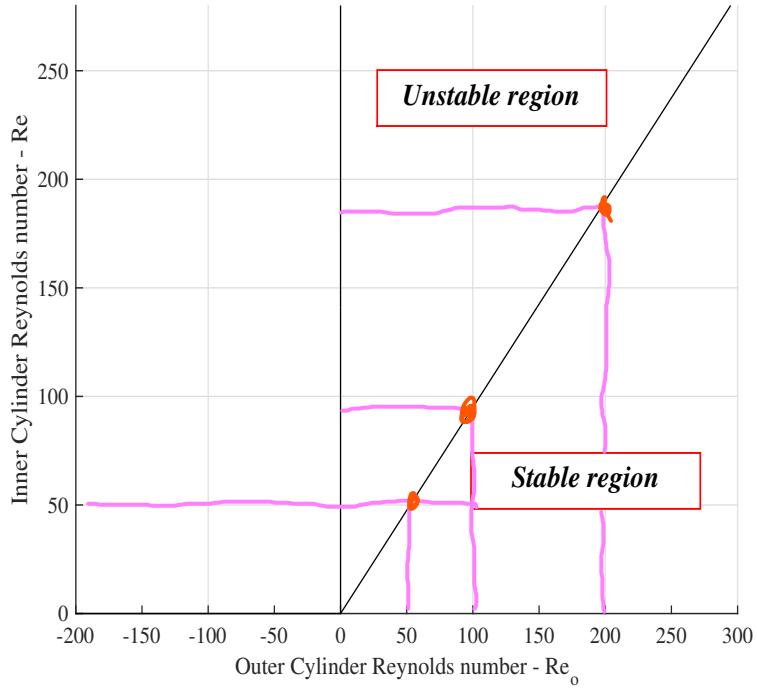


Figure 4.1: Rayleigh's line

### 4.3.2 Derivation of Rayleigh's criterion and analysis of some particular disturbances

Let us consider the equations in the form (2.11) by neglecting the viscous term, i.e. under the hypothesis that  $Re \rightarrow \infty$  as  $\nu \rightarrow 0$ . The equations in this circumstance become

$$\begin{aligned} \frac{\partial u'_r}{\partial t} + \frac{U}{r} \left( \frac{\partial u'_r}{\partial \theta} - 2u'_\theta \right) &= -\frac{\partial p'}{\partial r}, \\ \frac{\partial u'_\theta}{\partial t} + \frac{U}{r} \left( \frac{\partial u'_\theta}{\partial \theta} + u'_r \right) + u'_r \frac{dU}{dr} &= -\frac{1}{r} \frac{\partial p'}{\partial \theta}, \\ \frac{\partial u'_z}{\partial t} + \frac{U}{R} \frac{\partial u'_z}{\partial \theta} &= -\frac{\partial p'}{\partial z}, \\ \frac{1}{r} \frac{\partial}{\partial r} (ru'_r) + \frac{1}{r} \frac{\partial u'_\theta}{\partial \theta} + \frac{\partial u'_z}{\partial z} &= 0. \end{aligned} \quad (4.31)$$

Now, as  $\frac{U}{r} = \Omega(r)$ , by expressing the unknowns as travelling waves

$$\begin{aligned} u'_r(r, \theta, z) &= \tilde{u}_r(r)e^{i\alpha\theta+i\beta z+st}, \\ u'_\theta(r, \theta, z) &= \tilde{u}_\theta(r)e^{i\alpha\theta+i\beta z+st}, \\ u'_z(r, \theta, z) &= \tilde{u}_z(r)e^{i\alpha\theta+i\beta z+st}, \\ p'(r, \theta, z) &= \tilde{p}(r)e^{i\alpha\theta+i\beta z+st}, \end{aligned} \quad (4.32)$$

the system (4.31) can be written as

$$\begin{aligned} (s + i\alpha\Omega) \tilde{u}_r - 2\Omega \tilde{u}_\theta &= -\mathcal{D}\tilde{p}, \\ \left( \Omega + \frac{d(r\Omega)}{dr} \right) \tilde{u}_r + (s + i\alpha\Omega) \tilde{u}_\theta &= -\frac{i\alpha}{r} \tilde{p}, \\ (s + i\alpha\Omega) \tilde{u}_z &= -i\beta \tilde{p}, \\ \mathcal{D}_\diamond \tilde{u}_r + \frac{i\alpha}{r} \tilde{u}_\theta + i\beta \tilde{u}_z &= 0, \end{aligned} \quad (4.33)$$

where two new differential operators have been introduced to make the formulation more elegant. These operators are  $\mathcal{D} = \frac{d}{dr}$  and  $\mathcal{D}_\diamond = \frac{d}{dr} + \frac{1}{r}$ . For what concerns the boundary conditions, we have to impose homogeneous Dirichlet boundary conditions on the cylinders walls

$$\begin{aligned} \tilde{u}_r(a) &= \tilde{u}_r(b) = 0, \\ \tilde{u}_\theta(a) &= \tilde{u}_\theta(b) = 0, \\ \tilde{u}_z(a) &= \tilde{u}_z(b) = 0. \end{aligned} \quad (4.34)$$

In the following sections some results concerning the inviscid stability of the Taylor–Couette flow are presented, in particular when the disturbances are axisymmetric or not. These two conditions will be analysed in the viscous case too.

### 4.3.3 Axisymmetric disturbances

We start by considering axisymmetric disturbances, for which the governing equations (4.31) simplify a lot, as there is no dependence on the variable  $\theta$ . As the dependence on this variable is given by the term  $e^{i\alpha\theta}$ , it is sufficient to set  $\alpha = 0$  in the travelling waves formulation of the problem. The equations (4.33) therefore simplify into

$$\begin{aligned} s\tilde{u}_r - 2\Omega \tilde{u}_\theta &= -\mathcal{D}\tilde{p}, \\ \left( \Omega + \frac{d(r\Omega)}{dr} \right) \tilde{u}_r + s\tilde{u}_\theta &= 0, \\ s\tilde{u}_z &= -i\beta \tilde{p}, \\ \mathcal{D}_\diamond \tilde{u}_r + i\beta \tilde{u}_z &= 0. \end{aligned} \quad (4.35)$$

The system of equations (4.35) can be reduced to a single equation by making use of some algebra. This unique equation has only  $\tilde{u}_r$  as unknown and takes the form

$$(\mathcal{D}\mathcal{D}_\diamond - \beta^2) \tilde{u}_r - \frac{\beta^2}{s^2} \Phi(r) \tilde{u}_r = 0, \quad (4.36)$$

with boundary conditions

$$\begin{aligned} \tilde{u}_r(a) &= 0, \\ \tilde{u}_r(b) &= 0. \end{aligned} \quad (4.37)$$

By substituting the operator  $\mathcal{D}\mathcal{D}_\diamond$ , the equation (4.36) can be rewritten in the following form

$$\frac{d}{dr} \left( \frac{1}{r} \frac{d(r\tilde{u}_r)}{dr} \right) - \beta^2 \tilde{u}_r = \frac{\beta^2}{s^2} \Phi \tilde{u}_r, \quad (4.38)$$

which constitutes a generalised Sturm–Liouville eigenvalue problem, where the eigenvalue is given by  $\lambda = \frac{\beta^2}{s^2}$ . It is possible to demonstrate that the eigenvalues  $\lambda$  are all negative if  $\Phi > 0$  in the whole radial domain  $[a, b]$ ; conversely they are all positive if  $\Phi < 0$ . In addition, if  $\Phi$  changes sign in  $[a, b]$ , then there are both negative and positive eigenvalues with limit points at  $-\infty$  and  $+\infty$  [2](p. 78), [35](p. 103-108). In the axisymmetric case, if there is at least one point where  $\Phi < 0$ , then we can immediately conclude that the basic flow is unstable, whereas if the  $\Phi > 0 \forall r$ , the flow is stable (as also Rayleigh's criterion predicts). The situation, however, is not so easy for non-axisymmetric disturbances for which  $\alpha \neq 0$ , even though a generalization of Rayleigh's criterion has been derived by Billant–Gallaire [30] also for this case.

In order to confirm the validity of Rayleigh's criterion, we now show some numerical results obtained in the case of axisymmetric disturbances. The following figure shows the trend of the dispersion relation for a fixed value of the ratio between the angular velocities of the cylinders  $\omega = -1$  and under the small gap hypothesis, for which the gap between the length of the radii is small  $\eta = 0.95$ . The figure 4.2 shows the behaviour of the real part of the eigenvalues as a

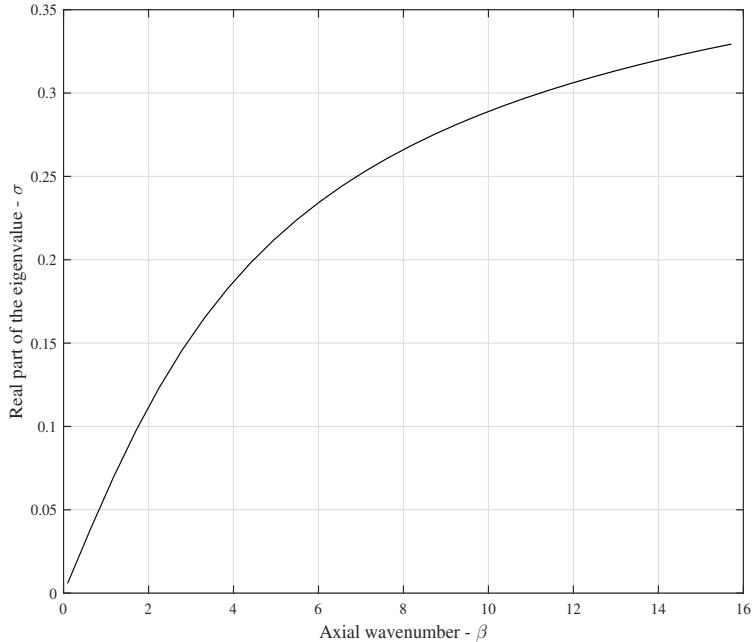
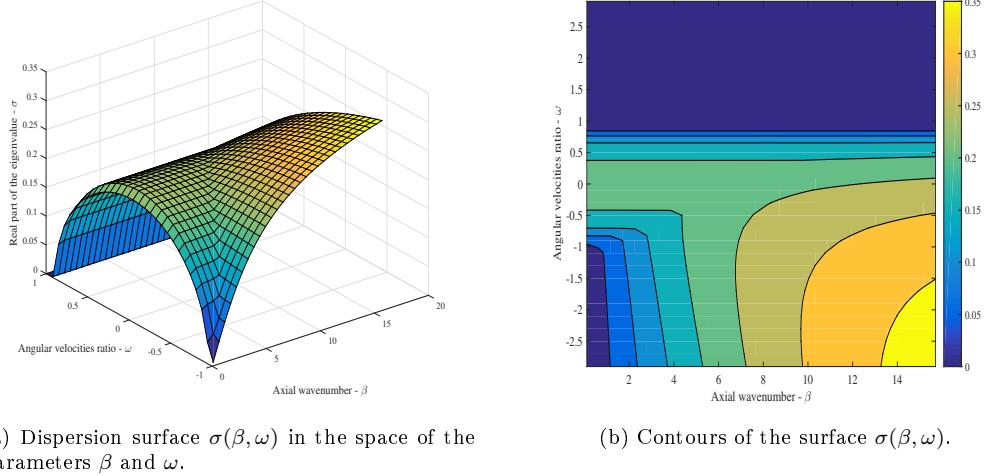


Figure 4.2: Dispersion relation  $\sigma(\beta)$  for  $\alpha = 0$ ,  $\eta = 0.95$  and  $\omega = -1$ .

function of the axial wavenumber  $\beta$ . We indicate the real part of  $s$  as  $\sigma$ . Since the values of  $\sigma$  are positive, the flow in this case is unstable. This trend is comparable to that obtained by

Chandrasekhar in his book ([4], p. 291). Figure 4.3 shows the surface given by the real part of the eigenvalues as a function of  $\beta$  and  $\omega$ , and its view on the plane  $\beta - \omega$ . From this latter trend, it is worthy to note that for positive values of  $\omega$  such that  $\omega > \eta^2 \simeq 0.90$ , the real part of the eigenvalues is null, as indeed in this case the eigenvalues are purely imaginary. On the other hand, for  $0 < \omega < \eta^2 \simeq 0.90$ , we have positive real eigenvalues, so the flow is linearly unstable, as a confirmation of Rayleigh's criterion.



(a) Dispersion surface  $\sigma(\beta, \omega)$  in the space of the parameters  $\beta$  and  $\omega$ .

(b) Contours of the surface  $\sigma(\beta, \omega)$ .

Figure 4.3: Dispersion relation  $\sigma(\beta, \omega)$  as a function of the axial wavenumber and of the ratio between the angular velocities, computed for  $\alpha = 0$ ,  $\eta = 0.95$ .

Let us now study the case when the gap between the two cylinders is not narrow, but larger. The specific value of  $\eta$  taken as example is 0.3. The results in this specific context are illustrated in figures 4.4 and 4.5. By comparing the dispersion relations at  $\omega = -1$ , it is noticeable how the growth rate in the wide gap case is higher; on the other hand the region where the instability arises is more confined than in the small gap case, figure 4.5b.

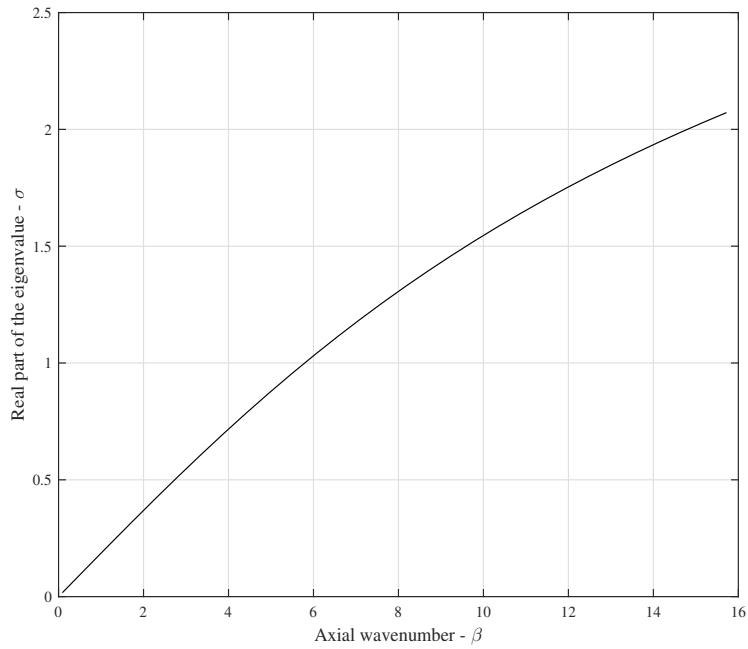


Figure 4.4: Dispersion relation  $\sigma(\beta)$  for  $\alpha = 0$ ,  $\eta = 0.3$  and  $\omega = -1$ .

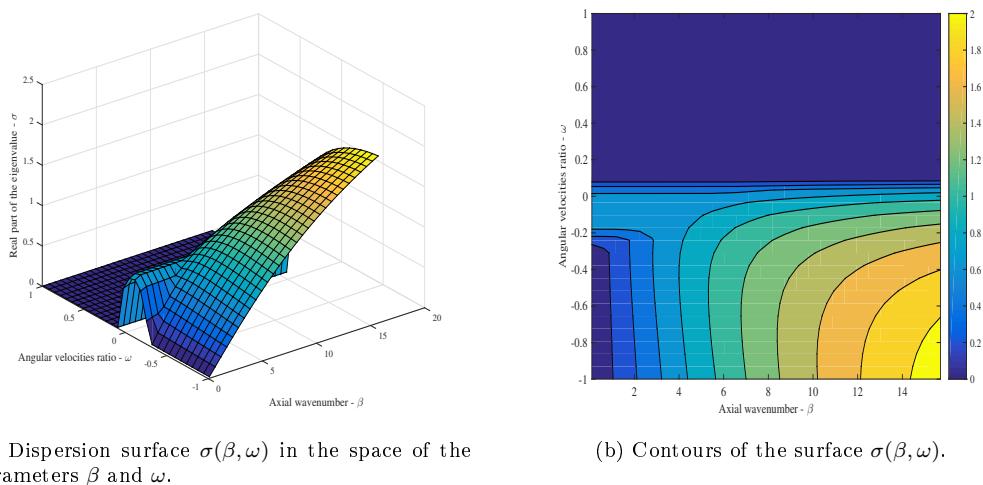


Figure 4.5: Dispersion relation  $\sigma(\beta, \omega)$  as a function of the axial wavenumber and of the ratio between the angular velocities, computed for  $\alpha = 0$ ,  $\eta = 0.3$ .

#### 4.3.4 Generic disturbances

In this section we analyse the case in which the disturbances depend on the angular variable  $\theta$ , that is when the azimuthal wave number is different from zero. The governing equations, in this case, are the general Euler equations described by the system (4.33) to which we must add the usual boundary conditions of zero velocity at the cylinder walls. As before, we first study the small gap case  $\eta = 0.95$ , and then the finite gap solution for  $\eta = 0.3$ . Figure 4.6 shows the dispersion relation computed at  $\eta = 0.95$ ,  $\omega = -1$ ,  $\alpha = 1$ .

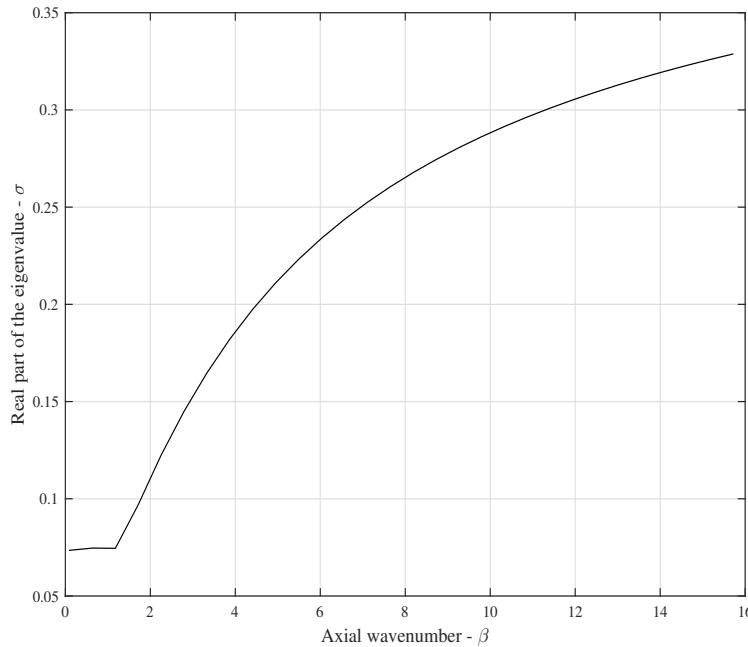


Figure 4.6: Dispersion relation  $\sigma(\beta)$  for  $\alpha = 1$ ,  $\eta = 0.95$  and  $\omega = -1$ .

As previously done, in figure 4.7 we show the results in terms of dispersion surface relatively to the real part of the eigenvalues. As can be seen by comparing the dispersion relations, they are very similar except for wave numbers close to zero, where the curve at  $\alpha = 1$  reaches an asymptotic constant value, while the curve at  $\alpha = 0$  tends to zero. Moreover, by looking at the figure 4.7, the purple region which indicates stability is very small. Indeed only for  $\omega > 0.90$  all modes are asymptotically stable. In all the other cases, there will be at least one unstable mode.

We now pass to the case with  $\eta = 0.3$ . The dispersion relation is given in figure 4.8. The surface  $\sigma(\beta, \omega)$  is shown in figure 4.9. In this case, the dispersion surface has an extended stable region (purple region) compared to the previous case ( $\alpha = 1, \eta = 0.95$ ). Furthermore, at  $\omega = -1$ , the eigenvalues grow very quickly as function of the axial wavenumber. As it can be seen by comparing the graphs for the two different values of  $\eta$  in the non-axisymmetric case, when the gap is very small, the dispersion curves and the dispersion surfaces are more regular than when the gap is fixed at  $\eta = 0.3$ . This fact can be traced back to the analytical form describing the Taylor–Couette flow. Indeed, by making use of an asymptotic analysis, the expression for the Taylor–Couette velocity can be reduced to a linear function of the radial coordinate. In addition, in the small gap case, the operator  $\mathcal{DD}_\diamond$  can be approximated by  $\mathcal{D}^2$ . In contrast when the gap is not small, these approximations are no longer valid and the nonlinear terms that are present both in the expression of the Taylor–Couette velocity field and in the definition of the operator  $\mathcal{DD}_\diamond = \frac{d^2}{dr^2} + \frac{1}{r} \frac{d}{dr} - \frac{1}{r^2}$ , play a significant role in the governing equations.

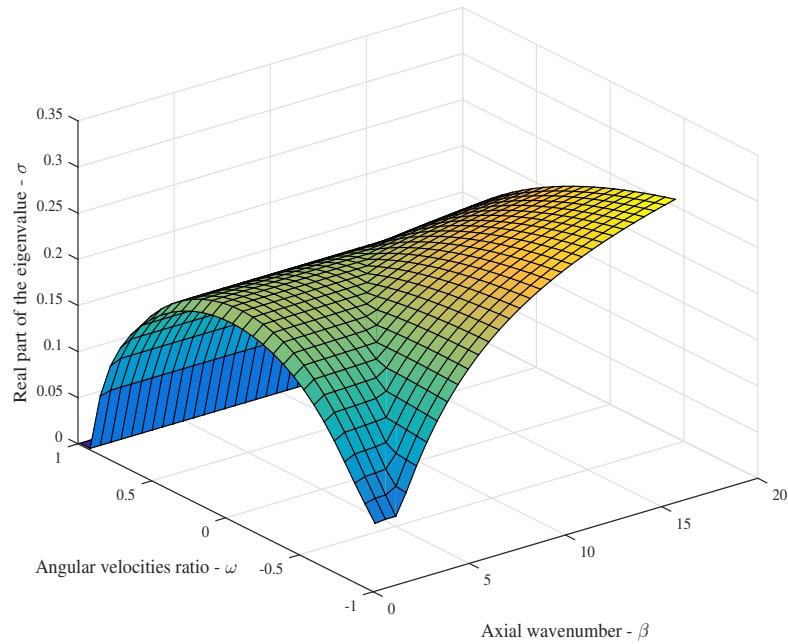
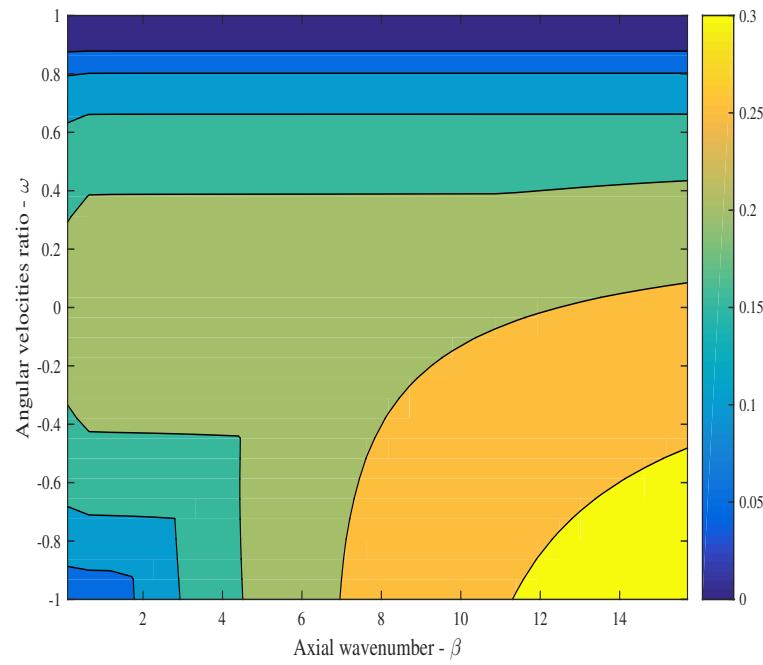
(a) Dispersion surface  $\sigma(\beta, \omega)$  in the space of the parameters  $\beta$  and  $\omega$ .(b) Contours of the surface  $\sigma(\beta, \omega)$ .

Figure 4.7: Dispersion relation  $\sigma(\beta, \omega)$  as a function of the axial wavenumber and of the ratio between the angular velocities, computed for  $\alpha = 1$ ,  $\eta = 0.95$ .

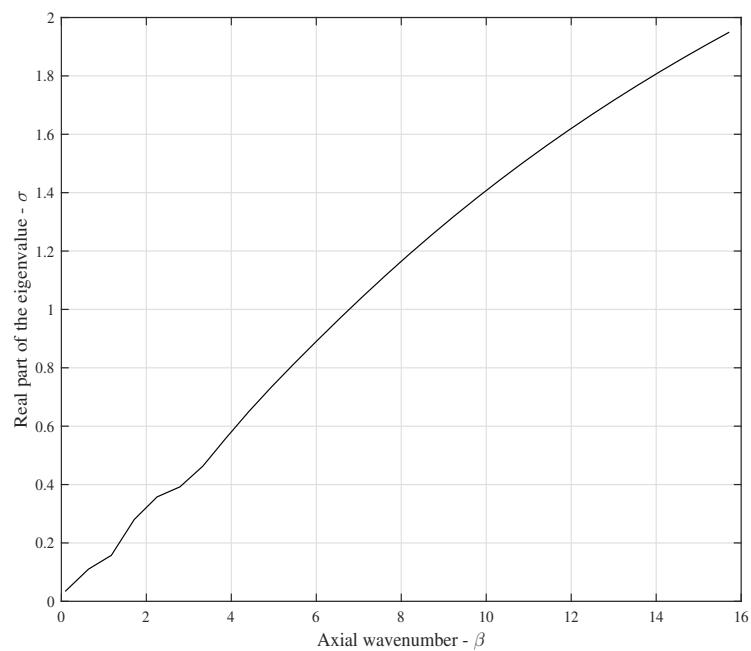


Figure 4.8: Dispersion relation  $\sigma(\beta)$  for  $\alpha = 1$ ,  $\eta = 0.3$  and  $\omega = -1$ .

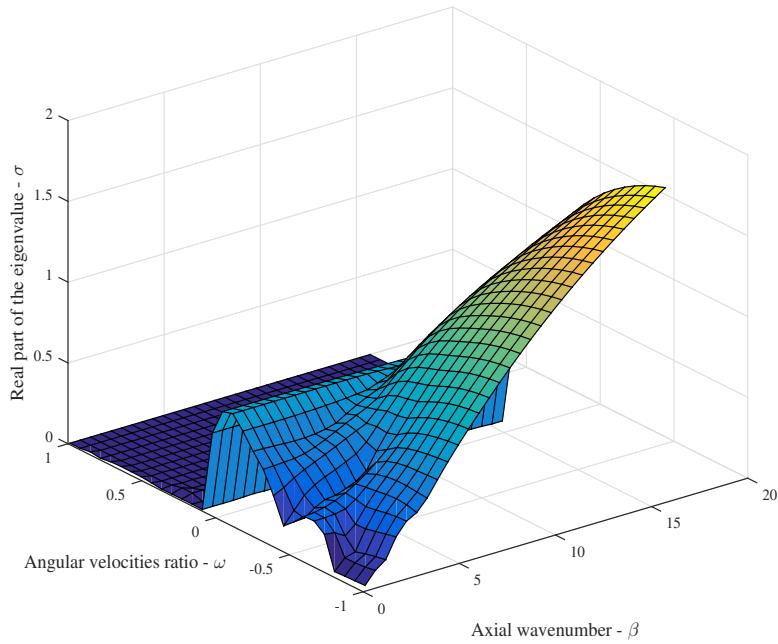
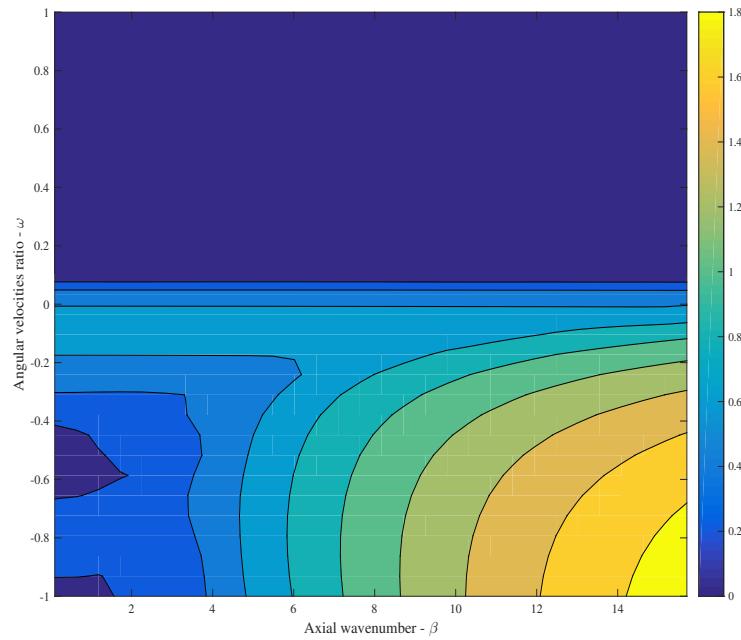
(a) Dispersion surface  $\sigma(\beta, \omega)$  in the space of the parameters  $\beta$  and  $\omega$ .(b) Contours of the surface  $\sigma(\beta, \omega)$ .

Figure 4.9: Dispersion relation  $\sigma(\beta, \omega)$  as a function of the axial wavenumber and of the ratio between the angular velocities, computed for  $\alpha = 1$ ,  $\eta = 0.3$ .

## 4.4 Linear stability analysis of a viscous flow

In the present section, we want to study the linear stability associated to the Taylor–Couette flow, in the real case when the effects of the viscosity are taken into account. The equations that govern the problem have been already derived in paragraph 4.1 and are rewritten here for the reader's convenience.

$$\begin{aligned} & \left[ s + i\alpha \frac{U}{r} - \frac{1}{Re} \left( \mathcal{D}^2 - \frac{1}{r^2} \right) \right] \tilde{u}_r + \left( \frac{2i\alpha}{Re r^2} - 2 \frac{U}{r} \right) \tilde{u}_\theta + \frac{d\tilde{p}}{dr} = 0, \\ & \left( \frac{U}{r} + U' - \frac{2i\alpha}{Re r^2} \right) \tilde{u}_r + \left[ s + i\alpha \frac{U}{r} - \frac{1}{Re} \left( \mathcal{D}^2 - \frac{1}{r^2} \right) \right] \tilde{u}_\theta + \frac{i\alpha}{r} \tilde{p} = 0, \\ & \left( s + i\alpha \frac{U}{r} - \frac{\mathcal{D}^2}{Re} \right) \tilde{u}_z + i\beta \tilde{p} = 0, \\ & \mathcal{D} \tilde{u}_r + \frac{i\alpha}{r} \tilde{u}_\theta + i\beta \tilde{u}_z = 0. \end{aligned} \quad (4.39)$$

We remind that by deriving these equations, the hypothesis of considering travelling waves solutions, both for the velocity and the pressure, has been introduced. We also remind that the function  $U(r)$  represents the Taylor–Couette basic flow. The system above, as discussed in paragraph 4.1, produces an eigenvalue problem, which can be written in the form

$$\mathcal{A}(Re, \alpha, \beta, \eta, \omega) \mathbf{w}(r) = s \mathcal{B}(Re, \alpha, \beta, \eta, \omega) \mathbf{w}(r), \quad (4.40)$$

or equivalently, by introducing the linear operator  $\mathcal{L}(Re, \alpha, \beta, \eta, \omega) = \mathcal{A}(Re, \alpha, \beta, \eta, \omega) - s \mathcal{B}(Re, \alpha, \beta, \eta, \omega)$ , in the homogeneous form

$$\mathcal{L}(Re, \alpha, \beta, \eta, \omega, s) \mathbf{w}(r) = 0. \quad (4.41)$$

From equation (4.41) the dispersion relation  $s = s(\alpha, \beta, Re, \eta, \omega)$  can be derived which represents a hypersurface in the parameters space  $[\alpha, \beta, Re, \eta, \omega]$ . Note how the dependency on the two parameters  $\eta$  and  $\omega$  is hidden inside the expression of the Taylor–Couette solution. From this scenario, it follows that in general, at each value of the parameters, i.e. at each point of the hypersurface, there is a new eigenvalue problem to be solved. It is known from the literature that the first instability of the Taylor–Couette flow leads to the appearance of two possible secondary flows: the first one is known as "Taylor vortices", whereas the second one is known as "Spiral vortices". The former derives from a steady state bifurcation and is composed of counter rotating vortices whose size propagates unchanged along the azimuthal direction, forming a toroidal surface around the inner cylinder. The latter instead comes from a Hopf bifurcation and its structure is made of vortices that roll up, like spirals around the cylinders. By considering the Fourier series expansion of the complete solution, in the case of Taylor vortices, the first modes of the disturbances which become unstable are the axisymmetric ones, for which  $\alpha = 0$ . As we will show in the paragraph, Taylor vortices exist for positive, null and at least small negative values of  $\omega$ . On the contrary, if the value of  $\omega$  becomes negatively large enough, the Taylor–Couette flow will become linearly unstable by forming spiral vortices as the first instability. It can be demonstrated that spiral vortices are generated necessarily by non-axisymmetric disturbances; in particular, the higher the value of the modulus of  $\omega$ , the higher the value of  $\alpha$  that makes the Taylor–Couette solution unstable.

### 4.4.1 Taylor vortices

We have said that Taylor vortices (TV), represent the flow that arises from a bifurcation of the Taylor–Couette basic solution when  $\alpha = 0$ . Taylor vortices emerge when the ratio between the angular velocities of the two cylinders is positive, null or slightly negative up to a threshold value, figure (4.10). In addition also the works made by G.I. Taylor [9], Chossat-Ioos [3], C.D.Andereck - S.S.Liu - H.L.Swinney [8], J.Sánchez - D.Crespo - F.Marquès [12], R.C.DiPrima - P.M.Eagles [7], show that the axisymmetric modes are the first to become unstable starting from the steady equilibrium solution of the Taylor–Couette flow. Along the neutral curve that

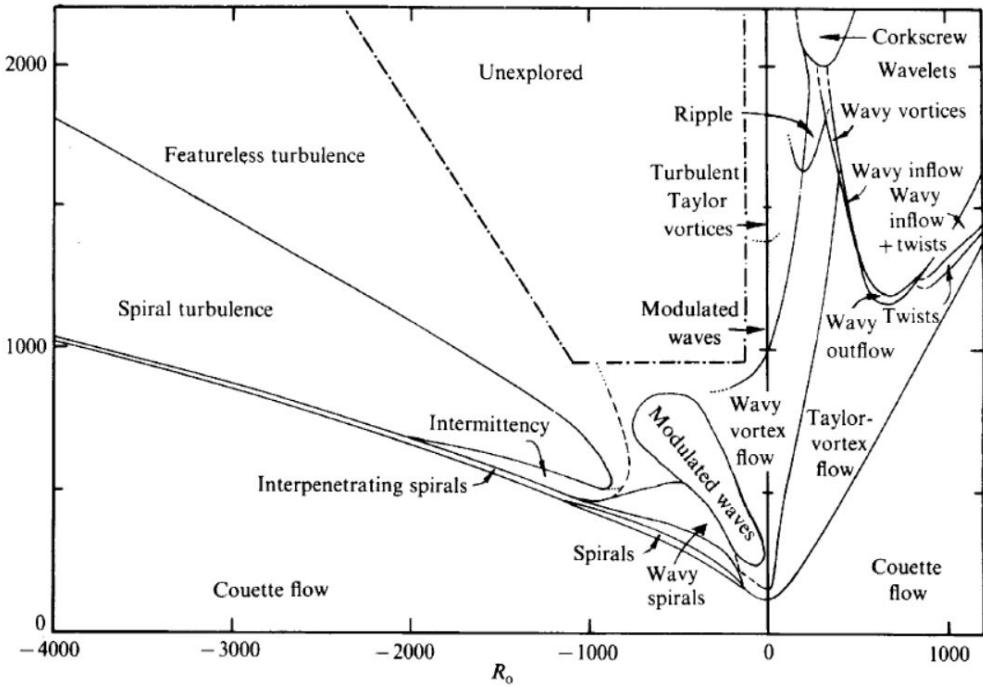


Figure 4.10: Complete bifurcation diagram for the basic Taylor–Couette flow [8].

causes the development of the vortices as a bifurcation of the T–C flow, the marginally stable modes are real, i.e.  $s = 0$  with  $s \in \mathbb{R}$ . It follows that Taylor vortices are a stationary bifurcation of the basic flow. By studying the eigenvalue problem for  $\alpha = 0$ , for different values of  $\eta$  and  $\omega$  we get different neutral curves in the space of the parameters; in the plane described by the Reynolds number and the axial wave number, two of these dispersion relations obtained are given. The curves are plotted in figure (4.11). We will analyze more in detail these two particular situations, assuming that the outer cylinder is at rest, while the inner cylinder rotates at a positive angular velocity. The first case analyzed is when the ratio of the radii tends to unity, while the second case refers to the wide gap case.

As it is possible to underline from figure 4.11) as the ratio between the radii increases, the critical Reynolds number grows very quickly, whereas the critical wavenumber becomes lower. We now presents some results concerning the study of the formation of the vortices starting from the small gap case, for which we take  $\eta = 0.95$ . The neutral curve in the plane  $Re - \beta$  is shown in figure 4.12: the critical point, i.e. the point at which the curve has its minimum, is found to be  $(\beta_c, Re_c) = (3.13, 185)$  and it is in agreement with the critical point obtained by DiPrima-Eagles [7]. The curve also highlights that above the critical value of the Reynolds number, there is always a band of axial wave numbers such that the Taylor–Couette flow is linearly unstable.

For a more general description of how the instability can be interpreted geometrically, in figure 4.13, we show the surface dispersion relation as function of the Reynolds number and of the axial wavenumber. In this figure, also the critical point and its neighbourhood has been plotted as there, a weakly nonlinear expansion will be performed when dealing with the nonlinear stability. At the critical point, the behaviour of the real part of the eigenvalue function is seen in figure 4.14 and in figure 4.15. In particular, from the latter, it is evident how, beyond the critical Reynolds number, there is a bandwidth of axial wavenumbers such that the real part of the eigenvalues becomes positive, leading the basic flow to instability.

We now analyse the situation of loss of stability, introducing a new variable in the space of the parameters, that is the Reynolds number associated to the outer cylinder denoted with  $Re_o$ . The dispersion relation, now in the  $Re - Re_o$  plane, is given in figure 4.16 and it is computed

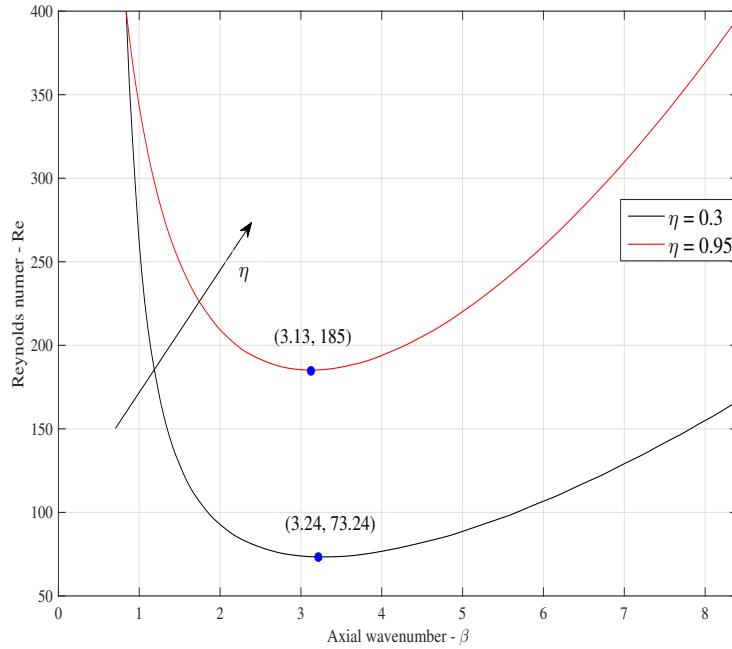


Figure 4.11: Neutral curves in the plane  $Re - \beta$  computed for  $\alpha = 0$ ,  $\omega = 0$  and for two different values of  $\eta$ . The red curve shows the neutral curve for  $\eta = 0.95$ . The black curve shows the neutral curve for  $\eta = 0.3$ . The critical points in the two cases are shown with a blue dot.

at  $\beta = \beta_c$ . As a comparison with the corresponding inviscid case, the Rayleigh's line has been plotted too. By looking for the minimum of this neutral curve, we find out that the critical point is at  $(Re_o, Re) = (0, 185)$ . Another comment that emerges from figure 4.16 is that the neutral curve in the viscous case is quite distant from Rayleigh's line and the viscous flow is much more stable than the corresponding inviscid flow. Only for high Reynolds numbers, the viscous curve tend to reach the asymptotic behaviour and lie on the Rayleigh's line. As we will show, this fact is not so evident instead by decreasing the ratio  $\eta$ . For instance, with  $\eta = 0.3$  and  $\beta = \beta_c$ , the marginal stability curve in the plane  $Re - Re_o$  is nearer the Rayleigh's line still at low Reynolds numbers. Anyway we will come back to this topic in the next paragraph. Continuing the analysis of the Taylor vortices in the small gap case and with fixed external cylinder, we now show the pattern of these vortices in figure 4.17a. This figure represents the streamlines of the vortices generated as the Taylor–Couette flow bifurcates. As it can be seen, TV are counter rotating vortices, whose size is a half of the critical wavelength. The last thing we illustrate, is the trend of the velocity components related to the marginally stable mode, along the scaled radial coordinate  $x = -c + E/r$ , where  $c = \frac{b+a}{b-a}$  and  $E = \frac{b-a}{2}$ . From this change of variables, we have that the interval of variation of  $x$  is  $[-1, 1]$ . Having defined this new variable, the behaviour of the velocity components are shown in figure 4.17b for the real part of the eigenmode and in figure 4.17c for the imaginary part of the eigenmode. As it can be seen, the radial and azimuthal components,  $\tilde{u}_r, \tilde{u}_\theta$ , are real marginally stable eigenfunctions. The axial component  $\tilde{u}_z$  instead is a purely imaginary marginally stable eigenfunction. Looking at the figure 4.17b, the most amplified mode is in the azimuthal direction (red curve).

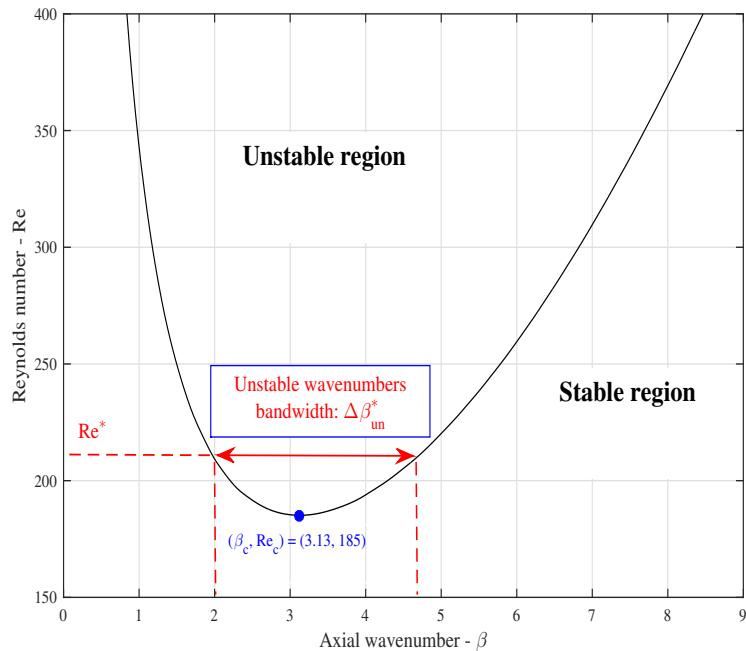


Figure 4.12: Neutral curve  $Re(\beta)$  for  $\alpha = 0$ ,  $\omega = 0$ ,  $\eta = 0.95$ .

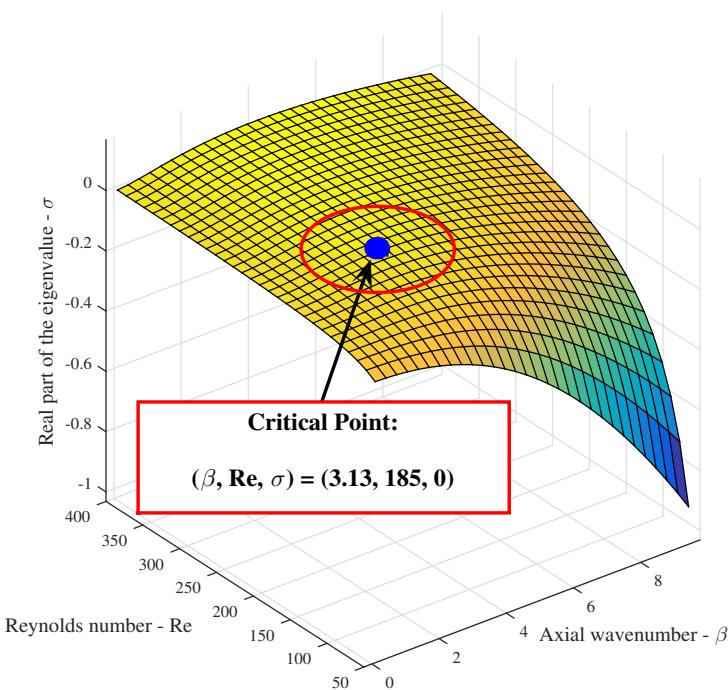


Figure 4.13: Dispersion surface  $\sigma(\beta, Re)$  for  $\alpha = 0$ ,  $\omega = 0$ ,  $\eta = 0.95$ . The figure also emphasizes the character of the dispersion relation close to the critical point.

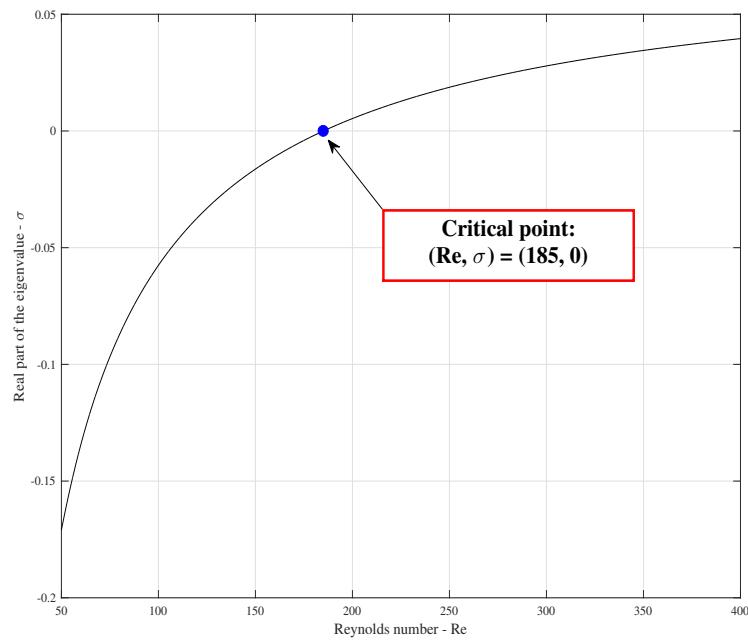


Figure 4.14: Dispersion relation curve  $\sigma(Re)$  computed at  $\beta = \beta_c$ ,  $\alpha = 0$ ,  $\omega = 0$ ,  $\eta = 0.95$ .

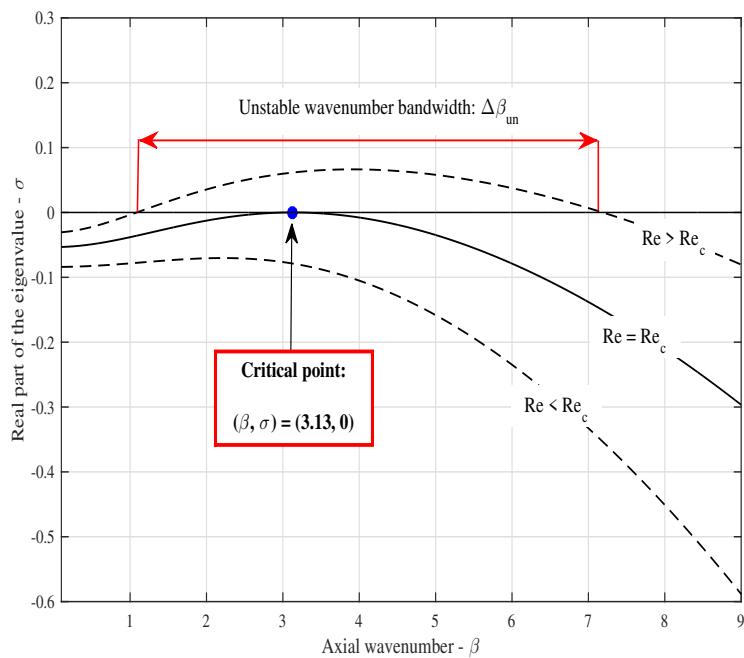


Figure 4.15: Dispersion relation curves  $\sigma(\beta)$  for different values of the Reynolds number. The curves are computed for  $\alpha = 0$ ,  $\omega = 0$ ,  $\eta = 0.95$ .

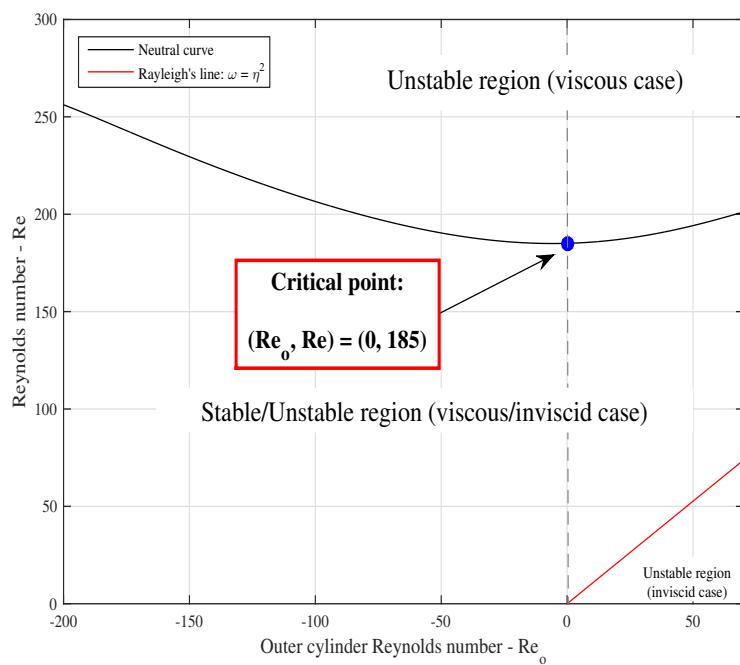


Figure 4.16: Neutral curve in the plane  $Re - Re_o$  computed at the critical value of the axial wavenumber  $\beta = \beta_c = 3.13$  and for  $\alpha = 0$ ,  $\eta = 0.95$ .

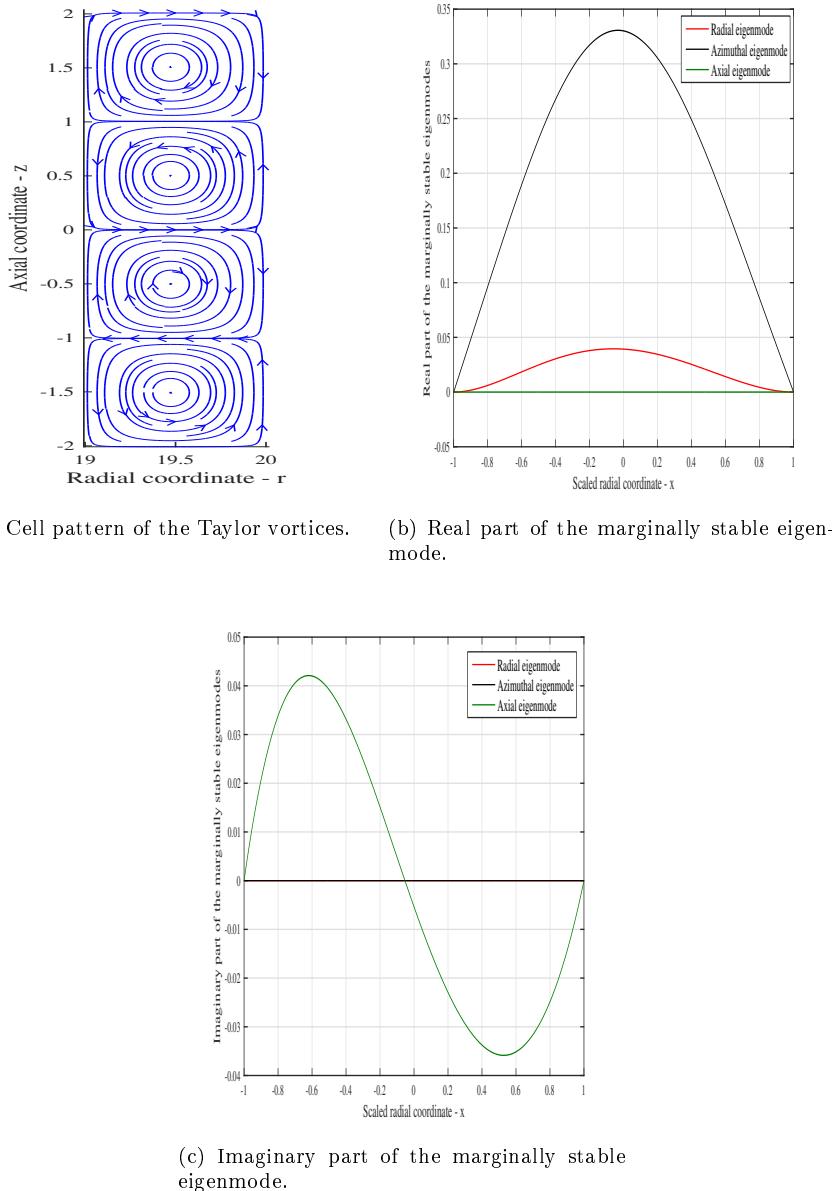


Figure 4.17: Structure of the Taylor vortices in the case  $\alpha = 0$ ,  $\omega = 0$ ,  $\eta = 0.95$ ,  $Re = Re_c = 185$ ,  $\beta = \beta_c = 3.13$ .

Now we begin the analysis of the perturbation response to axisymmetric disturbances, under the assumption that the gap is not small anymore, but it assumes values near the unity, or equivalently under the assumption that  $\eta \rightarrow 0$ . As seen by figure 4.11, the critical point in the plane  $Re - \beta$ , translates downwards and backwards as long as the ratio of the cylinders radii becomes lower. In the case, for  $\eta = 0.3$  and  $\omega = 0$  the dispersion relation is represented by the two curves 4.18 and 4.19. In the former we have the relationship that links the Reynolds number to the axial wave number, and we obtain a critical point  $(Re_c, \beta_c) = (73.24, 3.24)$ . In the plane  $Re_o - Re$  instead, the critical point is  $(Re_o, Re) = (-15.20, 68.87)$ .

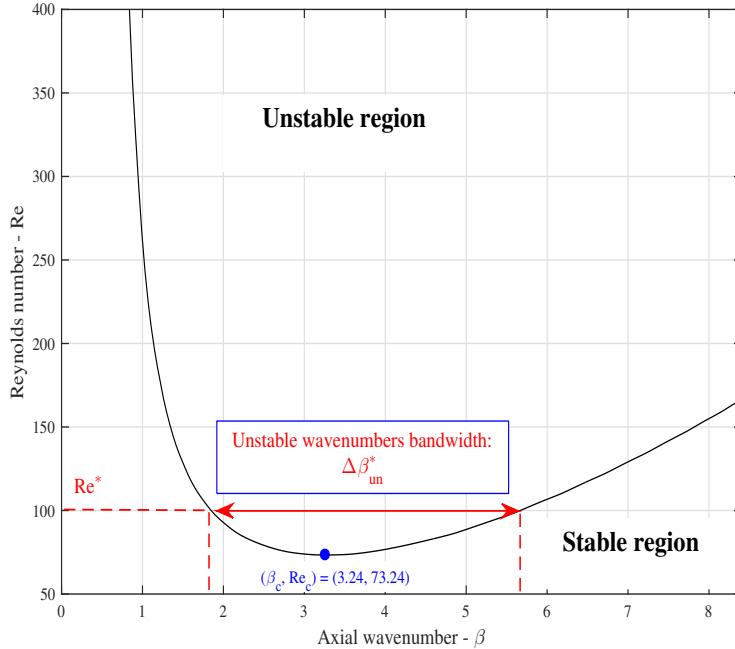


Figure 4.18: Neutral curve  $Re(\beta)$  for  $\alpha = 0$ ,  $\omega = 0$ ,  $\eta = 0.3$

By comparing the neutral curves in the  $\beta - Re$  diagram for the narrow gap case and the wide gap case, it is remarkable that the bandwidth of the unstable modes is much larger in the wide gap case because the curve tends to have a less steep growth rate for large wavenumbers. About the neutral curve in the  $Re_o - Re$  plane, it is appreciable how the neutral curve is much closer to Rayleigh's line in the wide gap situation, in contrast to the narrow gap case. Moreover, at the critical wavenumber for the wide gap case considered, the critical point is found for a negative value of the outer cylinder Reynolds number, that is when the cylinders rotate in opposite directions. The dispersion relation at the critical point  $(\beta_c, Re_c)$  is shown in figure 4.20.

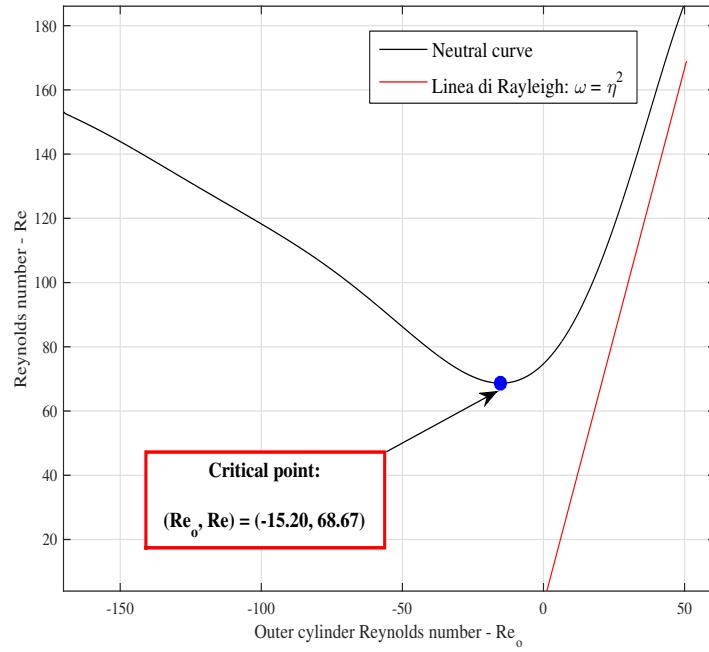
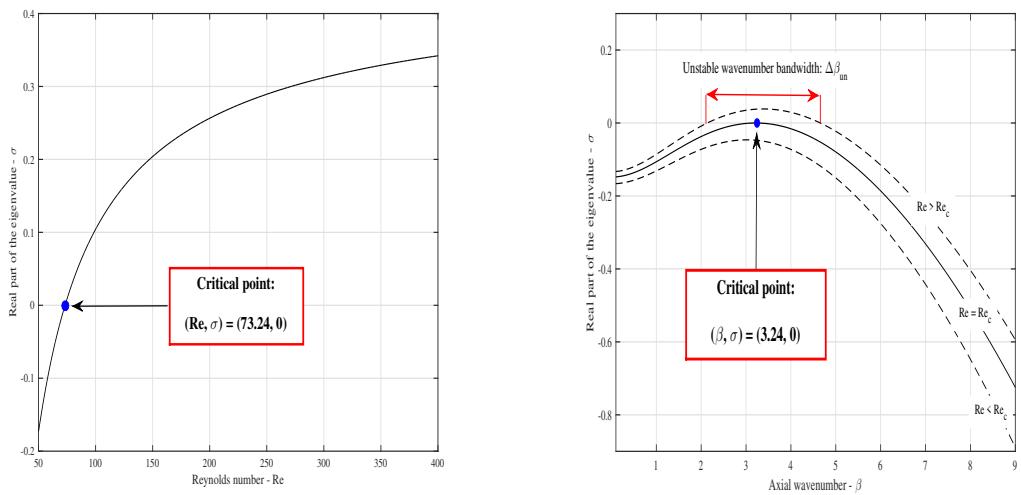


Figure 4.19: Neutral curve in the plane  $Re_o - Re$  computed at the critical axial wavenumber  $\beta = \beta_c = 3.24$  and for  $\alpha = 0$ ,  $\eta = 0.3$



(a) Dispersion relation curve  $\sigma(Re)$  computed at  $\beta = \beta_c$ ,  $\alpha = 0$ ,  $\eta = 0.3$ .

(b) Dispersion relation curve  $\sigma(\beta)$  computed at  $Re = Re_c$ ,  $\alpha = 0$ ,  $\omega = 0$ ,  $\eta = 0.3$ .

Figure 4.20: Dispersion relation curves in the wide gap case  $\eta = 0.3$ . The curves are computed also for  $\alpha = 0$ ,  $\omega = 0$ .

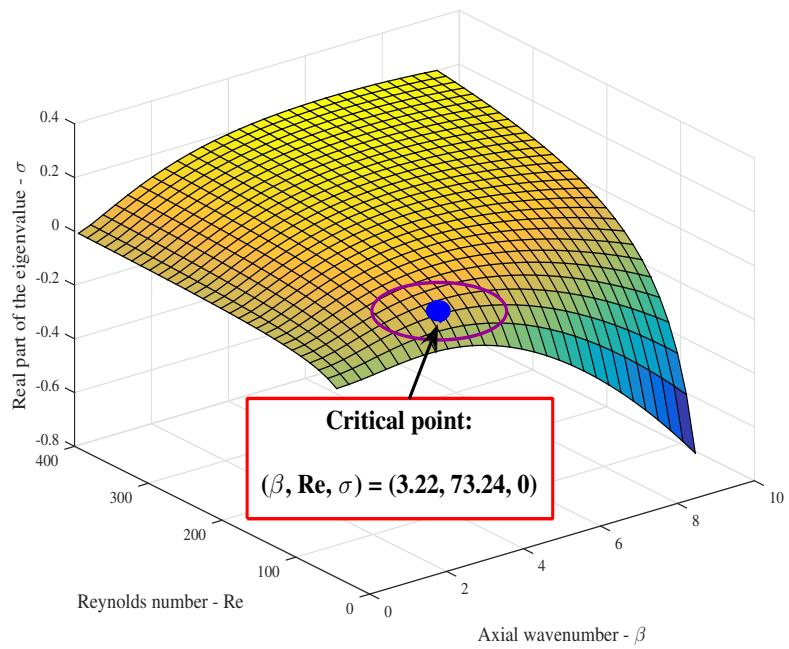


Figure 4.21: Dispersion surface  $\sigma(\beta, Re)$  computed for  $\alpha = 0$ ,  $\omega = 0$  and  $\eta = 0.3$ . The figure emphasizes the character of the dispersion relation in the neighbourhood of the critical point.

For what concerns the structure of the Taylor vortices, they are shown in figure 4.22a together with the trend of the velocity components along the scaled radial coordinate  $x$ . Two

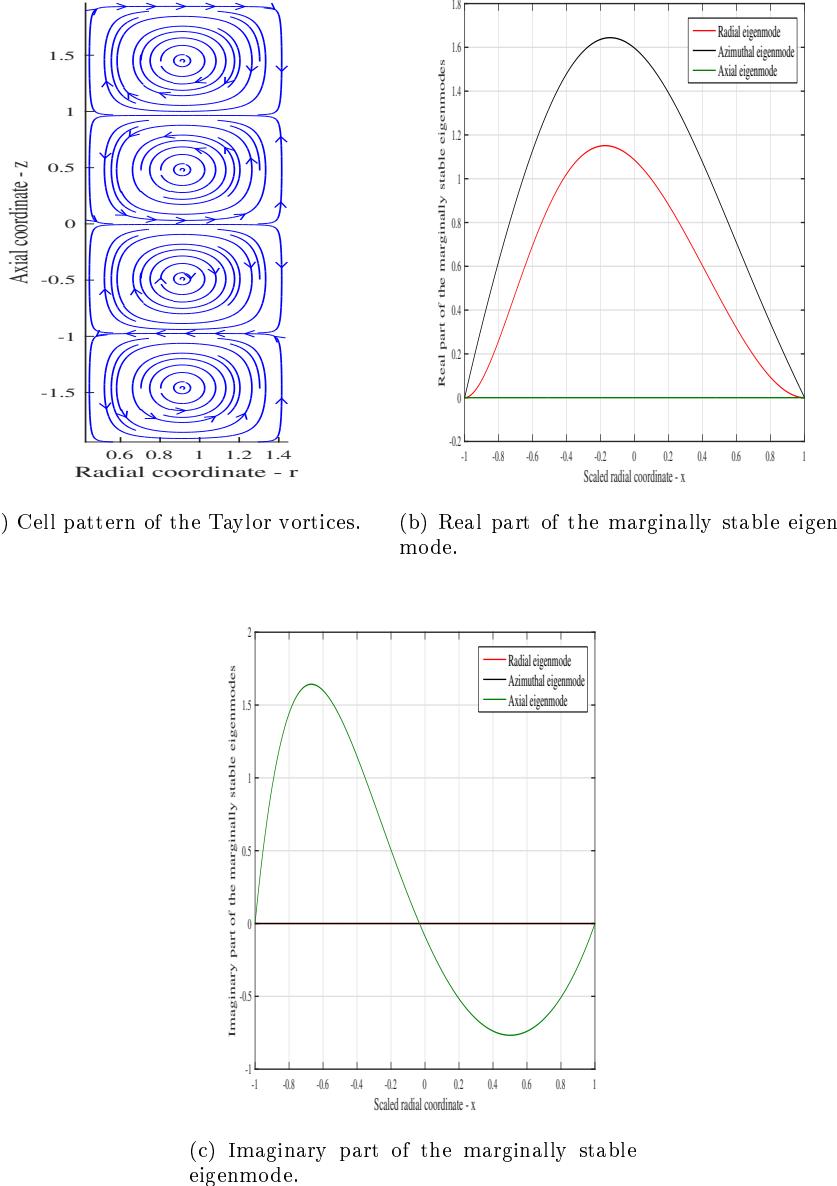


Figure 4.22: Structure of the Taylor vortices in the case  $\alpha = 0$ ,  $\omega = 0$ ,  $\eta = 0.3$ ,  $Re = Re_c = 73.24$ ,  $\beta = \beta_c = 3.24$ .

main comments can be made comparing figure 4.22 with figure 4.17. The first is about the size of the vortices in the two cases. In particular, as the ratio of the radii is decreased, the wavelength of the flow is decreased too since the critical mode in the wide gap case is higher than the one in the small gap case. Hence, the vortices in the finite gap situation are less extended in the axial direction than in the radial direction. As a second comment it can be observed that the behaviour of the velocity components is very different in the two cases. In the narrow gap case, the profiles are symmetric with respect to the vertical axis at  $x = 0$  with a dominant component along the azimuthal direction. In the wide gap case instead, they are no more symmetric and the order of magnitude of the three components is the same.

#### 4.4.2 Spiral vortices

We study now the other type of flow that arises from the first linear instability of the Taylor–Couette flow: the spiral-vortex flow. As the name may suggest, this flow is composed of travelling waves, both in the azimuthal and in the axial direction, which propagate periodically in time. This kind of instability is caused by a Hopf bifurcation, since the eigenvalues associated to the marginally stable mode are complex conjugates each with multiplicity two due to symmetry reasons. As a matter of fact, owing to the multiplicity of the eigenvalues, and ultimately to symmetry, we obtain waves that propagate downwards, called right handed spirals (R-SPI), and waves that propagate upwards, called left handed spirals (L-SPI). The kind of spiral that is observed experimentally actually, depends on the initial condition of the problem and on the set of parameters. An example of left-handed spirals is given in figure 4.23a and compared with the pattern formed by a Taylor vortex flow. In the case of the spiral vortices, the whirling structure rolls around the cylinders. In the following we will analyse only travelling waves which

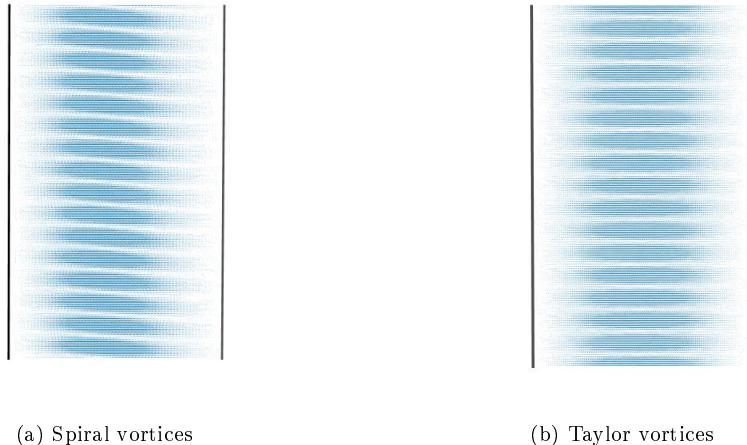
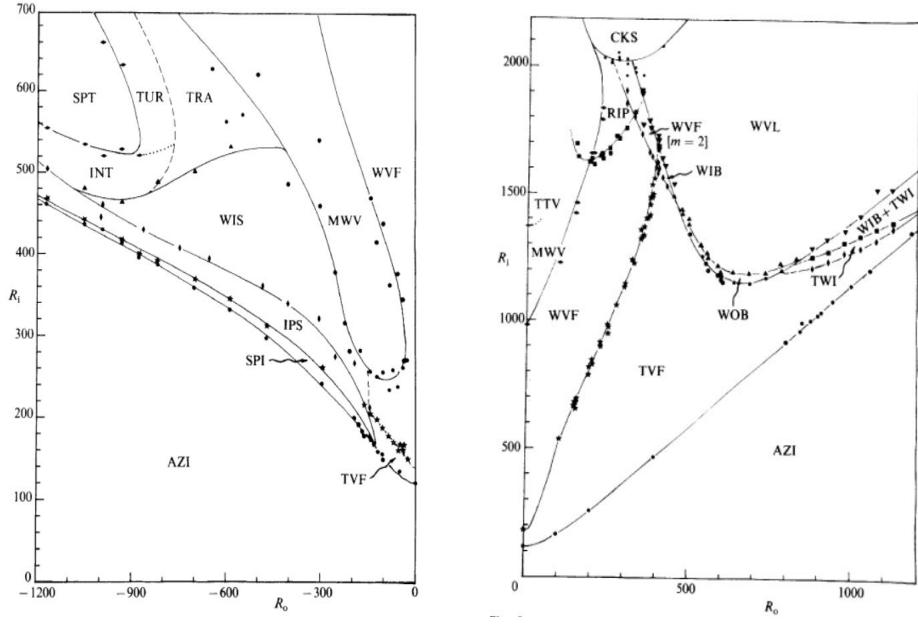


Figure 4.23: Visualization of the patterns around the Cylinders: Spiral vortices 4.23a; Taylor vortices 4.23b

propagate in the sense of the positive  $z$  axis. As shown in figure 4.24a and in figure 4.24b, taken from the works of Chossat–Ioos [3] and Andereck [8], spiral vortices are generated only when the two cylinders rotate in opposite directions. Unlike Taylor vortices, which persist for a large variation both in the Reynolds number and in the values of  $\omega$ , spiral vortices tend to disappear very soon, letting the formation of more and more complicated flows that soon become turbulent: interpenetrating spirals (IPS), turbulent spots (INT), spiral turbulence (SPT).

Spiral vortices are inherently a non-axisymmetric bifurcation solution. Indeed it can be observed that for negative values of  $\omega$  beyond a certain threshold, the first mode which becomes unstable is no longer axisymmetric. As an example, by looking for the neutral curves at a fixed negative value of  $\omega$  and letting the azimuthal wavenumber vary, it can be seen in figure 4.25 that the first unstable mode arises for  $\alpha = 3$ . All the other modes are represented by curves that are above the neutral curve for  $\alpha = 3$ . Although the mode with  $\alpha = 3$  is the most unstable, all the modes are very close one another. Therefore, as soon as the Reynolds number increases, other non-axysymmetric modes become immediately unstable.



(a) Bifurcating solutions for negative values of the ratio of the angular velocities of the cylinders [8]

(b) Bifurcating solutions for positive values of the ratio of the angular velocities of the cylinders [8]

Figure 4.24: Bifurcations of the Taylor–Couette basic flow. The chart shows the bifurcations that occur for negative values of  $\omega$ , 4.24a, and the bifurcations that occur for positive values of  $\omega$ , 4.24b.

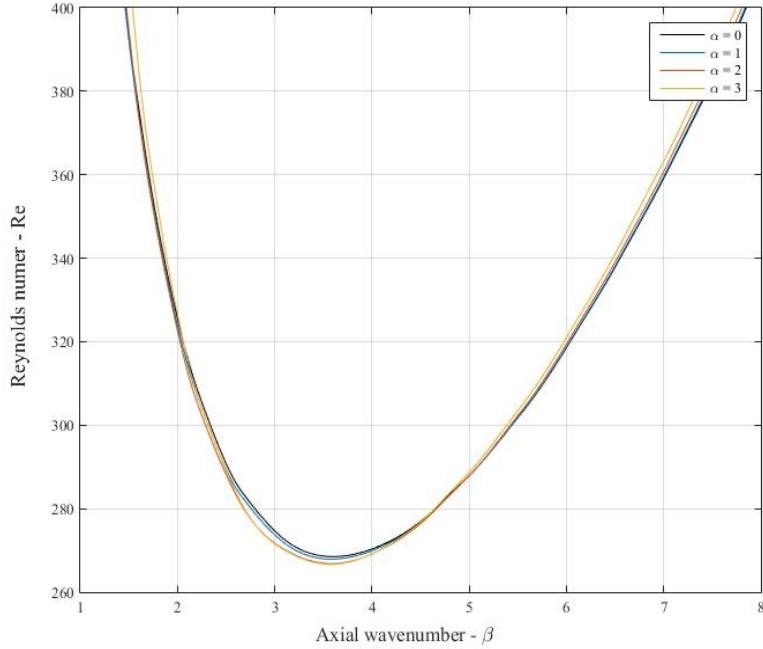


Figure 4.25: Comparison of neutral curves in the plane  $\beta - Re$  at  $\eta = 0.95$  and  $\omega = -0.8$  for different values of  $\alpha$

To conclude the view of our results about spiral vortices, in figure 4.26a the streamlines of a typical pattern arising from this kind of bifurcating solution are shown. The pattern is computed by taking the following values of the parameters:  $\alpha = 3, \omega = -0.8, \eta = 0.95, Re_c = 266.3, \beta_c = 3.56$ . These data are very close to those obtained by Chossat-Ioos in their book [3](p. 49, 52). The streamlines are displayed in the cross section for  $\theta = 0$  and the eigenmodes plotted as a function of  $x$ , figures 4.26b, 4.26c.

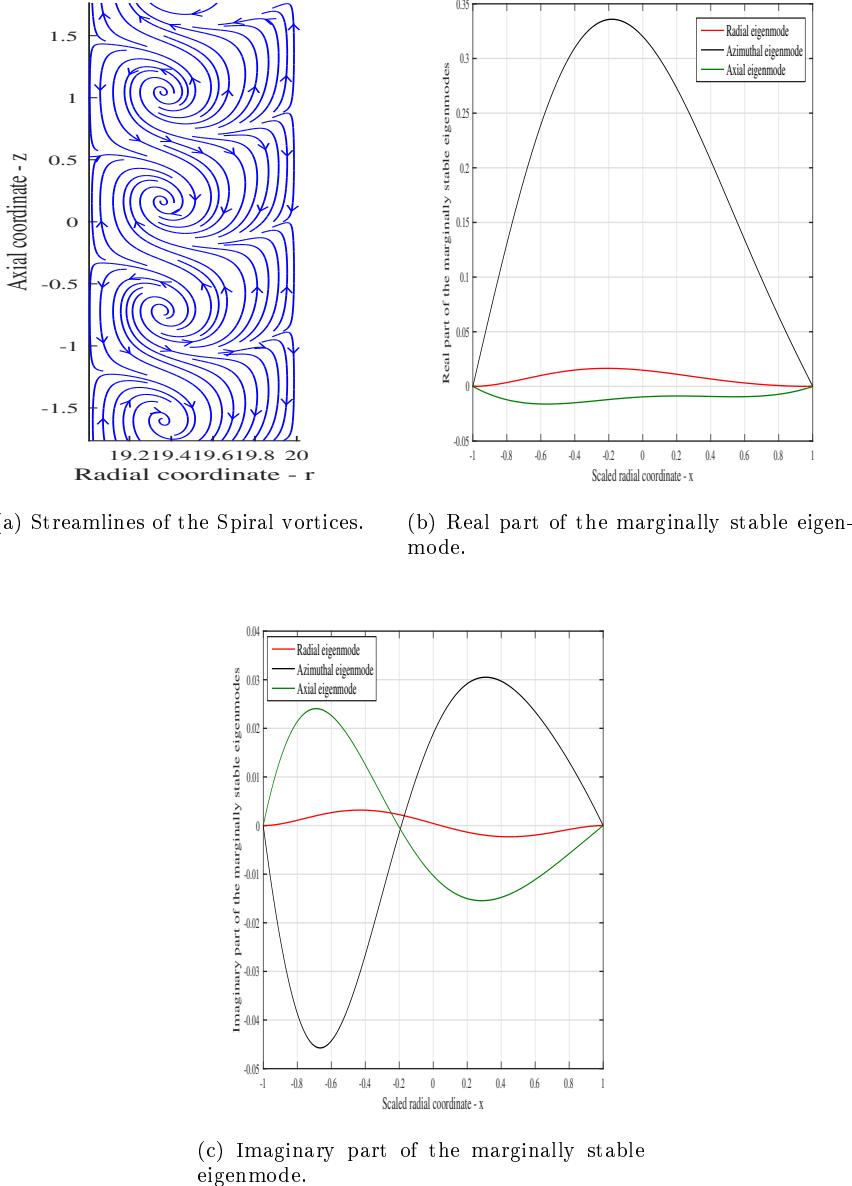


Figure 4.26: Structure of Spiral vortices for  $\alpha = 3, \omega = -0.8, \eta = 0.95, Re_c = 266.3, \beta_c = 3.56$ .

# Chapter 5

## Nonlinear stability

It has been seen that the study of the linear stability of a generic dynamical system leads to the determination of the stability or instability of an equilibrium solution, under the hypothesis that the perturbations remain infinitesimal in time. According to this theory, in fluid dynamics, the velocity and pressure perturbations can generally be described by a vector state  $\mathbf{w} = (\mathbf{u}', p')$  such that

$$\mathbf{w} = A(t)\mathbf{f}(\mathbf{r}) + A(t)^*\mathbf{f}(\mathbf{r})^*, \quad (5.1)$$

where the function  $\mathbf{f}(\mathbf{r})$  describes the spatial structure of the modes of the system and the function  $A(t)$  its amplitude as a function of time. From now on, the asterisk symbol will be used to indicate the complex conjugate of a generic quantity. The representation of the solution according to the relation (5.1) is valid under the hypothesis of the linear stability, i.e. as long as the amplitude of the perturbations remains sufficiently small so that the nonlinearities can be neglected in the governing equations. Indeed, under the hypothesis of the linear theory, the amplitude of the perturbation  $A(t)$  grows exponentially with the associated eigenvalue  $s = \sigma + i\omega$ , following an equation like

$$\frac{dA}{dt} = sA. \quad (5.2)$$

From now on, we will always denote the real part of the eigenvalue as  $\sigma$  and the imaginary part of the eigenvalue as  $\omega$ . From equation (5.2) it is clear that if the real part of the eigenvalue  $\sigma$  is negative, then the associated mode is stable. The need to account for nonlinearities arises when the eigenvalue crosses the imaginary axis, giving birth to a marginally stable mode. In this case, the marginally stable mode becomes dominant among the other modes and, as mentioned in the introduction, the linear stability cannot predict the stability or instability of the system. Therefore, in order to analyse the stability of the system, the nonlinear terms must be included and they will be responsible in stabilizing or not the system. Moreover, the study of the nonlinear stability can give useful indications on the behaviour of the system when perturbations grow in such a way for the nonlinear terms to become relevant.

In order to study the nonlinear dynamics of a system, however, there is still no universally valid instrument, but different approaches have been proposed to face the problem. The approach adopted in this work is part of the perturbation methods and is known as "weakly nonlinear analysis". We will explain it deeply in the next paragraphs, however, the basic idea is that the growth rate of the amplitude of a disturbance in time  $\frac{dA}{dt}$  can be seen as a Taylor series expansion in powers of the amplitude itself. The first who tried to deal with the weakly nonlinear analysis was the physicist Lev Landau [23]. He started from the linear stability result, so that the amplitude of an eigenmode relative to the linearized system grows exponentially in time according to the equation (5.2). Then he noted that, for  $A$  sufficiently small, that equation could be seen as a Taylor series expansion truncated at first order in the amplitude  $A$ . Thus he proposed to treat the nonlinearities simply by adding terms to this expansion, which will no longer be truncated at first order but at higher orders starting from the second, up to the desired one. As the amplitude is in general a complex function, at second order the terms which have to be added to the expansion are of the form  $A^2$ ,  $|A|^2$ ,  $(A^*)^2$ . Proceeding at the

third order they are  $A|A|^2$ ,  $A^3$ ,  $A^*|A|^2$ ,  $(A^*)^3$ , and so on for higher orders. Let us suppose that the truncation is at order  $r$ , the terms that have to be added at this order are of the form  $A^{r-j}(A^*)^j$ ,  $\forall j = 0, \dots, r$ . Anyway, by analysing the symmetries of the problem, many of these terms can be cancelled out. A particular case, also very important in fluid dynamic stability problems, is about the symmetry with respect to the time. That is, assuming the system is invariant along to the temporal direction  $t \rightarrow t + t_0$ , with  $t_0$  arbitrarily chosen, then if  $A = a_0 e^{st}$  is a solution, also  $A = a_0 e^{st+i\phi}$  must be a solution for any value of  $\phi$ . This means that the equation describing the dynamics of the amplitude  $A(t)$  must be invariant under rotations in the complex plane. For instance, coming back to the expansion at the second and third order previously cited, the only term that guarantees this invariance is the term  $A|A|^2$ , and its conjugate for the function  $A^*$ . Hence, by truncating the expansion at the third order [23] [1], the nonlinear dynamics of our system is described by the equation

$$\frac{dA}{dt} = sA - \kappa A|A|^2. \quad (5.3)$$

The equation (5.3) is called "Landau equation" or even "Stuart–Landau equation". In this equation, with respect to the linear approximation, there is a new constant term  $\kappa$  called "Landau coefficient". This term represents the contribution given by the nonlinear terms to the stability of the equilibrium solution. Particularly, based on the sign of the Landau constant, the system may reach another equilibrium solution, or may grow indefinitely leading to the instability. In fluid dynamics, the determination of the Landau coefficient is usually very laborious as it may originate from different causes: the nonlinear term, a nonlinear constitutive law, boundary conditions. However, once the Landau coefficient has been determined, the Landau equation is helpful in studying two phenomena that typically arise in fluid dynamic problems, namely

- the saturation of the amplitude for the perturbations,
- the variation of the frequency at which the perturbation propagates.

These two characteristics can be properly understood by studying the Landau equation for two one-dimensional model problems: the van der Pol oscillator and the Duffing oscillator.

## 5.1 Van der Pol oscillator: modulation of the amplitude in time

Let  $u = u(t)$  be the unknown function which satisfies the differential equation

$$\frac{d^2u}{dt^2} - \epsilon(1-u^2)\frac{du}{dt} + u = 0, \quad (5.4)$$

where  $\epsilon \ll 1$  is a small parameter. By linearizing the equation around the equilibrium solution  $u = 0$ , we can show that the growth rate of the perturbation in time is proportional to  $\epsilon$ . Indeed we have that

$$s_{1,2} = \frac{\epsilon \pm \sqrt{\epsilon^2 - 4}}{2}, \quad (5.5)$$

and, as  $\epsilon \ll 1$ , the previous expression can be expanded in Taylor series leading to

$$s_{1,2} = \pm i + \frac{\epsilon}{2} \pm \frac{i}{2}\epsilon^2 + \mathcal{O}(\epsilon^3). \quad (5.6)$$

As  $\sigma = \Re[s_{1,2}] = \frac{\epsilon}{2} + \mathcal{O}(\epsilon^3)$ , the nonlinear terms are expected to appear after a time of order  $\mathcal{O}(\epsilon^{-1})$ . Thus we can define a new time scale  $T = \epsilon t$ , so that the unknown depends on two variables: a variable  $t$  that expresses the fast time scale, responsible for the exponential decay of the stable modes; and a slow time scale  $T$  which expresses the dynamics of the system related to the non-hyperbolic modes. Then we have, with a notation abuse

$$u = u(t, T). \quad (5.7)$$

By expanding the solution in series of  $\epsilon$  and by truncating it at first order, we get

$$u(t, T) = u_0(t, T) + \epsilon u_1(t, T) + \mathcal{O}(\epsilon^2). \quad (5.8)$$

In this way, the derivative and the quadratic term which appear in the differential equation become

$$\begin{aligned} \frac{du(t, T)}{dt} &= \partial_t u_0 + \epsilon (\partial_t u_1 + \partial_T u_0) + \mathcal{O}(\epsilon^2), \\ \frac{d^2 u(t, T)}{dt^2} &= \partial_t^2 u_0 + \epsilon (\partial_t^2 u_1 + 2\partial_t \partial_T u_0) + \mathcal{O}(\epsilon^2), \\ u^2(t, T) &= u_0^2 + 2\epsilon u_0 u_1 + \mathcal{O}(\epsilon^2). \end{aligned} \quad (5.9)$$

By inserting these terms in the governing equation and by collecting the terms at the different powers of  $\epsilon$ , we have at zero order ( $\epsilon^0$ )

$$\partial_t^2 u_0 + u_0 = 0, \quad (5.10)$$

which gives the general solution

$$u_0(t, T) = A(T)e^{it} + A^*(T)e^{-it}. \quad (5.11)$$

The amplitude of the perturbation is indeed a function of the slow time scale  $T$ . By proceeding the expansion to the next order we find at the first order ( $\epsilon^1$ )

$$\partial_t^2 u_1 + u_1 = -2\partial_t \partial_T u_0 + (1 - u_0^2)\partial_t u_0. \quad (5.12)$$

By substituting the expression found for the solution at order zero in the equation at first order we have

$$\partial_t^2 u_1 + u_1 = \left[ -2i\frac{dA}{dT} - iA(1 - 2|A|^2) - iA^2 A^* \right] e^{it} + iA^3 e^{3it} + c.c., \quad (5.13)$$

where the notation c.c stands for "complex conjugate" and contains all the terms proportional to  $e^{-it}$  and to  $e^{-3it}$ . The equation (5.13) contains terms in the right-hand side which can give rise to a resonance condition and since the solution must be limited at any order in  $\epsilon$ , these terms must be imposed equal to zero. This condition expresses the solvability condition which permits to derive the Stuart–Landau equation. By equalling to zero the resonant terms, we obtain the equation

$$2\frac{dA}{dT} = A - A|A|^2, \quad (5.14)$$

and the corresponding complex conjugate. By rescaling by a factor two the unknown  $A \rightarrow \frac{A}{2}$ , we get the Stuart–Landau equation in the final form

$$\frac{dA}{dT} = \frac{1}{2}A - \frac{1}{8}|A|^2. \quad (5.15)$$

The Landau coefficient in this case is a real number and equal to  $\frac{1}{8}$ . This implies that the equilibrium solution  $u = 0$  becomes unstable via a supercritical Hopf bifurcation. The formal solution of the equation (5.15) can be found by firstly writing  $A$  as  $A = a(T)e^{i\phi(T)}$ . Secondly, performing the derivative with respect to  $T$  and dividing the terms for the real part and the ones for the imaginary part, we obtain the following system of two ordinary differential equations in the unknowns  $a(T), \phi(T)$

$$\begin{aligned} \frac{da}{dT} &= \frac{1}{2}a - \frac{1}{8}a^3, \\ \frac{d\phi}{dT} &= 0, \end{aligned} \quad (5.16)$$

for which the solution is

$$\begin{aligned} a(T) &= a_0 \left[ \frac{1}{4}a_0^2 + \left( 1 - \frac{1}{4}a_0^2 \right) e^{-T} \right]^{-1/2}, \\ \phi(T) &= \phi_0. \end{aligned} \quad (5.17)$$

Hence, coming back to the original physical unknown  $u(t)$ , the final solution will be given by

$$u(t) = \Re \left[ a(\epsilon t) e^{i(\phi_0 + t)} + c.c. \right]. \quad (5.18)$$

Notice how, as  $T \rightarrow \infty$ , the amplitude reaches an asymptotic value given by  $a = 2$ . This is in fact the non-trivial equilibrium solution given by equation (5.17). Hence, the amplitude of the perturbation saturates to a constant value  $a = 2$ .

The results concerning the time behaviour of the solution and the phase portrait of the system are given in figures 5.1 and 5.2 respectively for  $\epsilon = 0.01$ , while in figures 5.4 and 5.5 for  $\epsilon = 1$ . From figure 5.3 the agreement between the two solution is very high also for higher

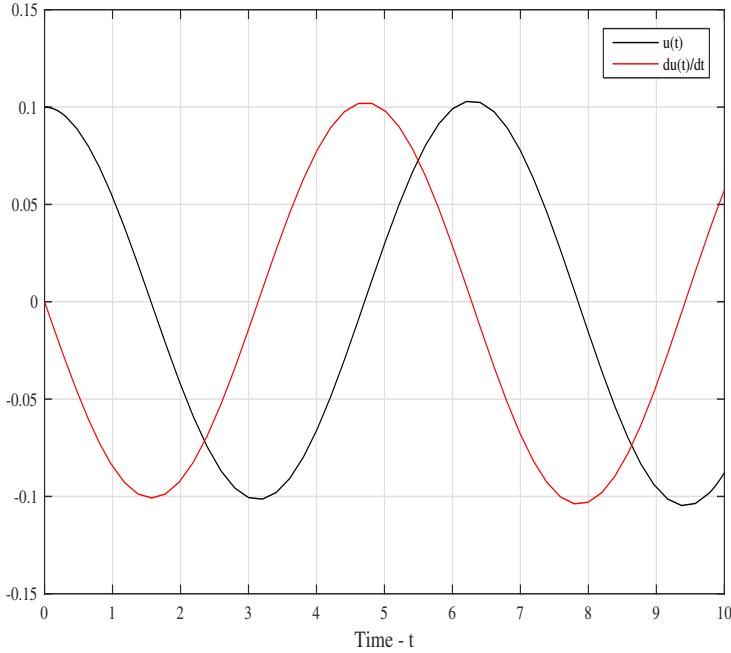


Figure 5.1: Behaviour of the exact solution  $u$  and of its temporal derivative  $\frac{du}{dt}$  for the Van der Pol problem with  $\epsilon = 0.01$ ,  $u(0) = 0.1$ ,  $\frac{du(0)}{dt} = 0$ .

times, due to the small value of  $\epsilon$  considered. Instead, from figure 5.6, as  $\epsilon = 1$  in this case, the two curves agree well for a time  $t \simeq 10$ . For increasing values of time, the two behaviours differ due to the presence of higher harmonics in the solution and a consequent shift in the frequency.

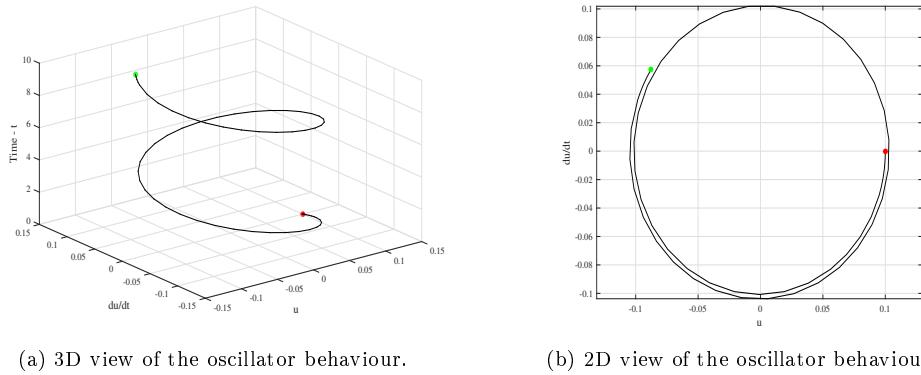


Figure 5.2: Van der Pol exact solution for  $\epsilon = 0.01$ ,  $u(0) = 0.1$ ,  $\frac{du(0)}{dt} = 0$ . The red point shows the starting point of the trajectory. The green point the final one.

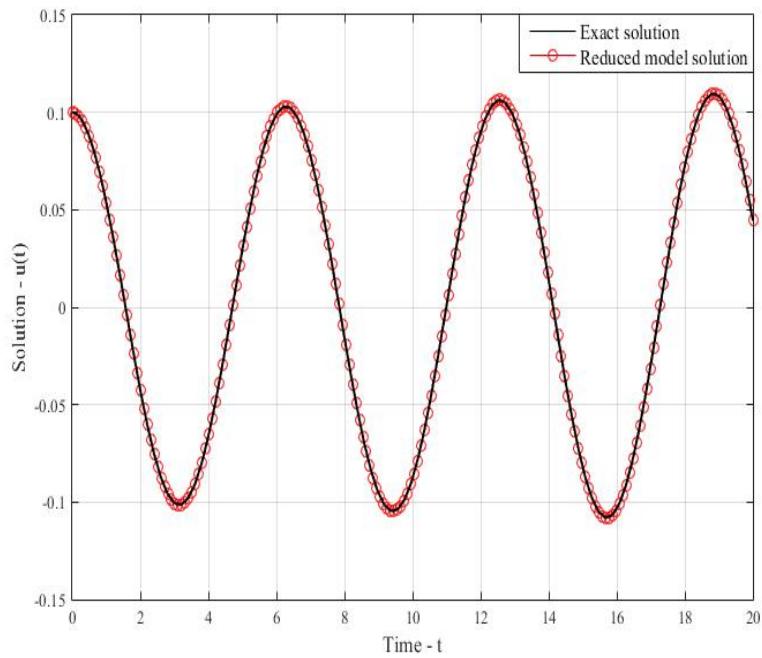


Figure 5.3: Comparison between the exact solution (black curve) and the one obtained by using the Landau equation (red dot-curve) for  $\epsilon = 0.01$ ,  $u(0) = 0.1$ .

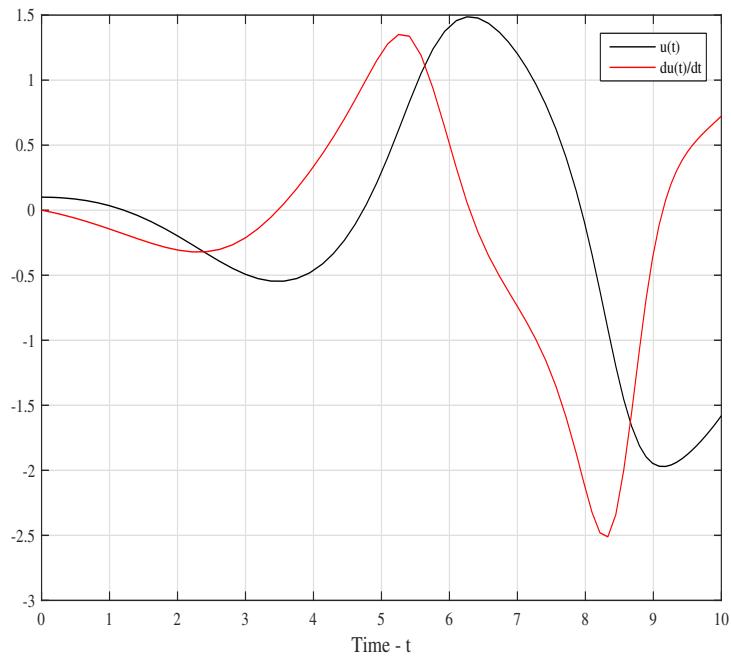
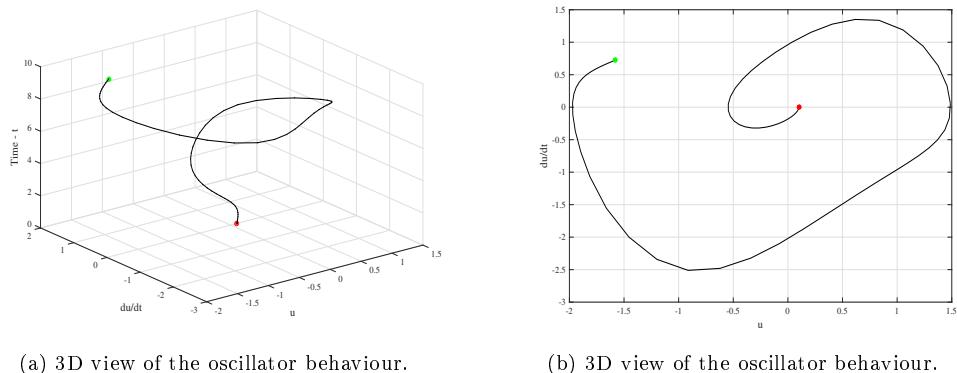


Figure 5.4: Behaviour of the exact solution  $u$  and of its temporal derivative  $\frac{du}{dt}$  for the Van der Pol problem with  $\epsilon = 1$ ,  $u(0) = 0.1$ ,  $\frac{du(0)}{dt} = 0$ .



(a) 3D view of the oscillator behaviour.

(b) 3D view of the oscillator behaviour.

Figure 5.5: Van der Pol exact solution for  $\epsilon = 1$ ,  $u(0) = 0.1$ ,  $\frac{du(0)}{dt} = 0$ . The red point shows the starting point of the trajectory. The green point the final one.

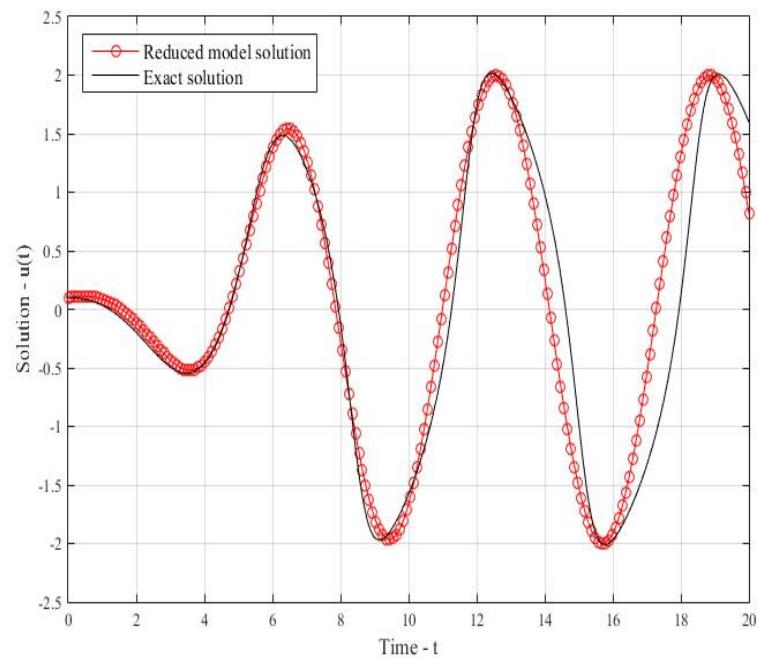


Figure 5.6: Comparison between the exact solution (black curve) and the one obtained by using the Landau equation (red dot-curve) for  $\epsilon = 1$ ,  $u(0) = 0.1$ .

## 5.2 Duffing oscillator: the shift in the frequency

Let us consider now the Duffing oscillator, whose dynamics is governed by the following differential equation

$$\frac{d^2u}{dt^2} + u + \epsilon u^3 = 0, \quad \epsilon \ll 1. \quad (5.19)$$

By proceeding in a way analogous to what done before, we expand the solution in series of powers of  $\epsilon$  and we introduce the slow time scale  $T = \epsilon t$ . By solving the equations at the various orders we find, at order  $\epsilon^0$

$$Lu_0 = 0, \quad L = \partial_t^2 + 1, \quad (5.20)$$

whose general solution is given by

$$u_0(t, T) = \frac{1}{2}A(T)e^{it} + c.c. \quad (5.21)$$

At order  $\epsilon^1$

$$\begin{aligned} Lu_1 &= -2\partial_t\partial_T u_0 - u_0^3 \\ &= \left(-i\frac{dA}{dT} - \frac{3}{8}A|A|^2\right)e^{it} - \frac{1}{8}A^3e^{3it} + c.c. \end{aligned} \quad (5.22)$$

The solvability condition in this case reads as

$$\frac{dA}{dT} = \frac{3i}{8}A|A|^2. \quad (5.23)$$

It is worthy to notice that in this case the Stuart–Landau equation does not contain the linear term proportional to  $A$  and moreover the Landau coefficient is complex.

By searching a solution in the form  $A(T) = a(T)e^{i\phi(T)}$  we have to solve the following ordinary differential system

$$\begin{aligned} \frac{da}{dT} &= 0, \\ \frac{d\phi}{dT} &= \frac{3}{8}a^2, \end{aligned} \quad (5.24)$$

whose solution is

$$\begin{aligned} a &= a_0, \\ \phi &= \frac{3}{8}a_0^2T + \phi_0. \end{aligned} \quad (5.25)$$

As it is clear from the solution of the problem, the nonlinearity in the governing equation does not modify the amplitude of the perturbation but instead it modifies the frequency at which the perturbation propagates. The results concerning the Duffing oscillator are shown in figure 5.7 and in figure 5.8 for  $\epsilon = 0.01$  and in figure 5.10 and 5.11 for  $\epsilon = 1$ .

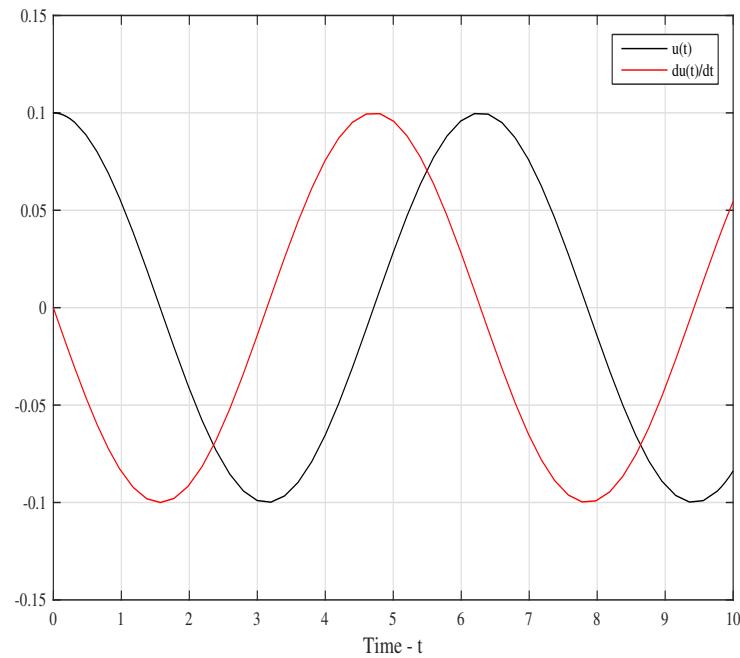


Figure 5.7: Behaviour of the exact solution  $u$  and of its temporal derivative  $\frac{du}{dt}$  for the Duffing problem with  $\epsilon = 0.01$ ,  $u(0) = 0.1$ ,  $\frac{du(0)}{dt} = 0$ .

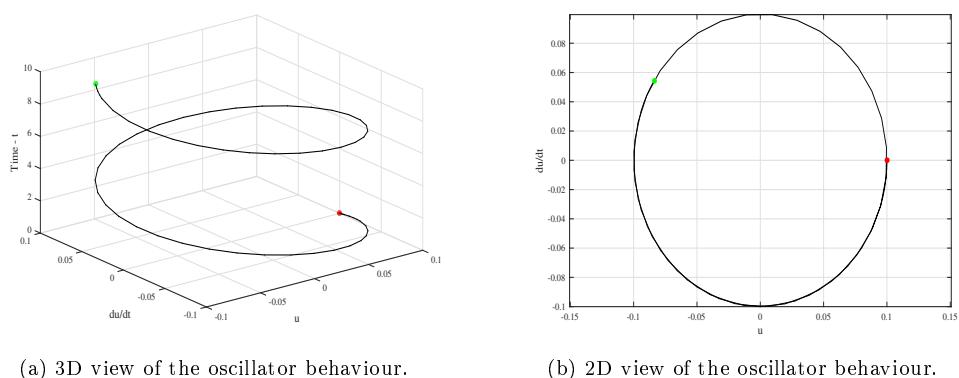


Figure 5.8: Duffing exact solution computed for  $\epsilon = 0.01$ ,  $u(0) = 0.1$ ,  $\frac{du(0)}{dt} = 0$ . The red point shows the starting point of the trajectory. The green point the final one.

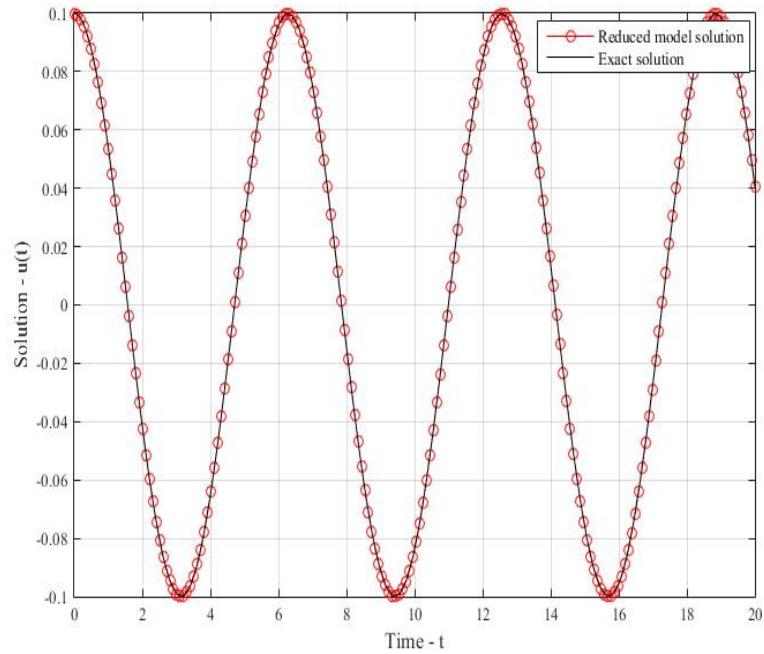


Figure 5.9: Comparison between the exact solution (black curve) and the one obtained by using the Landau equation (red dot-curve) for  $\epsilon = 0.01$ ,  $u(0) = 0.1$ .

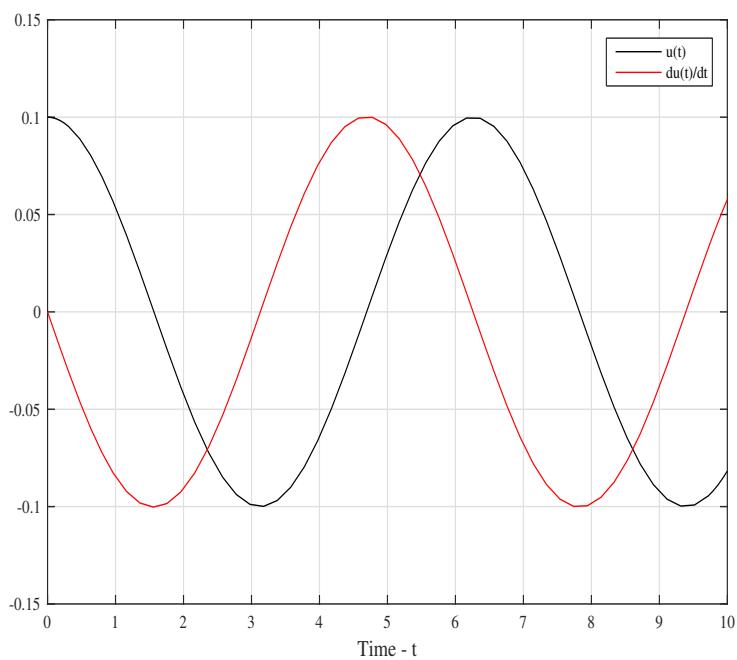
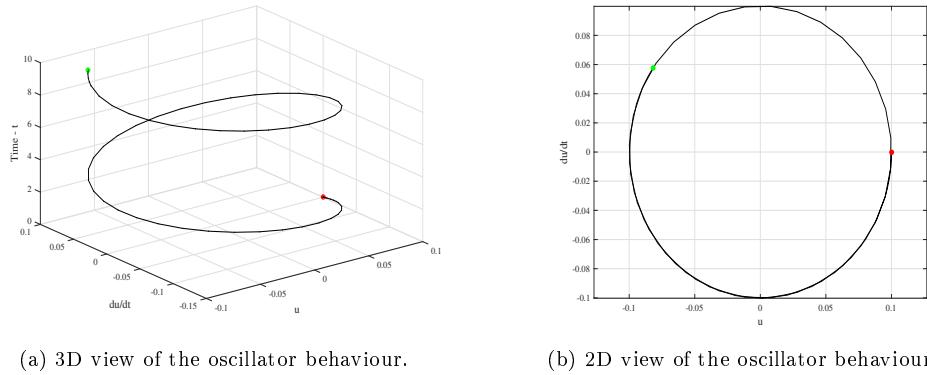


Figure 5.10: Behaviour of the exact solution  $u$  and of its temporal derivative  $\frac{du}{dt}$  for the Duffing problem with  $\epsilon = 1$ ,  $u(0) = 0.1$ ,  $\frac{du(0)}{dt} = 0$ .



(a) 3D view of the oscillator behaviour.

(b) 2D view of the oscillator behaviour.

Figure 5.11: Duffing exact solution computed for  $\epsilon = 1$ ,  $u(0) = 0.1$ ,  $\frac{du(0)}{dt} = 0$ . The red point shows the starting point of the trajectory. The green point the final one.

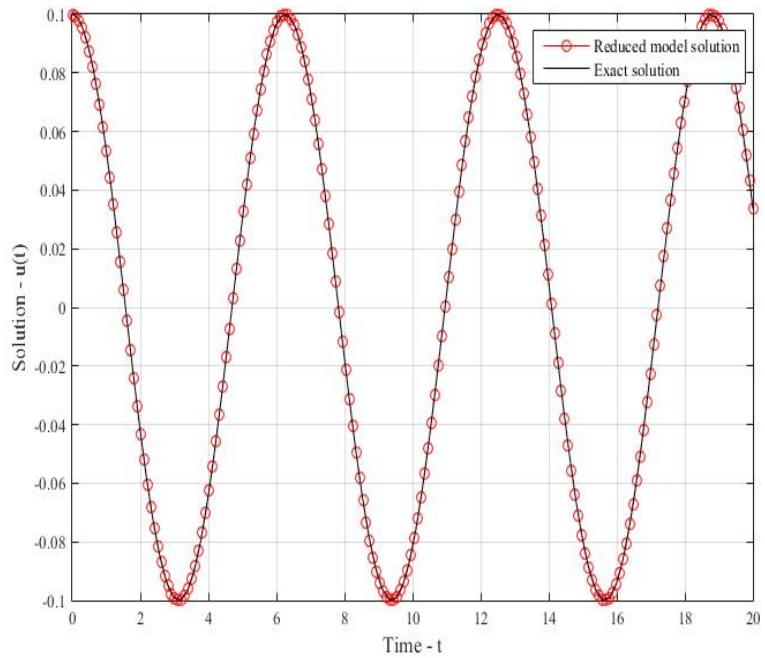


Figure 5.12: Comparison between the exact solution (black curve) and the one obtained by using the Landau equation (red dot-curve) for  $\epsilon = 1$ ,  $u(0) = 0.1$ .

### 5.3 Nonlinear dynamics of systems governed by partial differential equations

In the previous section two examples were studied—the van der Pol oscillator and the Duffing oscillator—which highlighted how the nonlinear effects can modify the amplitude and the phase of the perturbations. However, these models are based on governing equations that depend only on time. In fluid dynamic problems, in addition to the temporal dimension, we also have the spatial dimensions. It is therefore reasonable to wonder whether and how the spatial variation of a certain variable can lead to the onset of instability in the flow. From the linear stability analysis, we know that a steady fixed point of a dissipative system can become linearly unstable when the value of the control parameter  $\mathcal{R}$  exceeds a critical value  $\mathcal{R}_c$ , in our case the parameter can be chosen as the Reynolds number. Depending on the type of bifurcation for which the fixed point becomes linearly unstable, the instability can occur both with the appearance of stationary and spatially periodic structures, or as travelling waves. In both cases, the amplitude manifests a slow modulation, as discussed in the introduction, and may grow in time as well as in space. Then, it is possible to derive an equation which describes this slow modulation of the amplitude along time and space. This equation is known as Ginzburg–Landau equation. It differs from the Stuart–Landau equation because it contains the spatial dependence of the unknown and not only the temporal dependence. The idea at the base of the derivation of the Ginzburg–Landau equation is to describe the amplitude as the envelope of a wave packet defined close to the critical point at which the fixed point becomes non-hyperbolic. The method used to obtain the nonlinear version of such an equation is the multiple-scale method. In the following paragraphs, we will first derive the G–L equation for a model problem, the Swift–Hohenberg equation, and then for the Navier–Stokes equations applied to the Taylor–Couette base flow.

The Ginzburg–Landau (G–L) equation is a partial differential equation, with constant coefficients. These coefficients can be real or complex, depending on the bifurcation of the steady basic solution. In particular, the G–L equation is termed "real G–L equation", if the solution that arises from the linear instability has a stationary structure, i.e. if the marginally stable mode is stationary. It also implies that the corresponding eigenvalue evaluated at the critical point  $(\mathcal{R}_c, \beta_c)$  is real. From the point of view of bifurcation theory, in this case the system becomes linearly unstable through a "saddle-node" bifurcation, or a "pitchfork" bifurcation or even a "transcritical" bifurcation. Thus in this case the coefficients of the G–L equation are real. On the other hand, if the secondary solution arising from a bifurcation of the equilibrium solution is a non-stationary solution, i.e. the marginally stable mode is an oscillatory mode, then the G–L equation is termed "complex G–L equation" because its coefficients are complex. In this case, the marginally stable eigenvalue is purely imaginary and the fixed point becomes linearly unstable via a Hopf bifurcation.

#### 5.3.1 Weakly nonlinear dynamics: from the evolution equation of a wave packet to the Ginzburg–Landau equation

##### The real Ginzburg–Landau equation

We consider the case when the system passes from a stable state to a linearly unstable state through a stationary bifurcation, by increasing the control parameter  $\mathcal{R}$  beyond a critical value  $\mathcal{R}_c$ . In this situation, we have that the imaginary part of the marginally stable eigenvalue  $\omega$  does not play a role in governing the dynamics of the system near the threshold point. In fact, it can be written that  $\omega_c = 0$  and  $c_g = \frac{\partial \omega(\beta_c, \mathcal{R}_c)}{\partial \beta} = 0$ . Thus it is possible to consider only the real part of  $s$ , i.e.  $s = \sigma$ . The eigenvalue evaluated in the vicinity of the critical point, which expresses the growth rate of the amplitude of the perturbation in a neighbourhood of the non-hyperbolic point, can be expanded in Taylor series up to the desired order. For simplicity,

we limit ourselves to the second order, yielding

$$\sigma(\mathcal{R}, \beta) = \sigma(\mathcal{R}_c, \beta_c) + \frac{\partial\sigma(\mathcal{R}_c, \beta_c)}{\partial\beta}(\beta - \beta_c) + \frac{\partial\sigma(\mathcal{R}_c, \beta_c)}{\partial\mathcal{R}}(\mathcal{R} - \mathcal{R}_c) + \frac{1}{2} \frac{\partial^2\sigma(\mathcal{R}_c, \beta_c)}{\partial\beta^2}(\beta - \beta_c)^2 + \dots \quad (5.26)$$

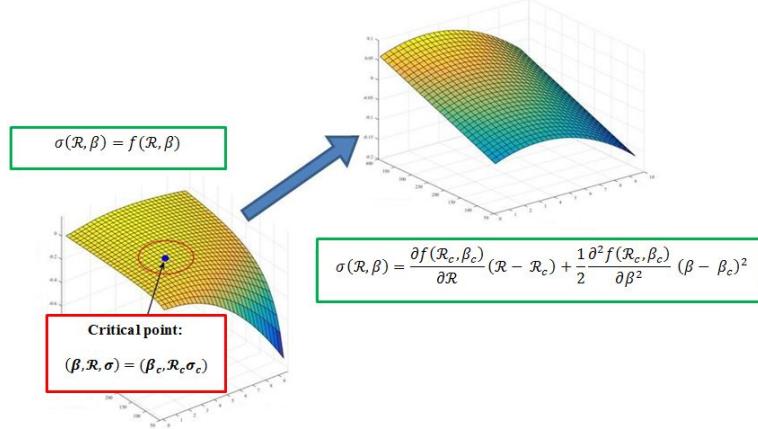


Figure 5.13: Approximation of the dispersion relation in the neighbourhood of the non-hyperbolic point in the plane  $\beta - \mathcal{R}$

The first two terms in the expansion are null as, in the critical point  $(\mathcal{R}_c, \beta_c)$ , the eigenvalue  $\sigma$  is by definition a real eigenvalue associated to a marginally stable mode. Geometrically this can be seen by the condition of tangentiality of  $\sigma(\mathcal{R}_c, \beta)$  with respect to the axis  $\beta$ . The expression for the expansion of  $\sigma$  can so be rewritten in a more compact form as follows

$$\tau_c \sigma(\mathcal{R}, \beta) = (\mathcal{R} - \mathcal{R}_c) - \xi_c^2(\beta - \beta_c)^2 + \dots, \quad (5.27)$$

where the quantities  $\tau_c = \left( \frac{\partial\sigma(\mathcal{R}_c, \beta_c)}{\partial\mathcal{R}} \right)^{-1}$  and  $\xi_c^2 = -\frac{\tau_c}{2} \frac{\partial^2\sigma(\mathcal{R}_c, \beta_c)}{\partial\beta^2}$  have been introduced. From the relation (5.27), it is possible to obtain the neutral stability curve corresponding to  $\sigma = 0$ . In the plane  $(\mathcal{R}, \beta)$ , this curve is a parabola

$$\mathcal{R} - \mathcal{R}_c = \xi_c^2(\beta - \beta_c)^2. \quad (5.28)$$

Let us analyse this expression. By calling  $\mathcal{R} - \mathcal{R}_c = \epsilon^2$ , such that  $\epsilon$  is sufficiently small, for  $\mathcal{R} > \mathcal{R}_c$  the axial wavenumbers inside the parabola have a band width whose amplitude is of order  $\epsilon$ .

Now, let us consider a perturbation  $u(x, t)$  of a basic state. It can be written in general as the Fourier integral

$$u(x, t) = \frac{1}{2} \int_0^{+\infty} \hat{u}(\beta) e^{\sigma(\mathcal{R}, \beta)t + i\beta x} d\beta + \text{c.c..} \quad (5.29)$$

In the neighbourhood of the critical point, the evolution of the perturbation is led by the non-hyperbolic state, therefore, by expanding the function  $u(x, t)$  around the point  $(\mathcal{R}_c, \beta_c)$ , we obtain

$$u(x, t) = \frac{1}{2} \int_0^{+\infty} \hat{u}(\beta) e^{\sigma_{app}(\mathcal{R}, \beta)t + i\beta x + i(\beta - \beta_c)x} d\beta + \text{c.c.}, \quad (5.30)$$

where the function  $\sigma_{app}(\mathcal{R}, \beta)$  indicates the approximation of the dispersion relation up to a desired order:

$$\sigma_{app}(\mathcal{R}, \beta) = \sigma(\mathcal{R}_c, \beta_c) + \frac{\partial\sigma(\mathcal{R}_c, \beta_c)}{\partial\beta}(\beta - \beta_c) + \frac{\partial\sigma(\mathcal{R}_c, \beta_c)}{\partial\mathcal{R}}(\mathcal{R} - \mathcal{R}_c) + \frac{1}{2} \frac{\partial^2\sigma(\mathcal{R}_c, \beta_c)}{\partial\beta^2}(\beta - \beta_c)^2 + \dots \quad (5.31)$$

Now, as  $\sigma(\mathcal{R}_c, \beta_c) = \sigma_c = 0$  and  $\frac{\partial\sigma(\mathcal{R}_c, \beta_c)}{\partial\beta} = 0$ , by substituting the expression for  $\sigma_{app}$  in the equation (5.30) we get

$$u(x, t) = \frac{1}{2} \int_0^{+\infty} \hat{u}(\beta) e^{\left( \frac{\partial\sigma(\mathcal{R}_c, \beta_c)}{\partial\mathcal{R}} (\mathcal{R} - \mathcal{R}_c) + \frac{1}{2} \frac{\partial^2\sigma(\mathcal{R}_c, \beta_c)}{\partial\beta^2} (\beta - \beta_c)^2 + \dots \right) t + i\beta_c x + i(\beta - \beta_c)x} d\beta + c.c.. \quad (5.32)$$

The term  $e^{i\beta_c x}$  does not depend on  $\beta$  and can be brought out of the integral operator, yielding

$$u(x, t) = \frac{1}{2} \left[ \int_0^{+\infty} \hat{u}(\beta) e^{\left( \frac{\partial\sigma(\mathcal{R}_c, \beta_c)}{\partial\mathcal{R}} (\mathcal{R} - \mathcal{R}_c) + \frac{1}{2} \frac{\partial^2\sigma(\mathcal{R}_c, \beta_c)}{\partial\beta^2} (\beta - \beta_c)^2 + \dots \right) t + i(\beta - \beta_c)x} d\beta \right] e^{i\beta_c x} + c.c.. \quad (5.33)$$

The term inside square brackets, represents the envelope of a wave packet in the neighbourhood of the critical point and defines the amplitude of the wave packet near the critical point. This means that the perturbation near the point  $(\mathcal{R}_c, \beta_c)$  has an amplitude which is given by the evolution of the function  $\mathcal{A}$ , defined according to

$$\mathcal{A}(x, t) = \int_0^{+\infty} \hat{u}(\beta) e^{\left( \frac{\partial\sigma(\mathcal{R}_c, \beta_c)}{\partial\mathcal{R}} (\mathcal{R} - \mathcal{R}_c) + \frac{1}{2} \frac{\partial^2\sigma(\mathcal{R}_c, \beta_c)}{\partial\beta^2} (\beta - \beta_c)^2 + \dots \right) t + i(\beta - \beta_c)x} d\beta. \quad (5.34)$$

As a consequence, the equation (5.30) can be rewritten as

$$u(x, t) = \frac{1}{2} \mathcal{A}(x, t) e^{i\beta_c x} + c.c. \quad (5.35)$$

We remark the fact that the integral which defines the amplitude  $\mathcal{A}(x, t)$  is governed by the wave numbers close to the critical one  $\beta_c$  since the other modes are asymptotically stable; indeed, the relation (5.35) expresses the (linear) behaviour of the perturbation guided by critical mode. We now want to derive an evolution equation for the wave packet. Such an equation, will be described by the amplitude  $\mathcal{A}$ . By performing the derivative with respect to time of the envelope, we can write, up to the second order

$$\begin{aligned} \partial_t \mathcal{A}(x, t) &= \left( \frac{\partial\sigma(\mathcal{R}_c, \beta_c)}{\partial\mathcal{R}} (\mathcal{R} - \mathcal{R}_c) + \frac{1}{2} \frac{\partial^2\sigma(\mathcal{R}_c, \beta_c)}{\partial\beta^2} (\beta - \beta_c)^2 + \dots \right) \int_0^{+\infty} \hat{u}(\beta) e^{\sigma_{app}(\mathcal{R}, \beta)t + i(\beta - \beta_c)x} d\beta \\ &= \frac{\partial\sigma(\mathcal{R}_c, \beta_c)}{\partial\mathcal{R}} (\mathcal{R} - \mathcal{R}_c) \mathcal{A} - \frac{1}{2} \frac{\partial^2\sigma(\mathcal{R}_c, \beta_c)}{\partial\beta^2} \partial_x^2 \mathcal{A}. \end{aligned} \quad (5.36)$$

Reminding the expression of the coefficients  $\tau_c$  and  $\xi_c$ , the evolution equation for the amplitude can be written as

$$\tau_c \partial_t \mathcal{A} = (\mathcal{R} - \mathcal{R}_c) \mathcal{A} + \xi_c^2 \partial_x^2 \mathcal{A}. \quad (5.37)$$

The equation above describes the linear dynamics of a wave packet near the critical point  $(\mathcal{R}_c, \beta_c)$ . Notice how this equation has real coefficients, according to the initial assumption to consider a marginally steady state. Moreover, by analysing the terms that form the equation, we have that the term proportional to  $\mathcal{A}$  at the right-hand side expresses the exponential growth of the perturbations near the critical point; in addition, the term that contains the second derivative of  $\mathcal{A}$  with respect to  $x$  is a diffusive term and indicates the spread of the envelope. Our ultimate goal is to derive the Ginzburg–Landau equation which instead expresses the nonlinear dynamics of a wave packet in the neighbourhood of the marginally stable state. The G–L equation can be deduced rigorously by making use of a weakly nonlinear expansion around the critical point. Anyway, it can be also written by analysing the symmetries that the dynamical system possesses. In particular, assuming that the system is invariant under translations in time and space, it will have to be invariant under rotations in the complex plane, as discussed previously for the Stuart–Landau equation. The first nonlinear term that satisfies this constraint is the term  $\mathcal{A}|\mathcal{A}|^2$ . Then, the general form of the Ginzburg–Landau equation truncated at third order is obtained simply by adding the nonlinear contribution to the right-hand side of the relation (5.37)

$$\tau_c \partial_t \mathcal{A} = (\mathcal{R} - \mathcal{R}_c) \mathcal{A} + \xi_c^2 \partial_x^2 \mathcal{A} - \kappa \mathcal{A} |\mathcal{A}|^2. \quad (5.38)$$

As it can be seen, the Ginzburg–Landau equation represents a generalization of the Stuart–Landau equation, allowing a modulation of the amplitude not only in time, but also along one, or even more, spatial directions.

### The complex Ginzburg–Landau equation

The Ginzburg–Landau equation with complex coefficients arises from the instability of a fixed point producing a travelling wave that propagates at a non-zero velocity. In this situation, the marginally stable mode is not necessarily stationary but it can be periodic in time.

As already mentioned, the rigorous derivation of the G–L equation, both with real or complex coefficients, can be obtained using the multiple-scale method. In this section, we limit ourselves to the derivation of the equation using again symmetry arguments. We start by deriving the equation that describes the linear dynamics of a wave packet that propagates at non-zero velocity, around the critical point  $(\mathcal{R}_c, \beta_c)$ . In this point, the non-hyperbolic eigenvalue  $s = \sigma - i\omega$  crosses the imaginary axis with an imaginary part different from zero. As done before, the real and imaginary part can be expressed in Taylor series truncated at least to the second order as

$$\begin{aligned}\tau_c \sigma &= (\mathcal{R} - \mathcal{R}_c) - \xi_c^2(\beta - \beta_c)^2 + \dots, \\ \omega &= \omega_c + c_g(\beta - \beta_c) + \omega'_R(\mathcal{R} - \mathcal{R}_c) + \frac{\omega''_c}{2}(\beta - \beta_c)^2 + \dots,\end{aligned}\tag{5.39}$$

where  $c_g = \frac{\partial \omega(\mathcal{R}_c, \beta_c)}{\partial \beta}$  represents the group velocity of the wave, that is the velocity at which the wave packet propagates. Instead, the quantity  $\omega''_c = \frac{\partial^2 \omega(\mathcal{R}_c, \beta_c)}{\partial \beta^2}$  indicates the growth rate of the group velocity with the axial wave number, whereas the quantity  $\omega'_R = \frac{\partial \omega(\mathcal{R}_c, \beta_c)}{\partial \mathcal{R}}$  expresses the growth rate of the frequency with the control parameter  $\mathcal{R}$ . As in this case the perturbation cannot be considered a stationary perturbation, we will have an explicit dependence on time of the exponential term  $e^{i\beta_c x + i\omega_c t}$ . In particular, in the neighbourhood of the critical point, the perturbation is expressed in terms of the amplitude  $A$  by the relation

$$u(x, t) = \frac{1}{2} \mathcal{A}(x, t) e^{i\beta_c x - i\omega_c t} + \text{c.c.},\tag{5.40}$$

where  $\mathcal{A}(x, t)$  is defined through the Fourier transform

$$\mathcal{A}(x, t) = \int_0^{+\infty} \hat{u}(\beta) e^{(\sigma_{app}(\mathcal{R}, \beta) - i\omega_{app}(\mathcal{R}, \beta)t + i(\beta - \beta_c)x)}.\tag{5.41}$$

From the expressions of  $\sigma$  and  $\omega$  described in the equation (5.39), by performing the same passages seen in the paragraph for the real Ginzburg–Landau equation, it can be proven that  $\mathcal{A}$  satisfies the following linear differential equation

$$\gamma_c(\partial_t \mathcal{A} + c_g \partial_x \mathcal{A}) = (\mathcal{R} - \mathcal{R}_c)\mathcal{A} + (\zeta_c^2 + i\frac{\gamma_c \omega''_c}{2})\partial_x^2 \mathcal{A},\tag{5.42}$$

where  $\gamma_c$  is such that  $\frac{1}{\gamma_c} = \frac{\partial \sigma(\mathcal{R}_c, \beta_c)}{\partial \mathcal{R}} - i\frac{\partial \omega(\mathcal{R}_c, \beta_c)}{\partial \mathcal{R}}$  and  $\zeta_c^2 = -\frac{1}{2}\gamma_c \frac{\partial^2 \sigma(\mathcal{R}_c, \beta_c)}{\partial \beta^2}$ . Now, in order to obtain the G–L equation truncated at third order, we add the first of the nonlinear terms at the right-hand side, getting the complex Ginzburg–Landau equation, which reads as

$$\gamma_c(\partial_t \mathcal{A} + c_g \partial_x \mathcal{A}) = (\mathcal{R} - \mathcal{R}_c)\mathcal{A} + (\zeta_c^2 + i\frac{\gamma_c \omega''_c}{2})\partial_x^2 \mathcal{A} - \kappa \mathcal{A} |\mathcal{A}|^2.\tag{5.43}$$

In general, the Landau coefficient is such that  $k \in \mathbb{C}$ , and so can be written as  $\kappa = \kappa_r + i\kappa_i$ . By a physical point of view, the complex Ginzburg–Landau equation describes the nonlinear dynamics of a wave packet which travels at a velocity group  $c_g$ . The equation can be expressed

in a more elegant formulation, by making the following change of variables

$$\begin{aligned}\xi &= \frac{\epsilon(x - c_g t)}{\zeta_c}, \\ T &= \frac{\epsilon^2}{\gamma_c} t, \\ A &= \frac{\sqrt{\kappa_r}}{\epsilon} \mathcal{A},\end{aligned}\tag{5.44}$$

thus, reminding that  $\mathcal{R} - \mathcal{R}_c = \epsilon^2$ , the equation (5.43) becomes

$$\partial_T A = A + (1 + ic_1) \partial_\xi^2 A - (1 + ic_2) A |A|^2,\tag{5.45}$$

where the coefficients  $c_1$  and  $c_2$  are given by

$$\begin{aligned}c_1 &= \frac{1}{2} \frac{\omega_c'' \gamma_c}{\zeta_c^2}, \\ c_2 &= \frac{k_i}{k_r}.\end{aligned}\tag{5.46}$$

It is worthy to notice how the term that was linked to the group velocity and was expressed by the first derivative of the amplitude with respect to  $x$  has disappeared and the equation has become a pure reaction-diffusion equation in the spatial variable  $\xi$ . Finally, concerning the stability of the G-L equation, it will depend on the two parameters  $c_1$  and  $c_2$ .

### The multiple-scale method for the Ginzburg-Landau equation

The Ginzburg-Landau equation can be derived formally by introducing some auxiliary variables in the problem formulation, to be able to better approximate the dynamics of the original system in the neighbourhood of the critical point. The number of such variables will depend on the order of approximation. These variables are also called "slow variables" because they are responsible for the description of the slow dynamics of the original system, i.e. the dynamics governed by the non-hyperbolic state in terms of the slowly varying amplitude. Indeed, for sufficiently large time the dynamics of the system produce nonlinear dynamics led by the non-hyperbolic state, as there exists at least one mode which is not attracted exponentially to a stable equilibrium solution.

This being said, it can be assumed that the amplitude  $\mathcal{A}$  of the perturbation in the neighbourhood of the critical point depends on  $p$  slowly varying time scales and  $q$  slowly varying spatial scales by the functional relation

$$\mathcal{A} = \mathcal{A}(T_1, T_2, \dots, T_p, X_1, X_2, \dots, X_q), \quad (5.47)$$

with  $T_k = \epsilon^k t$ ,  $X_k = \epsilon^k x$  and  $\epsilon$  the usual control parameter. As a consequence, the derivatives of the amplitude are given by

$$\begin{aligned} \partial_t \mathcal{A} &= (\epsilon \partial_{T_1} + \epsilon^2 \partial_{T_2} + \dots + \epsilon^p \partial_{T_p}) \mathcal{A}, \\ \partial_x \mathcal{A} &= (\epsilon \partial_{X_1} + \epsilon^2 \partial_{X_2} + \dots + \epsilon^q \partial_{X_q}) \mathcal{A}, \\ \partial_x^2 \mathcal{A} &= (\epsilon \partial_{X_1} + \epsilon^2 \partial_{X_2} + \dots + \epsilon^q \partial_{X_q})^2 \mathcal{A} \\ &= (\epsilon^2 \partial_{X_1}^2 + \epsilon^3 2 \partial_{X_1} \partial_{X_2} + \dots) \mathcal{A}. \end{aligned} \quad (5.48)$$

In the real coefficients case, the G-L equation reads as

$$\begin{aligned} \partial_t \mathcal{A}(x, t) &= \left( \frac{\partial \sigma(\mathcal{R}_c, \beta_c)}{\partial \mathcal{R}} (\mathcal{R} - \mathcal{R}_c) + \frac{1}{2} \frac{\partial^2 \sigma(\mathcal{R}_c, \beta_c)}{\partial \beta^2} (\beta - \beta_c)^2 + \dots \right) \int_0^{+\infty} \hat{u}(\beta) e^{\sigma_{app}(\mathcal{R}, \beta)t + i(\beta - \beta_c)x} d\beta \\ &= \frac{\partial \sigma(\mathcal{R}_c, \beta_c)}{\partial \mathcal{R}} (\mathcal{R} - \mathcal{R}_c) \mathcal{A} - \frac{1}{2} \frac{\partial^2 \sigma(\mathcal{R}_c, \beta_c)}{\partial \beta^2} \partial_x^2 \mathcal{A}. \end{aligned} \quad (5.49)$$

Therefore, calling  $\mathcal{R} - \mathcal{R}_c = \epsilon^2$ , by substituting the derivatives previously exploited we can write

$$(\epsilon \partial_{T_1} + \epsilon^2 \partial_{T_2} + \dots + \epsilon^p \partial_{T_p}) \mathcal{A} = \frac{\partial \sigma(\mathcal{R}_c, \beta_c)}{\partial \mathcal{R}} \epsilon^2 \mathcal{A} - \frac{1}{2} \frac{\partial^2 \sigma(\mathcal{R}_c, \beta_c)}{\beta^2} (\epsilon^2 \partial_{X_1}^2 + 2\epsilon^3 \partial_{X_1} \partial_{X_2} + \dots) \mathcal{A} - \kappa \mathcal{A} |\mathcal{A}|^2. \quad (5.50)$$

It is worthy to notice that the only term which has no dependence on  $\epsilon$  is the nonlinear one. In order to balance the order of magnitude of the terms in the expression we also expand the amplitude in series of  $\epsilon$ . However, the expansion must respect the constraint for the invariance of the equation by a rotation in the complex plane. This implies that the only terms that enter the expansion are the odd terms. Thus we can write

$$\mathcal{A} = \epsilon A + \epsilon^3 A |A|^2 + \epsilon^5 A |A|^4 + \epsilon^7 A |A|^6 + \dots \quad (5.51)$$

By inserting the expansion in equation (5.50) and by collecting all the terms at every power of  $\epsilon$ , we find, up to third order in  $\epsilon$

$$\begin{aligned} \partial_{T_1} A &= 0, \\ \partial_{T_2} A &= \frac{\partial \sigma(\mathcal{R}_c, \beta_c)}{\partial \mathcal{R}} A - \frac{1}{2} \frac{\partial^2 \sigma(\mathcal{R}_c, \beta_c)}{\partial \beta^2} \partial_{X_1}^2 A - \kappa A |\mathcal{A}|^2. \end{aligned} \quad (5.52)$$

From the first of the two equations, the amplitude does not depend on the time scale  $T_1$ . This is in accordance with the fact that the marginally stable state is stationary. Physically, this means that for times of order less than  $\epsilon^{-1}$ , the solution is still stationary. Only after a time of

order  $\epsilon^{-2}$ , the solution may become unsteady and its evolution is given by the second equation of the (5.52).

Concerning instead the complex G–L equation, it reads

$$\partial_t \mathcal{A} + c_g \partial_x \mathcal{A} = \left( \frac{\partial \sigma(\mathcal{R}_c, \beta_c)}{\partial \mathcal{R}} - i \frac{\partial \omega(\mathcal{R}_c, \beta_c)}{\partial \mathcal{R}} \right) (\mathcal{R} - \mathcal{R}_c) \mathcal{A} + \left( \frac{i}{2} \omega_c'' - \frac{1}{2} \frac{\partial^2 \sigma(\mathcal{R}_c, \beta_c)}{\partial \beta^2} \right) \partial_x^2 \mathcal{A} - \kappa \mathcal{A} |\mathcal{A}|^2. \quad (5.53)$$

By exploiting the time derivatives up to second order and the space derivatives up to first order and by equalling the terms at the various powers of  $\epsilon$ , we get the system of equations

$$\begin{aligned} \partial_{T_1} \mathcal{A} &= -c_g \partial_{X_1} \mathcal{A}, \\ \partial_{T_2} \mathcal{A} &= \left( \frac{\partial \sigma(\mathcal{R}_c, \beta_c)}{\partial \mathcal{R}} - i \frac{\partial \omega(\mathcal{R}_c, \beta_c)}{\partial \mathcal{R}} \right) \mathcal{A} + \left( \frac{i}{2} \omega_c'' - \frac{1}{2} \frac{\partial^2 \sigma(\mathcal{R}_c, \beta_c)}{\partial \beta^2} \right) \partial_{X_1}^2 \mathcal{A} - \kappa \mathcal{A} |\mathcal{A}|^2. \end{aligned} \quad (5.54)$$

In this case, contrary to the previous one, as the marginally stable state is not stationary, we have that the right-hand side of the first equation is different from zero ( $c_g \neq 0$ ). Thus,  $\mathcal{A}$  depends both on  $T_1$  and  $T_2$ . Particularly, the first of the two equations can be solved by introducing the new variable  $\xi = X_1 - c_g T_1 = \epsilon(x - c_g t)$ , so that we can assume  $\mathcal{A} = \mathcal{A}(\xi, T_2)$ . By doing so, the first equation is automatically satisfied. The second equation becomes a parabolic equation in the variables  $(T_2, \xi)$  which reads

$$\partial_{T_2} \mathcal{A} = \left( \frac{\partial \sigma(\mathcal{R}_c, \beta_c)}{\partial \mathcal{R}} - i \frac{\partial \omega(\mathcal{R}_c, \beta_c)}{\partial \mathcal{R}} \right) \mathcal{A} + \left( \frac{i}{2} \omega_c'' - \frac{1}{2} \frac{\partial^2 \sigma(\mathcal{R}_c, \beta_c)}{\partial \beta^2} \right) \partial_\xi^2 \mathcal{A} - \kappa \mathcal{A} |\mathcal{A}|^2. \quad (5.55)$$

In the next paragraphs, we will apply the procedure shown in this section in order to obtain the Ginzburg–Landau equation for two partial differential problems: the first one is a model problem, the Swift–Hohenberg equation. The second one is related to the Navier–Stokes equations.

### 5.3.2 A model problem: the Swift–Hohenberg equation

As an example we consider a model problem, governed by a single partial differential equation, depending on the two variables  $t$  and  $x$ . The equation is called "Swift–Hohenberg equation", (S–H). The objective of this section is to formally derive the Ginzburg–Landau equation associated with the S–H equation, using the multiple-scale method.

This method consists in supposing that new variables can be introduced in the problem and such that they express the modulation in time and space of the amplitude of the perturbation. In this way, the unknown function will not depend only on the original variables, in this case the time  $t$  and the space  $x$ , but also on the other auxiliary variables just introduced. As we will rigorously show, with this method the Ginzburg–Landau equation arises from a solvability condition that the equation has to satisfy to get a bounded solution. Indeed, if this condition is not satisfied there would be some secular terms in the right-hand side of the equation that would cause a resonance condition, leading the solution to grow linearly in time. So, let us consider the following Swift–Hohenberg equation

$$\partial_t u + u \partial_x u + \partial_x^4 u + \mathcal{R} \partial_x^2 u + u = 0, \quad (5.56)$$

where  $\mathcal{R}$  is the control parameter, the equivalent of the Reynolds number in the Navier–Stokes equations. Let us suppose the equation to have a stationary equilibrium solution  $u_0 = 0$ . By linearizing the governing equation around this solution, we obtain

$$\partial_t u + \partial_x^4 u + \mathcal{R} \partial_x^2 u + u = 0. \quad (5.57)$$

We search for a solution as a travelling wave of the form  $u = Ae^{\sigma t + i\alpha x}$ , where  $\sigma$  represents the growth rate in time of the perturbation, while  $\alpha$  is the wavenumber along the homogeneous direction  $x$ . By substituting this assumption into the equation (5.57), the dispersion relation, see also figure 5.14, reads

$$\sigma + \alpha^4 - \mathcal{R}\alpha^2 + 1 = 0, \Rightarrow \sigma = -\alpha^4 + \mathcal{R}\alpha^2 - 1. \quad (5.58)$$

Now, as  $\alpha \in \mathbb{R}$ ,  $\sigma$  can be a function of real values only, so that the relation expressing the neutral curve is given by

$$\mathcal{R}(\alpha) = \alpha^2 + \frac{1}{\alpha^2}. \quad (5.59)$$

By applying the derivative of  $\mathcal{R}$  with respect to  $\alpha$ , we get the critical values of the control parameter and the wave number respectively

$$\frac{d\mathcal{R}}{d\alpha} = 2\alpha - \frac{2}{\alpha^3} = 0, \quad (5.60)$$

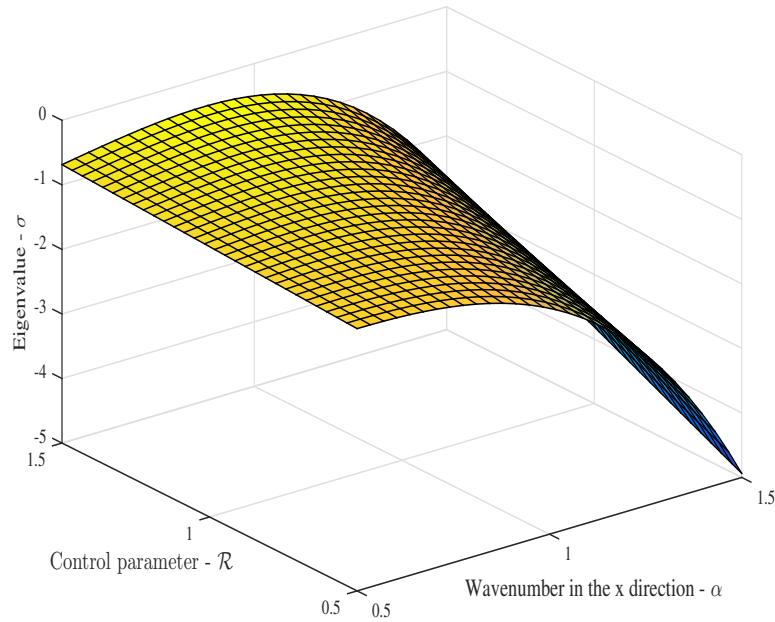
$$\Rightarrow \begin{cases} \alpha_c = 1, \\ \mathcal{R}_c = 2. \end{cases} \quad (5.61)$$

As shown before in paragraph 5.3.1, in a neighbourhood of the critical point  $(\mathcal{R}_c, \alpha_c) = (2, 1)$ , the dispersion relation can be approximated up to the second order like

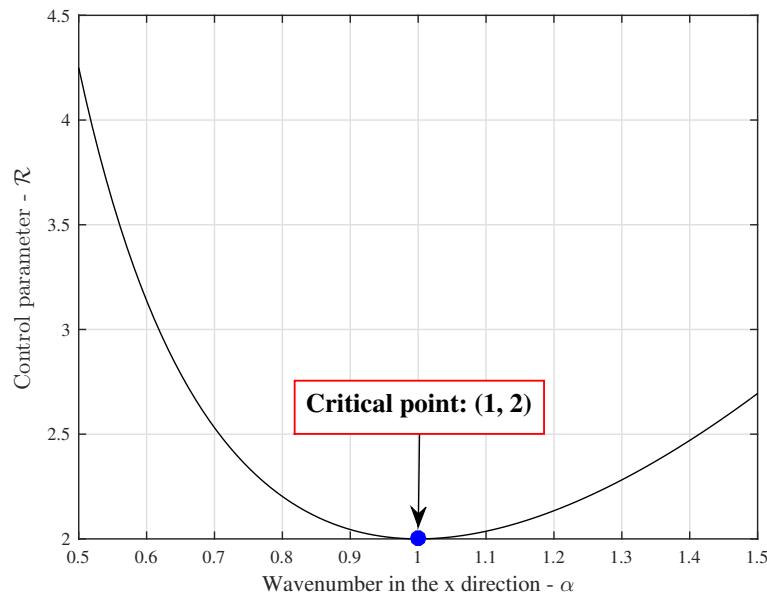
$$\sigma(\mathcal{R}, \alpha) = \frac{\partial \sigma(\mathcal{R}_c, \alpha_c)}{\partial \mathcal{R}} (\mathcal{R} - \mathcal{R}_c) + \frac{1}{2} \frac{\partial^2 \sigma(\mathcal{R}_c, \beta_c)}{\partial \alpha^2} (\alpha - \alpha_c)^2 + \mathcal{O}(\epsilon^2), \Rightarrow \sigma(\mathcal{R}, \alpha) = (\mathcal{R} - 2) - 4(\alpha - 1)^2. \quad (5.62)$$

By calling  $\mathcal{R} - \mathcal{R}_c = \epsilon^2$ , we have that  $\sigma \simeq \mathcal{O}(\epsilon^2)$ , and  $\alpha - \alpha_c \simeq \mathcal{O}(\epsilon)$ . Due to this, it is possible to introduce two slow scales: a slow time scale  $T = \epsilon^2 t$  and a "slow" length scale  $X = \epsilon x$ . The Swift–Hohenberg equation can be rewritten by exploiting the dependence on  $\epsilon$  and by adding and subtracting the term  $\mathcal{R}_c \partial_x^2 u$  as follows

$$\partial_t u + u \partial_x u + \partial_x^4 u + (\mathcal{R} - \mathcal{R}_c) \partial_x^2 u + u + \mathcal{R}_c \partial_x^2 u = 0. \quad (5.63)$$



(a) Dispersion surface.



(b) Neutral stability curve.

Figure 5.14: Dispersion surface  $\sigma(\mathcal{R}, \alpha)$  and neutral curve  $\mathcal{R}(\alpha)$ .

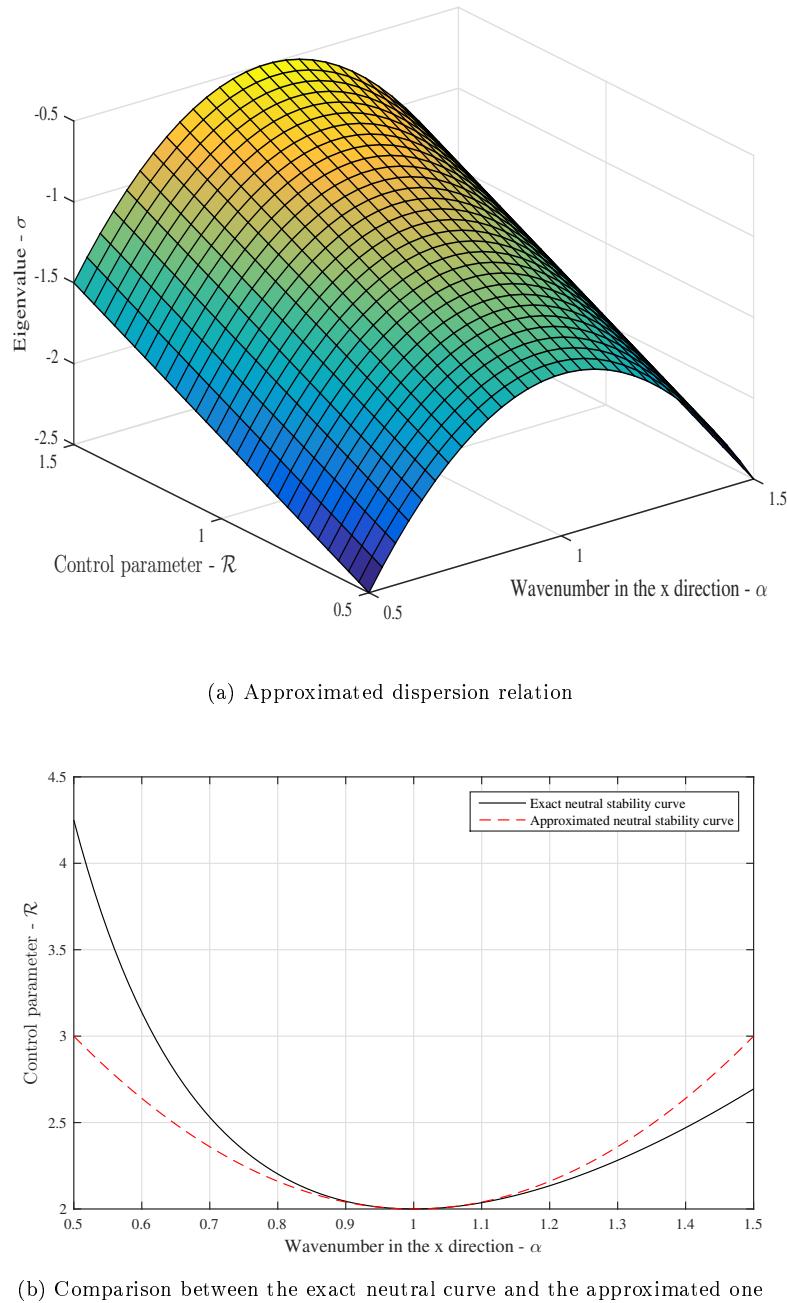


Figure 5.15: Approximated behaviour of the dispersion relation close to the critical point. Figure shows the approximated dispersion surface  $\sigma_{app}(\mathcal{R}, \beta)$  in the neighbourhood of the critical point  $(\beta_c, \mathcal{R}_c) = (1, 2)$ . Figure shows the approximated neutral curve  $\sigma_{app}(\mathcal{R}, \beta) = 0$ .

However, as  $\epsilon^2 = \mathcal{R} - \mathcal{R}_c$ , we can write the equation as

$$\partial_t u + u \partial_x u + \partial_x^4 u + \epsilon^2 \partial_x^2 u + u + \mathcal{R}_c \partial_x^2 u = 0. \quad (5.64)$$

At this point we expand the solution in series of  $\epsilon$  up to the third order. Reminding  $u_0 = 0$ , the expansion takes the form

$$u(T, x, X) = \epsilon u_1(T, x, X) + \epsilon^2 u_2(T, x, X) + \epsilon^3 u_3(T, x, X) + \mathcal{O}(\epsilon^4). \quad (5.65)$$

The derivatives become

$$\begin{aligned} \partial_t u &= \epsilon^3 \partial_T u_1 + \mathcal{O}(\epsilon^4), \\ u \partial_x u &= \epsilon^2 u_1 \partial_x u_1 + \epsilon^3 (u_1 \partial_X u_1 + u_1 \partial_x u_2 + u_2 \partial_x u_1) + \mathcal{O}(\epsilon^4), \\ \partial_x^2 u &= \epsilon \partial_x^2 u_1 + \epsilon^2 (2 \partial_x \partial_X u_1 + \partial_x^2 u_2) + \epsilon^3 (2 \partial_x \partial_X u_2 + \partial_X^2 u_1 + \partial_x^2 u_3) + \mathcal{O}(\epsilon^4), \\ \partial_x^4 u &= \epsilon \partial_x^4 u_1 + \epsilon^2 (4 \partial_x^3 \partial_X u_1 + \partial_x^4 u_2) + \epsilon^3 (6 \partial_x^2 \partial_X^2 u_1 + 4 \partial_x^3 \partial_X u_2 + \partial_x^4 u_3) + \mathcal{O}(\epsilon^4), \\ \epsilon^2 \partial_x^2 u &= \epsilon^3 \partial_x^2 u_1 + \mathcal{O}(\epsilon^4). \end{aligned} \quad (5.66)$$

By substituting the derivatives into the governing equation and collecting the term at different powers of  $\epsilon$ , we obtain at order  $\epsilon^1$

$$\partial_x^4 u_1 + \mathcal{R}_c \partial_x^2 u_1 + u_1 = 0, \quad (5.67)$$

but, as  $\mathcal{R}_c = 2$ , the general solution of the equation (5.67) is

$$u_1(T, x, X) = \mathcal{A}_1(T, X) e^{ix} + \mathcal{A}_1^*(T, X) e^{-ix}. \quad (5.68)$$

The term  $\mathcal{A}_1^*$  refers to the complex conjugate of the amplitude  $\mathcal{A}_1$ . In order to make shorter and clearer the notation, we call  $\mathcal{L}$  the linear operator such that  $\mathcal{L} = \partial_x^4 + 2\partial_x^2 + 1$ . By doing so, the governing equation at first order can be written in the form

$$\mathcal{L} u_1 = 0. \quad (5.69)$$

By proceeding we obtain that at order  $\epsilon^2$  the problem is governed by the following differential equation

$$\mathcal{L} u_2 = -u_1 \partial_x u_1 - (4 \partial_x^3 \partial_X u_1 + 4 \partial_x \partial_X u_1), \quad (5.70)$$

but, as  $4 \partial_x^3 \partial_X u_1 + 4 \partial_x \partial_X u_1 = 0$ , the equation (5.70) becomes

$$\mathcal{L} u_2 = -u_1 \partial_x u_1 \Rightarrow \mathcal{L} u_2 = -i \mathcal{A}_1^2 e^{2ix} + i \mathcal{A}_1^{*2} e^{-2ix}. \quad (5.71)$$

Therefore, at second order there are no secular terms and the solution consists of a general solution of the associated homogeneous equation and of a particular solution of the same equation, taking into account the forcing term which appears on the right-hand side. The final solution at this order is

$$u_2(T, x, X) = \mathcal{A}_2(T, X) e^{ix} + \mathcal{A}_2^*(T, X) e^{-ix} - \frac{i}{9} \mathcal{A}_1^2(T, X) e^{2ix} + \frac{i}{9} \mathcal{A}_1^{*2}(T, X) e^{-2ix}. \quad (5.72)$$

As the general solution of the equation (5.71) does not play a role in guiding the dynamics of the system, the functions  $\mathcal{A}_2$  and  $\mathcal{A}_2^*$  can be set equal to zero. Thus, the solution at the second order reduces to

$$u_2 = -\frac{i}{9} \mathcal{A}_1^2 e^{2ix} + \frac{i}{9} \mathcal{A}_1^{*2} e^{-2ix}. \quad (5.73)$$

Finally, by writing the problem at the final order in  $\epsilon$ , we find at order  $\epsilon^3$

$$\mathcal{L} u_3 = -\partial_T u_1 - u_1 \partial_X u_1 - \partial_x^2 u_1 - 2 \partial_X^2 u_1 - 6 \partial_x^2 \partial_X^2 u_1 - u_1 \partial_x u_2 - u_2 \partial_x u_1 - 4 \partial_x^3 \partial_X u_2 - 4 \partial_x \partial_X u_2. \quad (5.74)$$

By summing similar terms, we notice that the terms which give rise to resonance are given by

$$-\partial_T u_1 - \partial_x^2 u_1 + 4 \partial_X^2 u_1 - u_1 \partial_x u_2 - u_2 \partial_x u_1. \quad (5.75)$$

Particularly, by imposing these terms to be zero, we can find the following system of equation in the unknowns  $\mathcal{A}_1$  and  $\mathcal{A}^*_1$

$$\begin{cases} -\partial_T \mathcal{A}_1 + \mathcal{A}_1 + 4\partial_X^2 \mathcal{A}_1 - \frac{1}{9}\mathcal{A}_1^2 \mathcal{A}^*_1 = 0, \\ -\partial_T \mathcal{A}^*_1 + \mathcal{A}^*_1 + 4\partial_X^2 \mathcal{A}^*_1 - \frac{1}{9}\mathcal{A}_1 \mathcal{A}^{*2}_1 = 0, \end{cases} \quad (5.76)$$

where the second equation of the system is just the complex conjugate of the first one. Thus we are allowed to solve just the first equation, an by the fact that

$$\mathcal{A}_1^2 \mathcal{A}^*_1 = |\mathcal{A}_1|^2 \mathcal{A}_1, \quad (5.77)$$

and by simply calling  $\mathcal{A} = \mathcal{A}_1$ , the equation which expresses the dynamics of the amplitude is the Ginzburg–Landau equation that we had to find. It reads as

$$\partial_T \mathcal{A} = \mathcal{A} + 4\partial_X^2 \mathcal{A} - \frac{1}{9}\mathcal{A}|\mathcal{A}|^2. \quad (5.78)$$

Obviously, in order for the Ginzburg–Landau equation to have a unique solution, it must be equipped with appropriate boundary conditions and an initial condition. The equation deduced here, describes the dynamics of our original system in a neighbourhood of the critical point in the space of the parameters  $(\alpha_c, \mathcal{R}_c)$  associated with the fixed point  $u_0 = 0$ . Indeed, we can recognise in the coefficients of the linear terms of the G–L equation, the coefficients of the linearised dispersion relation. In fact, from equation (5.62) we have that

$$\begin{aligned} \frac{\partial \sigma(\mathcal{R}_c, \alpha_c)}{\partial \mathcal{R}} &= 1, \\ \frac{1}{2} \frac{\partial^2 \sigma(\mathcal{R}_c, \alpha_c)}{\partial \alpha^2} &= -4, \end{aligned} \quad (5.79)$$

that are in accordance with the properties that the coefficients of the G–L equation have to satisfy, as discussed in the previous paragraphs. It is worthy to notice that the G–L equation highlights the fact that the stability of the system does not depend only on its linear character, but the nonlinear terms that arise in the dynamics may change the stability of the whole system. This fact is clearly represented by the right-hand side of the equation, where, in addition to the linear terms, the non-linear term  $\frac{1}{9}\mathcal{A}|\mathcal{A}|^2$  appears. Particularly, as the Landau coefficient is positive, it is expected that the nonlinearity saturates the amplitude and the system reaches a new stable state of equilibrium for  $\mathcal{R} - \mathcal{R}_c \geq 0$ .

## 5.4 Weakly nonlinear expansion of the Navier–Stokes equations

In this paragraph, we want to adopt a procedure similar to that used to derive the Ginzburg–Landau equation for the Swift–Hohenberg model. However, now the difference is that we are dealing with a system of differential equations much more complex, namely the Navier–Stokes equations.

Firstly, in order to perform an asymptotic expansion of the Navier–Stokes equations, we begin by rewriting them in a convenient form, which also points out the dependence of the governing equations on the parameter  $\epsilon$  that will be used in the expansion. The equations in dimensionless form are defined by the following system

$$\begin{cases} \frac{\partial \mathbf{u}}{\partial t} + (\mathbf{u} \cdot \nabla) \mathbf{u} + \nabla p - \frac{1}{\mathcal{R}} \nabla^2 \mathbf{u} = 0, \\ \nabla \cdot \mathbf{u} = 0, \end{cases} \quad (5.80)$$

where  $\mathcal{R}$  stands for the Reynolds number of the flow. Now, in order to write the Navier–Stokes equation in a form similar to (5.64), we call  $\mathcal{R}_c$  the critical Reynolds number computed with the linear theory. It's reminded that at every critical Reynolds number is associated an axial critical wavenumber. In fact the relation  $\mathcal{R}_c = \min \mathcal{R}(\beta, \alpha) | \sigma(\mathcal{R}(\beta, \alpha)) = 0$  holds.

By adding and subtracting the quantity  $\frac{1}{\mathcal{R}_c} \nabla^2 \mathbf{u}$ , the Navier–Stokes equations can be written as

$$\begin{cases} \frac{\partial \mathbf{u}}{\partial t} + (\mathbf{u} \cdot \nabla) \mathbf{u} + \nabla p + \frac{(\mathcal{R} - \mathcal{R}_c)}{\mathcal{R} \mathcal{R}_c} \nabla^2 \mathbf{u} - \frac{1}{\mathcal{R}_c} \nabla^2 \mathbf{u} = 0, \\ \nabla \cdot \mathbf{u} = 0. \end{cases} \quad (5.81)$$

Now, we define  $g(\mathcal{R}) = \frac{(\mathcal{R} - \mathcal{R}_c)}{\mathcal{R} \mathcal{R}_c}$ . In the limit  $\mathcal{R} \rightarrow \mathcal{R}_c$ , we can expand  $g$  in Taylor series to have

$$\begin{aligned} g(\mathcal{R}) &= g(\mathcal{R}_c) + g'(\mathcal{R}_c)(\mathcal{R} - \mathcal{R}_c) + \mathcal{O}((\mathcal{R} - \mathcal{R}_c)^2), \\ &= \frac{1}{\mathcal{R}_c^2}(\mathcal{R} - \mathcal{R}_c) + \mathcal{O}((\mathcal{R} - \mathcal{R}_c)^2). \end{aligned} \quad (5.82)$$

In this case, we define  $\epsilon^2 = \frac{\mathcal{R} - \mathcal{R}_c}{\mathcal{R}_c}$ , so that the condition  $\epsilon \ll 1$  is satisfied. Thus, the expression (5.82) becomes

$$g(\mathcal{R}) = \frac{1}{\mathcal{R}_c} \epsilon^2 + \mathcal{O}((\mathcal{R} - \mathcal{R}_c)^2), \quad (5.83)$$

and the Navier–Stokes equations read

$$\begin{cases} \frac{\partial \mathbf{u}}{\partial t} + (\mathbf{u} \cdot \nabla) \mathbf{u} + \nabla p + \frac{\epsilon^2}{\mathcal{R}_c} \nabla^2 \mathbf{u} - \frac{1}{\mathcal{R}_c} \nabla^2 \mathbf{u} = 0, \\ \nabla \cdot \mathbf{u} = 0. \end{cases} \quad (5.84)$$

As discussed in the previous paragraphs, near the critical point, the eigenvalue  $s = \sigma(\mathcal{R}, \beta) - i\omega(\mathcal{R}, \beta)$  can be expanded in Taylor series at least up to the second order with a relation like

$$\begin{aligned} \sigma(\mathcal{R}, \beta) &= \frac{\partial \sigma(\mathcal{R}_c, \beta_c)}{\partial \mathcal{R}} (\mathcal{R} - \mathcal{R}_c) + \frac{1}{2} \frac{\partial^2 \sigma(\mathcal{R}_c, \beta_c)}{\partial \beta^2} (\beta - \beta_c)^2 + \mathcal{O}(\epsilon^2), \\ \omega(\mathcal{R}, \beta) &= \omega(\mathcal{R}_c, \beta_c) + \frac{\partial \omega(\mathcal{R}_c, \beta_c)}{\partial \beta} + \frac{1}{2} \frac{\partial^2 \omega(\mathcal{R}_c, \beta_c)}{\partial \beta^2} + \mathcal{O}(\epsilon^2), \end{aligned} \quad (5.85)$$

being  $\sigma(\mathcal{R}, \beta)$  and  $\frac{\partial \sigma(\mathcal{R}_c, \beta_c)}{\partial \beta}$  both null as the dispersion relation is tangent to the straight line  $\sigma = 0$ . From equation (5.85) it is clear that as  $\mathcal{R} - \mathcal{R}_c \sim \epsilon^2$ , then  $\beta - \beta_c \sim \epsilon$ . Hence we have that  $\sigma \simeq \mathcal{O}(\epsilon^2)$  while  $\beta \simeq \mathcal{O}(\epsilon)$ . Based on this dimensional analysis, we can introduce two slow scales: a slow time scale  $T = \epsilon^2 t$  and a slow spatial scale  $\mathbf{R} = (0, \eta, \xi) = \epsilon(0, \theta - \omega_g t, z - c_g t)$ , where  $\omega_g = \omega(\mathcal{R}_c, \beta_c)$ . We now proceed by deriving the Ginzburg–Landau equation in the more general case in which the critical eigenvalue has null real part, whereas the imaginary part is different from zero. This case is more general because it permits to include in the

formulation also those base flows which are marginally oscillatory and not necessary stationary. As a matter of fact, if the basic state is stationary it will be sufficient to set  $\omega(\mathcal{R}_c, \beta_c) = \omega_c = 0$ ,  $\frac{\partial \omega(\mathcal{R}_c, \beta_c)}{\partial \beta} = c_g = 0$  and perform the same analysis as well. It is reminded that in the case the equilibrium state is stationary, the explicit dependence of the solution on the fast time  $t$  disappears. Therefore, in the general case we can write

$$\begin{aligned}\mathbf{u} &= \mathbf{u}(t, T, \mathbf{r}, \mathbf{R}), \\ p &= p(t, T, \mathbf{r}, \mathbf{R}).\end{aligned}\tag{5.86}$$

By expanding the velocity and pressure fields in series of  $\epsilon$ , at the third order for simplicity, we have

$$\begin{aligned}\mathbf{u} &= \mathbf{u}_0(\mathbf{r}) + \epsilon \mathbf{u}_1(t, T, \mathbf{r}, \mathbf{R}) + \epsilon^2 \mathbf{u}_2(t, T, \mathbf{r}, \mathbf{R}) + \epsilon^3 \mathbf{u}_3(t, T, \mathbf{r}, \mathbf{R}) + \mathcal{O}(\epsilon^4), \\ p &= p_0(\mathbf{r}) + \epsilon p_1(t, T, \mathbf{r}, \mathbf{R}) + \epsilon^2 p_2(t, T, \mathbf{r}, \mathbf{R}) + \epsilon^3 p_3(t, T, \mathbf{r}, \mathbf{R}) + \mathcal{O}(\epsilon^4).\end{aligned}\tag{5.87}$$

The differential operators become

$$\begin{aligned}\partial_t &= \partial_t - \epsilon (\omega_g \partial_\eta + c_g \partial_\xi) + \epsilon^2 \partial_T, \\ \nabla &= \nabla + \epsilon \nabla_\diamond, \\ \nabla^2 &= \nabla^2 + 2\epsilon L_\diamond + \epsilon^2 \nabla_\diamond^2,\end{aligned}\tag{5.88}$$

where  $\nabla_\diamond = \frac{\partial}{\partial \mathbf{R}} = \left(0, \frac{1}{r} \frac{\partial}{\partial \eta}, \frac{\partial}{\partial \xi}\right)$ ,  $\nabla_\diamond^2 = \frac{1}{r^2} \frac{\partial^2}{\partial \eta^2} + \frac{\partial^2}{\partial \xi^2}$ , while the operator  $L_\diamond$  reads as

$$L_\diamond = \begin{pmatrix} \frac{1}{r^2} \frac{\partial^2}{\partial \theta \partial \eta} + \frac{\partial^2}{\partial z \partial \xi}, & -\frac{1}{r^2} \frac{\partial}{\partial \eta}, & 0 \\ \frac{1}{r^2} \frac{\partial}{\partial \eta}, & \frac{1}{r^2} \frac{\partial^2}{\partial \theta \partial \eta} + \frac{\partial^2}{\partial z \partial \xi}, & 0 \\ 0, & 0, & \frac{1}{r^2} \frac{\partial^2}{\partial \theta \partial \eta} + \frac{\partial^2}{\partial z \partial \xi} \end{pmatrix}.\tag{5.89}$$

By exploiting the derivatives along the different spatial directions and with respect to time, we obtain

$$\partial_t \mathbf{u} = \epsilon \partial_t \mathbf{u}_1 + \epsilon^2 [\partial_t \mathbf{u}_2 - (\omega_g \partial_\eta \mathbf{u}_1 + c_g \partial_\xi \mathbf{u}_1)] + \epsilon^3 [\partial_t \mathbf{u}_3 - (\omega_g \partial_\eta \mathbf{u}_2 + c_g \partial_\xi \mathbf{u}_2) + \partial_T \mathbf{u}_1] + \mathcal{O}(\epsilon^4),$$

$$\begin{aligned}(\mathbf{u} \cdot \nabla) \mathbf{u} &= (\mathbf{u}_0 \cdot \nabla) \mathbf{u}_0 + \epsilon [(\mathbf{u}_0 \cdot \nabla) \mathbf{u}_1 + (\mathbf{u}_1 \cdot \nabla) \mathbf{u}_0] + \epsilon^2 [(\mathbf{u}_0 \cdot \nabla_\diamond) \mathbf{u}_1 + (\mathbf{u}_0 \cdot \nabla) \mathbf{u}_2 + (\mathbf{u}_2 \cdot \nabla) \mathbf{u}_0 + (\mathbf{u}_1 \cdot \nabla) \mathbf{u}_1] \\ &\quad + \epsilon^3 [(\mathbf{u}_0 \cdot \nabla_\diamond) \mathbf{u}_2 + (\mathbf{u}_0 \cdot \nabla) \mathbf{u}_3 + (\mathbf{u}_1 \cdot \nabla_\diamond) \mathbf{u}_1 + (\mathbf{u}_1 \cdot \nabla) \mathbf{u}_2 + (\mathbf{u}_2 \cdot \nabla) \mathbf{u}_1 + (\mathbf{u}_3 \cdot \nabla) \mathbf{u}_0] + \mathcal{O}(\epsilon^4),\end{aligned}$$

$$\nabla p = \nabla p_0 + \epsilon \nabla p_1 + \epsilon^2 [\nabla_\diamond p_1 + \nabla p_2] + \epsilon^3 [\nabla_\diamond p_2 + \nabla p_3] + \mathcal{O}(\epsilon^4),$$

$$\begin{aligned}\nabla^2 \mathbf{u} &= \nabla^2 \mathbf{u}_0 + \epsilon \nabla^2 \mathbf{u}_1 + \epsilon^2 [\nabla^2 \mathbf{u}_2 + 2L_\diamond \mathbf{u}_1] \\ &\quad + \epsilon^3 [\nabla^2 \mathbf{u}_3 + 2L_\diamond \mathbf{u}_2 + \nabla_\diamond^2 \mathbf{u}_1] + \mathcal{O}(\epsilon^4),\end{aligned}$$

$$\nabla \cdot \mathbf{u} = \nabla \cdot \mathbf{u}_0 + \epsilon \nabla \cdot \mathbf{u}_1 + \epsilon^2 [\nabla \cdot \mathbf{u}_2 + \nabla_\diamond \cdot \mathbf{u}_1] + \epsilon^3 [\nabla \cdot \mathbf{u}_3 + \nabla_\diamond \cdot \mathbf{u}_2].\tag{5.90}$$

We put these expressions in the equations (5.84) and we collect the terms with equal exponents of  $\epsilon$ . At the order  $\epsilon^0$  we have the base flow equations

$$\begin{cases} (\mathbf{u}_0 \cdot \nabla) \mathbf{u}_0 + \nabla p_0 - \frac{1}{\mathcal{R}_c} \nabla^2 \mathbf{u}_0 = 0, \\ \nabla \cdot \mathbf{u}_0 = 0, \end{cases}\tag{5.91}$$

whose solution gives the Taylor–Couette flow. We define the differential operator  $\mathcal{L}$  such that

$$\mathcal{L} = \begin{pmatrix} \partial_t + (\mathbf{u}_0 \cdot \nabla) + (\dots \cdot \nabla) \mathbf{u}_0 - \frac{1}{\mathcal{R}_c} \nabla^2, & \nabla \\ \nabla \cdot, & 0 \end{pmatrix}.\tag{5.92}$$

By developing the problems to the higher orders, we obtain at order  $\epsilon$

$$\mathcal{L} \begin{pmatrix} \mathbf{u}_1 \\ p_1 \end{pmatrix} = 0. \quad (5.93)$$

The problem (5.93) is related to the linear stability of the base flow. At order  $\epsilon^2$ , we have

$$\mathcal{L} \begin{pmatrix} \mathbf{u}_2 \\ p_2 \end{pmatrix} = \begin{pmatrix} (\omega_g \partial_\eta + c_g \partial_\xi) \mathbf{u}_1 - (\mathbf{u}_0 \cdot \nabla_\diamond) \mathbf{u}_1 - (\mathbf{u}_1 \cdot \nabla) \mathbf{u}_1 - \nabla_\diamond p_1 + \frac{1}{\mathcal{R}_c} \nabla^2 \mathbf{u}_0 + \frac{2}{\mathcal{R}_c} L_\diamond \mathbf{u}_1 \\ -\nabla_\diamond \cdot \mathbf{u}_1 \end{pmatrix}. \quad (5.94)$$

At order  $\epsilon^3$ , we have

$$\mathcal{L} \begin{pmatrix} \mathbf{u}_3 \\ p_3 \end{pmatrix} = \begin{pmatrix} (\omega_g \partial_\eta + c_g \partial_\xi) \mathbf{u}_2 - \partial_T \mathbf{u}_1 - (\mathbf{u}_0 \cdot \nabla_\diamond) \mathbf{u}_2 - (\mathbf{u}_1 \cdot \nabla_\diamond) \mathbf{u}_1 - (\mathbf{u}_1 \cdot \nabla) \mathbf{u}_2 - (\mathbf{u}_2 \cdot \nabla) \mathbf{u}_1 \\ -\nabla_\diamond p_2 - \frac{1}{\mathcal{R}_c} \nabla^2 \mathbf{u}_1 + \frac{1}{\mathcal{R}_c} (2L_\diamond \mathbf{u}_2 + \nabla_\diamond^2 \mathbf{u}_1) \\ -\nabla_\diamond \cdot \mathbf{u}_2 \end{pmatrix}. \quad (5.95)$$

#### 5.4.1 Resolution of the systems at the different orders

At this point, we want to solve the problem by finding the solution of the three systems obtained before; a solution that will give us the Ginzburg–Landau equation for the Taylor–Couette flow. Let us start with the system at first order. As mentioned before, it is equivalent to the system that describes the linear stability of the flow, so we can assume in a completely general way that the shape of the solution is given by the following velocity and pressure fields

$$\begin{aligned} \mathbf{u}_1 &= \mathcal{A}_1(T, \eta, \xi) \psi_1(r) e^{-i\omega_c t + i\alpha_c \theta + i\beta_c z} + \mathcal{A}_1^*(T, \eta, \xi) \psi_1^*(r) e^{i\omega_c t - i\alpha_c \theta - i\beta_c z}, \\ p_1 &= \mathcal{A}_1(T, \eta, \xi) \phi_1(r) e^{-i\omega_c t + i\alpha_c \theta + i\beta_c z} + \mathcal{A}_1^*(T, \eta, \xi) \phi_1^*(r) e^{i\omega_c t - i\alpha_c \theta - i\beta_c z}, \end{aligned} \quad (5.96)$$

where the following quantities have been introduced:

- $\mathcal{A}_1$  is the function that expresses the modulation in the amplitude of the perturbations, for both velocity and pressure. As discussed earlier, it represents the envelope of the wavepacket centred in the critical wavenumber.  $\mathcal{A}_1^*$  is its complex conjugate.
- $(s_c, \psi_1(r), \phi_1(r))$  represents the general solution of the first order problem, i.e. the solution coming from the linear stability analysis. In particular the critical eigenvalue  $s_c = i\omega_c$  and  $(\psi_1(r), \phi_1(r))$  are the corresponding eigenvectors.
- $\omega_c, \alpha_c, \beta_c$  represent the critical frequency, the azimuthal critical wavenumber and the axial critical wavenumber, respectively. In particular,  $\omega_c \equiv \omega_g = \omega(\mathcal{R}_c, \beta_c)$ .

From now on, to simplify the notation, we will avoid the explicit dependence of the amplitude on the variables  $T, \eta, \xi$ ; moreover, we will indicate with  $e^\pm$  the exponential term  $e^{\pm(-i\omega_c + i\alpha_c \theta + i\beta_c z)}$ . This being said, we search a solution of the second order system, which is rewritten here for convenience,

$$\mathcal{L} \begin{pmatrix} \mathbf{u}_2 \\ p_2 \end{pmatrix} = \begin{pmatrix} (\omega_g \partial_\eta + c_g \partial_\xi) \mathbf{u}_1 - (\mathbf{u}_0 \cdot \nabla_\diamond) \mathbf{u}_1 - (\mathbf{u}_1 \cdot \nabla) \mathbf{u}_1 - \nabla_\diamond p_1 + \nabla^2 \mathbf{u}_0 + \frac{2}{\mathcal{R}_c} L_\diamond \mathbf{u}_1 \\ -\nabla_\diamond \cdot \mathbf{u}_1 \end{pmatrix}. \quad (5.97)$$

As it can be seen from the expression (5.97), the right-hand side is composed of various terms, some of them are going to give rise to secular terms. In particular these will be the one proportional to  $e^\pm$ . By analysing them separately, we have

$$(\omega_g \partial_\eta + c_g \partial_\xi) \mathbf{u}_1 = \left( \omega_g \frac{\partial \mathcal{A}_1}{\partial \eta} + c_g \frac{\partial \mathcal{A}_1}{\partial \xi} \right) \psi_1 e^+ + \left( \omega_g \frac{\partial \mathcal{A}_1^*}{\partial \eta} + c_g \frac{\partial \mathcal{A}_1^*}{\partial \xi} \right) \psi_1^* e^-,$$

$$(\mathbf{u}_0 \cdot \nabla_\diamond) \mathbf{u}_1 = \frac{U(r)}{r} \frac{\partial \mathbf{u}_1}{\partial \eta} = \frac{U(r)}{r} \frac{\partial \mathcal{A}_1}{\partial \eta} \psi_1 e^+ + \frac{U(r)}{r} \frac{\partial \mathcal{A}_1^*}{\partial \eta} \psi_1^* e^-,$$

$$\begin{aligned} (\mathbf{u}_1 \cdot \nabla) \mathbf{u}_1 &= (\mathcal{A}_1 \psi_1 e^+ + \mathcal{A}_1^* \psi_1^* e^-) \cdot \nabla (\mathcal{A}_1 \psi_1 e^+ + \mathcal{A}_1^* \psi_1^* e^-) \\ &= \mathcal{A}_1^2 (\psi_1 \cdot \nabla) \psi_1 e^{2+} + |\mathcal{A}_1|^2 [(\psi_1 \cdot \nabla) \psi_1^* + (\psi_1^* \cdot \nabla) \psi_1] + (\mathcal{A}_1^*)^2 (\psi_1^* \cdot \nabla) \psi_1 e^{2-}, \end{aligned}$$

$$\nabla_\diamond p_1 = (\nabla_\diamond \mathcal{A}_1) \phi_1 e^+ + (\nabla_\diamond \mathcal{A}_1^*) \phi_1^* e^-,$$

$$\nabla^2 \mathbf{u}_0 = 0,$$

$$\begin{aligned} \frac{2}{\mathcal{R}_c} L_\diamond \mathbf{u}_1 &= \frac{2}{\mathcal{R}_c} \begin{pmatrix} \frac{1}{r^2} \frac{\partial^2 u_{1r}}{\partial \theta \partial \eta} + \frac{\partial^2 u_{1r}}{\partial z \partial \xi} - \frac{1}{r^2} \frac{\partial u_{1\theta}}{\partial \eta} \\ \frac{1}{r^2} \frac{\partial u_{1r}}{\partial \eta} + \frac{1}{r^2} \frac{\partial^2 u_{1\theta}}{\partial \theta \partial \eta} + \frac{\partial^2 u_{1\theta}}{\partial z \partial \xi} \\ \frac{1}{r^2} \frac{\partial^2 u_{1z}}{\partial \theta \partial \eta} + \frac{\partial^2 u_{1z}}{\partial z \partial \xi} \end{pmatrix} \\ &= \frac{2}{\mathcal{R}_c} \begin{pmatrix} \left[ \left( \frac{i\alpha_c}{r^2} \frac{\partial \mathcal{A}_1}{\partial \eta} + i\beta_c \frac{\partial \mathcal{A}_1}{\partial \xi} \right) \psi_{1r} - \frac{1}{r^2} \frac{\partial \mathcal{A}_1}{\partial \eta} \psi_{1\theta} \right] e^+ - \left[ \left( \frac{i\alpha_c}{r^2} \frac{\partial \mathcal{A}_1^*}{\partial \eta} + i\beta_c \frac{\partial \mathcal{A}_1^*}{\partial \xi} \right) \psi_{1r}^* + \frac{1}{r^2} \frac{\partial \mathcal{A}_1^*}{\partial \eta} \psi_{1\theta}^* \right] e^- \\ \left[ \left( \frac{i\alpha_c}{r^2} \frac{\partial \mathcal{A}_1}{\partial \eta} + i\beta_c \frac{\partial \mathcal{A}_1}{\partial \xi} \right) \psi_{1\theta} + \frac{1}{r^2} \frac{\partial \mathcal{A}_1}{\partial \eta} \psi_{1r} \right] e^+ - \left[ \left( \frac{i\alpha_c}{r^2} \frac{\partial \mathcal{A}_1^*}{\partial \eta} + i\beta_c \frac{\partial \mathcal{A}_1^*}{\partial \xi} \right) \psi_{1\theta}^* - \frac{1}{r^2} \frac{\partial \mathcal{A}_1^*}{\partial \eta} \psi_{1r}^* \right] e^- \\ \left[ \left( \frac{i\alpha_c}{r^2} \frac{\partial \mathcal{A}_1}{\partial \eta} + i\beta_c \frac{\partial \mathcal{A}_1}{\partial \xi} \right) \psi_{1z} \right] e^+ - \left[ \left( \frac{i\alpha_c}{r^2} \frac{\partial \mathcal{A}_1^*}{\partial \eta} + i\beta_c \frac{\partial \mathcal{A}_1^*}{\partial \xi} \right) \psi_{1z}^* \right] e^- \end{pmatrix} \\ &= \frac{2}{\mathcal{R}_c} \left[ \left( \frac{i\alpha_c}{r^2} \frac{\partial \mathcal{A}_1}{\partial \eta} + i\beta_c \frac{\partial \mathcal{A}_1}{\partial \xi} \right) \psi_1 + \frac{1}{r^2} \frac{\partial \mathcal{A}_1}{\partial \eta} \psi_{1\perp} \right] e^+ \\ &\quad - \frac{2}{\mathcal{R}_c} \left[ \left( \frac{i\alpha_c}{r^2} \frac{\partial \mathcal{A}_1^*}{\partial \eta} + i\beta_c \frac{\partial \mathcal{A}_1^*}{\partial \xi} \right) \psi_1^* + \frac{1}{r^2} \frac{\partial \mathcal{A}_1^*}{\partial \eta} \psi_{1\perp}^* \right] e^-, \\ \nabla_\diamond \cdot \mathbf{u}_1 &= \left( \frac{1}{r} \frac{\partial \mathcal{A}_1}{\partial \eta} \psi_{1\theta} + \frac{\partial \mathcal{A}_1}{\partial \xi} \psi_{1z} \right) e^+ + \left( \frac{1}{r} \frac{\partial \mathcal{A}_1^*}{\partial \eta} \psi_{1\theta}^* + \frac{\partial \mathcal{A}_1^*}{\partial \xi} \psi_{1z}^* \right) e^-. \end{aligned} \tag{5.98}$$

The secular terms that appear at the right side are those proportional to  $e^\pm$  and can give rise to resonant modes. Therefore these terms must be set equal to zero, as we are looking for a solution that remains bounded in time and space. To do this, we need to take advantage of Fredholm's alternative. We proceed as follows: given the linear problem  $\mathcal{L}(\mathbf{u}_1, p_1) = 0$ , we define the adjoint problem as

$$\int_V (\mathbf{u}_1^a, p_1^a)^T \mathcal{L}(\mathbf{u}_1, p_1) = \int_V (\mathbf{u}_1, p_1)^T \mathcal{L}^*(\mathbf{u}_1^a, p_1^a). \tag{5.99}$$

where  $\mathcal{L}^*$  is the adjoint operator of  $\mathcal{L}$ . Now, due to the fact that  $\mathcal{L}(\mathbf{u}_1, p_1) = 0$ , we have also that the corresponding adjoint problem have to be null, i.e.

$$\int_V (\mathbf{u}_1, p_1)^T \mathcal{L}^*(\mathbf{u}_1^a, p_1^a) = 0. \tag{5.100}$$

Obviously, in order for the adjoint problem to admit a unique solution, suitable boundary conditions have to be imposed. These boundary conditions are derived directly from the weak formulation of the original linear problem by annihilating the bilinear concomitant [24]. In our case the adjoint problem takes the form

$$\begin{cases} \mathcal{L}^*(\mathbf{u}_1^a, p_1^a) = 0, \\ \mathbf{u}_1^a|_{r=a,b} = 0, \quad \forall \theta, z \in \mathbb{R}. \end{cases} \quad (5.101)$$

As concerns our particular problem, since it is invariant with respect to the azimuthal and axial directions, the integration on the whole three-dimensional domain reduces to an integration along the radial direction only. Hence, in order to cancel the secular terms out from the original problem, Fredholm's alternative is exploited. Fredholm's alternative states that in order for a linear system to admit a solution, it is necessary that its right hand side is orthogonal to the Kernel of the corresponding adjoint problem. For this reason, by multiplying the sequence of terms proportional to  $e^{\pm(-i\omega_c t + i\alpha_c \theta + \beta_c z)}$  by the adjoint critical eigenmodes, integrating along  $r$  and setting the integral equal to zero, we obtain the solvability condition of the problem.

Going back to our second order problem, the solvability condition referred to the secular terms proportional to  $e^{-i\omega_c t + i\alpha_c \theta + i\beta_c z}$  is given by

$$\begin{aligned} \int_a^b \psi_1^a \cdot \left[ \left( \omega_g \frac{\partial \mathcal{A}_1}{\partial \eta} + c_g \frac{\partial \mathcal{A}_1}{\partial \xi} \right) \psi_1 - \frac{U}{r} \frac{\partial \mathcal{A}_1}{\partial \eta} \psi_1 + \frac{2}{\mathcal{R}_c} \left( \frac{i\alpha_c}{r^2} \frac{\partial \mathcal{A}_1}{\partial \eta} + i\beta_c \frac{\partial \mathcal{A}_1}{\partial \xi} \right) \psi_1 - \phi_1 \nabla_\diamond \mathcal{A}_1 + \frac{2}{\mathcal{R}_c} r^2 \frac{\partial \mathcal{A}_1}{\partial \eta} \psi_{1\perp} \right] \\ + \int_a^b \phi_1^a \left[ \frac{1}{r} \frac{\partial \mathcal{A}_1}{\partial \eta} \psi_{1\theta} + \frac{\partial \mathcal{A}_1}{\partial \xi} \psi_{1z} \right] = 0, \end{aligned} \quad (5.102)$$

having omitted the differential symbol  $dr$  for notation consistency. For the corresponding complex conjugate terms, the ones proportional to  $e^{i\omega_c t - i\alpha_c \theta - i\beta_c z}$ , the solvability condition implies

$$\begin{aligned} \int_a^b (\psi_1^a)^* \cdot \left[ \left( \omega_g \frac{\partial \mathcal{A}_1^*}{\partial \eta} + c_g \frac{\partial \mathcal{A}_1^*}{\partial \xi} \right) - \frac{U}{r} \frac{\partial \mathcal{A}_1^*}{\partial \eta} + 2\mathcal{R}_c \left( \frac{i\alpha_c}{r^2} \frac{\partial \mathcal{A}_1^*}{\partial \eta} + i\beta_c \frac{\partial \mathcal{A}_1^*}{\partial \xi} \right) \psi_1^* - \phi_1^* \nabla_\diamond \mathcal{A}_1^* - 2 \frac{\mathcal{R}_c}{r^2} \frac{\partial \mathcal{A}_1^*}{\partial \eta} \psi_{1\perp}^* \right] \\ + \int_a^b (\phi_1^a)^* \left[ \frac{1}{r} \frac{\partial \mathcal{A}_1^*}{\partial \eta} \psi_{1\theta}^* + \frac{\partial \mathcal{A}_1^*}{\partial \xi} \psi_{1z}^* \right] = 0. \end{aligned} \quad (5.103)$$

Having deleted the resonant terms from the problem, the second order problem reduces to find a solution of the form  $(\mathbf{u}_2, p_2)$  such that

$$\mathcal{L} \begin{pmatrix} \mathbf{u}_2 \\ p_2 \end{pmatrix} = \begin{pmatrix} -\mathcal{A}_1^2 (\psi_1 \cdot \nabla) \psi_1 e^{2+} - |\mathcal{A}_1|^2 [(\psi_1 \cdot \nabla) \psi_1^* + (\psi_1^* \cdot \nabla) \psi_1] - (\mathcal{A}_1^*)^2 (\psi_1^* \cdot \nabla) \psi_1^* e^{2-} \\ 0 \end{pmatrix}. \quad (5.104)$$

The solution can generally be written as

$$\begin{cases} \mathbf{u}_2 = \mathcal{A}_1^2 \psi_2 e^{2+} + |\mathcal{A}_1|^2 \psi_2^{(0)} + (\mathcal{A}_1^*)^2 \psi_2^* e^{2+}, \\ p_2 = \mathcal{A}_1^2 \phi_2 e^{2+} + |\mathcal{A}_1|^2 \phi_2^{(0)} + (\mathcal{A}_1^*)^2 \phi_2^* e^{2-}, \end{cases} \quad (5.105)$$

where, reminding that  $e^{2\pm} = e^{\pm(-2i\omega_c t + 2i\alpha_c \theta + 2i\beta_c z)}$ , the functions  $(\psi_2, \phi_2), (\psi_2^*, \phi_2^*)$  can be computed by solving the differential problems

$$\mathcal{L} \begin{pmatrix} \psi_2 \\ \phi_2 \end{pmatrix} = \begin{pmatrix} -(\psi_1 \cdot \nabla) \psi_1 \\ 0 \end{pmatrix}, \quad (5.106)$$

$$\mathcal{L} \begin{pmatrix} \psi_2^{(0)} \\ \phi_2^{(0)} \end{pmatrix} = \begin{pmatrix} -|\mathcal{A}_1|^2 [(\psi_1 \cdot \nabla) \psi_1^* + (\psi_1^* \cdot \nabla) \psi_1] \\ 0 \end{pmatrix}, \quad (5.107)$$

$$\mathcal{L} \begin{pmatrix} \psi_2^* \\ \phi_2^* \end{pmatrix} = \begin{pmatrix} -(\mathcal{A}_1^*)^2(\psi_1^* \cdot \nabla) \psi_1^* \\ 0 \end{pmatrix}. \quad (5.108)$$

By proceeding at third order, we have to solve the system

$$\mathcal{L} \begin{pmatrix} u_3 \\ p_3 \end{pmatrix} = \begin{pmatrix} (\omega_g \partial_\eta + c_g \partial_\xi) \mathbf{u}_2 - \partial_T \mathbf{u}_1 - (\mathbf{u}_0 \cdot \nabla_\diamond) \mathbf{u}_2 - (\mathbf{u}_1 \cdot \nabla_\diamond) \mathbf{u}_1 - (\mathbf{u}_1 \cdot \nabla) \mathbf{u}_2 - (\mathbf{u}_2 \cdot \nabla) \mathbf{u}_1 \\ -\nabla_\diamond p_2 - \frac{1}{\mathcal{R}_c^2} \nabla^2 \mathbf{u}_1 + \frac{1}{\mathcal{R}_c} (2L_\diamond \mathbf{u}_2 + \nabla_\diamond^2 \mathbf{u}_1) \\ -\nabla_\diamond \cdot \mathbf{u}_2 \end{pmatrix}. \quad (5.109)$$

As previously done, we proceed step by step showing every single term, so as to finally identify the secular terms

$$(\omega_g \partial_\eta + c_g \partial_\xi) \mathbf{u}_2 = \left( \omega_g \frac{\partial \mathcal{A}_1^2}{\partial \eta} + c_g \frac{\partial \mathcal{A}_1^2}{\partial \xi} \right) \psi_2 e^{2+} + \left( \omega_g \frac{\partial |\mathcal{A}_1|^2}{\partial \eta} + c_g \frac{\partial |\mathcal{A}_1|^2}{\partial \xi} \right) \psi_2^{(0)} + \left( \omega_g \frac{\partial (\mathcal{A}_1^*)^2}{\partial \eta} + c_g \frac{\partial (\mathcal{A}_1^*)^2}{\partial \xi} \right) \psi_2^* e^{2-}$$

$$\partial_T \mathbf{u}_1 = \partial_T \mathcal{A}_1 \psi_1 e^+ + \partial_T \mathcal{A}_1^* \psi_1^* e^-,$$

$$(\mathbf{u}_0 \cdot \nabla_\diamond) \mathbf{u}_2 = \frac{U(r)}{r} \frac{\partial \mathbf{u}_2}{\partial \eta} = \frac{U(r)}{r} \frac{\partial \mathcal{A}_1^2}{\partial \eta} \psi_2 e^{2+} + \frac{U(r)}{r} \frac{\partial |\mathcal{A}_1|^2}{\partial \eta} \psi_2^{(0)} + \frac{U(r)}{r} \frac{\partial (\mathcal{A}_1^*)^2}{\partial \eta} \psi_2^* e^{2-},$$

$$\begin{aligned} (\mathbf{u}_1 \cdot \nabla) \mathbf{u}_2 &= (\mathcal{A}_1 \psi_1 e^+ + \mathcal{A}_1^* \psi_1^* e^-) \cdot \nabla (\mathcal{A}_1^2 \psi_2 e^{2+} + |\mathcal{A}_1|^2 \psi_2^{(0)} + (\mathcal{A}_1^*)^2 \psi_2^* e^{2-}) \\ &= \mathcal{A}_1 |\mathcal{A}_1|^2 \left[ (\psi_1 \cdot \nabla) \psi_2^{(0)} + (\psi_1^* \cdot \nabla) \psi_2 \right] e^+ + \mathcal{A}_1^* |\mathcal{A}_1|^2 \left[ (\psi_1 \cdot \nabla) \psi_2^* + (\psi_1^* \cdot \nabla) \psi_2^{(0)} \right] e^- \\ &\quad + \mathcal{A}_1^3 (\psi_1 \cdot \nabla) \psi_2 e^{3+} + (\mathcal{A}_1^*)^3 (\psi_1^* \cdot \nabla) \psi_2^* e^{3-}, \end{aligned}$$

$$\begin{aligned} (\mathbf{u}_2 \cdot \nabla) \mathbf{u}_1 &= (\mathcal{A}_1^2 \psi_2 e^{2+} + |\mathcal{A}_1|^2 \psi_2^{(0)} + (\mathcal{A}_1^*)^2 \psi_2^* e^{2-}) \cdot \nabla (\mathcal{A}_1 \psi_1 e^+ + \mathcal{A}_1^* \psi_1^* e^-) \\ &= \mathcal{A}_1 |\mathcal{A}_1|^2 \left[ (\psi_2 \cdot \nabla) \psi_1^* + (\psi_2^{(0)} \cdot \nabla) \psi_1 \right] e^+ + \mathcal{A}_1^* |\mathcal{A}_1|^2 \left[ (\psi_2^* \cdot \nabla) \psi_1 + (\psi_2^{(0)} \cdot \nabla) \psi_1^* \right] e^- \\ &\quad + \mathcal{A}_1^3 (\psi_2 \cdot \nabla) \psi_1 e^{3+} + (\mathcal{A}_1^*)^3 (\psi_2^* \cdot \nabla) \psi_1^* e^{3-}, \end{aligned}$$

$$\nabla_\diamond p_2 = (\nabla_\diamond \mathcal{A}_1^2) \phi_2 e^{2+} + (\nabla_\diamond |\mathcal{A}_1|^2) \phi_2^{(0)} + (\nabla_\diamond (\mathcal{A}_1^*)^2) \phi_2^* e^{2-},$$

$$\nabla^2 \mathbf{u}_1 = \mathcal{A}_1 \Delta_r \psi_1 e^+ + \mathcal{A}_1^* \Delta_r \psi_1^* e^-,$$

$$\frac{2}{\mathcal{R}_c} L_\diamond \mathbf{u}_2 = \frac{2}{\mathcal{R}_c} \left[ \frac{\partial \mathcal{A}_1^2}{\partial \eta} \varphi_\eta + \frac{\partial \mathcal{A}_1^2}{\partial \xi} \varphi_\xi \right] e^{2+} + \frac{2}{\mathcal{R}_c} \left[ \frac{\partial |\mathcal{A}_1|^2}{\partial \eta} \varphi_\eta^{(0)} + \frac{\partial |\mathcal{A}_1|^2}{\partial \xi} \varphi_\xi^{(0)} \right] + \frac{2}{\mathcal{R}_c} \left[ \frac{\partial (\mathcal{A}_1^*)^2}{\partial \eta} \varphi_\eta^* + \frac{\partial (\mathcal{A}_1^*)^2}{\partial \xi} \varphi_\xi^* \right] e^{2-},$$

$$\frac{1}{\mathcal{R}_c} \nabla_\diamond^2 \mathbf{u}_1 = \frac{1}{\mathcal{R}_c} \left( \frac{1}{r^2} \frac{\partial^2 \mathcal{A}_1}{\partial \eta^2} + \frac{\partial^2 \mathcal{A}_1}{\partial \xi^2} \right) \psi_1 e + \frac{1}{\mathcal{R}_c} \left( \frac{1}{r^2} \frac{\partial^2 \mathcal{A}_1^*}{\partial \eta^2} + \frac{\partial^2 \mathcal{A}_1^*}{\partial \xi^2} \right) \psi_1^* e^-,$$

$$\nabla_\diamond \cdot \mathbf{u}_2 = \left( \frac{1}{r} \frac{\partial \mathcal{A}_1^2}{\partial \eta} \psi_{2\theta} + \frac{\partial \mathcal{A}_1^2}{\partial \xi} \psi_{2z} \right) e^{2+} + \left( \frac{1}{r} \frac{\partial |\mathcal{A}_1|^2}{\partial \eta} \psi_{2\theta}^{(0)} + \frac{\partial |\mathcal{A}_1|^2}{\partial \xi} \psi_{2z}^{(0)} \right) + \left( \frac{1}{r} \frac{\partial (\mathcal{A}_1^*)^2}{\partial \eta} \psi_{2\theta}^* + \frac{\partial (\mathcal{A}_1^*)^2}{\partial \xi} \psi_{2z}^* \right) e^{2-}.$$

(5.110)

As regards the last forcing term for the third-order system, that is  $(\mathbf{u}_1 \cdot \nabla_\diamond) \mathbf{u}_1$ , it will contain the nonlinear terms coming from the product of the derivatives of the amplitude with the amplitude itself. Thus, as it is quite complicated to write, we firstly decompose it into three components and then write it in a more compact form using a special vector notation. We proceed by starting from the radial component:

$$\begin{aligned}
 [(\mathbf{u}_1 \cdot \nabla_\diamond) \mathbf{u}_1]_r &= (\mathcal{A}_1 \psi_{1\theta} e^+ + \mathcal{A}_1^* \psi_{1\theta}^* e^-) \frac{1}{r} \left( \frac{\partial \mathcal{A}_1}{\partial \eta} \psi_{1r} e^+ + \frac{\partial \mathcal{A}_1^*}{\partial \eta} \psi_{1r}^* e^- \right) \\
 &\quad + (\mathcal{A}_1 \psi_{1z} e^+ + \mathcal{A}_1^* \psi_{1z}^* e^-) \left( \frac{\partial \mathcal{A}_1}{\partial \xi} \psi_{1r} e^+ + \frac{\partial \mathcal{A}_1^*}{\partial \xi} \psi_{1r}^* e^- \right) \\
 &= \left( \mathcal{A}_1 \partial_\eta \mathcal{A}_1 \frac{\psi_{1\theta} \psi_{1r}}{r} + \mathcal{A}_1 \partial_\xi \mathcal{A}_1 \psi_{1z} \psi_{1r} \right) e^{2+} \\
 &\quad + \left( \mathcal{A}_1 \partial_\eta \mathcal{A}_1^* \frac{\psi_{1\theta}^* \psi_{1r}^*}{r} + \mathcal{A}_1^* \partial_\eta \mathcal{A}_1 \frac{\psi_{1\theta}^* \psi_{1r}}{r} + \mathcal{A}_1 \partial_\xi \mathcal{A}_1^* \psi_{1z} \psi_{1r}^* + \mathcal{A}_1^* \partial_\xi \mathcal{A}_1 \psi_{1z}^* \psi_{1r} \right) \\
 &\quad + \left( \mathcal{A}_1^* \partial_\eta \mathcal{A}_1^* \frac{\psi_{1\theta}^* \psi_{1r}^*}{r} + \mathcal{A}_1^* \partial_\xi \mathcal{A}_1^* \psi_{1z}^* \psi_{1r}^* \right) e^{2-}.
 \end{aligned} \tag{5.111}$$

For what concerns the angular component we have

$$\begin{aligned}
 [(\mathbf{u}_1 \cdot \nabla_\diamond) \mathbf{u}_1]_\theta &= (\mathcal{A}_1 \psi_{1\theta} e^+ + \mathcal{A}_1^* \psi_{1\theta}^* e^-) \frac{1}{r} \left( \frac{\partial \mathcal{A}_1}{\partial \eta} \psi_{1\theta} e^+ + \frac{\partial \mathcal{A}_1^*}{\partial \eta} \psi_{1\theta}^* e^- \right) \\
 &\quad + (\mathcal{A}_1 \psi_{1z} e^+ + \mathcal{A}_1^* \psi_{1z}^* e^-) \left( \frac{\partial \mathcal{A}_1}{\partial \xi} \psi_{1\theta} e^+ + \frac{\partial \mathcal{A}_1^*}{\partial \xi} \psi_{1\theta}^* e^- \right) \\
 &= \left( \mathcal{A}_1 \partial_\eta \mathcal{A}_1 \frac{\psi_{1\theta}^2}{r} + \mathcal{A}_1 \partial_\xi \mathcal{A}_1 \psi_{1z} \psi_{1\theta} \right) e^{2+} \\
 &\quad + \left( \mathcal{A}_1 \partial_\eta \mathcal{A}_1^* \frac{\psi_{1\theta} \psi_{1\theta}^*}{r} + \mathcal{A}_1^* \partial_\eta \mathcal{A}_1 \frac{\psi_{1\theta}^* \psi_{1\theta}}{r} + \mathcal{A}_1 \partial_\xi \mathcal{A}_1^* \psi_{1z} \psi_{1\theta}^* + \mathcal{A}_1^* \partial_\xi \mathcal{A}_1 \psi_{1z}^* \psi_{1\theta} \right) \\
 &\quad + \left( \mathcal{A}_1^* \partial_\eta \mathcal{A}_1^* \frac{(\psi_{1\theta}^*)^2}{r} + \mathcal{A}_1^* \partial_\xi \mathcal{A}_1^* \psi_{1z}^* \psi_{1\theta}^* \right) e^{2-}.
 \end{aligned} \tag{5.112}$$

Finally, for the axial component we have

$$\begin{aligned}
 [(\mathbf{u}_1 \cdot \nabla_\diamond) \mathbf{u}_1]_z &= (\mathcal{A}_1 \psi_{1\theta} e^+ + \mathcal{A}_1^* \psi_{1\theta}^* e^-) \frac{1}{r} \left( \frac{\partial \mathcal{A}_1}{\partial \eta} \psi_{1z} e^+ + \frac{\partial \mathcal{A}_1^*}{\partial \eta} \psi_{1z}^* e^- \right) \\
 &\quad + (\mathcal{A}_1 \psi_{1z} e^+ + \mathcal{A}_1^* \psi_{1z}^* e^-) \left( \frac{\partial \mathcal{A}_1}{\partial \xi} \psi_{1z} e^+ + \frac{\partial \mathcal{A}_1^*}{\partial \xi} \psi_{1z}^* e^- \right) \\
 &= \left( \mathcal{A}_1 \partial_\eta \mathcal{A}_1 \frac{\psi_{1\theta} \psi_{1z}}{r} + \mathcal{A}_1 \partial_\xi \mathcal{A}_1 \psi_{1z}^2 \right) e^{2+} \\
 &\quad + \left( \mathcal{A}_1 \partial_\eta \mathcal{A}_1^* \frac{\psi_{1\theta} \psi_{1z}^*}{r} + \mathcal{A}_1^* \partial_\eta \mathcal{A}_1 \frac{\psi_{1\theta}^* \psi_{1z}}{r} + \mathcal{A}_1 \partial_\xi \mathcal{A}_1^* \psi_{1z} \psi_{1z}^* + \mathcal{A}_1^* \partial_\xi \mathcal{A}_1 \psi_{1z}^* \psi_{1z} \right) \\
 &\quad + \left( \mathcal{A}_1^* \partial_\eta \mathcal{A}_1^* \frac{(\psi_{1\theta}^*) \psi_{1z}^*}{r} + \mathcal{A}_1^* \partial_\xi \mathcal{A}_1^* (\psi_{1z}^*)^2 \right) e^{2-}.
 \end{aligned} \tag{5.113}$$

By putting together the three components, we can write the operator in a general way as

$$\begin{aligned}
 (\mathbf{u}_1 \cdot \nabla_\diamond) \mathbf{u}_1 &= (\mathcal{A}_1 \partial_\eta \mathcal{A}_1 \chi_\eta + \mathcal{A}_1 \partial_\xi \mathcal{A}_1 \chi_\xi) e^{2+} \\
 &\quad + (\mathcal{A}_1 \partial_\eta \mathcal{A}_1^* \varphi_\eta + \mathcal{A}_1^* \partial_\eta \mathcal{A}_1 \varphi_\eta^* + \mathcal{A}_1 \partial_\xi \mathcal{A}_1^* \varphi_\xi + \mathcal{A}_1^* \partial_\xi \mathcal{A}_1 \varphi_\xi^*) \\
 &\quad + (\mathcal{A}_1^* \partial_\eta \mathcal{A}_1^* \mathbf{v}_\eta + \mathcal{A}_1^* \partial_\xi \mathcal{A}_1^* \mathbf{v}_\xi) e^{2-},
 \end{aligned} \tag{5.114}$$

where the following vectors have been defined

$$\begin{aligned}\boldsymbol{\chi}_\eta &= \left( \frac{\psi_{1\theta}\psi_{1r}}{r}, \frac{\psi_{1\theta}^2}{r}, \frac{\psi_{1\theta}\psi_{1z}}{r} \right), \\ \boldsymbol{\chi}_\xi &= (\psi_{1z}\psi_{1r}, \psi_{1z}\psi_{1\theta}, \psi_{1z}^2), \\ \boldsymbol{\varphi}_\eta &= \left( \frac{\psi_{1\theta}\psi_{1r}^*}{r}, \frac{\psi_{1\theta}\psi_{1\theta}^*}{r}, \frac{\psi_{1\theta}\psi_{1z}^*}{r} \right), \\ \boldsymbol{\varphi}_\eta^* &= \left( \frac{\psi_{1\theta}^*\psi_{1r}}{r}, \frac{\psi_{1\theta}\psi_{1\theta}^*}{r}, \frac{\psi_{1\theta}^*\psi_{1z}}{r} \right), \\ \boldsymbol{\varphi}_\xi &= (\psi_{1z}\psi_{1r}^*, \psi_{1z}\psi_{1\theta}^*, \psi_{1z}^*\psi_{1z}), \\ \boldsymbol{\varphi}_\xi^* &= (\psi_{1z}^*\psi_{1r}, \psi_{1z}^*\psi_{1\theta}, \psi_{1z}^*\psi_{1z}), \\ \boldsymbol{v}_\eta &= \left( \frac{\psi_{1\theta}^*\psi_{1r}^*}{r}, \frac{(\psi_{1\theta}^*)^2}{r}, \frac{\psi_{1\theta}^*\psi_{1z}^*}{r} \right), \\ \boldsymbol{v}_\xi &= (\psi_{1z}^*\psi_{1r}^*, \psi_{1\theta}^*\psi_{1z}^*, (\psi_{1z}^*)^2).\end{aligned}\tag{5.115}$$

As previously done, the resonant terms must be set equal to zero through the use of Fredholm's alternative so that the system (5.109) admit a solution. These resonant terms are given by

$$\begin{aligned}-\partial_T \mathcal{A}_1 - \mathcal{A}_1 |\mathcal{A}_1|^2 &\left( (\boldsymbol{\psi}_1 \cdot \nabla) \boldsymbol{\psi}_2^{(0)} + (\boldsymbol{\psi}_1^* \cdot \nabla) \boldsymbol{\psi}_2 + (\boldsymbol{\psi}_2 \cdot \nabla) \boldsymbol{\psi}_1^* + (\boldsymbol{\psi}_2^{(0)} \cdot \nabla) \boldsymbol{\psi}_1 \right) - \\ &\frac{1}{\mathcal{R}_c} \mathcal{A}_1 \Delta_r \boldsymbol{\psi}_1 + \frac{1}{\mathcal{R}_c} \left( \frac{1}{r^2} \partial_\eta^2 \mathcal{A}_1 + \partial_\xi^2 \mathcal{A}_1 \right) \boldsymbol{\psi}_1,\end{aligned}\tag{5.116}$$

where the operator  $\Delta_r$  identifies the Laplacian acting on the radial variable, the second derivatives with respect to  $\theta$  and  $z$  reduce to an algebraic relation.

Now, by multiplying expression (5.116) by the solution  $\boldsymbol{\psi}_1^a$  of the linear adjoint problem, integrating along the radial coordinate, and setting the integral equal to zero, we obtain a new solvability condition for the third order system. By virtue of the integral operator, the dependence of the coefficients on the variable  $r$  disappears and so we get a partial differential equation with constant coefficients which is the Ginzburg–Landau equation we were looking for. By exploiting the passages listed above step by step we have

$$\begin{aligned}\int_a^b \boldsymbol{\psi}_1^a \cdot \left[ -\partial_T \mathcal{A}_1 \boldsymbol{\psi}_1 - \mathcal{A}_1 |\mathcal{A}_1|^2 \left( (\boldsymbol{\psi}_1 \cdot \nabla) \boldsymbol{\psi}_2^{(0)} + (\boldsymbol{\psi}_1^* \cdot \nabla) \boldsymbol{\psi}_2 + (\boldsymbol{\psi}_2 \cdot \nabla) \boldsymbol{\psi}_1^* + (\boldsymbol{\psi}_2^{(0)} \cdot \nabla) \boldsymbol{\psi}_1 \right) \right] - \\ \int_a^b \boldsymbol{\psi}_1^a \cdot \left[ \frac{1}{\mathcal{R}_c} \mathcal{A}_1 \Delta_r \boldsymbol{\psi}_1 - \frac{1}{\mathcal{R}_c} \left( \frac{1}{r^2} \partial_\eta^2 \mathcal{A}_1 + \partial_\xi^2 \mathcal{A}_1 \right) \boldsymbol{\psi}_1 \right] = 0.\end{aligned}\tag{5.117}$$

However, the terms proportional to  $\mathcal{A}_1$  can be taken out of the integral operator, so that the equation takes the form

$$-\tau \partial_T \mathcal{A}_1 - \kappa \mathcal{A}_1 |\mathcal{A}_1|^2 - \frac{a_1}{\mathcal{R}_c^2} \mathcal{A}_1 + \frac{1}{\mathcal{R}_c} (a_2 \partial_\eta^2 \mathcal{A}_1 + \tau \partial_\xi^2 \mathcal{A}_1) = 0,\tag{5.118}$$

where the coefficients are given by evaluating the following integrals

$$\begin{aligned}\tau &= \int_a^b \boldsymbol{\psi}_1^a \cdot \boldsymbol{\psi}_1, \\ \kappa &= \int_a^b \boldsymbol{\psi}_1^a \cdot \left( (\boldsymbol{\psi}_1 \cdot \nabla) \boldsymbol{\psi}_2^{(0)} + (\boldsymbol{\psi}_1^* \cdot \nabla) \boldsymbol{\psi}_2 + (\boldsymbol{\psi}_2 \cdot \nabla) \boldsymbol{\psi}_1^* + (\boldsymbol{\psi}_2^{(0)} \cdot \nabla) \boldsymbol{\psi}_1 \right), \\ a_1 &= \int_a^b \boldsymbol{\psi}_1^a \cdot \Delta_r \boldsymbol{\psi}_1, \\ a_2 &= \int_a^b \boldsymbol{\psi}_1^a \cdot \frac{1}{r^2} \boldsymbol{\psi}_1.\end{aligned}\tag{5.119}$$

By imposing the normalization condition  $\tau = \int_a^b \psi^a_1 \cdot \psi_1 = 1$  the G–L equation in the final form reads as

$$\partial_T \mathcal{A}_1 = -\frac{a_1}{\mathcal{R}_c} \mathcal{A}_1 + \frac{a_2}{\mathcal{R}_c} \partial_\eta^2 \mathcal{A}_1 + \frac{1}{\mathcal{R}_c} \partial_\xi^2 \mathcal{A}_1 - \kappa \mathcal{A}_1 |\mathcal{A}_1|^2. \quad (5.120)$$

In the following, we will assume that the spatial dependence of the amplitude  $\mathcal{A}$  is given only by  $\xi$  and not also by  $\eta$ . This is because we have always assumed that along the angular direction  $\theta$ , only integer values of the wavenumber are allowed and there is no modulation of the amplitude along the azimuthal direction. By changing the angular wave number, the coefficients of the G–L equation will change and the nonlinear dynamics of our system close to the critical point will be described by a different G–L equation. In particular, if the marginally stable mode is not axisymmetric, its contribution will affect both the coefficient  $a_1$  and  $k$ . Indeed, in the case of the Taylor–Couette flow, both  $\alpha, \omega_c$  will not be null. Having simplified the general formal aspect of equation (5.120), for our purposes it will finally read as

$$\partial_T \mathcal{A}_1 = -\frac{a_1}{\mathcal{R}_c} \mathcal{A}_1 + \frac{1}{\mathcal{R}_c} \partial_\xi^2 \mathcal{A}_1 - \kappa \mathcal{A}_1 |\mathcal{A}_1|^2. \quad (5.121)$$

## 5.5 Alternative derivation of the Ginzburg-Landau equation

In this section we want to use a more abstract approach to derive the G–L equation for the Navier–Stokes system and in general for any dynamical system described by partial differential equations.

Let a general dynamical system be described through a state vector  $\mathbf{w}$  such that

$$\frac{\partial \mathbf{w}}{\partial t} + L\mathbf{w} = \mathbf{f}(\mathbf{w}), \quad (5.122)$$

where  $\mathbf{f}$  is supposed to be a quadratic function of the unknown  $\mathbf{w}$ . By expanding in series of the small parameter  $\epsilon$  the function  $\mathbf{w}$ , and by writing the generic  $n$ -th order function by means of the amplitude  $\mathcal{A}$ , we have

$$\begin{aligned} \mathbf{w}_n &= \sum_{k=0}^n \binom{n}{k} (\mathcal{A}\psi_1 e^+)^{n-k} (\mathcal{A}^*\psi_1^* e^-)^k \\ &= \sum_{k=0}^n \mathcal{A}^{n-k} (\mathcal{A}^*)^k \psi_{n,n-2k} e^{n-2k}. \end{aligned} \quad (5.123)$$

Thus, by extending the summation to the  $n$  powers of  $\epsilon$ , the vector of the unknowns  $\mathbf{w}$  is given by the summation on all the values of  $n$  up to the desired order, say  $r$

$$\mathbf{w} = \sum_{n=0}^r \sum_{k=0}^n \epsilon^n \mathcal{A}^{n-k} (\mathcal{A}^*)^k \psi_{n,n-2k} e^{n-2k}. \quad (5.124)$$

We begin by treating the various operators which appear in the equation (5.122), starting from the nonlinear one. As it is quadratic in the unknown  $\mathbf{w}$ , we can think of expressing it in the form

$$\mathbb{A}\mathbf{w} \otimes \mathbb{B}\mathbf{w}, \quad (5.125)$$

where  $\mathbb{A}$  and  $\mathbb{B}$  represent two matrices with constant coefficients. From this, by introducing the generic operator  $D$  that acts on the nonlinear term, we can write

$$\mathbf{f} = D(\mathbb{A}\mathbf{w} \otimes \mathbb{B}\mathbf{w}), \quad (5.126)$$

The expression inside the relation (5.125), will be given by

$$\begin{aligned} \mathbb{A}\mathbf{w} \otimes \mathbb{B}\mathbf{w} &= \sum_{n=0}^r \sum_{k=0}^n \epsilon^n \mathcal{A}^{n-k} (\mathcal{A}^*)^k [\mathbb{A}\psi_{n,n-2k}] e^{n-2k} \otimes \sum_{p=0}^r \sum_{q=0}^n \epsilon^p \mathcal{A}^{p-q} (\mathcal{A}^*)^q [\mathbb{B}\psi_{p,p-2q}] e^{p-2q} \\ &= \sum_{n=0}^r \sum_{k=0}^n \epsilon^n \mathcal{A}^{n-k} (\mathcal{A}^*)^k [\mathbb{F}_{n,n-2k}] e^{n-2k} \otimes \sum_{p=0}^r \sum_{q=0}^n \epsilon^p \mathcal{A}^{p-q} (\mathcal{A}^*)^q [\mathbb{G}_{p,p-2q}] e^{p-2q}, \end{aligned} \quad (5.127)$$

where

$$\begin{aligned} \mathbb{F}_{n,n-2k} &= \mathbb{A}\psi_{n,n-2k}, \quad \forall n, k, \\ \mathbb{G}_{n,n-2k} &= \mathbb{B}\psi_{n,n-2k}, \quad \forall p, q. \end{aligned} \quad (5.128)$$

From equation (5.127), by exploiting the terms we get

$$\begin{aligned}
\mathbb{A}\mathbf{w} \otimes \mathbb{B}\mathbf{w} &= [\mathbb{F}_{0,0} + \epsilon (\mathcal{A}\mathbb{F}_{1,1}e^+ + \mathcal{A}^*\mathbb{F}_{1,-1}e^-) + \epsilon^2 (\mathcal{A}^2\mathbb{F}_{2,2}e^{2+} + |\mathcal{A}|^2\mathbb{F}_{2,0} + (\mathcal{A}^*)^2\mathbb{F}_{2,-2}e^{2-}) + \dots] \otimes \\
&\quad [\mathbb{G}_{0,0} + \epsilon (\mathcal{A}\mathbb{G}_{1,1}e^+ + \mathcal{A}^*\mathbb{G}_{1,-1}e^-) + \epsilon^2 (\mathcal{A}^2\mathbb{G}_{2,2}e^{2+} + |\mathcal{A}|^2\mathbb{G}_{2,0} + (\mathcal{A}^*)^2\mathbb{G}_{2,-2}e^{2-}) + \dots] \\
&= \mathbb{F}_{0,0} \otimes \mathbb{G}_{0,0} + \epsilon [\mathcal{A}(\mathbb{F}_{0,0} \otimes \mathbb{G}_{1,1} + \mathbb{F}_{1,1} \otimes \mathbb{G}_{0,0})e^+ + \mathcal{A}^*(\mathbb{F}_{0,0} \otimes \mathbb{G}_{1,-1} + \mathbb{F}_{1,-1} \otimes \mathbb{G}_{0,0})e^-] \\
&\quad + \epsilon^2 [\mathcal{A}^2(\mathbb{F}_{0,0} \otimes \mathbb{G}_{2,2} + \mathbb{F}_{1,1} \otimes \mathbb{G}_{1,1} + \mathbb{F}_{2,2} \otimes \mathbb{G}_{0,0})e^{2+} + \dots] + \dots \\
&= \mathbb{M}_{0,0} + \epsilon (\mathcal{A}\mathbb{M}_{1,1}e^+ + \mathcal{A}^*\mathbb{M}_{1,-1}e^-) + \epsilon^2 (\mathcal{A}^2\mathbb{M}_{2,2}e^{2+} + |\mathcal{A}|^2\mathbb{M}_{2,0} + (\mathcal{A}^*)^2\mathbb{M}_{2,-2}e^{2-}) + \dots \\
&= \sum_{n=0}^r \sum_{k=0}^n \epsilon^n \mathcal{A}^{n-k} (\mathcal{A}^*)^k [\mathbb{M}_{n,n-2k}] e^{n-2k}.
\end{aligned} \tag{5.129}$$

For what concerns the operator  $D$  acting on the nonlinear term, we assume it to be a linear operator and we may assume it depends on a linear algebraic transformation  $\mathbb{T}$  and on a linear differential operator, the classical Nabla operator  $\nabla$ . Thus we will have

$$D = D(\mathbb{T}, \nabla), \tag{5.130}$$

but as  $\nabla = \nabla + \epsilon\nabla_\diamond$  we obtain

$$\begin{aligned}
D &= D(\mathbb{T}, \nabla) + \epsilon D(\mathbb{T}, \nabla_\diamond) \\
&= D + \epsilon D_\diamond.
\end{aligned} \tag{5.131}$$

Finally, the nonlinear term reads

$$\mathbf{f}(\mathbf{w}) = D \sum_{n=0}^r \sum_{k=0}^n \epsilon^n \mathcal{A}^{n-k} (\mathcal{A}^*)^k [\mathbb{M}_{n,n-2k}] e^{n-2k} + D_\diamond \sum_{n=0}^{r-1} \sum_{k=0}^n \epsilon^{n+1} \mathcal{A}^{n-k} (\mathcal{A}^*)^k [\mathbb{M}_{n,n-2k}] e^{n-2k}. \tag{5.132}$$

About the linear terms instead, we proceed in the following way. The temporal derivative can be split as follows

$$\begin{aligned}
\frac{\partial \mathbf{w}}{\partial t} &= \partial_t \mathbf{w} - \epsilon(\mathbf{c} \cdot \nabla_\diamond) \mathbf{w} + \epsilon^2 \partial_T \mathbf{w} \\
&= \partial_t \mathbf{w} - \epsilon c_g \partial_\xi \mathbf{w} + \epsilon^2 \partial_T \mathbf{w} \\
&= \partial_t \mathbf{w} - \sum_{n=0}^{r-1} \sum_{k=0}^n \epsilon^{n+1} c_g \partial_\xi (\mathcal{A}^{n-k} (\mathcal{A}^*)^k) [\psi_{n,n-2k}] e^{n-2k} + \\
&\quad \sum_{n=0}^{r-2} \sum_{k=0}^n \epsilon^{n+2} \partial_T (\mathcal{A}^{n-k} (\mathcal{A}^*)^k) [\psi_{n,n-2k}] e^{n-2k}.
\end{aligned} \tag{5.133}$$

Regarding the other linear operator—the spatial operator—we can consider that it is a function of a linear algebraic operator  $\mathbb{L}$  which describes a possible rotation and expansion of the vector  $\mathbf{w}$ , by the Nabla operator under the form of both gradient and divergence, by the Laplacian operator and by a generic linear operator  $\tilde{L}$  which acts only on the primitive variables of the problem. After the introduction of these operators, we can write

$$L = L(\mathbb{L}, \nabla, \nabla^2) + \epsilon^2 \tilde{L}. \tag{5.134}$$

Now, as  $\nabla = \nabla + \epsilon\nabla_\diamond$  and  $\nabla^2 = \nabla^2 + 2\epsilon L_\diamond + \epsilon^2 \nabla_\diamond^2$ , by exploiting the linearity of the operator  $L$  we obtain

$$\begin{aligned}
L &= L + \epsilon (\nabla_\diamond + 2L_\diamond) + \epsilon^2 (\nabla_\diamond^2 + \tilde{L}) \\
&= L + \epsilon L'_\diamond + \epsilon^2 L'_{\diamond\diamond}.
\end{aligned} \tag{5.135}$$

In order to rewrite the governing equation at the various orders, we recognise firstly the linear "homogeneous" operator  $\mathcal{L}$  introduced in the previous paragraphs. Then the equation (5.122) can be rewritten as

$$\begin{aligned} \mathcal{L}\mathbf{w} = & \sum_{n=0}^{r-1} \sum_{k=0}^n \epsilon^{n+1} c_g \partial_\xi \left( \mathcal{A}^{n-k} (\mathcal{A}^*)^k \right) [\psi_{n,n-2k}] e^{n-2k} - \sum_{n=0}^{r-2} \sum_{k=0}^n \epsilon^{n+2} \partial_T \left( \mathcal{A}^{n-k} (\mathcal{A}^*)^k \right) [\psi_{n,n-2k}] e^{n-2k} - \\ & \sum_{n=0}^{r-1} \sum_{k=0}^n \epsilon^{n+1} L'_\diamond \left( \mathcal{A}^{n-k} (\mathcal{A}^*)^k [\psi_{n,n-2k}] e^{n-2k} \right) - \sum_{n=0}^{r-2} \sum_{k=0}^n \epsilon^{n+2} L'_{\diamond\diamond} \left( \mathcal{A}^{n-k} (\mathcal{A}^*)^k [\psi_{n,n-2k}] e^{n-2k} \right) + \\ & D \sum_{n=2}^r \sum_{k=0}^n \epsilon^n \mathcal{A}^{n-k} (\mathcal{A}^*)^k [\mathbb{M}_{n,n-2k}] e^{n-2k} + D_\diamond \sum_{n=0}^{r-1} \sum_{k=0}^n \epsilon^{n+1} \mathcal{A}^{n-k} (\mathcal{A}^*)^k [\mathbb{M}_{n,n-2k}] e^{n-2k}. \end{aligned} \quad (5.136)$$

Notice how the second to last summation is from  $n = 2$ , as the term for  $n = 0$  is null since  $\mathbb{M}_{0,0} = 0$ , while the term for  $n = 1$  falls into the  $\mathcal{L}$  operator as the term  $\mathbb{M}_{1,1} = \mathbb{F}_{1,1} \otimes \mathbb{G}_{1,1} + \mathbb{F}_{0,0} \otimes \mathbb{G}_{1,1}$  is equivalent to  $(\mathbf{u}_1 \cdot \nabla) \mathbf{u}_0 + (\mathbf{u}_0 \cdot \nabla) \mathbf{u}_1$  in the multiple-scale method presented in the previous paragraph.

By exploiting the summations to the different orders, at order  $\epsilon^0$  the system returns the base flow  $w_0 = (\mathbf{u}_0, p_0)$ . By proceeding at first order ( $\epsilon$ ) we have

$$\mathcal{L}\mathbf{w}_1 = 0, \quad (5.137)$$

which represents the linear stability problem. At order  $\epsilon^2$  we have

$$\mathcal{L}\mathbf{w}_2 = c_g \partial_\xi \mathcal{A} \psi_{1,1} e^+ + L'_\diamond (\mathcal{A} \psi_{1,1} e^+) + D (\mathcal{A}^2 \psi_{2,2} e^{2+} + |\mathcal{A}|^2 \psi_{2,0}) + D_\diamond (\mathcal{A} \mathbb{M}_{1,1} e^+) + c.c., \quad (5.138)$$

for which the solvability condition gives

$$\int_a^b \mathbf{w}_{1,1}^a \cdot [c_g \partial_\xi \mathcal{A} \psi_{1,1} + L'_\diamond (\mathcal{A} \psi_{1,1}) + D (\mathcal{A}^2 \mathbb{M}_{2,2} + |\mathcal{A}|^2 \mathbb{M}_{2,0}) + D_\diamond (\mathcal{A} \mathbb{M}_{1,1})] = 0, \quad (5.139)$$

for the terms proportional to  $e^+$ , while its complex conjugate for the terms proportional to  $e^-$ . Finally, at order  $\epsilon^3$  the system to be solved is given by

$$\begin{aligned} \mathcal{L}\mathbf{w}_3 = & c_g \partial_\xi (\mathcal{A}^2 \psi_{2,2} e^2 + |\mathcal{A}|^2 \psi_{2,0}) - \partial_T (\mathcal{A} \psi_{1,1} e) - L'_\diamond (\mathcal{A}^2 \psi_{2,2} e^2 + |\mathcal{A}| \psi_{2,0}) - \\ & L'_{\diamond\diamond} (\mathcal{A} \psi_{1,1} e) + D (\mathcal{A}^3 \mathbb{M}_{3,3} e^3 + \mathcal{A} |\mathcal{A}|^2 \mathbb{M}_{3,1} e) + D_\diamond (\mathcal{A}^2 \mathbb{M}_{2,2} e^2 + |\mathcal{A}|^2 \mathbb{M}_{2,0}) + c.c. \end{aligned} \quad (5.140)$$

The solvability condition for the terms proportional to  $e^+$  reads

$$\int_a^b \mathbf{w}_{1,1}^a \cdot [\partial_T (\mathcal{A} \psi_{1,1}) - L'_{\diamond\diamond} (\mathcal{A} \psi_{1,1}) + D (\mathcal{A} |\mathcal{A}|^2 \mathbb{M}_{3,1})] = 0. \quad (5.141)$$

Let  $\mathcal{D}_{\diamond\diamond}$  be a new operator such that  $\int_a^b \mathbf{w}_{1,1}^a \cdot [L'_{\diamond\diamond} (\mathcal{A} \psi_{1,1})] = \mathcal{D}_{\diamond\diamond} \mathcal{A}$ . The Ginzburg–Landau equation in symbolic form reads

$$\tau \partial_T \mathcal{A} - \mathcal{D}_{\diamond\diamond} \mathcal{A} + c \mathcal{A} |\mathcal{A}|^2 = 0, \quad (5.142)$$

where the constants  $\tau$  and  $c$  are computed by the integrals

$$\begin{aligned} \tau &= \int_a^b \mathbf{w}_{1,1}^a \cdot \psi_{1,1}, \\ c &= \int_a^b \mathbf{w}_{1,1}^a \cdot D (\mathbb{M}_{3,1}). \end{aligned} \quad (5.143)$$

By imposing the normalization condition  $\tau = 1$  and calling as usual the Landau coefficient  $k = c$  we obtain the relation

$$\partial_T \mathcal{A} - \mathcal{D}_{\diamond\diamond} \mathcal{A} + \kappa \mathcal{A} |\mathcal{A}|^2 = 0. \quad (5.144)$$

Now, it can be shown that the operator  $\mathcal{D}_{\diamond\diamond}$  is given by the linear combination of two operators:  $(\nabla_{\diamond})^2$  and  $\tilde{L}$ , where the former is the Laplacian computed with respect to the slow spatial variables, in the case of the Navier–Stokes equation only  $\xi \Rightarrow (\nabla_{\diamond})^2 = \partial_{\xi}^2$ . The latter operator instead, is a differential operator acting only on the primitive variables of the problem, thus is a linear algebraic operator in the amplitude  $\mathcal{A}$ . For what concerns the Navier–Stokes equations, it can be shown that  $\tilde{L} \equiv \nabla^2$ . Hence we can generally write

$$\mathcal{D}_{\diamond\diamond} = a_1 \tilde{L} + a_2 \partial_{\xi}^2. \quad (5.145)$$

By replacing the relation (5.145) in the equation (5.144) and by scaling the coefficients, we get the G-L equation in the final form

$$\partial_T \mathcal{A} - c_1 \mathcal{A} - c_2 \partial_{\xi}^2 \mathcal{A} + \kappa \mathcal{A} |\mathcal{A}|^2 = 0, \quad (5.146)$$

which is equivalent to the one obtained in the previous paragraph–equation(5.121).

## 5.6 High-order approximation

In the previous section we have derived the G–L equation for the Navier–Stokes equation up to the third order, so that the equation describing the modulation of the amplitude was a cubic equation. This came from the fact that we have approximated the dispersion relation with a parabola centred in the critical point  $(\beta_c, \mathcal{R}_c)$ . If we want to better approximate the solution of our problem, we have to add high-order terms in the expansion of the dispersion relation. This implies that we also have to add new slow variables. By doing so, the Ginzburg–Landau equation will contain terms to the fifth, seventh power and so on, up to the desired order of approximation.

This being said, we start to approximate the dispersion relation to higher orders with respect to the control parameter  $\mathcal{R}$  and the axial wave number  $\beta$ . We still treat the case for which there exist an imaginary part of the eigenvalue. Thus, the dispersion relation  $s = \sigma(\mathcal{R}, \beta) - i\omega(\mathcal{R}, \beta)$  can be expanded as

$$\begin{aligned} \sigma(\mathcal{R}, \beta) &= \frac{\partial\sigma(\mathcal{R}_c, \beta_c)}{\partial\mathcal{R}}(\mathcal{R} - \mathcal{R}_c) + \frac{1}{2}\frac{\partial^2\sigma(\mathcal{R}_c, \beta_c)}{\partial\mathcal{R}^2}(\mathcal{R} - \mathcal{R}_c)^2 + \\ &\quad \frac{\partial^2\sigma(\mathcal{R}_c, \beta_c)}{\partial\mathcal{R}\partial\beta}(\mathcal{R} - \mathcal{R}_c)(\beta - \beta_c) + \frac{1}{2}\frac{\partial^2\sigma(\mathcal{R}_c, \beta_c)}{\partial\beta^2}(\beta - \beta_c)^2 + \\ &\quad \frac{1}{3!}\frac{\partial^3\sigma(\mathcal{R}_c, \beta_c)}{\partial\mathcal{R}^3}(\mathcal{R} - \mathcal{R}_c)^3 + \frac{3}{3!}\frac{\partial^3\sigma(\mathcal{R}_c, \beta_c)}{\partial\mathcal{R}^2\partial\beta}(\mathcal{R} - \mathcal{R}_c)^2(\beta - \beta_c) + \\ &\quad \frac{3}{3!}\frac{\partial^3\sigma(\mathcal{R}_c, \beta_c)}{\partial\mathcal{R}\partial\beta^2}(\mathcal{R} - \mathcal{R}_c)(\beta - \beta_c)^2 + \frac{1}{3!}\frac{\partial^3\sigma(\mathcal{R}_c, \beta_c)}{\partial\beta^3}(\beta - \beta_c)^3 + \\ &\quad \frac{1}{4!}\frac{\partial^4\sigma(\mathcal{R}_c, \beta_c)}{\partial\mathcal{R}^4}(\mathcal{R} - \mathcal{R}_c)^4 + \frac{4}{4!}\frac{\partial^4\sigma(\mathcal{R}_c, \beta_c)}{\partial\mathcal{R}^3\partial\beta}(\mathcal{R} - \mathcal{R}_c)^3(\beta - \beta_c) + \\ &\quad \frac{6}{4!}\frac{\partial^4\sigma(\mathcal{R}_c, \beta_c)}{\partial\mathcal{R}^2\partial\beta^2}(\mathcal{R} - \mathcal{R}_c)^2(\beta - \beta_c)^2 + \frac{4}{4!}\frac{\partial^4\sigma(\mathcal{R}_c, \beta_c)}{\partial\mathcal{R}\partial\beta^3}(\mathcal{R} - \mathcal{R}_c)(\beta - \beta_c)^3 + \\ &\quad \frac{1}{4!}\frac{\partial^4\sigma(\mathcal{R}_c, \beta_c)}{\partial\beta^4}(\beta - \beta_c)^4 + \mathcal{O}(5), \\ \omega(\mathcal{R}, \beta) &= \omega_c + c_g(\beta - \beta_c) + \frac{\partial\omega(\mathcal{R}_c, \beta_c)}{\partial\mathcal{R}}(\mathcal{R} - \mathcal{R}_c) + \frac{1}{2!}\frac{\partial^2\omega(\mathcal{R}_c, \beta_c)}{\partial\mathcal{R}^2}(\mathcal{R} - \mathcal{R}_c)^2 + \end{aligned} \tag{5.147}$$

$$\begin{aligned} &\quad \frac{2}{2!}\frac{\partial^2\omega(\mathcal{R}_c, \beta_c)}{\partial\mathcal{R}\partial\beta}(\mathcal{R} - \mathcal{R}_c)(\beta - \beta_c) + \frac{1}{2!}\frac{\partial^2\omega(\mathcal{R}_c, \beta_c)}{\partial\beta^2}(\beta - \beta_c)^2 + \\ &\quad \frac{1}{3!}\frac{\partial^3\omega(\mathcal{R}_c, \beta_c)}{\partial\mathcal{R}^3}(\mathcal{R} - \mathcal{R}_c)^3 + \frac{3}{3!}\frac{\partial^3\omega(\mathcal{R}_c, \beta_c)}{\partial\mathcal{R}^2\partial\beta}(\mathcal{R} - \mathcal{R}_c)^2(\beta - \beta_c) + \\ &\quad \frac{3}{3!}\frac{\partial^3\omega(\mathcal{R}_c, \beta_c)}{\partial\mathcal{R}\partial\beta^2}(\mathcal{R} - \mathcal{R}_c)(\beta - \beta_c)^2 + \frac{1}{3!}\frac{\partial^3\omega(\mathcal{R}_c, \beta_c)}{\partial\beta^3}(\beta - \beta_c)^3 + \\ &\quad \frac{1}{4!}\frac{\partial^4\omega(\mathcal{R}_c, \beta_c)}{\partial\mathcal{R}^4}(\mathcal{R} - \mathcal{R}_c)^4 + \frac{4}{4!}\frac{\partial^4\omega(\mathcal{R}_c, \beta_c)}{\partial\mathcal{R}^3\partial\beta}(\mathcal{R} - \mathcal{R}_c)^3(\beta - \beta_c) + \\ &\quad \frac{6}{4!}\frac{\partial^4\omega(\mathcal{R}_c, \beta_c)}{\partial\mathcal{R}^2\partial\beta^2}(\mathcal{R} - \mathcal{R}_c)^2(\beta - \beta_c)^2 + \frac{4}{4!}\frac{\partial^4\omega(\mathcal{R}_c, \beta_c)}{\partial\mathcal{R}\partial\beta^3}(\mathcal{R} - \mathcal{R}_c)(\beta - \beta_c)^3 + \\ &\quad \frac{1}{4!}\frac{\partial^4\omega(\mathcal{R}_c, \beta_c)}{\partial\beta^4}(\beta - \beta_c)^4 + \mathcal{O}(5), \end{aligned}$$

where the symbol  $\mathcal{O}(5)$  stands for terms of fifth order and higher. By subtracting the expression for  $i\omega$  from that for  $\sigma$ , the expansion for the dispersion relation is obtained

$$\begin{aligned}
 s_{app}(\mathcal{R}, \beta) &= -i\omega_c + \left( \frac{\partial\sigma(\mathcal{R}_c, \beta_c)}{\partial\mathcal{R}} - i\frac{\partial\omega(\mathcal{R}_c, \beta_c)}{\partial\mathcal{R}} \right) (\mathcal{R} - \mathcal{R}_c) - \\
 &\quad ic_g(\beta - \beta_c) + \frac{1}{2!} \left[ \frac{\partial^2\sigma(\mathcal{R}_c, \beta_c)}{\partial\mathcal{R}^2} - i\frac{\partial^2\omega(\mathcal{R}_c, \beta_c)}{\partial\mathcal{R}^2} \right] (\mathcal{R} - \mathcal{R}_c)^2 + \\
 &\quad \left[ \frac{\partial^2\sigma(\mathcal{R}_c, \beta_c)}{\partial\mathcal{R}\partial\beta} - i\frac{\partial^2\omega(\mathcal{R}_c, \beta_c)}{\partial\mathcal{R}\partial\beta} \right] (\mathcal{R} - \mathcal{R}_c)(\beta - \beta_c) + \frac{1}{2!} \left[ \frac{\partial^2\sigma(\mathcal{R}_c, \beta_c)}{\partial\beta^2} - i\frac{\partial^2\omega(\mathcal{R}_c, \beta_c)}{\partial\beta^2} \right] (\beta - \beta_c)^2 + \\
 &\quad \frac{1}{3!} [...] + \frac{1}{4!} [...] + \mathcal{O}(5), \\
 &= -i\omega_c + \frac{1}{\gamma_c}(\mathcal{R} - \mathcal{R}_c) - ic_g(\beta - \beta_c) + a(\beta - \beta_c)^2 + b(\mathcal{R} - \mathcal{R}_c)(\beta - \beta_c) + c(\mathcal{R} - \mathcal{R}_c)^2 + \\
 &\quad d(\mathcal{R} - \mathcal{R}_c)^3 + e(\mathcal{R} - \mathcal{R}_c)^2(\beta - \beta_c) + f(\mathcal{R} - \mathcal{R}_c)(\beta - \beta_c)^2 + g(\beta - \beta_c)^3 + h(\mathcal{R} - \mathcal{R}_c)^4 + \\
 &\quad k(\mathcal{R} - \mathcal{R}_c)^3(\beta - \beta_c) + m(\mathcal{R} - \mathcal{R}_c)^2(\beta - \beta_c)^2 + n(\mathcal{R} - \mathcal{R}_c)(\beta - \beta_c)^3 + p(\beta - \beta_c)^4 + \mathcal{O}(5).
 \end{aligned} \tag{5.148}$$

Now, as  $\mathcal{A}$  is the envelope of a wave packet, in the neighbourhood of the critical point  $(\mathcal{R}_c, \beta_c)$  it can be expressed as

$$\begin{aligned}
 \mathcal{A} &= \int_0^\infty \tilde{u}(\beta) e^{s_{app}(\mathcal{R}, \beta)t + i(\beta - \beta_c)x} \\
 &= \int_0^\infty \tilde{u}(\beta) e^{\tilde{s}_{app}(\mathcal{R}, \beta)t + i(\beta - \beta_c)x - i\omega_c t},
 \end{aligned} \tag{5.149}$$

where  $\tilde{s}_{app} = s_{app} + i\omega_c$ . By taking the time derivative of  $\mathcal{A}$ , it can be shown that it satisfies the equation

$$\begin{aligned}
 \partial_t \mathcal{A} &= \left[ \frac{1}{\gamma_c}(\mathcal{R} - \mathcal{R}_c) + c(\mathcal{R} - \mathcal{R}_c)^2 + d(\mathcal{R} - \mathcal{R}_c)^3 + h(\mathcal{R} - \mathcal{R}_c)^4 \right] \mathcal{A} \\
 &\quad + [-c_g - ib(\mathcal{R} - \mathcal{R}_c) - ie(\mathcal{R} - \mathcal{R}_c)^2 - ik(\mathcal{R} - \mathcal{R}_c)^3] \partial_x \mathcal{A} \\
 &\quad + [-a - f(\mathcal{R} - \mathcal{R}_c) - m(\mathcal{R} - \mathcal{R}_c)^2] \partial_x^2 \mathcal{A} \\
 &\quad + [ig + in(\mathcal{R} - \mathcal{R}_c)] \partial_x^3 \mathcal{A} + p \partial_x^4 \mathcal{A}.
 \end{aligned} \tag{5.150}$$

The equation above describes the linear dynamics of a wave packet with a fourth order approximation. As we want to derive the G-L equation, we have to add the nonlinear terms to this equation. As previously done, these terms are added in the right-hand side, firstly a cubic term, then a fifth order term and so on up to the desired order. We obtain the following expression

$$\begin{aligned}
 \partial_t \mathcal{A} &= \left[ \frac{1}{\gamma_c}(\mathcal{R} - \mathcal{R}_c) + c(\mathcal{R} - \mathcal{R}_c)^2 + d(\mathcal{R} - \mathcal{R}_c)^3 + h(\mathcal{R} - \mathcal{R}_c)^4 \right] \mathcal{A} \\
 &\quad + [-c_g - ib(\mathcal{R} - \mathcal{R}_c) - ie(\mathcal{R} - \mathcal{R}_c)^2 - ik(\mathcal{R} - \mathcal{R}_c)^3] \partial_x \mathcal{A} \\
 &\quad + [-a - f(\mathcal{R} - \mathcal{R}_c) - m(\mathcal{R} - \mathcal{R}_c)^2] \partial_x^2 \mathcal{A} \\
 &\quad + [ig + in(\mathcal{R} - \mathcal{R}_c)] \partial_x^3 \mathcal{A} + p \partial_x^4 \mathcal{A} - k_1 A |A|^2 - k_2 A |A|^4.
 \end{aligned} \tag{5.151}$$

Equation (5.151) is the Ginzburg–Landau equation truncated at fifth order. By adopting a multiple-scale approach, we introduce the slow time scales and spatial time scales as done in paragraph 5.3.1, so that the amplitude is a function of these new variables and can be expanded in series of  $\epsilon$  as

$$\begin{aligned}
 \mathcal{A}(T_1, T_2, \dots, T_p, X_1, X_2, \dots, X_q) &= \epsilon A(T_1, T_2, \dots, T_p, X_1, X_2, \dots, X_q) \\
 &\quad + \epsilon^3 A(T_1, T_2, \dots, T_p, X_1, X_2, \dots, X_q) |A(T_1, T_2, \dots, T_p, X_1, X_2, \dots, X_q)|^2 \\
 &\quad + \epsilon^5 A(T_1, T_2, \dots, T_p, X_1, X_2, \dots, X_q) |A(T_1, T_2, \dots, T_p, X_1, X_2, \dots, X_q)|^4 + \mathcal{O}(\epsilon^6).
 \end{aligned} \tag{5.152}$$

As a consequence, the differential operators change in the following way

$$\partial_t \mathcal{A} = \epsilon^2 \partial_{T_1} A + \epsilon^3 \partial_{T_2} A + \epsilon^4 (\partial_{T_1} A |A|^2 + \partial_{T_3} A) + \epsilon^5 (\partial_{T_2} A |A|^2 + \partial_{T_4} A) + \mathcal{O}(\epsilon^6),$$

$$\partial_x \mathcal{A} = \epsilon^2 \partial_{X_1} A + \epsilon^3 \partial_{X_2} A + \epsilon^4 (\partial_{X_1} A |A|^2 + \partial_{X_3} A) + \epsilon^5 (\partial_{X_2} A |A|^2 + \partial_{X_4} A) + \mathcal{O}(\epsilon^6), \quad (5.153)$$

$$\partial_x^2 \mathcal{A} = \epsilon^3 \partial_{X_1}^2 A + \epsilon^4 2 \partial_{X_1} \partial_{X_2} A + \epsilon^5 (\partial_{X_1}^2 A |A|^2 + \partial_{X_2}^2 A + 2 \partial_{X_1} \partial_{X_2} A) + \mathcal{O}(\epsilon^6), \quad (5.154)$$

$$\partial_x^3 \mathcal{A} = \epsilon^4 \partial_{X_1}^3 A + \epsilon^5 3 \partial_{X_1}^2 \partial_{X_2} A + \mathcal{O}(\epsilon^6), \quad (5.155)$$

$$(5.156)$$

$$\partial_x^4 \mathcal{A} = \epsilon^5 \partial_{X_1}^4 A + \mathcal{O}(\epsilon^6). \quad (5.157)$$

Now, reminding that  $\mathcal{R} - \mathcal{R}_c = \epsilon^2$  we substitute these expressions in equation (5.151) at the different orders of  $\epsilon$ . At order  $\epsilon$  we find the identity  $0 = 0$ . At order  $\epsilon^2$  we obtain

$$\partial_{T_1} A = -c_g \partial_{X_1} A, \quad (5.158)$$

that is one of the equations obtained in the paragraph 5.3.1. By proceeding to the next order we find at order  $\epsilon^3$

$$\partial_{T_2} A = \frac{1}{\gamma_c} A - c_g \partial_{X_2} A - a \partial_{X_1}^2 A - k_1 A |A|^2, \quad (5.159)$$

that is the well known Ginzburg–Landau equation truncated at third order. At order  $\epsilon^4$  the equation in the amplitude reads

$$\partial_{T_3} A + \partial_{T_1} A |A|^2 = -c_g (\partial_{X_1} A |A|^2 + \partial_{X_3} A) - i b \partial_{X_1} A - 2 a \partial_{X_1} \partial_{X_2} A + i g \partial_{X_1}^3 A. \quad (5.160)$$

Finally, at order  $\epsilon^5$  the Ginzburg–Landau equation reads

$$\begin{aligned} \partial_{T_4} A + \partial_{T_2} A |A|^2 &= c A + \frac{1}{\gamma_c} A |A|^2 - c_g (\partial_{X_2} A |A|^2 + \partial_{X_4} A) - i b \partial_{X_2} A - a (\partial_{X_1}^2 A |A|^2 + \partial_{X_2}^2 A + 2 \partial_{X_1} \partial_{X_2} A) \\ &\quad - f \partial_{X_1}^2 A + 3 i g \partial_{X_1}^2 \partial_{X_2} A + \partial_{X_1}^4 A - (k_1 + k_2) A |A|^4. \end{aligned} \quad (5.161)$$

It is remarkable that only at the fifth order, the term  $A |A|^4$  appears. Moreover, from the fourth order on, the nonlinearity is hidden also in the derivatives of the nonlinear terms  $A |A|^2, A |A|^4, \dots$ . These equations thus, express the nonlinear dynamics of the wave packet on the multiple scales that govern the phenomenon close to the non-hyperbolic state. Obviously, by increasing the order of  $\epsilon$ , the solution of the resulting equation will be more accurate, although more complicated to figure out, since the nonlinear term will play a role in the amplitude equation.

At this point, we want to use the above theory to write the solution at higher orders for the general dynamical system introduced in the paragraph 5.5 and then apply it to the Taylor–Couette problem. As the expressions derived previously show, the thing that changes now, is the expansion of the operators that appear in the governing equation. In the following, the governing equation is briefly rewritten

$$\frac{\partial \mathbf{w}}{\partial t} + L \mathbf{w} = \mathbf{f}(\mathbf{w}). \quad (5.162)$$

We start by writing the operators properly. Concerning the operator  $D$  acting on the nonlinear term, we can expand it as

$$D = D_0 + \epsilon D_1 + \epsilon^2 D_2 + \dots \epsilon^q D_q, \quad (5.163)$$

where inside each operator  $D_m$ , there are the derivatives with respect to the  $m$ -th spatial coordinate. Accordingly, the time differential operator can be expanded as

$$\partial_t = \partial_t + \epsilon \partial_{T_1} + \epsilon^2 \partial_{T_2} + \dots \epsilon^p \partial_{T_p}. \quad (5.164)$$

For what concerns the linear operator  $L$  we can write it as

$$L = L(\mathbb{L}, \nabla, \nabla^2) + \epsilon^2 \tilde{L}, \quad (5.165)$$

where the nabla operator reads as

$$\begin{aligned} \nabla &= \nabla_\perp + \partial_z, \\ &= \nabla_\perp + \partial_z + \epsilon \partial_{Z_1} + \epsilon^2 \partial_{Z_2} + \dots \epsilon^q \partial_{Z_q}, \\ &= \nabla + \epsilon \partial_{Z_1} + \epsilon^2 \partial_{Z_2} + \dots + \epsilon^q \partial_{Z_q}. \end{aligned} \quad (5.166)$$

Notice that, in this context, the slow spatial variable has been written as  $Z$  in place of  $X$ . This because in the application to the Taylor–Couette problem, the modulation of the amplitude acts on the  $z$ -axis. The operator  $\nabla_\perp$  denotes the gradient along the radial and azimuthal direction, i.e. the directions along which there is no modulation of the amplitude. The Laplacian instead can be expressed as

$$\begin{aligned} \nabla^2 &= \nabla_\perp^2 + \partial_z^2, \\ &= \nabla_\perp^2 + (\partial_z + \epsilon \partial_{Z_1} + \epsilon^2 \partial_{Z_2} + \dots \epsilon^q \partial_{Z_q})(\partial_z + \epsilon \partial_{Z_1} + \epsilon^2 \partial_{Z_2} + \dots \epsilon^q \partial_{Z_q}), \\ &= \nabla^2 + \epsilon 2 \partial_z \partial_{Z_1} + \epsilon^2 (2 \partial_z \partial_{Z_2} + \partial_{Z_1}^2) + \dots + \epsilon^{2q} \partial_{Z_q}^2. \end{aligned} \quad (5.167)$$

Hence, exploiting the linearity of the operator  $L$ , it can be written in compact form as

$$L = L + \epsilon L_1 + \epsilon^2 L_2 + \dots + \epsilon^{2q} L_{2q}. \quad (5.168)$$

In order emphasize the second derivative with respect to each slow variable, we rewrite the expression (5.168) in the following form

$$L = L + \epsilon L_1 + \epsilon^2 (\mathbb{L}_2 + \partial_{Z_1}^2) + \epsilon^3 L_3 + \epsilon^4 (\mathbb{L}_4 + \partial_{Z_2}^2) + \dots + \epsilon^{2q} (\mathbb{L}_{2q} + \partial_{Z_q}^2). \quad (5.169)$$

It is useful to notice that only even terms in the expansion of the linear operator  $L$  contain the second derivative with respect to the slow spatial variables. The operators of odd powers in the parameter  $\epsilon$  and the operators  $\mathbb{L}_n$ ,  $\forall n$  even, contain on the contrary the second mixed derivatives with respect to the appropriate variables. Now, we insert the expression in the governing equation. Reminding that

$$\mathbf{w} = \sum_{n=0}^r \sum_{k=0}^n \epsilon^n \mathcal{A}^{n-k} (\mathcal{A}^*)^k \psi_{n,n-2k} e^{n-2k}, \quad (5.170)$$

without writing the summation for convenience, except for the nonlinear operator  $D_0$  because of the reasons explained in the previous paragraph, we can write

$$\begin{aligned} \mathcal{L}\mathbf{w} = & -\epsilon^{n+1} \partial_{T_1} (\mathcal{A}^{n-k} (\mathcal{A}^*)^k) [\psi_{n,n-2k}] e^{n-2k} - \epsilon^{n+2} \partial_{T_2} (\mathcal{A}^{n-k} (\mathcal{A}^*)^k) [\psi_{n,n-2k}] e^{n-2k} - \dots \\ & - \epsilon^{n+p} \partial_{T_p} (\mathcal{A}^{n-k} (\mathcal{A}^*)^k) [\psi_{n,n-2k}] e^{n-2k} - \epsilon^{n+1} L_1 (\mathcal{A}^{n-k} (\mathcal{A}^*)^k [\psi_{n,n-2k}] e^{n-2k}) - \\ & \epsilon^{n+2} L_2 (\mathcal{A}^{n-k} (\mathcal{A}^*)^k [\psi_{n,n-2k}] e^{n-2k}) - \dots - \epsilon^{n+2q} L_{2q} (\mathcal{A}^{n-k} (\mathcal{A}^*)^k [\psi_{n,n-2k}] e^{n-2k}) + \\ & \sum_{n=2}^r \sum_{k=0}^n \epsilon^n D_0 \mathcal{A}^{n-k} (\mathcal{A}^*)^k [\mathbb{M}_{n,n-2k}] e^{n-2k} + \epsilon^{n+1} D_1 \mathcal{A}^{n-k} (\mathcal{A}^*)^k [\mathbb{M}_{n,n-2k}] e^{n-2k} + \\ & \epsilon^{n+2} D_2 \mathcal{A}^{n-k} (\mathcal{A}^*)^k [\mathbb{M}_{n,n-2k}] e^{n-2k} + \dots + \epsilon^{n+q} D_q \mathcal{A}^{n-k} (\mathcal{A}^*)^k [\mathbb{M}_{n,n-2k}] e^{n-2k}. \end{aligned} \quad (5.171)$$

We now solve the systems for any power of  $\epsilon$ , starting from the second one. For each system we multiply the resonant terms by the solution of the linear adjoint problem and integrate in the domain, yielding to a set of partial differential equations with constant coefficients. Thus at order  $\epsilon^2$ , the resonant terms give rise to an equation like

$$-\partial_{T_1} \mathcal{A} - a_1 L_1 \mathcal{A} + a_2 D_1 \mathcal{A} = 0. \quad (5.172)$$

At order  $\epsilon^3$  we get

$$-\partial_{T_2} \mathcal{A} - b_1 L_2 \mathcal{A} + b_2 \mathcal{A} |\mathcal{A}|^2 + b_3 D_2 \mathcal{A} = 0. \quad (5.173)$$

At order  $\epsilon^4$  we have

$$-\partial_{T_3} \mathcal{A} - c_1 \partial_{T_1} (\mathcal{A} |\mathcal{A}|^2) - c_2 L_1 (\mathcal{A} |\mathcal{A}|^2) - c_3 L_3 \mathcal{A} + c_4 D_1 (\mathcal{A} |\mathcal{A}|^2) + c_5 D_3 \mathcal{A} = 0. \quad (5.174)$$

Finally, at order  $\epsilon^5$  we obtain

$$-\partial_{T_4} \mathcal{A} - k_1 \partial_{T_2} (\mathcal{A} |\mathcal{A}|^2) - k_2 L_2 (\mathcal{A} |\mathcal{A}|^2) - k_3 L_4 \mathcal{A} + k_4 (\mathcal{A} |\mathcal{A}|^4) + k_5 D_2 (\mathcal{A} |\mathcal{A}|^2) + k_6 D_4 \mathcal{A} = 0. \quad (5.175)$$

We notice that at fifth order a new nonlinear term arises, that is the term  $\mathcal{A} |\mathcal{A}|^4$ . By going further on the approximation, one can find terms proportional to  $\mathcal{A} |\mathcal{A}|^6, \mathcal{A} |\mathcal{A}|^8, \dots$  and so on. Obviously, having introduced new time and space variables, the unknown will depend on more than two variables, as explained in the previous two paragraphs. Indeed, for example, at the order 3 now, we have also the terms  $D_2 \mathcal{A}$  and  $L_2 \mathcal{A}$  which contain, in addition to the term  $\partial_{Z_1}^2$ , the derivatives of  $\mathcal{A}$  with respect to  $Z_2$ . As a matter of fact, if we exploit the particular form of the operators  $L_2, D_2$  we can write an equation which will read as

$$-\partial_{T_2} \mathcal{A} - h_1 \mathcal{A} - h_2 \partial_{Z_1}^2 \mathcal{A} + h_3 \mathcal{A} |\mathcal{A}|^2 + h_4 \partial_{Z_2} \mathcal{A} = 0, \quad (5.176)$$

that is equivalent, after having exploited the coefficients, to the formulation (5.159) previously derived.

## 5.7 Solutions of the Ginzburg–Landau equation in the case of axisymmetric disturbances

In this section we show the results obtained by solving the Ginzburg–Landau equation in the form (5.121), for the case of axisymmetric disturbances of the Taylor–Couette basic flow when the outer cylinder is at rest and when the gap between the two cylinders is very small. The linear stability analysis associated to this case has been discussed in paragraph 4.4.1 and has implied the formation of axially periodic swirling structures, namely the Taylor vortices. Now we investigate a range of solutions of the Ginzburg–Landau equation related to this situation. The equation we want to solve is here rewritten in the form

$$\partial_T A = c_1 A + c_2 \partial_\xi^2 A - \kappa A |A|^2. \quad (5.177)$$

The coefficients  $c_1$  and  $c_2$  are such that  $c_1 = \frac{-a_1}{\mathcal{R}_c}$  and  $c_2 = \frac{1}{\mathcal{R}_c}$ , with  $a_1, a_2, \kappa$  computed by performing the integrals written in equation (5.119). The coefficients  $c_1, c_2, \kappa$  are reported in table 5.1 for three different values of  $\eta$ . As the Landau coefficient is positive, when the gap is small the Taylor vortices are a supercritical bifurcation of the Taylor–Couette basic flow and the Ginzburg–Landau equation is real, with  $\xi = \epsilon z$ . The computed coefficients are also in accordance with the literature [3], [22], [1], [2]. In particular in table 5.2, the coefficients of the linear terms for  $\eta = 0.95$  are compared with those obtained by Tabeling [22] with a different scaling of the slow variables ( $t_2 = \frac{10}{\mathcal{R}_c^{3/2}} T$ ,  $z_1 = \frac{\sqrt{10}}{\mathcal{R}_c^{1/4}} \xi$ ). As it can be seen, they agree well.

In the following, as the aim is to describe the evolution of the amplitude of the perturbations

Table 5.1: Coefficients of the G–L equation for  $\alpha = 0$  and in the case the outer cylinder is fixed. The coefficients are also computed for three different values of  $\eta$ .

$\eta$	$c_1$	$c_2$	$\kappa$
0.95	0.1054	0.0054	0.030
0.90	0.1467	0.0075	0.090
0.85	0.1761	0.0092	0.1701

Table 5.2: Comparison of the coefficients of the linear terms in the G–L equation for  $\eta = 0.95$

	$c_1$	$c_2$
My coeff.	26.52	0.99
Tabeling coeff.	26.16	0.98

depending on the small parameter  $\epsilon$ , we rewrite the G–L equation making use of the physical variables  $(t, z)$ . This is done by reminding the definitions of  $T, \xi$  and  $A$ . In particular, by changing the variables into

$$\begin{aligned} t &= \frac{T}{\epsilon^2}, \\ z &= \frac{\xi}{\epsilon}, \\ A &= \frac{\mathcal{A}}{\epsilon}, \end{aligned} \quad (5.178)$$

the G–L equation reads as

$$\partial_t \mathcal{A} = c_1 \epsilon^2 \mathcal{A} + c_2 \partial_z^2 \mathcal{A} - \kappa \mathcal{A} |\mathcal{A}|^2. \quad (5.179)$$

In the following paragraphs, we are going to obtain some type of solutions by changing the value of the control parameter  $\epsilon$ . In particular, we will analyse solutions for which  $\epsilon^2 = (0.01, 0.1)$  relatively to the case with  $\eta = 0.85$ . This is due to the fact that in this case we can compare the results with those obtained from the DNS. By doing so, some hypothesis have to be made:

- we assume that in the interval of the values of  $\epsilon$  considered, the Taylor vortices do not become linearly unstable themselves, but they remain the only bifurcating solution related to the T-C flow.
- we assume that there exists only one marginally stable mode, that is the one used to obtain the Ginzburg–Landau equation in the form (5.179).
- after having found the solution of the G–L equation, i.e. the function  $\mathcal{A}(z, t)$ , we take the expansion of the solution in physical variables truncated at the first order, that is  $\mathbf{u} = \mathbf{u}_0 + \epsilon A \psi e^{i\beta_c z} + c.c. = \mathbf{u}_0 + \mathcal{A}(z, t) \psi e^{i\beta_c z} + c.c.$ . This is possible as if the control parameter is sufficiently small, then the higher order terms do not play a significant role in the summation of the higher-order terms.

Having introduced these assumptions, we proceed by deriving the solutions of the Ginzburg–Landau equation.

### 5.7.1 Stationary periodic solution

We look for a solution of equation (5.179) in the form

$$\mathcal{A} = a_0 e^{iqz}, \quad (5.180)$$

where  $q$  is a parameter defined in the interval  $[-|\epsilon| \sqrt{\frac{c_1}{c_2}}, |\epsilon| \sqrt{\frac{c_1}{c_2}}]$ , such that

$$q = \beta - \beta_c. \quad (5.181)$$

By substituting the expression (5.180) into the G–L equation, we get

$$a_0 (c_1 \epsilon^2 - c_2 q^2 - \kappa a_0^2) = 0, \quad (5.182)$$

therefore a family of non-trivial solutions exist

$$a_0 = \pm \sqrt{\frac{c_1 \epsilon^2 - c_2 q^2}{\kappa}}, \quad -|\epsilon| \sqrt{\frac{c_1}{c_2}} \leq q \leq |\epsilon| \sqrt{\frac{c_1}{c_2}}. \quad (5.183)$$

Now we define an important function, that will help us understanding the nonlinear behaviour of the solutions compared to the linear one, especially it will be very useful to characterize how the vortices evolve along the axis of the cylinders. The function is defined as  $f(z) = \mathcal{A}(z) e^{i\beta_c z}$ . In the particular case under analysis, this function is equal to

$$f(z) = \sqrt{\frac{\epsilon^2 c_1 - c_2 (\beta - \beta_c)^2}{\kappa}} e^{i\beta_c z}. \quad (5.184)$$

As it can be seen, it depends on the parameters  $\epsilon$  and  $\beta$ . Thus, depending on how far we are from the threshold, the nonlinear term may vary the amplitude and the wavelength of the vortices. The behaviour of the function  $f(z)$  is shown in the following figures for different values of  $\epsilon$  and  $\beta$  and compared with the one obtained from the linear theory, that is  $f_{lin}(z) = \epsilon e^{i\beta_c z}$ .

#### The case $\epsilon^2 = 0.01$

Define  $\epsilon^2 = 0.01$  means to investigate the nonlinear behaviour of the vortices for a Reynolds number  $\mathcal{R} = 109.40$ . In the following figures, we show the results of the G–L equation for two values of the axial wavenumber. From figure 5.16 it can be noted the shift in the wavelength, i.e. in the size of the vortices when  $\beta = (1 + 0.05)\beta_c$ . This is clearer by looking at the pattern of the vortices in figure 5.18 where instead in the case  $\beta = \beta_c$  the two pattern are very similar.

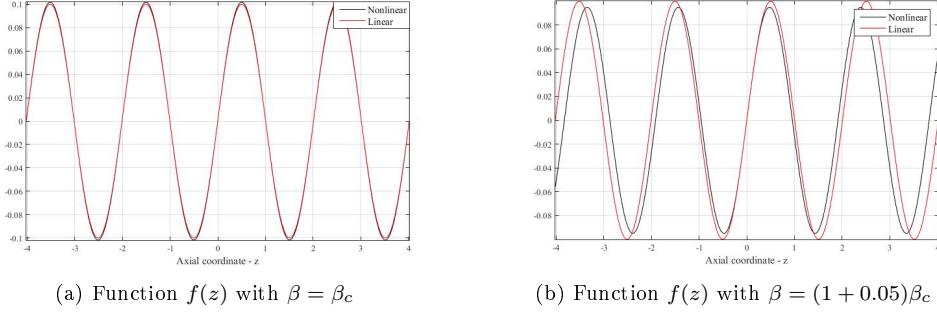


Figure 5.16: Behaviour of the function  $f(z) = \mathcal{A}(z)e^{i\beta_c z}$  for two different values of the axial wavenumber and with  $\epsilon^2 = 0.01$ . The critical wavenumber is  $\beta_c = 3.13$ .

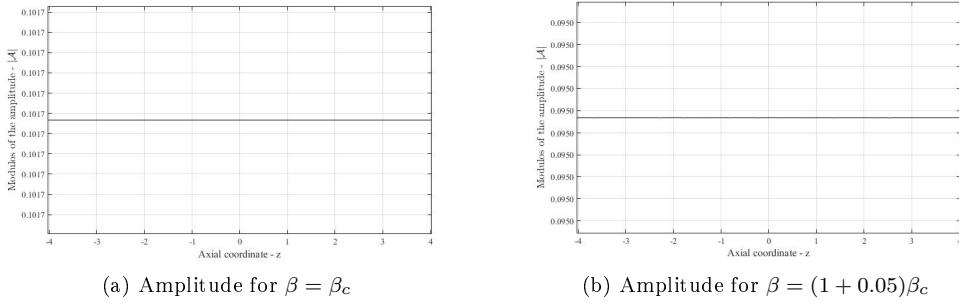


Figure 5.17: Comparison of the amplitude  $\mathcal{A}(z)$  for two different values of the axial wavenumber and with  $\epsilon^2 = 0.01$ . The critical wavenumber is  $\beta_c = 3.13$ .

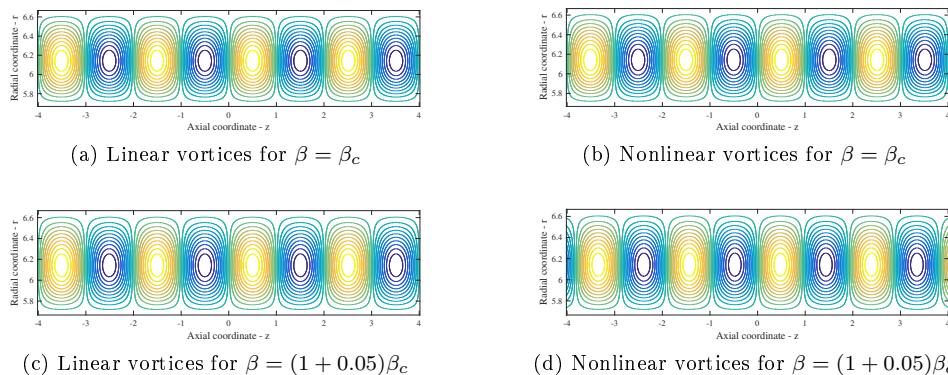


Figure 5.18: Streamline of the vortices for the two values of  $\beta$  and with  $\epsilon^2 = 0.01$ , both in the linear and nonlinear case.

### The case $\epsilon^2 = 0.1$

In this case, the Reynolds has been increased to  $\mathcal{R} = 119.15$ . As done in the previous example, the following figures show the results for two different values of  $\beta$ . Except the values in modulus of the amplitude and of the range of variation of the function  $f$ , the qualitative shape remains the same as for the previous case. Hence also the pattern formed will have the same characteristics.

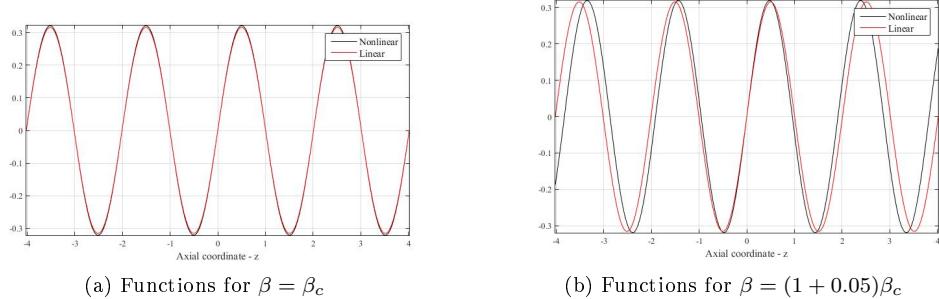


Figure 5.19: Behaviour of the function  $f(z) = \mathcal{A}(z)e^{i\beta_c z}$  for two different values of the axial wavenumber and with  $\epsilon^2 = 0.1$ . The critical wavenumber is  $\beta_c = 3.13$ .

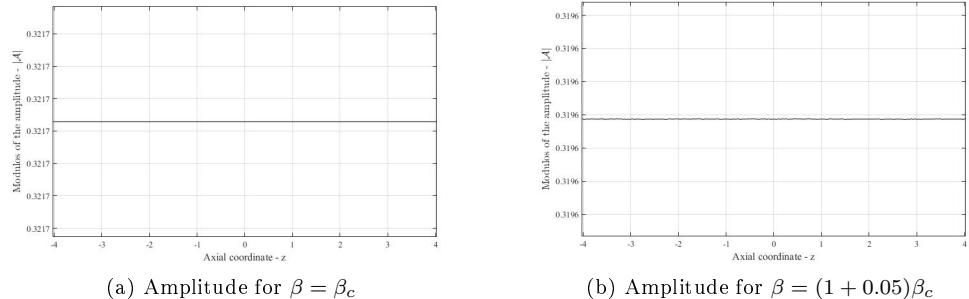


Figure 5.20: Comparison of the amplitude  $\mathcal{A}(z)$  for two different values of the axial wavenumber and with  $\epsilon^2 = 0.1$ . The critical wavenumber is  $\beta_c = 3.13$ .

### 5.7.2 Stationary non-periodic solution

In order to get a non-periodic solution of the G–L equation, we add boundaries to the axial domain, that mathematically means to impose boundary conditions to the equation (5.179). We define the axial domain  $z = [-L, L]$  and impose homogeneous Dirichlet boundary conditions at  $z = \pm L$ . Physically, this means to investigate if and how the Taylor vortices disappear along the cylinders, restoring the Taylor–Couette basic flow. In practice, this could be caused by the presence of a forcing term so that at  $z = \pm L$ , the Taylor–Couette solution holds. By looking for a steady solution, i.e.  $\mathcal{A} = \mathcal{A}(z)$ , the problem we want to solve is the following

$$\begin{aligned} c_1\epsilon^2 \mathcal{A} + c_2 \frac{d^2 \mathcal{A}}{dz^2} - \kappa \mathcal{A} |\mathcal{A}|^2 &= 0, \\ \mathcal{A}(-L) &= 0, \\ \mathcal{A}(L) &= 0. \end{aligned} \tag{5.185}$$

By virtue of the previous scenario, this problem is equivalent to solve the following Navier–Stokes problem

$$\begin{aligned} (\mathbf{u} \cdot \nabla) \mathbf{u} + \nabla p - \frac{1}{\mathcal{R}} \nabla^2 \mathbf{u} &= 0, \\ \nabla \cdot \mathbf{u} &= 0, \\ \mathbf{u}|_{S_L} &= \mathbf{u}_{TC}, \end{aligned} \tag{5.186}$$

where  $S_L$  is the total boundary of the flow inside the interval  $[-L, L]$  and  $\mathbf{u}_{TC}$  is the Taylor–Couette flow. We analyse two situations, depending on the value of  $\epsilon$ . The values taken into consideration are as usual  $\epsilon^2 = 0.01$  and  $\epsilon^2 = 0.1$ . Moreover, we will always assume that  $L = \frac{5}{0.85}$ , so that we can compare the results with those obtained from a DNS simulation performed using the software FreeFem++ [31]. About this point indeed, we assume that the flow simulated with the DNS has the same Reynolds number of our flow. In addition we assume that the ratio between the gap of the radii and the length of the cylinders is the same, that is  $\frac{d_{DNS}}{L_{DNS}} = \frac{d}{L}$ . For this reason we take  $d_{DNS} = 0.5$  and  $L_{DNS} = \frac{2.5}{0.85}$ . Moreover we take  $R_a = 2.83$  and  $R_b = 3.33$ , so that the ratio between the radii is 0.85. A representation of the computational domain and of the mesh used, is given in figure 5.21

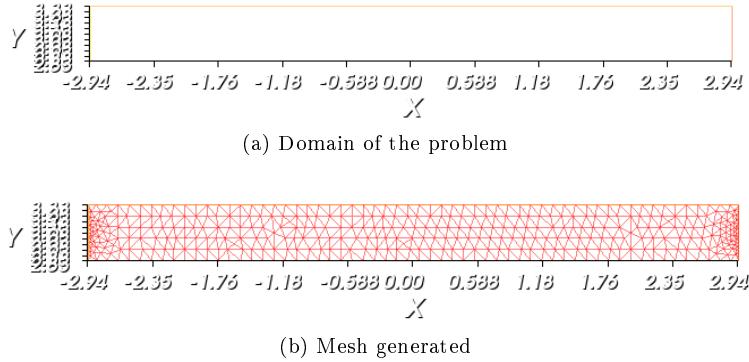
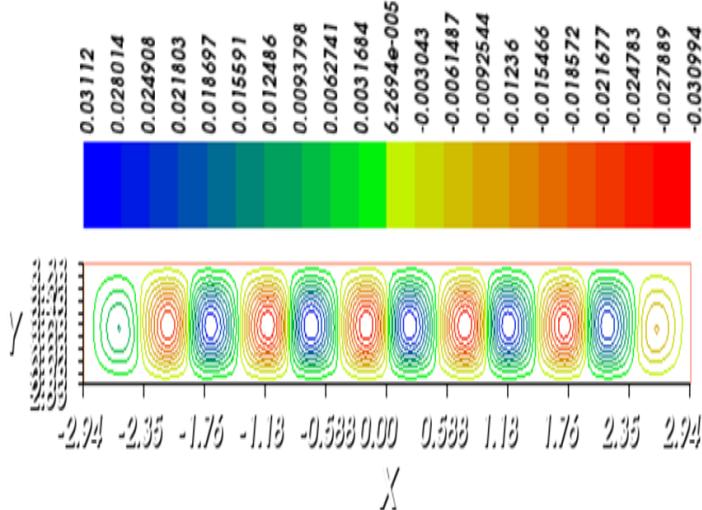


Figure 5.21: Computational domain used for the DNS

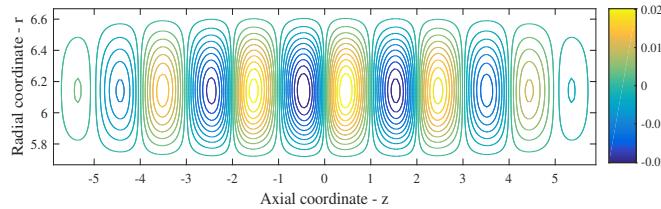
#### The case $\epsilon^2 = 0.01$

If  $\epsilon^2 = 0.01$ , the Reynolds number is  $\mathcal{R} = 109.40$ . By solving numerically the Ginzburg–Landau equation, we get the following results. In figure 5.22 the cell pattern of the solution is shown and compared with the one obtained solving the full Navier–Stokes problem by means of the DNS code. As it can be seen, they seem quite similar and moreover the values of the streamline function agree well just by using a first order approximation in the solution for the velocity. The difference in the maximum values of both the streamline functions is very small. In figures 5.22d and 5.22c the behaviour of the amplitude  $\mathcal{A}$  and the function  $f(z) = \mathcal{A}(z)e^{i\beta_c z}$  are shown

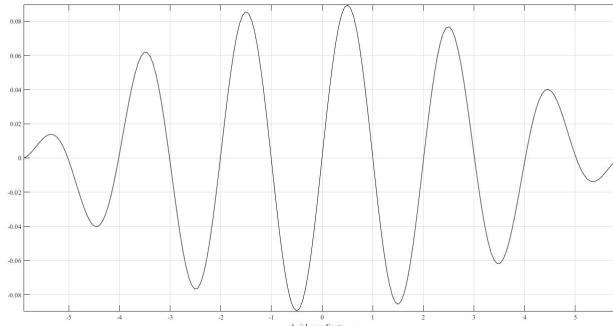
respectively. As it can be noticed, as the flow approaches the walls, the vortices deform and decrease their height and their width, disappearing totally at the walls. In figure 5.23c instead, it is given a comparison between the axial function  $f(z)$  in this specific case and that concerning the linear stability analysis, for which  $f_{lin}(z) = \epsilon e^{i\beta_c z}$ . From this figure it can appreciated how in the middle of the cylinders the two functions are similar so also the structure of the vortices. However due to the boundary conditions, there is a considerable damping close to the walls. In figure 5.23a and 5.23b, there is a comparison of the cell pattern given by the nonlinear theory and the one given by the linear theory, for which the assumption of infinite cylinders holds.



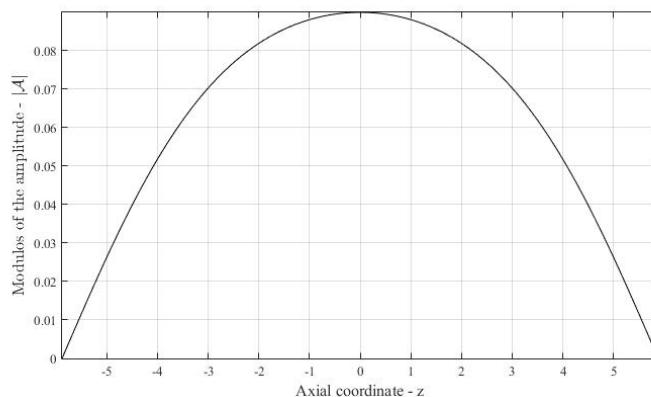
(a) Streamline function computed with the DNS. The function is scaled by a factor  $U_{DNS} d_{DNS}^2$ , where  $U_{DNS} = (\epsilon^2 + 1)\mathcal{R}_c/d_{DNS}$ .



(b) Streamline function computed by solving the G-L equation.

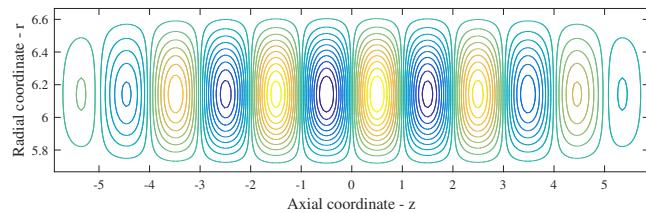


(c) Behaviour of the function  $f(z) = A(z)e^{i\beta_c z}$  for  $\epsilon^2 = 0.01$  which represents the periodic formation of the vortices along the axis. In the figure it is clear the damping close to the boundaries.

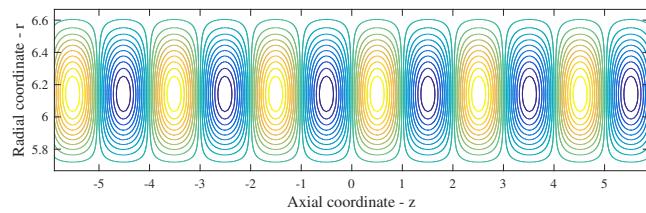


(d) Trend of the amplitude  $A$  along the axis for  $\epsilon^2 = 0.01$ .

Figure 5.22: Representation of the behaviour of the Taylor vortices in the steady case for  $\mathcal{R} = 109.40$ .



(a) Cell pattern in the nonlinear bounded case



(b) Cell pattern in the linear unbounded case

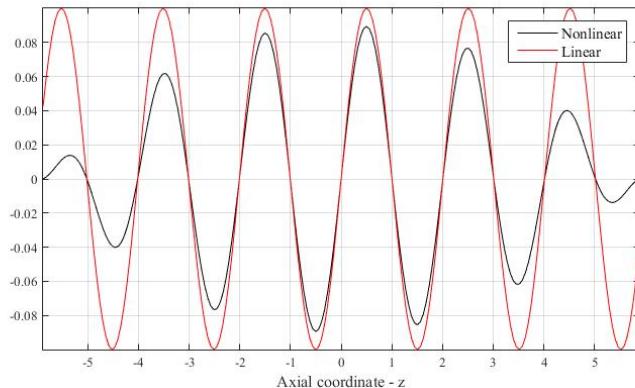
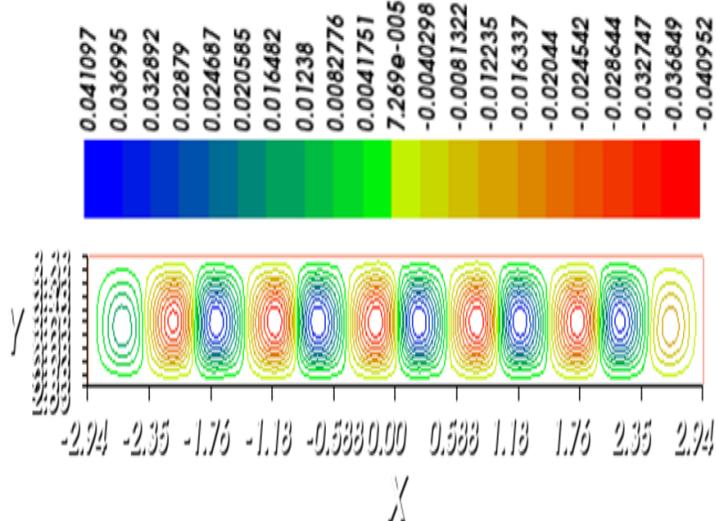
(c) Comparison between the function  $f(z)$  both in the linear and in the nonlinear case

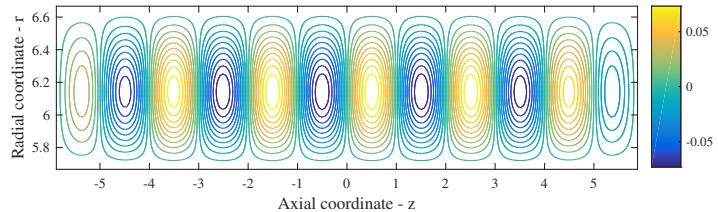
Figure 5.23: Comparison of the cell pattern formed both in the nonlinear and in the linear case.

### The case $\epsilon^2 = 0.1$

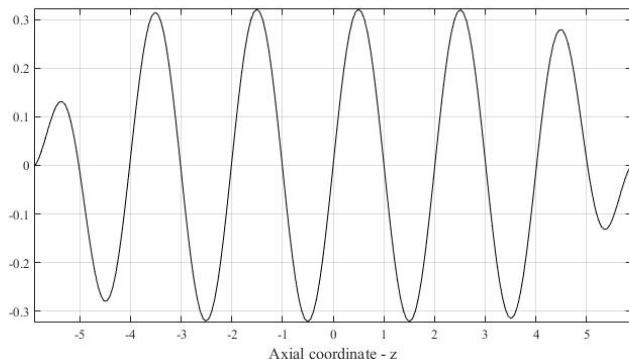
In this case, we consider a Reynolds number  $\mathcal{R} = 119.15$ . By solving the problem (5.185), we get the following results. As done before, in figure 5.24 we show the trend of the Taylor vortices highlighting the effects that the walls have on them. By making a comparison with the case  $\epsilon^2 = 0.01$ , the amplitude of the perturbation is higher and reaches the asymptotic value  $\left(\frac{c_1 \epsilon^2}{k}\right)^{1/2}$  very quickly going from the left wall to the centre of the axis and then goes back to zero on the opposite wall. It means we have a stronger and faster modulation of the amplitude near the boundaries. Moreover it can be said that the intensity of the vortices in the present case is higher than in the previous one and it is visible by the colour of the streamlines; the intensity of the colours become higher just at a short distance from the walls. For the comparison with the DNS, the behaviour is in agreement. The main difference is in the maximum value of the streamline function (0.06 for the G–L approximation, 0.04 for the exact solution from the DNS), however, thought the difference is not very high, it is present since we are at a greater distance from the critical point. In figure 5.25c the usual function  $f(z)$  is shown and compared with the one belonging to the linear theory. Finally in figure 5.25 the shape of the cells is compared both in the nonlinear bounded case and in the linear unbounded case.



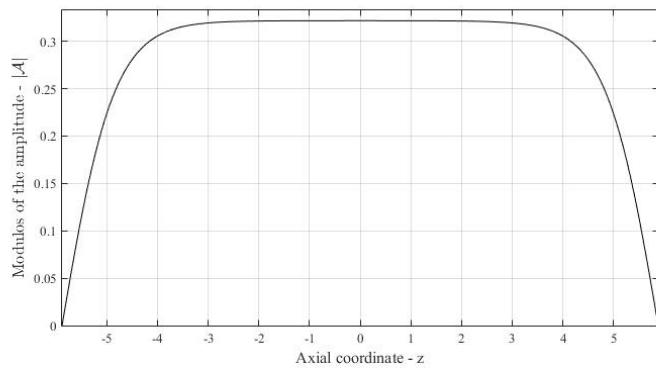
(a) Streamline function computed with the DNS. The function is scaled by a factor  $U_{DNS} d_{DNS}^2$ , where  $U_{DNS} = (\epsilon^2 + 1)\mathcal{R}_c/d_{DNS}$ .



(b) Streamline function computed by solving the G-L equation.

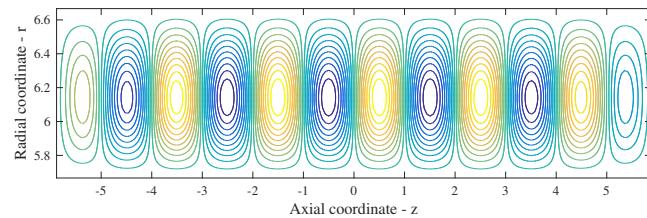


(c) Behaviour of the function  $f(z) = \mathcal{A}(z)e^{i\beta_c z}$  for  $\epsilon^2 = 0.1$  which represents the periodic formation of the vortices along the axis. In the figure it is clear the damping close to the boundaries.

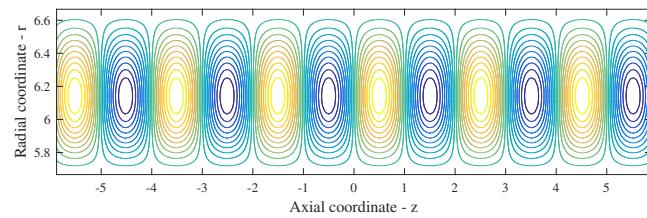


(d) Trend of the amplitude  $\mathcal{A}$  along the axis for  $\epsilon^2 = 0.1$ .

Figure 5.24: Representation of the behaviour of the Taylor vortices in the steady case for  $\mathcal{R} = 119.15$ .



(a) Cell pattern in the nonlinear bounded case.



(b) Cell pattern in the linear unbounded case.

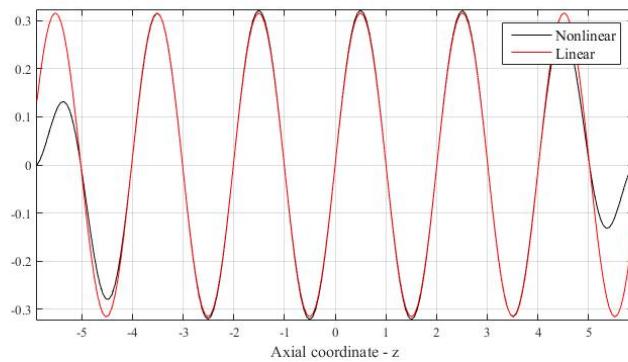
(c) Comparison between the function  $f(z)$  both in the linear and in the nonlinear case.

Figure 5.25: Comparison of the cell pattern formed both in the nonlinear and in the linear case

### 5.7.3 Unsteady periodic solution

Now we try to find a solution of the equation (5.177) that is still periodic along the z-axis, but such that the amplitude can vary in time. Hence we search a solution in the form

$$\mathcal{A}(z, t) = a(t)e^{iqz}. \quad (5.187)$$

By performing the derivatives, we get the following differential equation to be solved

$$\frac{da}{dt} = (c_1\epsilon^2 - c_2q^2)a - \kappa a^3. \quad (5.188)$$

In order to get a unique solution, we impose the initial condition  $a(0) = a_0$ . Thus the complete problem reads as

$$\begin{cases} \frac{da}{dt} = (c_1\epsilon^2 - c_2q^2)a - \kappa a^3, \\ a(0) = a_0. \end{cases} \quad (5.189)$$

By calling  $c$  the quantity  $c = c_1\epsilon^2 - c_2q^2$ , we can integrate analytically the equation (5.189), as it is equal to the Van der Pol oscillator equation. By doing so, the general solution is expressed as

$$a(t) = \sqrt{\frac{He^{2ct}}{1 + \frac{\kappa H}{c}e^{2ct}}}. \quad (5.190)$$

By imposing the initial condition we find out that  $H = \frac{a_0^2}{1 - \frac{\kappa}{c}a_0^2}$ , hence the final solution is

$$a(t) = \sqrt{\frac{\frac{a_0^2}{1 - \frac{\kappa}{c}a_0^2}e^{2ct}}{1 + \frac{\kappa}{c}\frac{a_0^2}{1 - \frac{\kappa}{c}a_0^2}e^{2ct}}}, \quad c = c(q, \epsilon), n \in \mathbb{N}. \quad (5.191)$$

In terms of the unknown for the G–L equation, the final result is given by

$$\mathcal{A}(z, t) = \left( \sqrt{\frac{\frac{a_0^2}{1 - \frac{\kappa}{c}a_0^2}e^{2ct}}{1 + \frac{\kappa}{c}\frac{a_0^2}{1 - \frac{\kappa}{c}a_0^2}e^{2ct}}} \right) e^{iq\xi}. \quad (5.192)$$

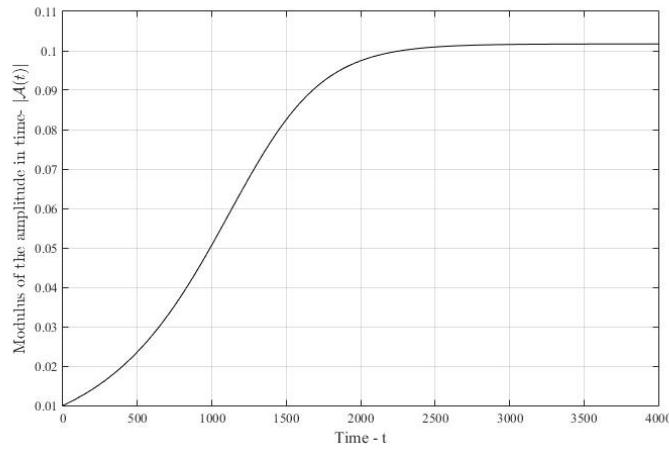
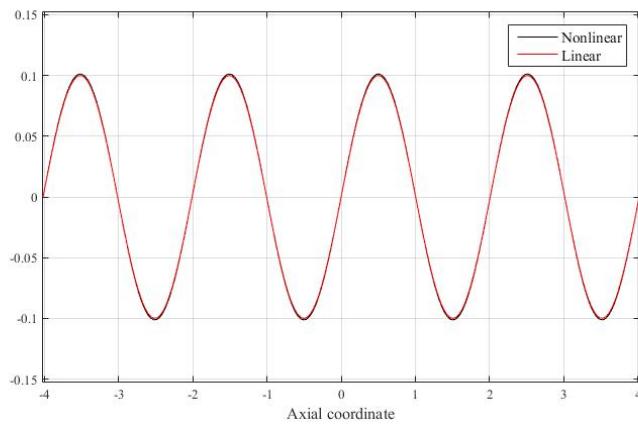
From the equation above, it is clear that the solution depends on the parameters  $q$  and  $\epsilon$ . In particular, depending on the sign of  $c(q, \epsilon)$ , there can exist stable finite-amplitude equilibrium solutions as  $t \rightarrow +\infty$  or, on the contrary, only infinitesimal trivial equilibrium solutions  $\mathcal{A} = 0$ . Indeed, we can distinguish two situations:

- if  $c(q, \epsilon) > 0$ , then the system reaches an asymptotic equilibrium state given by  $a_{eq} = \sqrt{c/\kappa} \Rightarrow \mathcal{A}_{eq}(\xi) = \sqrt{\frac{c}{\kappa}}e^{iq\xi}$ .
- if  $c(q, \epsilon) \leq 0$ , then the system doesn't reach a finite and stable equilibrium state, but it reaches just the trivial equilibrium solution  $a_{eq} = 0 \Rightarrow \mathcal{A}_{eq}(\xi) = 0$ .

In order to show the results, we take as initial condition a small sinusoidal disturbance, i.e.  $\mathcal{A}(z, 0) = 0.01e^{iqz} \Rightarrow a(0) = 0.01$ . Moreover we assume that  $\epsilon^2 = 0.01$  so that to show the results for two different wavenumbers.

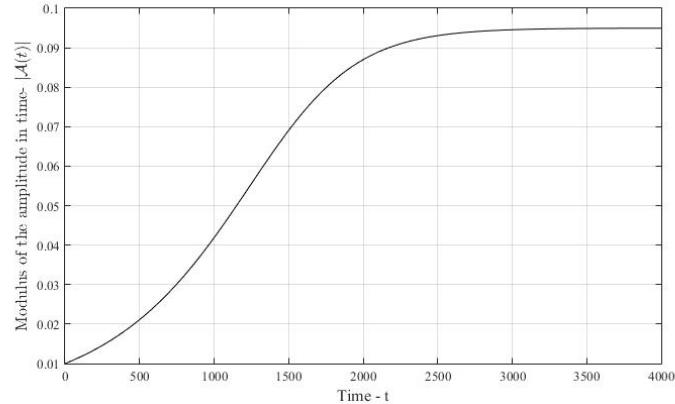
**The case  $\beta = \beta_c$**

In this context  $q = 0$ . This implies that  $c(q, \epsilon) = 0.0018 > 0$ . So, the system will reach an asymptotic equilibrium value given by  $\mathcal{A}_{eq} = \sqrt{\frac{c}{\kappa}}e^{iqz} = 0.1875$ . In figure 5.26a the variation in time of the amplitude is given. As  $t \rightarrow +\infty$  it reaches the equilibrium value  $a_{eq} = 0.1017$ . In figure 5.26b is given a comparison between the function  $f(z)$  in this case and in the usual linear case. As it is can be seen, in this situation there is no phase shift in the propagation of the disturbances, and variation in the amplitude is null in practise. As a consequence, the pattern of the vortices are the same.

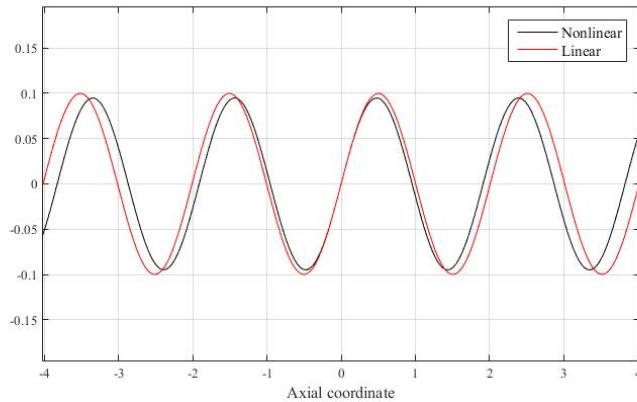
(a) Variation in time of the amplitude  $a(t)$ (b) Function  $f(z)$  computed at the final time  $t_{fin} = 4000$ Figure 5.26: Behaviour of the solution  $\mathcal{A}(z, t)$  for  $\beta = \beta_c = 3.13$ .

**The case  $\beta = (1 + 0.05)\beta_c$**

In this case  $q = 0.05\beta_c$ , so we expect a shift in the wavelength. Moreover, by calculation we get that  $c(q, \epsilon) = 0.0017 < 0$ . Again the system will tend to reach the asymptotic state  $\mathcal{A}_{eq} = 0.095e^{i0.05\beta_c z}$ . The behaviour of the amplitude in time at  $z = 0$  is shown in figure 5.27, whereas the function  $f(z)$  at  $t = 4000$  is shown in figure 5.27b and compared with the linear case. It is appreciable the change in the phase. As a consequence, the patterns in the nonlinear case will be shifted with respect to the linear one.

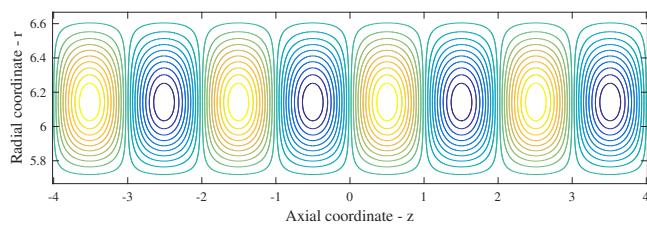


(a) Variation in time of the amplitude at  $z = 0$

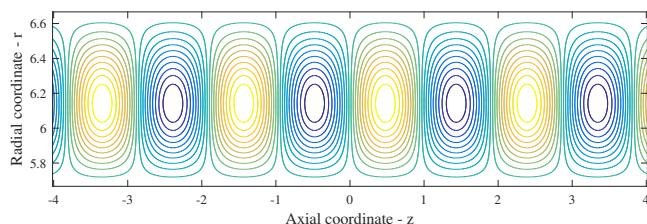


(b) Comparison of the  $f(z)$  at  $t = 4000$  both in the nonlinear and in the linear case

Figure 5.27: Behaviour of the solution  $\mathcal{A}(z, t)$  for  $\beta = (1 + 0.05)\beta_c$  and  $\beta_c = 3.13$ .



(a) Cell pattern in the linear case



(b) Cell pattern in the nonlinear case

Figure 5.28: Comparison of the structure of the Taylor vortices at  $t = 4000$  between the linear and the nonlinear case.

### 5.7.4 Unsteady non-periodic solution

In this paragraph, we investigate a solution of the unsteady G–L equation by imposing homogeneous Dirichlet boundary conditions at certain points along the axis and then we compare the results with a DNS simulation, as done for the stationary case. We consider a time domain of the order  $\mathcal{O}(10^3)$  to compare the results also with the steady case. For what concerns instead the axial domain we consider  $z \in [-L, L]$  with  $L = \frac{5}{0.85}$ . The domain of the DNS is the same as before:  $r \in [2.83, 3.33]$  and  $z \in [-\frac{2.5}{0.85}, \frac{2.5}{0.85}]$ . These values guarantees that the flows simulated by solving the Ginzburg–Landau equation and that given by the DNS, have the same Reynolds number, the same ratio between the gap of the radii and the length of the cylinders and the same ratio between the radii. In this case, as the G–L equation depends on time, we have to impose an initial condition. For this, we assume it to be a small disturbance of order  $\mathcal{O}(10^{-2})$  or less. This being said, the general problem we want to solve has the form

$$\begin{aligned} \partial_t \mathcal{A} &= c_1 \epsilon^2 \mathcal{A} + c_2 \partial_z^2 \mathcal{A} - \kappa \mathcal{A} |\mathcal{A}|^2, \\ \mathcal{A}(-L, t) &= 0, \\ \mathcal{A}(L, t) &= 0, \\ \mathcal{A}(z, 0) &= \mathcal{A}_0(z). \end{aligned} \tag{5.193}$$

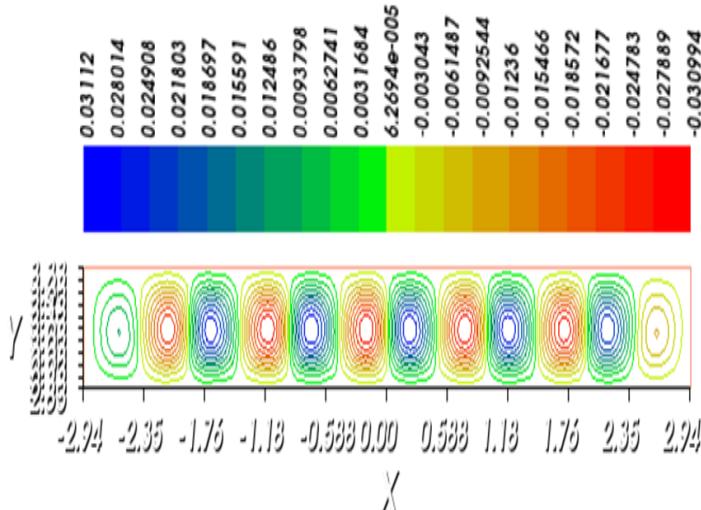
We assume that the amplitude  $\mathcal{A}$  is real only, i.e.  $\mathcal{A}(z, t) = a(z, t)$ , with no shift in the wavelength. As done in the steady case, the problem (5.193) is equivalent to solve the complete Navier–Stokes problem

$$\begin{aligned} \partial_t \mathbf{u} + (\mathbf{u} \cdot \nabla) \mathbf{u} + \nabla p - \frac{1}{\mathcal{R}} \nabla^2 \mathbf{u} &= 0, \\ \nabla \cdot \mathbf{u} &= 0, \\ \mathbf{u}|_{S_L} &= \mathbf{u}_{TC}, \\ \mathbf{u}|_{t=0} &= \mathbf{u}_{In}, \end{aligned} \tag{5.194}$$

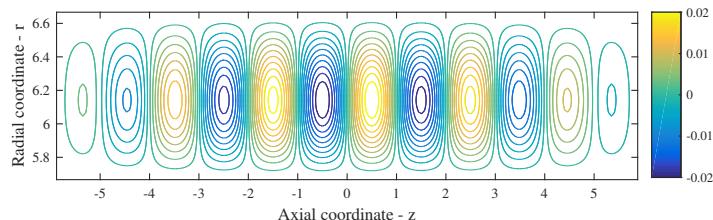
where  $S_L$  is the total boundary of the flow inside the interval  $[-L, L]$ ,  $\mathbf{u}_{TC}$  is the Taylor–Couette flow and  $\mathbf{u}_{In}$  is a suitable initial velocity field. For example, in our computations we set  $\mathbf{u}_{In} = \mathbf{0}$ .

#### Solution with $\epsilon^2 = 0.01$

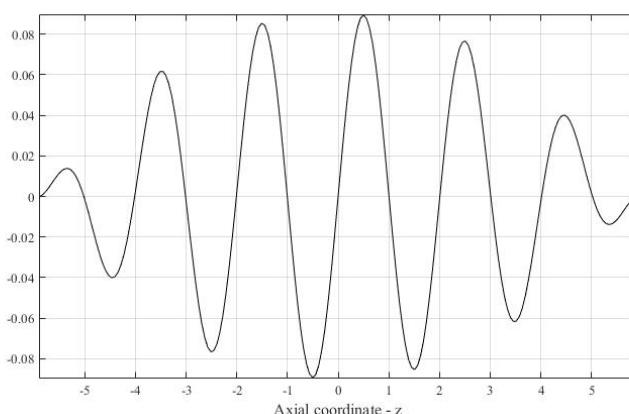
We want to simulate the trend of the solution given by the Ginzburg–Landau equation both in space and in time. We take a time interval  $t \in [0, 4000]$  and by solving the complete problem (5.193) assuming  $\mathcal{A}_0(z) = \bar{a}_0 = 1.e-02$ , the following results are derived. In figure 5.29 we show the structure of the vortices at the final time considered  $t_{fin} = 4000$  and we compare the behaviour with the DNS. As it can be noticed, the streamline function in both cases has a very similar shape with values comparable one another. Particularly, they are equal to the ones of the steady case as the system at  $t_{fin} = 4000$  has reached an asymptotic equilibrium condition that is stationary. In figure 5.30 instead is represented the complete solution of the G–L equation  $\mathcal{A}(z, t)$ , with a particular attention on its time evolution, figure 5.30c.



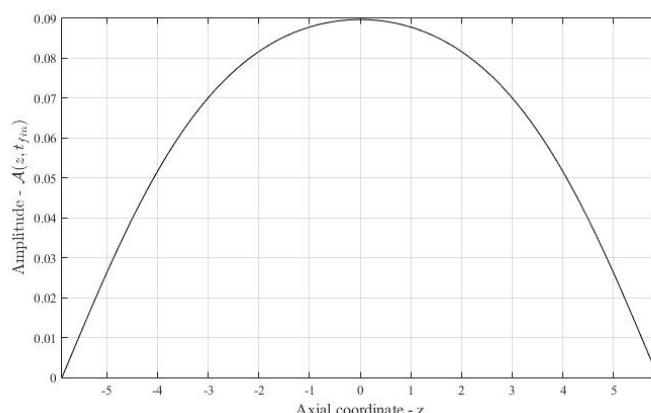
(a) Streamline function computed with the DNS. The function is scaled by a factor  $U_{DNS} d_{DNS}^2$ , where  $U_{DNS} = (\epsilon^2 + 1)\mathcal{R}_c/d_{DNS}$ .



(b) Cell pattern given by the solution of the G-L equation at  $t = 4000$ .

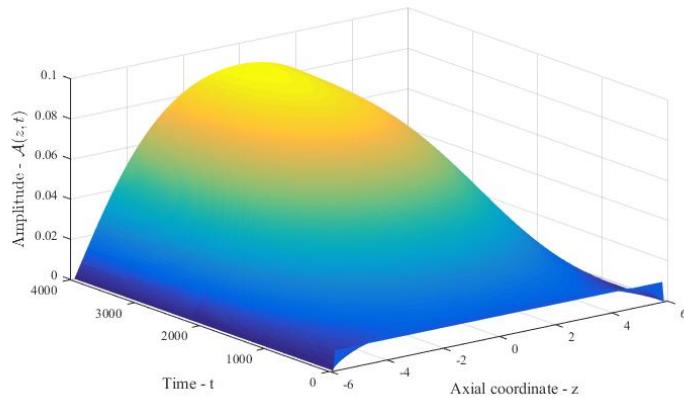
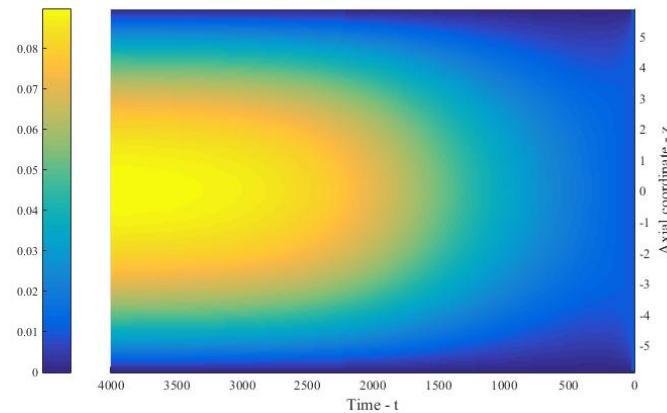
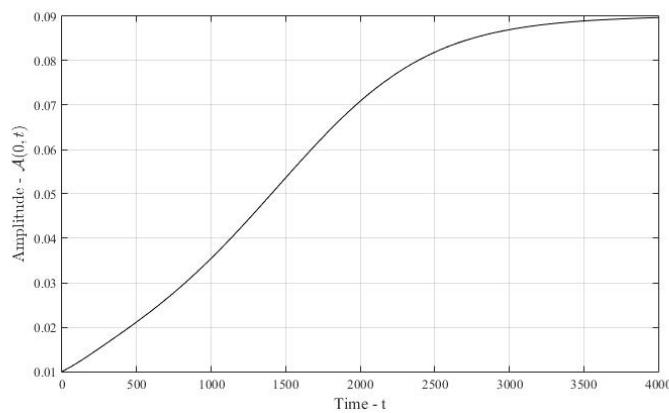


(c) Behaviour of the function  $f(z) = \mathcal{A}(z, t)e^{i\beta_c z}$  at  $t = 4000$ .



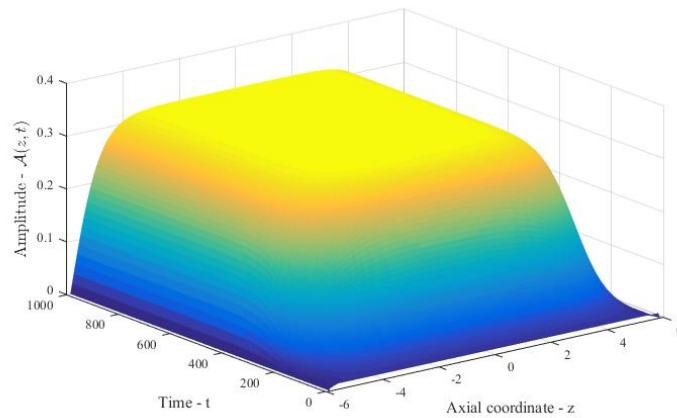
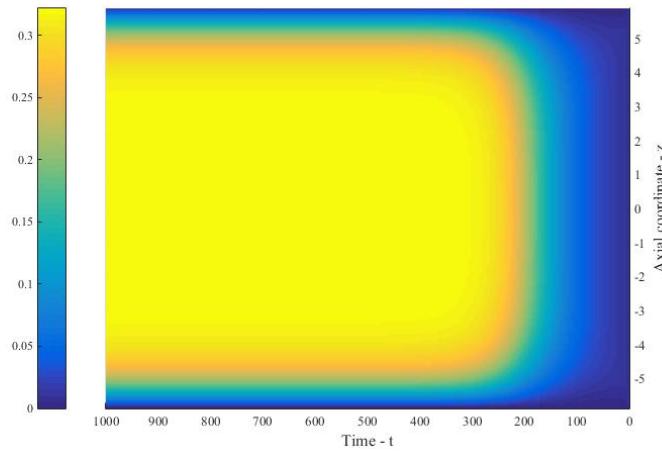
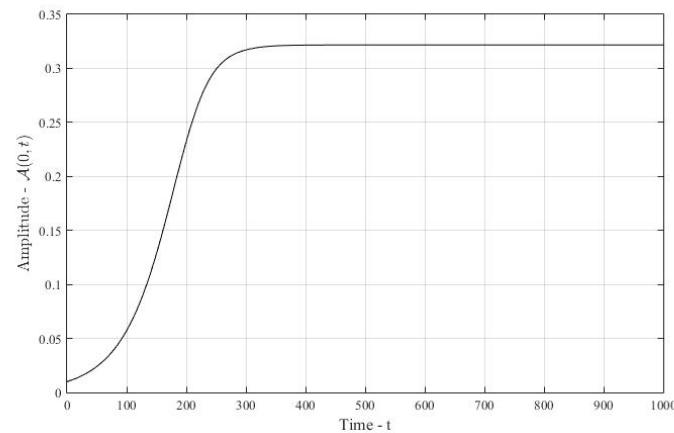
(d) Behaviour of the amplitude  $\mathcal{A}(z, t)$  at  $t = 4000$ .

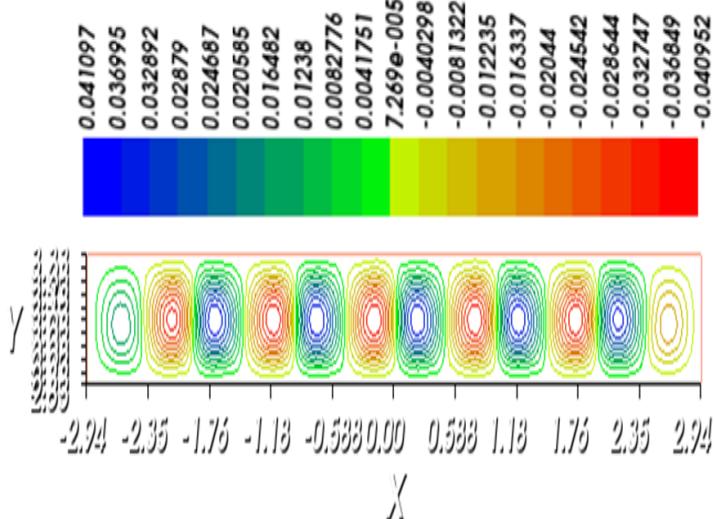
Figure 5.29: Structure of the Taylor vortices for  $t = t_{fin} = 4000$  in the case  $\epsilon^2 = 0.01$ .

(a) 3D visualization of the amplitude  $\mathcal{A}(z, t)$ .(b) 2D visualization of the amplitude  $\mathcal{A}(z, t)$ .(c) Time behaviour of the amplitude at the centreline point  $\mathcal{A}(0, t)$  when  $\epsilon^2 = 0.01$ .Figure 5.30: Complete solution  $\mathcal{A}(z, t)$  of the G–L equation with homogeneous Dirichlet boundary conditions at  $z = \pm L$  and with  $\epsilon^2 = 0.01$ .

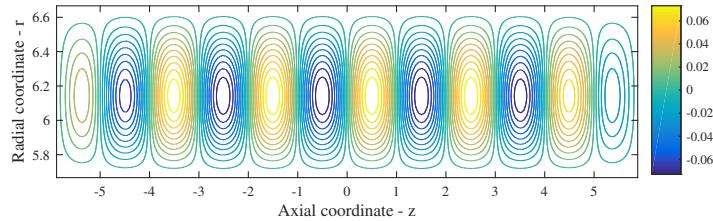
**Solution with  $\epsilon^2 = 0.1$** 

Now, we investigate the case for which  $\epsilon^2 = 0.1$  and again  $\bar{a}_0 = 1.e - 02$ . In this case we take a time interval  $t \in [0, 1000]$  and solve the G–L problem. As can be seen from figure 5.31c, due to the faster growth rate of the amplitude, at  $t = 1000$  the system has still reached a steady equilibrium solution, which is comparable with the one obtained by the steady solution. Indeed, as for  $t > 400$  the solution is stationary, the structure of the vortices is the same as the one given in the steady, non-periodic case. Also here, the number and shape of the vortices agrees well with the DNS simulation, figures 5.32a and 5.32b. As in the steady case, here the amplitude is more flat with respect to the case with  $\epsilon^2 = 0.01$  and it decreases more rapidly towards zero at the boundaries. Physically, this means that the vortices remain undeformed for the major part of the axial length and only very close to the walls they decrease their size and disappear. This behaviour is also clear looking at the function  $f(z)$  in figure 5.32c.

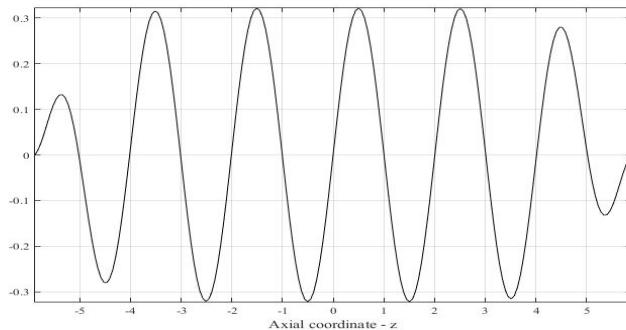
(a) 3D visualization of the amplitude  $\mathcal{A}(z, t)$ .(b) 2D visualization of the amplitude  $\mathcal{A}(z, t)$ .(c) Time behaviour of the amplitude at the centreline point  $\mathcal{A}(0, t)$  when  $\epsilon^2 = 0.1$ .Figure 5.31: Complete solution  $\mathcal{A}(z, t)$  of the G–L equation with homogeneous Dirichlet boundary conditions at  $z = \pm L$  and with  $\epsilon^2 = 0.1$ .



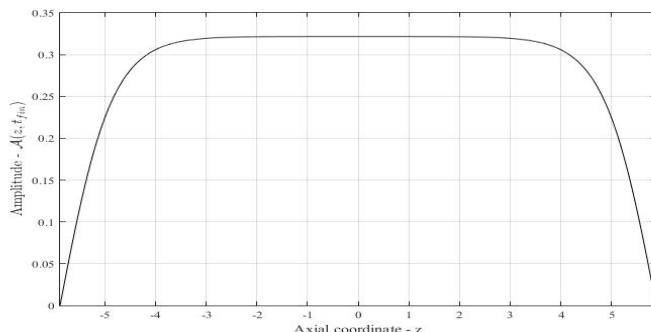
(a) Streamline function computed with the DNS. The function is scaled by a factor  $U_{DNS} d_{DNS}^2$ , where  $U_{DNS} = (\epsilon^2 + 1)\mathcal{R}_c/d_{DNS}$ .



(b) Cell pattern given by the solution of the G-L. equation at  $t = 1000$ .



(c) Behaviour of the function  $f(z) = \mathcal{A}(z, t)e^{i\beta_c z}$  at  $t = 1000$ .



(d) Behaviour of the amplitude  $\mathcal{A}(z, t)$  at  $t = 1000$ .

Figure 5.32: Structure of the Taylor vortices for  $t = t_{fin} = 1000$  in the case  $\epsilon^2 = 0.1$ , with  $\mathcal{A}(z, 0) = 1.e - 02$  and with homogeneous boundary conditions at  $z = \pm L$ .

### Solution with $\epsilon^2 = 0.1$ and with a random initial condition

In this paragraph we show the results obtained by solving the Ginzburg–Landau equation (5.193) with a random initial condition. We always take a time interval  $t \in [0, 1000]$  and we assume  $\mathcal{A}(z, 0) = (1.e - 04)\text{rand}(z)$ . By solving the problem taking  $\epsilon^2 = 0.1$ , the results obtained are the following. As it can be seen from figure 5.33, also in this case the system tends to a steady asymptotic equilibrium solution which is equivalent to that obtained in the previous section and in the stationary-non periodic case. The only difference however is the time needed for the amplitude to reach the flat behaviour visible in figures 5.33a, 5.33b and 5.33c. This is due to the smaller amplitude of the initial condition,  $1.e - 04$ , with respect to the previous cases,  $1.e - 02$ . Anyway, the vortices tend to reach a steady solution as time increases. Therefore, their structure for  $t \geq 700$  will be the same as the structure obtained in the previous mentioned paragraphs.

### Solution with $\epsilon^2 = 0.1$ , a random initial condition and with quadratic terms in the expansion of the solution

In this final paragraph we give a solution of the problem described in the previous paragraph, now expanding the solution for the velocity up to the second order. We write the solution as

$$\mathbf{u} = \mathbf{u}_{TC} + \mathcal{A}(z, t)\boldsymbol{\psi}_1 e^{i\beta_c z} + \mathcal{A}^2(z, t)\boldsymbol{\psi}_2 e^{i2\beta_c z} + |\mathcal{A}(z, t)|^2 \boldsymbol{\psi}_2^{(0)} + \text{c.c}, \quad (5.195)$$

where as usual  $\mathbf{u}_{TC}$  is the Taylor–Couette flow, whereas  $\boldsymbol{\psi}_1$  is the marginally stable eigenmode computed by solving the linear stability problem,  $\boldsymbol{\psi}_2$  and  $\boldsymbol{\psi}_2^{(0)}$  are the eigenmodes related to the solution of the second order problem as shown in equations (5.106) and (5.107). This being said, the amplitude  $\mathcal{A}(z, t)$  is obtained by solving the problem

$$\begin{aligned} \partial_t \mathcal{A} &= c_1 \epsilon^2 \mathcal{A} + c_2 \partial_z^2 \mathcal{A} - \kappa \mathcal{A} |\mathcal{A}|^2, \\ \mathcal{A}(-L, t) &= 0, \\ \mathcal{A}(L, t) &= 0, \\ \mathcal{A}(z, 0) &= (1.e - 04)\text{rand}(z). \end{aligned} \quad (5.196)$$

From its numerical solution, the following results are obtained. In figure 5.34 the structure of the Taylor vortices is shown and compared with the one given by the DNS simulation. What it is worthy to notice is that now the five couples of counter rotating vortices are much more visible and comparable with the ones from the DNS. Moreover, these counter rotating vortices break down in two smaller vortices at the boundaries. The particular shape of this whirling structure can be attributed to the presence of a second harmonic in the solution, as written in the expression (5.195). Finally, also in this case the system tends to a steady equilibrium state and in fact the behaviour of the amplitude at the final instant is the same as the one obtained in the previous two paragraphs, figure 5.35.

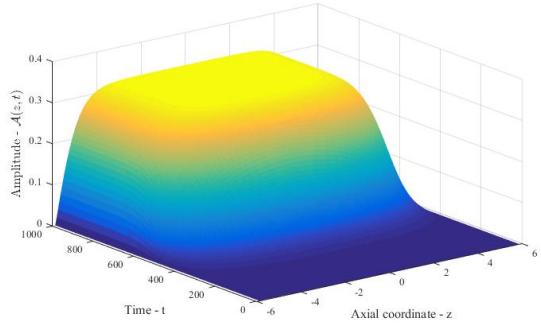
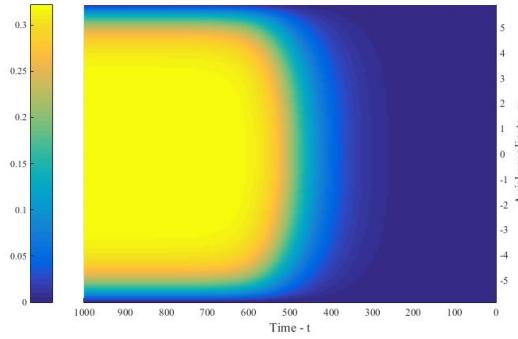
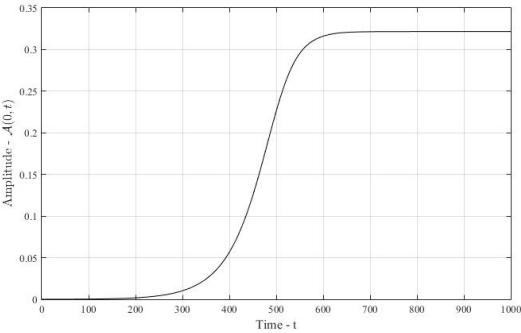
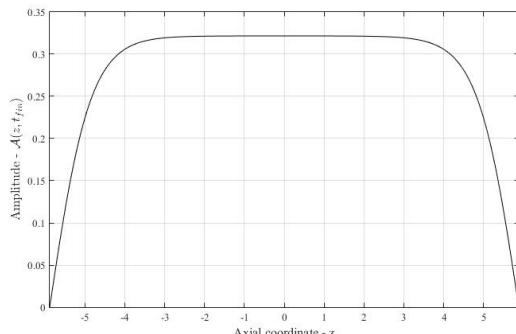
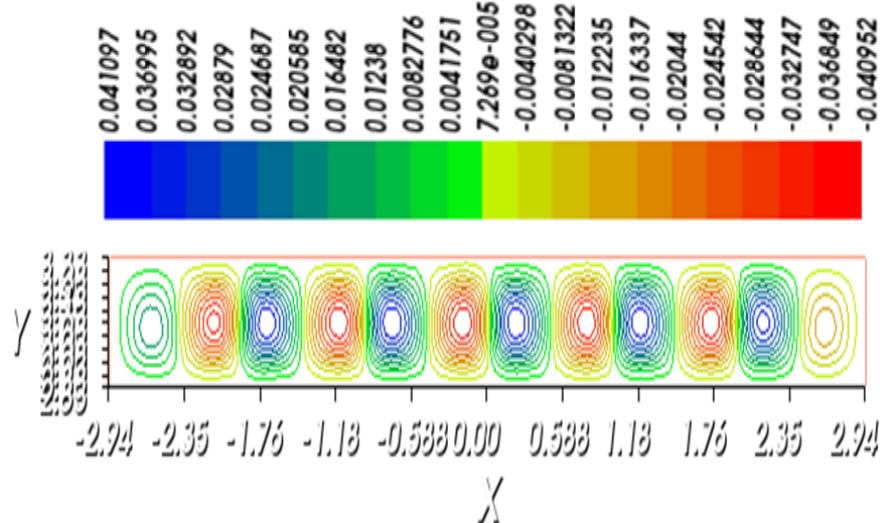
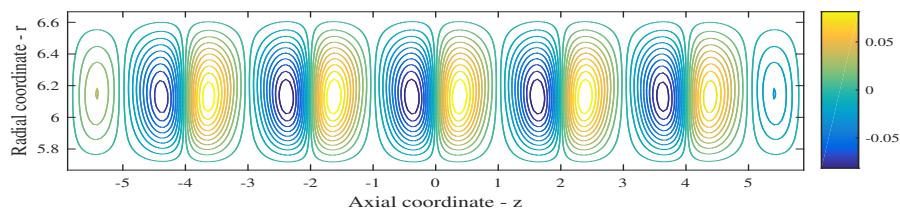
(a) 3D visualization of the amplitude  $\mathcal{A}(z,t)$ .(b) 2D visualization of the amplitude  $\mathcal{A}(z,t)$ .(c) Time behaviour of the amplitude at the centreline point  $\mathcal{A}(0,t)$  when  $\epsilon^2 = 0.1$  and  $\mathcal{A}(z,0) = (1.e - 04)rand(z)$ .(d) Behaviour of the amplitude  $\mathcal{A}(z,t)$  along the axis for  $t = 1000$ .

Figure 5.33: Complete solution  $\mathcal{A}(z,t)$  of the G–L equation with homogeneous Dirichlet boundary conditions at  $z = \pm L$ ,  $\epsilon^2 = 0.1$  and with a random initial condition  $\mathcal{A}(z,0) = (1.e - 04)rand(z)$ .



(a) Streamline function computed with the DNS. The function is scaled by a factor  $U_{DNS} d_{DNS}^2$ , where  $U_{DNS} = (\epsilon^2 + 1)\mathcal{R}_c/d_{DNS}$ .



(b) Cell pattern given by the solution of the G-L equation at  $t = 1000$ .

Figure 5.34: Structure of the Taylor vortices for  $t = t_{fin} = 800$  in the case  $\epsilon^2 = 0.1$ ,  $\mathcal{A}(z, 0) = (1.e - 04)rand(z)$  and with second order terms in the expansion of the solution.

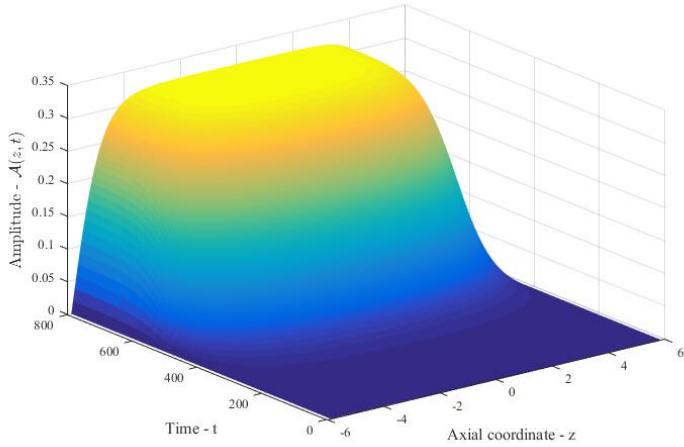
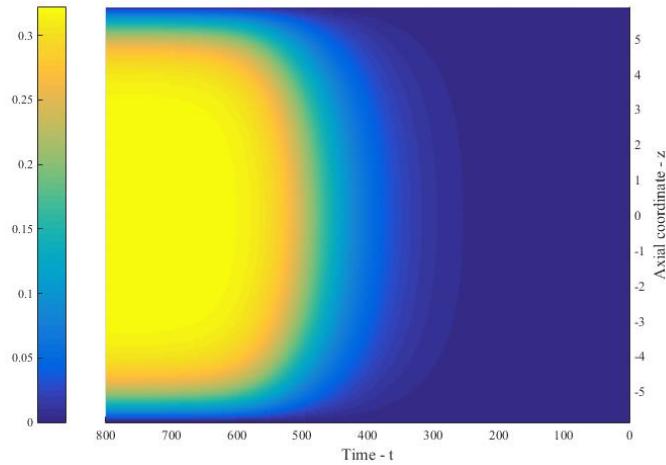
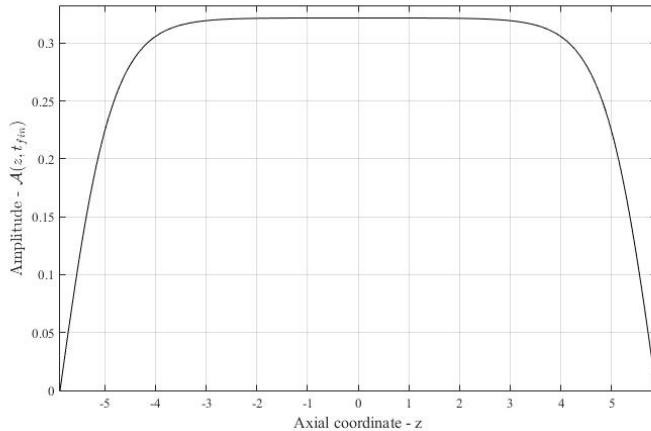
(a) 3D visualization of the amplitude  $\mathcal{A}(z, t)$ .(b) 2D visualization of the amplitude  $\mathcal{A}(z, t)$ .(c) Behaviour of the amplitude  $\mathcal{A}(z, t)$  along the axis for  $t = 800$ .

Figure 5.35: Complete solution  $\mathcal{A}(z, t)$  of the G–L equation with homogeneous Dirichlet boundary conditions at  $z = \pm L$ ,  $\epsilon^2 = 0.1$ , with a random initial condition  $\mathcal{A}(z, 0) = (1.e-04)\text{rand}(z)$ .

## 5.8 The Ginzburg-Landau equation with a forcing term

In this section we want to extend the theory seen so far that has lead us to the derivation of the Ginzburg-Landau equation in the classical form, i.e. in the autonomous form. In particular, now we want to derive the G-L equation which contains a forcing term and see how the solution evolves. A forcing term can be introduced in different ways in the governing equation. By doing so, the Navier-Stokes equation will read

$$\begin{aligned} \frac{\partial \mathbf{u}}{\partial t} + (\mathbf{u} \cdot \nabla) \mathbf{u} + \nabla p - \frac{1}{\mathcal{R}} \nabla^2 \mathbf{u} &= \mathbf{f}, \\ \nabla \cdot \mathbf{u} &= 0. \end{aligned} \quad (5.197)$$

We assume the forcing term to vary only along the axial direction, the radial direction and in time. Moreover, we assume it to be small in modulus, so that it can be expressed with a relation like

$$\mathbf{f}(r, z, t) = \epsilon^3 \mathbf{F}(r, z, t) e^{i\beta_c z}. \quad (5.198)$$

In this way, at order three in  $\epsilon$ , the forcing term will be a resonant term and so it will enter the Ginzburg-Landau equation by means of the solvability condition. In particular, its contribution in the solvability condition is given by

$$\int_a^b \psi_1^a \cdot \mathbf{F}, \quad (5.199)$$

therefore the complete solvability condition reads

$$\begin{aligned} \int_a^b \psi_1^a \cdot \left[ -\partial_T \mathcal{A}_1 \psi_1 - \mathcal{A}_1 |\mathcal{A}_1|^2 \left( (\psi_1 \cdot \nabla) \psi_2^{(0)} + (\psi_1^* \cdot \nabla) \psi_2 + (\psi_2 \cdot \nabla) \psi_1^* + (\psi_2^{(0)} \cdot \nabla) \psi_1 \right) \right] - \\ \int_a^b \psi_1^a \cdot \left[ \frac{1}{\mathcal{R}_c} \mathcal{A}_1 \Delta_r \psi_1 - \frac{1}{\mathcal{R}_c} \left( \frac{1}{r^2} \partial_\eta^2 \mathcal{A}_1 + \partial_\xi^2 \mathcal{A}_1 \right) \psi_1 + \mathbf{F} \right] = 0. \end{aligned} \quad (5.200)$$

By computing the integrals as written in expression (5.119), and rescaling the Ginzburg-Landau equation as done in (5.178), the final form of a forced Ginzburg-Landau equation reads

$$\partial_t \mathcal{A} = c_1 \epsilon^2 \mathcal{A} + c_2 \partial_z^2 \mathcal{A} - \kappa \mathcal{A} |\mathcal{A}|^2 + \epsilon^3 g(z, t), \quad (5.201)$$

where  $g(z, t) = \int_a^b \psi_1^a \cdot \mathbf{F}(r, z, t)$ .

### 5.8.1 Forcing term in the axial direction

Let us consider a forcing term that acts along the axial direction, that is

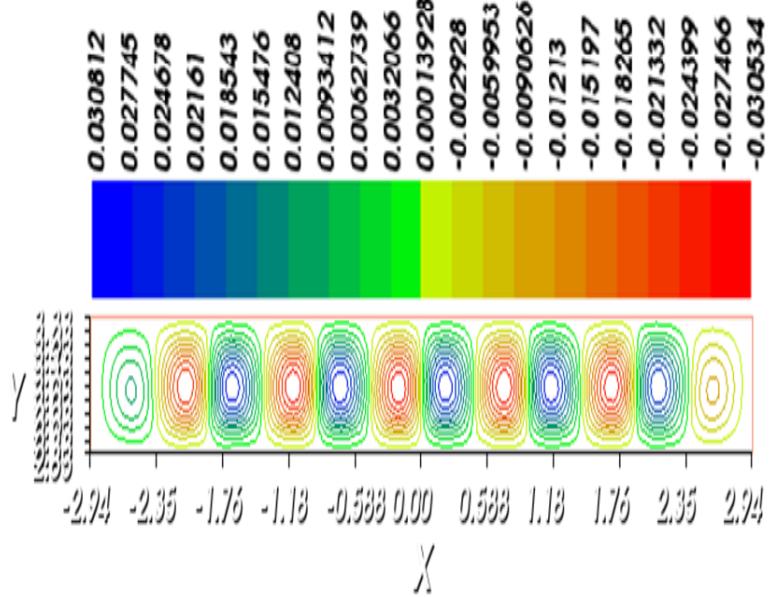
$$\mathbf{f}(r, z, t) = \epsilon^3 F_z(r, z, t) e^{i\beta_c z} \hat{z}. \quad (5.202)$$

In particular, we assume  $F_z(r, z, t) = \cos(\frac{2\pi}{L} z)(-r^2 + (a+b)r - ab)$ . In this way, the forcing term is null on the boundary of the cylinders. By imposing the solvability condition on the forcing term, its dependence on  $r$  disappears and it results in a coefficient,  $c_f$ , for the cosinusoidal behaviour along  $z$ . By solving the full G-L problem

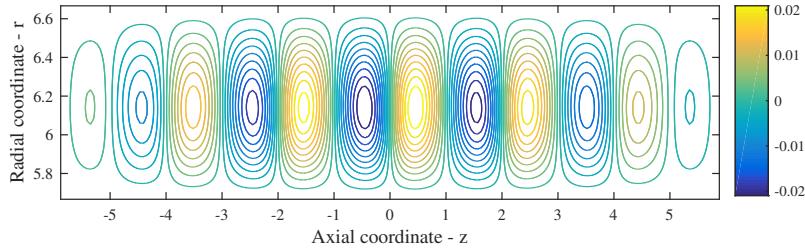
$$\begin{aligned} \partial_t \mathcal{A} &= c_1 \epsilon^2 \mathcal{A} + c_2 \partial_z^2 \mathcal{A} - \kappa \mathcal{A} |\mathcal{A}|^2 + \epsilon^3 c_f \cos\left(\frac{2\pi}{L} z\right), \\ \mathcal{A}(-L, t) &= 0, \\ \mathcal{A}(L, t) &= 0, \\ \mathcal{A}(z, 0) &= 1.e - 04rand(z), \end{aligned} \quad (5.203)$$

the following results are derived and compared with a DNS simulation. In figure 5.36 the cell patterns obtained for  $\epsilon^2 = 0.01$  is shown and compared with the one given by the DNS simulation. They are quite similar and also the quantitative value of both the stream functions

are in accordance (0.02 the maximum value for the G–L model, 0.030 the maximum value for the DNS simulation). In figure 5.37 instead, the complete solution of the Ginzburg–Landau problem is shown. It is worthy to notice that the asymptotic value reached by the amplitude as  $t \rightarrow +\infty$  is higher than the corresponding case without forcing. It is remarkable the fact that, though there is a forcing term, the whirling structure does not change, at least as the system tends to its asymptotic stationary state. Obviously the forcing taken into account has a very small amplitude, however under this condition, the Ginzburg–Landau equation predicts well the behaviour of the whole system.



(a) Streamline function computed with the DNS. The function is scaled by a factor  $U_{DNS} d_{DNS}^2$ , where  $U_{DNS} = (\epsilon^2 + 1)\mathcal{R}_c/d_{DNS}$ .



(b) Cell pattern given by the solution of the G–L equation at  $t = 1000$ .

Figure 5.36: Structure of the Taylor vortices for  $t = t_{fin} = 6000$  in the case  $\epsilon^2 = 0.01$ ,  $\mathcal{A}(z, 0) = (1.e-04)rand(z)$ , subject to a sinusoidal forcing term along the axial direction and with second order terms in the expansion of the solution.

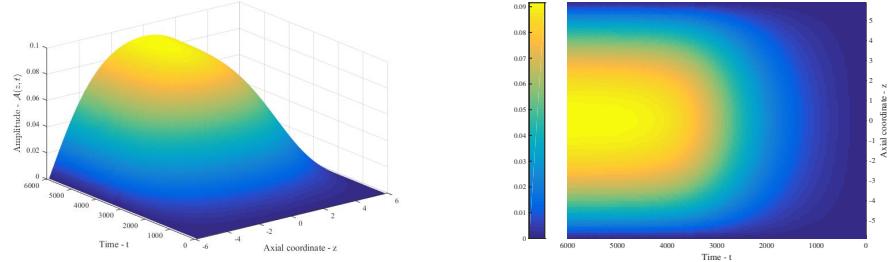
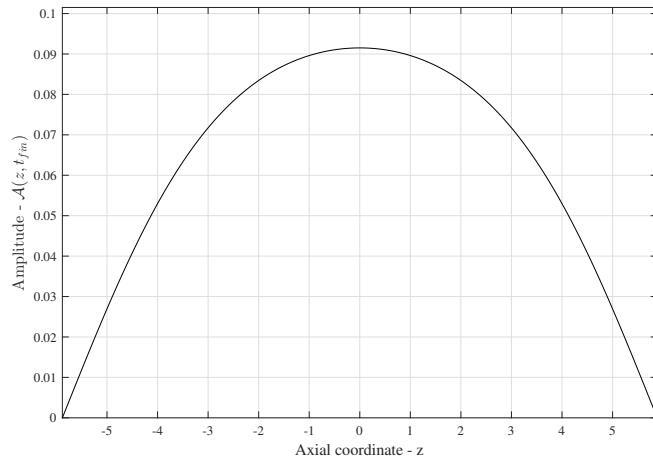
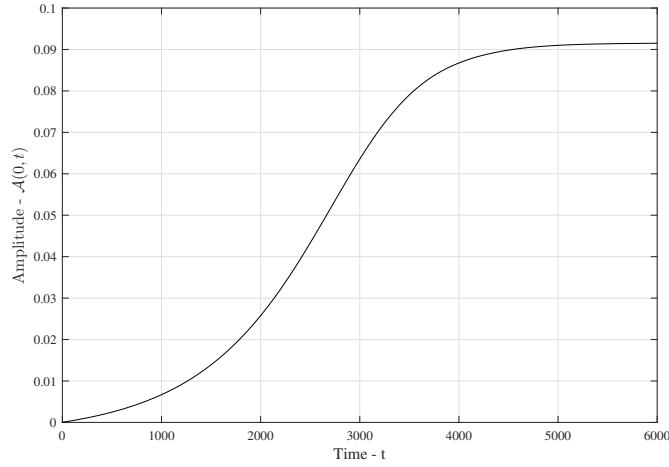
(a) 3D visualization of the amplitude  $\mathcal{A}(z, t)$ . (b) 2D visualization of the amplitude  $\mathcal{A}(z, t)$ .(c) Behaviour of the amplitude  $\mathcal{A}(z, t)$  along the axis for  $t = 6000$ .(d) Behaviour of the amplitude  $\mathcal{A}(0, t)$  in time.

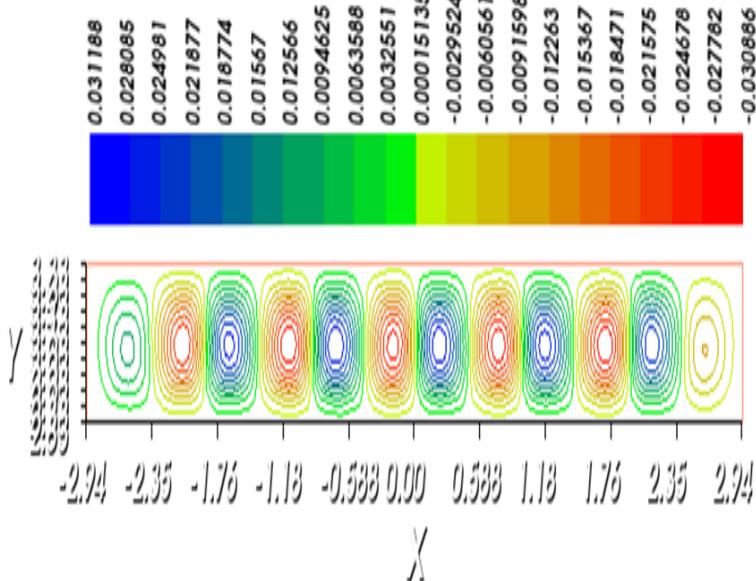
Figure 5.37: Complete solution  $\mathcal{A}(z, t)$  of the G–L equation with homogeneous Dirichlet boundary conditions at  $z = \pm L$ ,  $\epsilon^2 = 0.1$ , with a random initial condition  $\mathcal{A}(z, 0) = (1.e - 04)rand(z)$  and subject to a cosinusoidal forcing term.

### 5.8.2 Forcing term in the radial direction

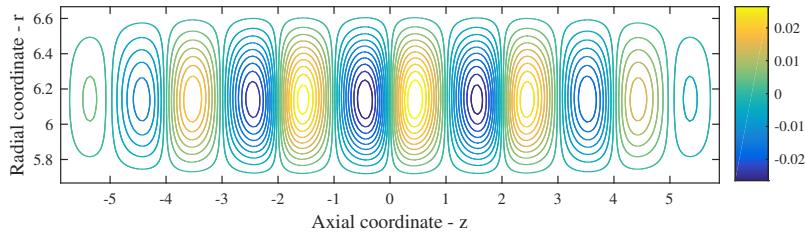
We now consider the same kind of forcing term analyzed in the previous paragraph, but now we assume it to act along the radial direction, i.e.

$$\mathbf{f}(r, z, t) = \epsilon^3 F_r(r, z, t) e^{i\beta_c z} \hat{\mathbf{r}}, \quad (5.204)$$

with  $F_r(r, z, t) = \cos(\frac{2\pi}{L}z)(-r^2 + (a+b)r - ab)$ . By doing so, the coefficient  $c_f$  given by the solvability condition changes. The complete problem (5.203) is solved with  $\epsilon^2 = 0.01$  and the following results are derived. As usual in figure 5.38 the pattern obtained is compared with the one given by the DNS simulation. The maximum value of the stream functions now are much closer one another (0.027 for the G-L model, 0.031 for the DNS simulation). In figure 5.39 instead, the complete solution of the Ginzburg–Landau problem is shown. Particularly, comparing this solution with the one obtained in the case of the axial forcing, one can appreciate the variation in time of the amplitude; with a radial forcing term, the amplitude reaches the steady state earlier and with an asymptotic value higher with respect to the previous one. Hence, we can say that a radial forcing term amplifies the intensity of the vortices more than a corresponding axial forcing.



(a) Streamline function computed with the DNS. The function is scaled by a factor  $U_{DNS} d_{DNS}^2$ , where  $U_{DNS} = (\epsilon^2 + 1)\mathcal{R}_c/d_{DNS}$ .



(b) Cell pattern given by the solution of the G-L equation at  $t = 1000$ .

Figure 5.38: Structure of the Taylor vortices for  $t = t_{fin} = 6000$  in the case  $\epsilon^2 = 0.01$ ,  $\mathcal{A}(z, 0) = (1.e - 04)rand(z)$ , subject to a sinusoidal forcing term along the radial direction and with second order terms in the expansion of the solution.

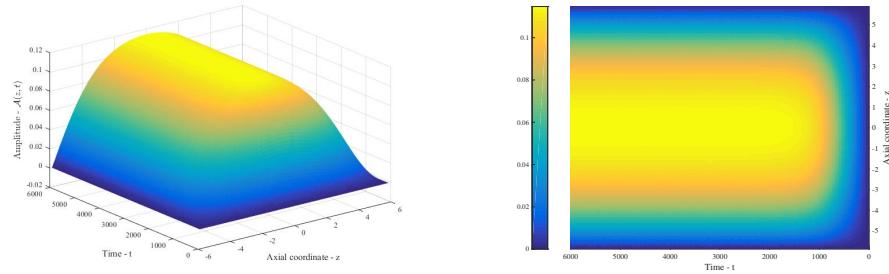
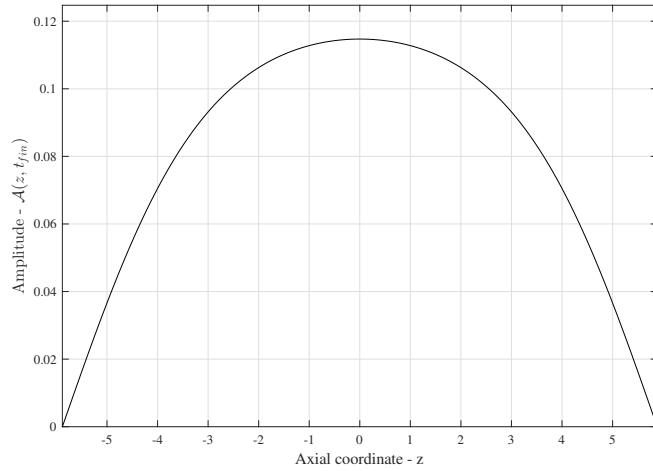
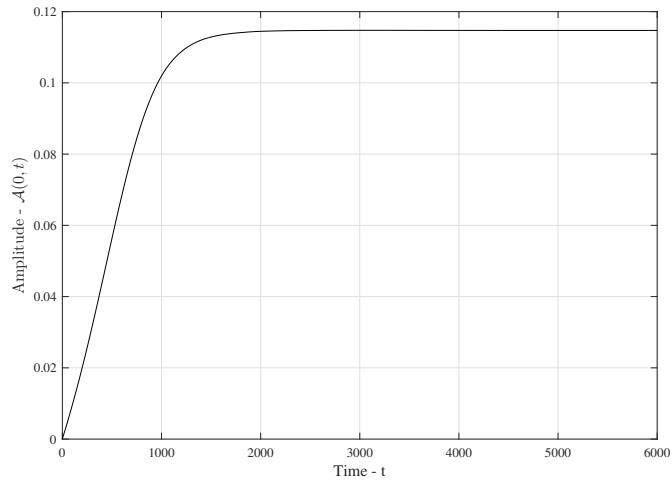
(a) 3D visualization of the amplitude  $\mathcal{A}(z, t)$ . (b) 2D visualization of the amplitude  $\mathcal{A}(z, t)$ .(c) Behaviour of the amplitude  $\mathcal{A}(z, t)$  along the axis for  $t = 6000$ .(d) Behaviour of the amplitude  $\mathcal{A}(0, t)$  in time.

Figure 5.39: Complete solution  $\mathcal{A}(z, t)$  of the G–L equation with homogeneous Dirichlet boundary conditions at  $z = \pm L$ ,  $\epsilon^2 = 0.1$ , with a random initial condition  $\mathcal{A}(z, 0) = (1.e-04)\text{rand}(z)$  and subject to a cosinusoidal forcing term.

### 5.8.3 Ginzburg–Landau equation with a uniform and steady forcing term

In this last section, we consider two particular forcing terms, both acting along the axial direction only, which give rise to a uniform and steady forcing term in the Ginzburg–Landau equation. In particular, the first forcing we analyze is given by the relation

$$\mathbf{f}_1(r, z, t) = \epsilon^3 e^{i\beta_c z} \hat{\mathbf{z}}, \quad (5.205)$$

whereas the second forcing term is given by

$$\mathbf{f}_2(r, z, t) = \epsilon^3 (-r^2 + (a+b)r - ab) e^{i\beta_c z} \hat{\mathbf{z}}. \quad (5.206)$$

In the first case, the solvability condition reduces to  $\int_a^b \psi_{1,z}^a = \bar{g}_1 = \text{const}$ . In the second case, the solvability condition reads  $\int_a^b \psi_{1,z}^a (-r^2 + (a+b)r - ab) = \bar{g}_2 = \text{const}$ . Thus, in both cases the function  $g(z, t)$  is a constant. As a consequence, the Ginzburg–Landau equation will be written in the form

$$\partial_t \mathcal{A} = c_1 \epsilon^2 \mathcal{A} + c_2 \partial_z^2 \mathcal{A} - \kappa \mathcal{A} |\mathcal{A}|^2 + \epsilon^3 \bar{g}_{1,2}. \quad (5.207)$$

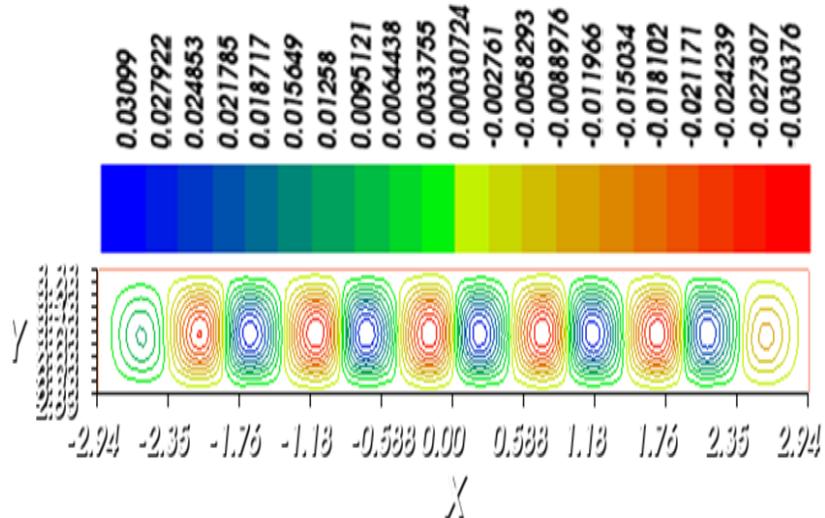
In the following paragraphs, we show some results concerning these two cases. In both cases, we consider a value of the control parameter  $\epsilon^2 = 0.01$ .

#### The case with $\mathbf{f} = \mathbf{f}_1$

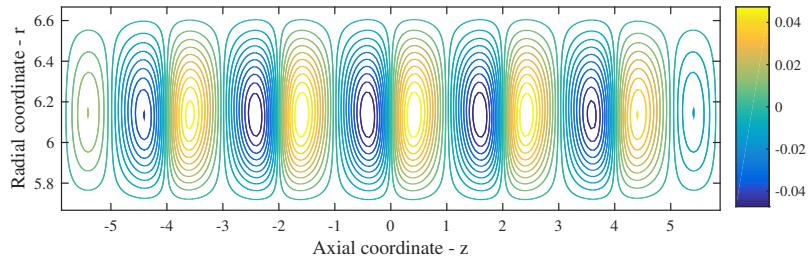
Let us consider the complete Ginzburg–Landau problem

$$\begin{aligned} \partial_t \mathcal{A} &= c_1 \epsilon^2 \mathcal{A} + c_2 \partial_z^2 \mathcal{A} - \kappa \mathcal{A} |\mathcal{A}|^2 + \epsilon^3 \bar{g}_1, \\ \mathcal{A}(-L, t) &= 0, \\ \mathcal{A}(L, t) &= 0, \\ \mathcal{A}(z, 0) &= 1.e - 04rand(z). \end{aligned} \quad (5.208)$$

From its numerical solution, the following results are obtained. In figure 5.40 as usual the whirling structure of the Taylor vortices is shown and compared with the one coming from the DNS simulation. Also in this case, the structure of the vortices at the final time  $t_{fin} = 1000$  remains practically unchanged with respect to the previous cases. In figure 5.41 the complete solution of the Ginzburg–Landau problem is shown.



(a) Streamline function computed with the DNS. The function is scaled by a factor  $U_{DNS} d_{DNS}^2$ , where  $U_{DNS} = (\epsilon^2 + 1)\mathcal{R}_c/d_{DNS}$ .



(b) Cell pattern given by the solution of the G-L equation at  $t = 1000$ .

Figure 5.40: Structure of the Taylor vortices for  $t = t_{fin} = 6000$  in the case  $\epsilon^2 = 0.01$ ,  $\mathcal{A}(z, 0) = (1.e-04)rand(z)$  and with forcing term  $\mathbf{f} = \mathbf{f}_1$ .

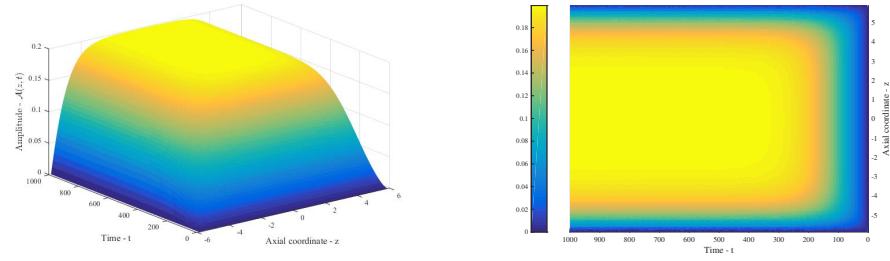
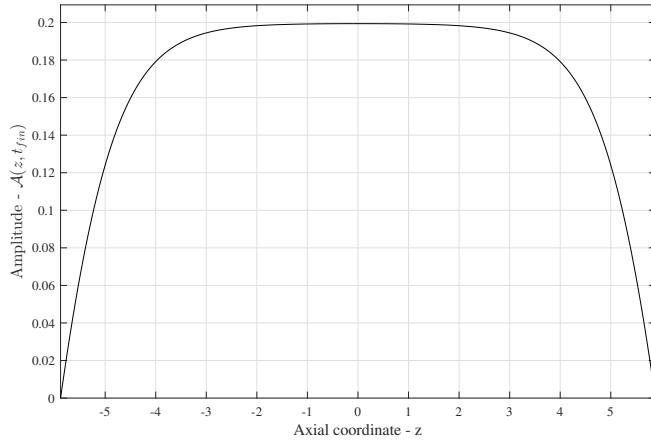
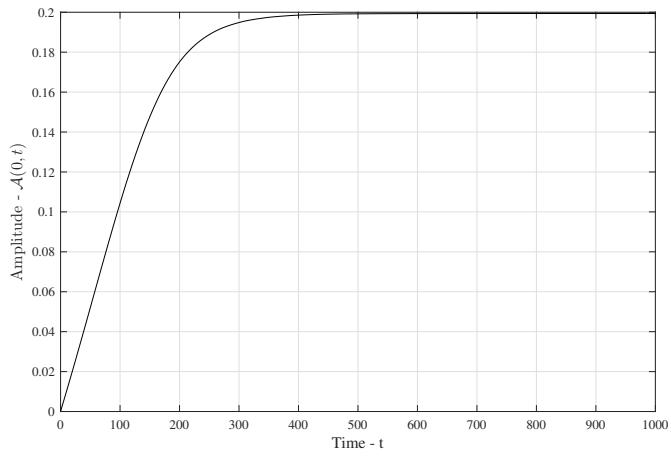
(a) 3D visualization of the amplitude  $\mathcal{A}(z, t)$ . (b) 2D visualization of the amplitude  $\mathcal{A}(z, t)$ .(c) Behaviour of the amplitude  $\mathcal{A}(z, t)$  along the axis for  $t = 6000$ .(d) Behaviour of the amplitude  $\mathcal{A}(0, t)$  in time.

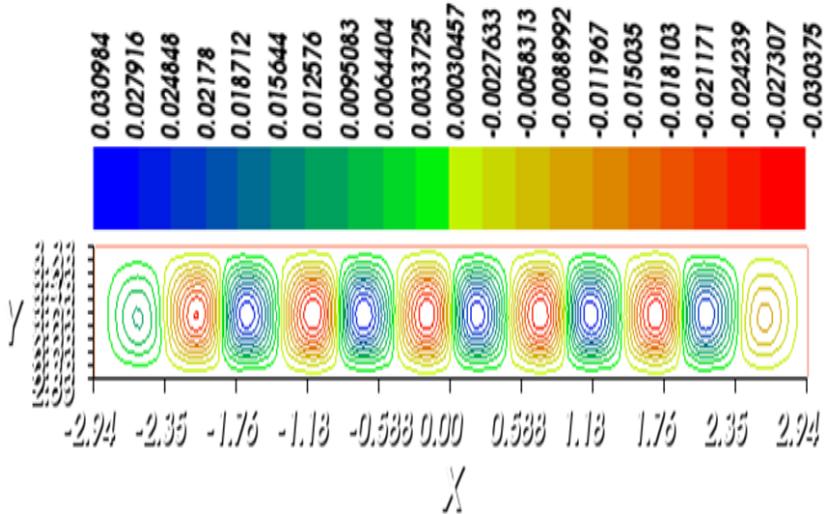
Figure 5.41: Complete solution  $\mathcal{A}(z, t)$  of the G–L equation with homogeneous Dirichlet boundary conditions at  $z = \pm L$ ,  $\epsilon^2 = 0.1$ , with a random initial condition  $\mathcal{A}(z, 0) = (1.e-04)\text{rand}(z)$  and subject to a uniform forcing term  $\bar{g}_1$ .

### The case with $f = f_2$

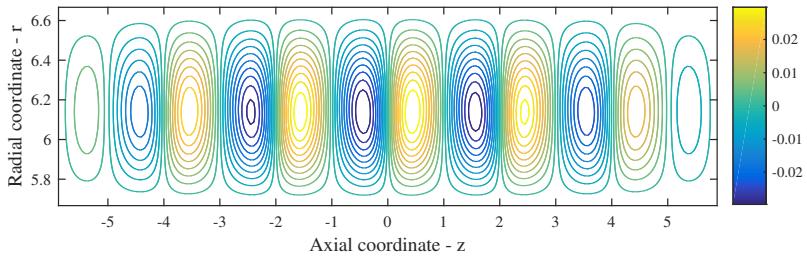
Let us consider the complete Ginzburg–Landau problem

$$\begin{aligned} \partial_t \mathcal{A} &= c_1 \epsilon^2 \mathcal{A} + c_2 \partial_z^2 \mathcal{A} - \kappa \mathcal{A} |\mathcal{A}|^2 + \epsilon^3 \bar{g}_2, \\ \mathcal{A}(-L, t) &= 0, \\ \mathcal{A}(L, t) &= 0, \\ \mathcal{A}(z, 0) &= 1.e - 04 \text{rand}(z). \end{aligned} \tag{5.209}$$

We investigate its solution and compare it with the one obtained from a DNS simulation. In figure 5.42 the structure of the vortices is shown both with the DNS simulation and with the Ginzburg–Landau model. In figure 5.43, the solution of the Ginzburg–Landau problem (5.209) is given. Also in this case, the vortices remain, however the difference in the values of the stream function computed with the DNS and that with the G–L equation is lower. The maximum value of the stream function computed with the G–L model is 0.026, whereas the maximum value computed with the DNS is 0.030. For what concerns the amplitude  $\mathcal{A}$ , its time behaviour shows that the growth rate of the curve in the centreline is much lower than in the case for  $f = f_1$ . Indeed, at the final time considered  $t_{fin} = 1000$ , the system has just reached its asymptotic steady state, whereas in the previous case the system reaches its asymptotic steady state at a time  $t \simeq 500$ .



(a) Streamline function computed with the DNS. The function is scaled by a factor  $U_{DNS} d_{DNS}^2$ , where  $U_{DNS} = (\epsilon^2 + 1) \mathcal{R}_c / d_{DNS}$ .



(b) Cell pattern given by the solution of the G–L equation at  $t = 1000$ .

Figure 5.42: Structure of the Taylor vortices for  $t = t_{fin} = 6000$  in the case  $\epsilon^2 = 0.01$ ,  $\mathcal{A}(z, 0) = (1.e - 04)\text{rand}(z)$  and with forcing term  $f = f_2$ .

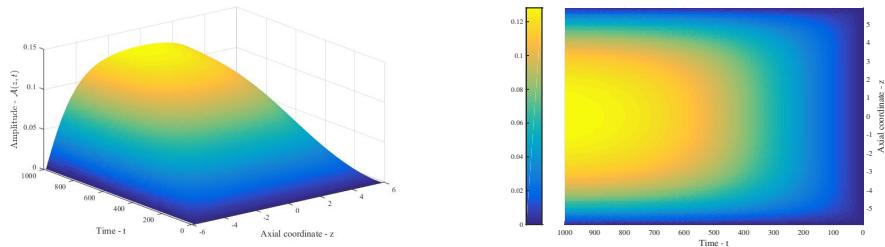
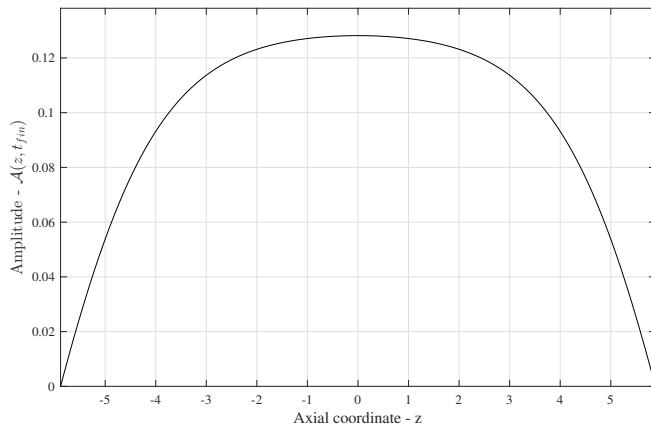
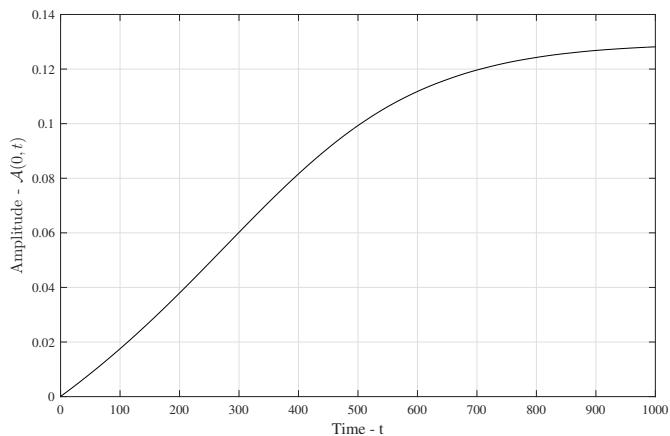
(a) 3D visualization of the amplitude  $\mathcal{A}(z, t)$ . (b) 2D visualization of the amplitude  $\mathcal{A}(z, t)$ .(c) Behaviour of the amplitude  $\mathcal{A}(z, t)$  along the axis for  $t = 6000$ .(d) Behaviour of the amplitude  $\mathcal{A}(0, t)$  in time.

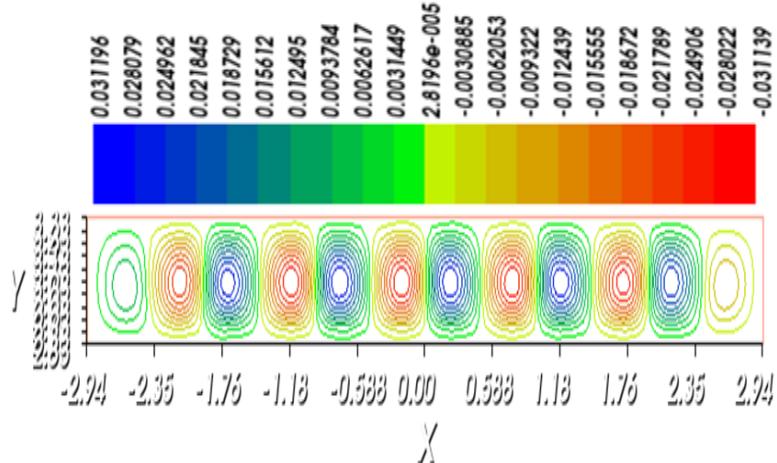
Figure 5.43: Complete solution  $\mathcal{A}(z, t)$  of the G–L equation with homogeneous Dirichlet boundary conditions at  $z = \pm L$ ,  $\epsilon^2 = 0.1$ , with a random initial condition  $\mathcal{A}(z, 0) = (1.e - 04)rand(z)$  and subject to a uniform forcing term  $\bar{g}_2$ .

### 5.8.4 Evolution of a steady state subject to an impulsive forcing term

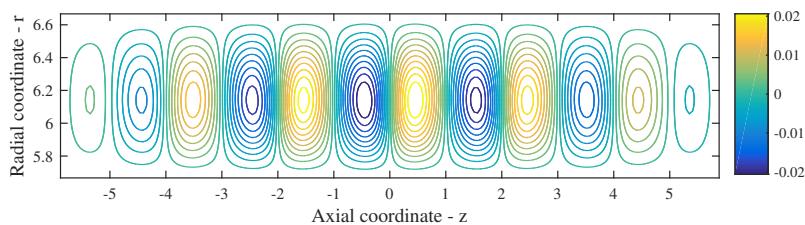
In this section we want to investigate how the amplitude evolves if it is perturbed by an impulsive forcing term starting from a steady equilibrium solution of the G–L equation obtained in the previous sections. In particular we investigate the case for  $\epsilon^2 = 0.01$ . The problem we want to simulate reads

$$\begin{aligned}\partial_t \mathcal{A} &= c_1 \epsilon^2 \mathcal{A} + c_2 \partial_z^2 \mathcal{A} - \kappa \mathcal{A} |\mathcal{A}|^2 + \epsilon^3 \delta(t), \\ \mathcal{A}(-L, t) &= 0, \\ \mathcal{A}(L, t) &= 0, \\ \mathcal{A}(z, 0) &= \mathcal{A}_{\text{steady}}^{GL}(z).\end{aligned}\tag{5.210}$$

By solving numerically the problem, the following results are obtained. In figure 5.45, the solution in terms of the amplitude is shown. In particular in figure 5.45a the time behaviour of the amplitude for  $z = 0$  is shown, whereas in figure 5.45b the asymptotic steady state is plotted as a function of  $z$ . From this, the asymptotic state is the same of the initial one, except for a very small difference in the maximum value of the amplitude at final steady state with respect to the maximum value of the solution at the initial time. Moreover, from the time behaviour it is clear that after a transient in which the amplitude varies very quickly, the system reaches again an asymptotic steady solution. As a consequence, at steady state, the structure of the vortices remains unchanged. The vortices are shown in figure 5.44 and compared with those coming from the DNS simulation. From the analysis of this problem we can say that a perturbation of a steady condition does not produce an instability of the vortices. Therefore a stationary equilibrium solution is obtained which is equal to the initial one.

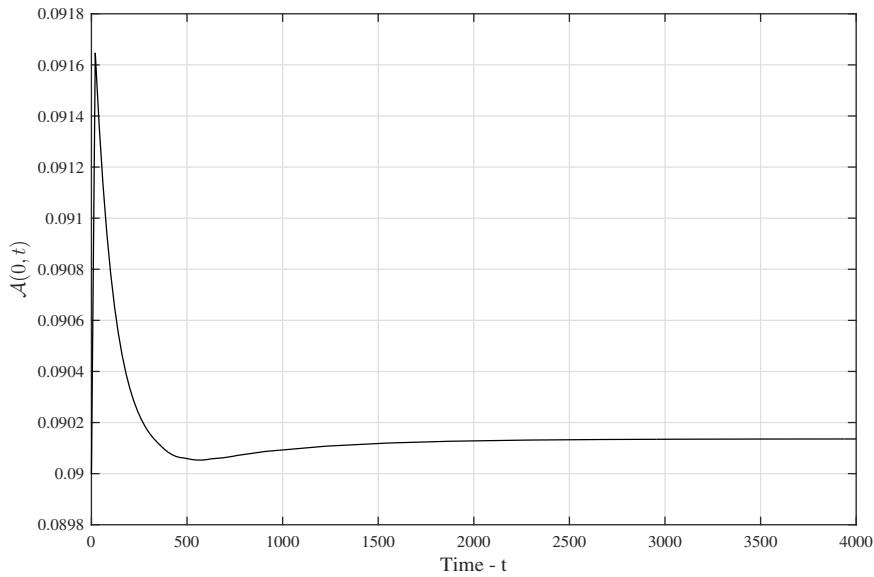
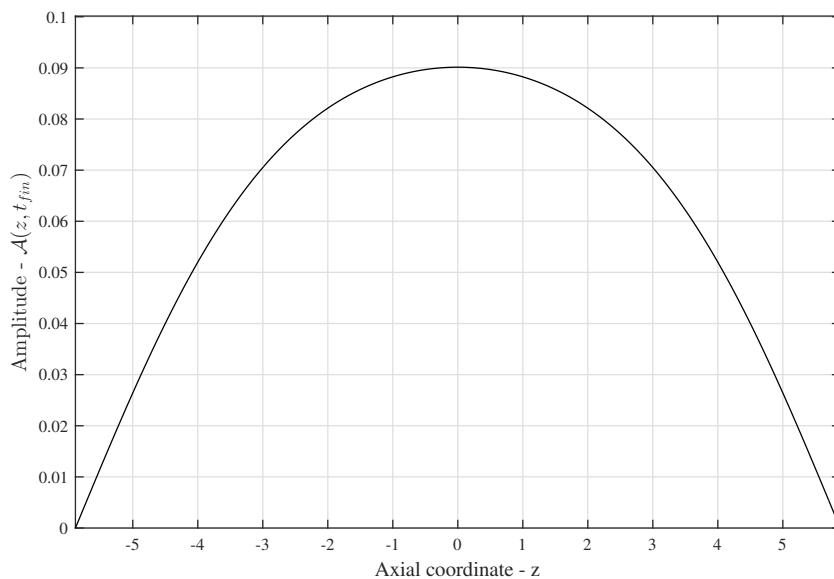


(a) Streamline function computed with the DNS. The function is scaled by a factor  $U_{DNS} d_{DNS}^2$ , where  $U_{DNS} = (\epsilon^2 + 1) \mathcal{R}_c / d_{DNS}$ .



(b) Cell pattern given by the solution of the G–L equation at  $t = 4000$ .

Figure 5.44: Structure of the Taylor vortices for  $t = t_{fin} = 4000$  in the case  $\epsilon^2 = 0.01$ . The pattern formed is the steady condition given by a perturbation of the steady Taylor vortices with an impulse forcing term.

(a) Behaviour of the amplitude at the centreline  $\mathcal{A}(0, t)$  as a function of the time.(b) Behaviour of the amplitude along the axis at the final time  $t = 4000$ .Figure 5.45: Solution of the complete G-L problem with  $\delta(t)$  as a forcing term and  $\mathcal{A}_{\text{steady}}^{GL}(z)$  as an initial condition.

## Chapter 6

# Conclusions and future developments

This thesis work deals with the study of the hydrodynamic stability applied to the Taylor–Couette flow, with a great emphasis on the nonlinear stability. The study of this branch of fluid dynamic stability has been possible by means of the rigorous derivation of the Ginzburg–Landau equation, a nonlinear PDE, which aims at describing the dynamics of the system close to some critical points for which the Taylor–Couette flow becomes a non-hyperbolic fixed point of the system. The equation has been analyzed for the first bifurcation of the Taylor–Couette flow, which originates the Taylor vortices.

The first conclusion that is possible to draw from this work is that the Ginzburg–Landau equation is a good model for the description of the dynamics of the vortices close to the critical point. Moreover, the model has been used to evaluate its accuracy for the description of the solution of more complicated Navier–Stokes problems, given for instance by the introduction of boundaries such as moving lids. The model has revealed good accuracy in predicting the pattern and in the quantitative properties of the flow beyond the instability threshold. In addition, the flow predicted by the Ginzburg–Landau equation has been compared with that obtained by the Navier–Stokes when a forcing term is applied. By assuming them to be small in amplitude, a forced Ginzburg–Landau equation has been obtained and analysed. The comparison of the solution given by the Ginzburg–Landau model and that given by the DNS simulation revealed a good accuracy in the prediction of asymptotic steady state.

Differently from what happens with the linear stability theory, the Ginzburg–Landau equation for the Taylor vortices correctly predicts that brings the amplitude to an asymptotic steady solution even for supercritical Reynolds numbers. Therefore the nonlinear term gives a saturation of the amplitude in time.

In writing this work, however, some constraints have been introduced and their removal could be the base for future developments concerning the nonlinear stability in fluid dynamics. A first limitation comes from the fact that the Ginzburg–Landau equation has been derived by assuming there could be a modulation of the amplitude of the perturbations only along the axial coordinate. Therefore, it could be interesting to allow the modulation along the azimuthal direction too and, by studying a two dimensional Ginzburg–Landau equation in space, to evaluate how the solution changes with respect to the case discussed here. Moreover, it has been decided to truncate the equation at third order. However, by increasing the order of the expansion, new solutions could be found and then other behaviours of the vortices may be explained. Furthermore, the accuracy of the solutions with respect to the complete Navier–Stokes problem discussed in this work, would increase. Only the Ginzburg–Landau equation related to axisymmetric disturbances has been studied. The other first bifurcating flow arising from the instability of the Taylor–Couette solution are the Spiral vortices as it has been shown in the thesis. In this context, as they come from the linear instability of non-axisymmetric

disturbances, the resulting Ginzburg–Landau equation will be complex. The study of this equation would allow to predict and analyse different solutions from that obtained here.

# Appendix A

## Estratto in italiano

### A.1 Capitolo 1: introduzione

Lo studio della stabilità in fluidodinamica è di grande importanza in quanto permette la comprensione di complessi meccanismi fisici che portano il flusso dal regime laminare al regime turbolento. La stabilità delle correnti fluide può essere studiata secondo due approcci: quello lineare e quello non lineare. In questo elaborato si è deciso di studiare la stabilità relativa alla corrente di Taylor–Couette, con una maggiore enfasi sulla parte non lineare.

#### A.1.1 Stabilità lineare

Lo studio della stabilità lineare presuppone di linearizzare le equazioni di Navier–Stokes attorno al flusso base e di studiare il comportamento delle perturbazioni a tale flusso base sotto l’ipotesi che queste rimangano di ampiezza infinitesima. Per valutare poi l’effettiva stabilità o meno, si deve valutare il segno della parte reale degli autovalori relativi al sistema linearizzato. In questa situazione infatti, tre sono i casi che possono emergere:

- se tutti gli autovalori hanno parte reale negativa, allora lo stato di equilibrio è asintoticamente stabile.
- se vi è almeno un autovalore ad aver parte reale positiva, allora lo stato di equilibrio è linearmente instabile.
- se il sistema possiede almeno un autovalore a parte reale nulla, lo stato di equilibrio è marginalmente stabile, o non-iperbolico, e la sua stabilità va necessariamente accertata mediante un’analisi di stabilità non lineare.

#### A.1.2 Stabilità non lineare

Lo studio della stabilità non lineare si basa pertanto sullo studio della stabilità lineare e mira a indagare la stabilità dei punti di equilibrio non-iperbolici. Il motivo che sta alla base dello studio della stabilità non lineare è che, al contrario di quanto predice la sola stabilità lineare per cui uno stato non-iperbolico possiede un tasso di crescita nullo delle perturbazioni nel tempo, andando ad includere nella trattazione del problema gli effetti legati alla non linearità delle equazioni di governo, il segno del tasso di crescita può essere determinato. Per descrivere quindi gli effetti non lineari, in questa tesi si è deciso di adottare un metodo perturbativo che consiste nell’effettuare un’espansione in serie di Taylor della soluzione nell’intorno del punto non iperbolico. Inoltre, mediante il metodo delle scale multiple, è stato possibile ricavare un’equazione differenziale alle derivate parziali, nota come equazione di Ginzburg–Landau, la cui incognita rappresenta la modulazione dello spazio e nel tempo delle perturbazioni nell’intorno di un punto critico per il quale il flusso base perde la sua iperbolicità.

## A.2 Capitolo 2: equazioni di Navier–Stokes adimensionali

Le equazioni che governano il moto dei fluidi sono chiamate equazioni di Navier–Stokes e discendono direttamente da tre principi fisici, quali la legge di conservazione della massa, la legge di bilancio della quantità di moto e la legge di bilancio dell'energia. Se si suppone che gli effetti legati alla comprimibilità del fluido e quelli legati alla sua capacità di scambiare calore siano trascurabili, si ricavano le equazioni di Navier–Stokes incomprimibili. Esse possono essere riscritte in una forma più comoda così da non dover tenere in considerazione le proprietà fisiche del fluido che si sta analizzando. Ossia, possono essere scritte in forma adimensionale. Nella loro forma adimensionale, le equazioni fanno emergere un unico parametro, detto numero di Reynolds, il quale può essere calcolato per un determinato fluido una volta che si siano specificate una lunghezza caratteristica del dominio nel quale il fluido si muove e una velocità caratteristica del fluido. Vi sono due modi principali per adimensionalizzare le equazioni; in questa tesi si è deciso di adottare quella per cui l'inverso del numero di Reynolds moltiplica il termine diffusivo delle equazioni di Navier–Stokes. Esse dunque appaiono nella forma

$$\begin{cases} \frac{\partial \mathbf{u}}{\partial t} + (\mathbf{u} \cdot \nabla) \mathbf{u} + \nabla p - \frac{1}{Re} \nabla^2 \mathbf{u} = 0, \\ \nabla \cdot \mathbf{u} = 0. \end{cases} \quad (\text{A.1})$$

Nel proseguo della tesi, le equazioni di governo saranno sempre trattate in questa forma.

## A.3 Capitolo 3: corrente stazionaria di Taylor–Couette

La corrente di Taylor–Couette è tra le correnti fluide più studiate nella storia della fluidodinamica in quanto rappresenta una delle poche soluzioni ricavabili in forma chiusa integrando le equazioni di Navier–Stokes. La corrente di Taylor–Couette è quel flusso stazionario che si sviluppa tra due cilindri concentrici rotanti, supposti di lunghezza infinita. Pertanto, date le proprietà di simmetria della corrente, essa è descrivibile come una corrente piana puramente azimutale, la cui intensità varia solo lungo la coordinata radiale interna ai cilindri. La sua espressione analitica è data dalla seguente relazione

$$u_\theta(r) = U(r) = \frac{\omega - \eta^2}{\eta(1 + \eta)} r + \frac{\eta(1 - \omega)}{(1 - \eta)(1 - \eta^2)} \frac{1}{r}, \quad (\text{A.2})$$

dove  $\eta$  e  $\omega$  sono due parametri caratteristici del nostro problema:  $\eta = \frac{R_a}{R_b}$  rappresenta il rapporto tra i raggi dei cilindri,  $\omega = \frac{\Omega_b}{\Omega_a}$  invece rappresenta il rapporto tra le velocità angolari a cui ruotano i cilindri.

## A.4 Capitolo 4: Stabilità lineare e sua applicazione alla corrente di Taylor-Couette

La stabilità lineare della corrente di Taylor–Couette può essere studiata trascurando il termine non lineare nelle equazioni di Navier–Stokes linearizzate attorno al flusso base di Taylor–Couette. Il problema dello studio della stabilità lineare si riconduce a un problema agli autovalori nel quale l'autovalore  $s$  è funzione dei parametri che intervengono nella scrittura delle equazioni linearizzate, ossia  $s = s(Re, \alpha, \beta, \eta, \omega)$ , dove  $\omega$  indica il rapporto tra le velocità angolari dei cilindri. Studiare la stabilità lineare significa determinare il segno della parte reale di  $s$  in funzione dei parametri da cui dipende. Poiché, nel caso generale, essa rappresenta una ipersuperficie nello spazio descritto da  $Re, \alpha, \beta, \eta, \omega$ , in questa tesi si è descritta la relazione di dispersione facendo variare al più solo due parametri alla volta. Dalla letteratura è noto che le prime biforcazioni a cui la corrente di Taylor–Couette va incontro sono due, e sono date rispettivamente da disturbi assalsimmetrici e non assalsimmetrici. La corrente che si genera nel primo caso forma i cosiddetti vortici di Taylor, la seconda forma i vortici a spirale. Sono stati studiati quindi questi flussi secondari, ricavando i punti critici prima nel piano  $\beta - Re$ , poi nel piano  $Re_o, Re$ , per due valori del rapporto tra i raggi  $\eta = 0.95$  e  $\eta = 0.3$ . Le curve neutre nel caso dei vortici di Taylor sono mostrate in figura A.1, mentre in figura A.2 viene mostrato il pattern formato e l'andamento del modo marginalmente stabile lungo la coordinata radiale scalata  $x$ . Per quanto riguarda invece i vortici a spirale, essi sono vortici che non si

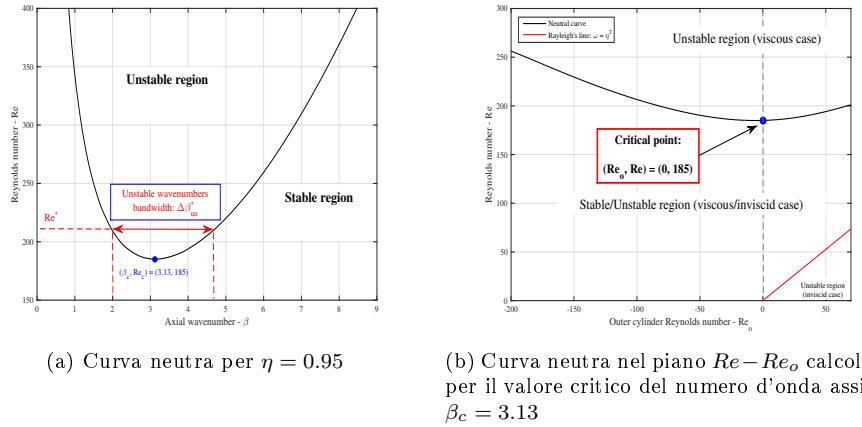


Figure A.1: Curve neutre per  $\eta = 0.95$

propagano inalterati lungo la direzione azimutale dal momento che non sono assalsimmetrici,  $\alpha \neq 0$ . Pertanto, come si evince dalla figura A.3, tendono ad avvolgersi a spirale attorno alle pareti del cilindro interno. Il pattern così generato e l'andamento delle componenti di velocità relative al modo marginalmente stabile sono mostrati nelle figure A.4a e A.4c.

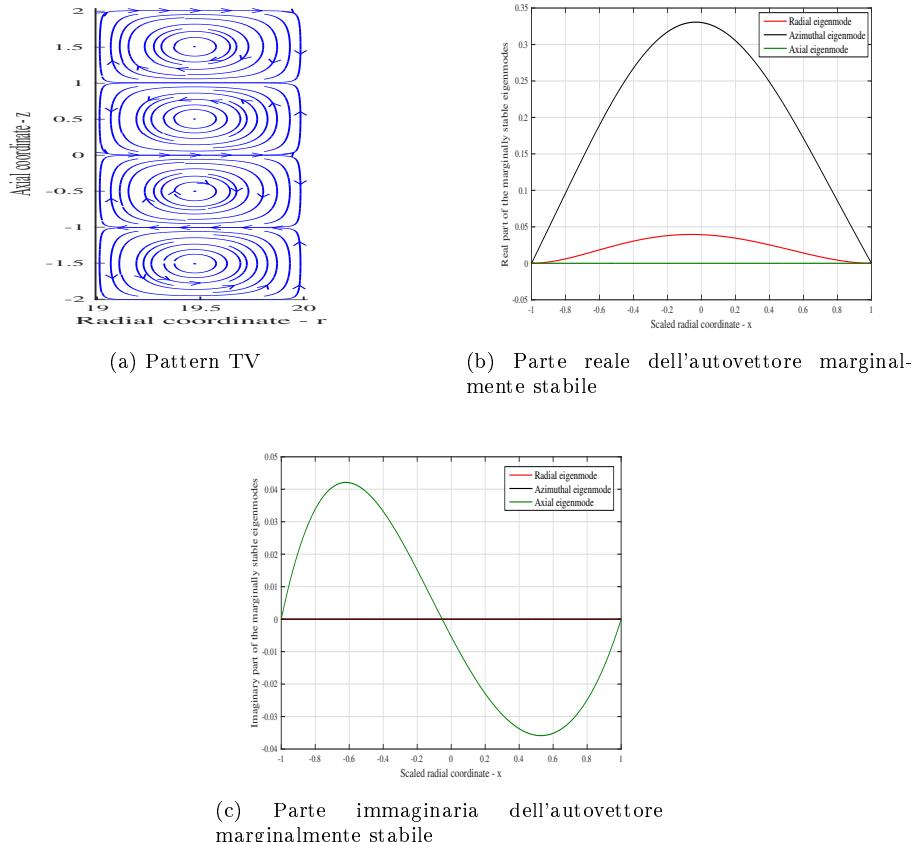


Figure A.2: Linee di corrente e andamento componenti di velocità relative ai vortici di Taylor per  $\eta = 0.95$

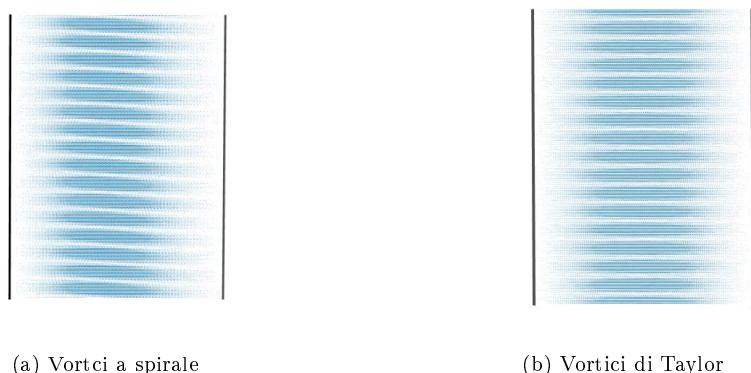


Figure A.3: Visualizzazione dei pattern caratteristici attorno ai cilindri: vortici a spirale A.3a; vortici di Taylor A.3b

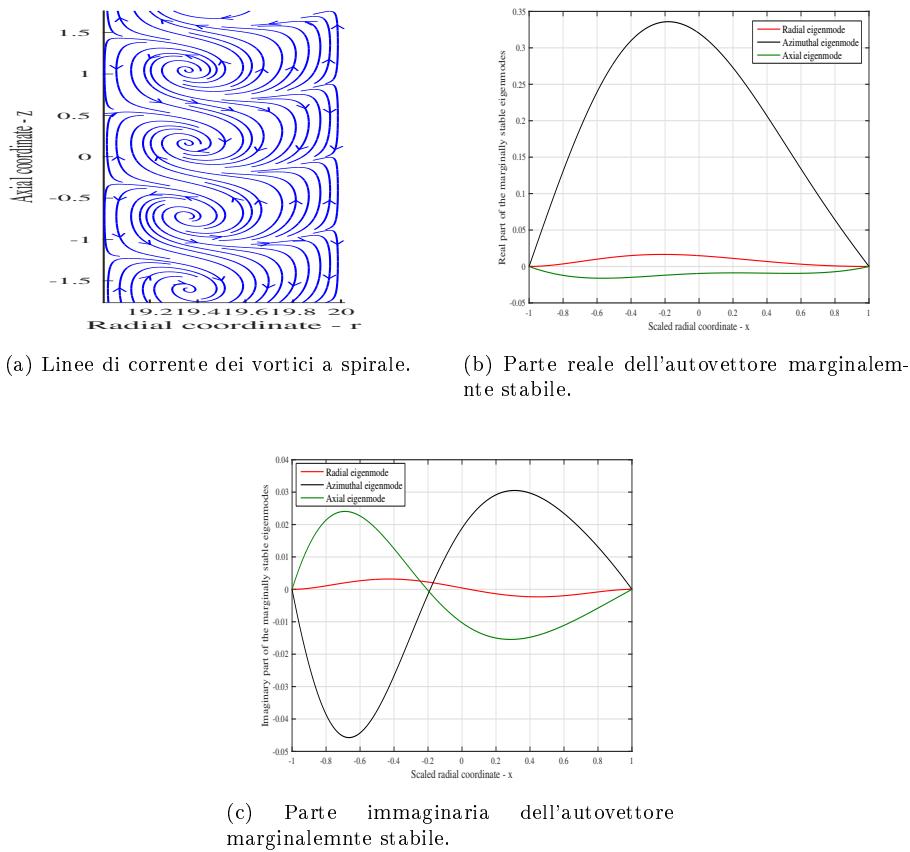


Figure A.4: Linee di corrente e componenti di velocità per i vortici a spirale generati ad  $\alpha = 3, \omega = -0.8, \eta = 0.95, Re_c = 266.1, \beta_c = 3.08$ .

## A.5 Capitolo 5: stabilità non lineare

Lo studio della stabilità non lineare riveste particolare importanza nell'andare a determinare la stabilità di punti non iperbolici del sistema dinamico in considerazione. Questi sono stati di equilibrio per cui il tasso di crescita delle perturbazioni predetto dalla teoria lineare nel tempo è nullo e dunque nulla può essere detto a riguardo della sua stabilità o meno. L'inclusione della non linearità nella trattazione del problema può aiutare a predire il segno del tasso di crescita e quindi portare alla stabilità o all'instabilità del punto non iperbolico. Nei problemi di fluidodinamica, e in particolare in quello trattato in questa tesi, il tasso di crescita delle perturbazioni è rappresentato da una funzione continua che definisce la parte reale degli autovalori del sistema lineare associato. Tale funzione, è stata ridotta a una funzione dipendente da solo due variabili: il numero di Reynolds  $\mathcal{R}$  e il numero d'onda assiale  $\beta$

$$\sigma = \sigma(\mathcal{R}, \beta). \quad (\text{A.3})$$

Dalla teoria lineare, si sa che in un determinato punto critico  $(\mathcal{R}_c, \beta_c)$ , il flusso base di Taylor–Couette diventa un punto fisso non iperbolico del sistema delle equazioni di Navier–Stokes e il tasso di crescita in quel punto si annulla. Allora, l'idea è quella di espandere in serie di Taylor la relazione di dispersione  $\sigma(\mathcal{R}, \beta)$  nell'intorno del punto critico e di andare quindi a trovare delle scale di tempo e di lunghezza che possano far intervenire nello studio della stabilità anche i termini non lineari responsabili della stabilizzazione o meno del sistema nell'intorno del punto critico. Espandendo la funzione  $\sigma$  fino al secondo ordine, si possono introdurre due scale "lente": una scala temporale  $T = \epsilon^2 t$  e una scala spaziale  $\xi = \epsilon z$ . Il parametro  $\epsilon = \sqrt{\frac{\mathcal{R} - \mathcal{R}_c}{\mathcal{R}_c}}$  è detto parametro d'ordine del problema non lineare ed è supposto essere sufficientemente piccolo. Andando quindi ad esprimere il campo di velocità e di pressione in funzione anche delle variabili lente, ossia  $\mathbf{u} = \mathbf{u}(\mathbf{r}, t, T, \xi)$ ,  $p = p(\mathbf{r}, t, T, \xi)$ , e chiamando  $A(T, \xi)$  l'ampiezza delle perturbazioni ai vari ordini in  $\epsilon$ , si è ottenuta l'equazione di Ginzburg–Landau nella forma

$$\partial_T A = c_1 A + c_2 \partial_\xi^2 A - k A |A|^2. \quad (\text{A.4})$$

L'equazione di Ginzburg–Landau descrive la dinamica debolmente non lineare del nostro sistema nell'intorno del punto critico  $(\mathcal{R}_c, \beta_c)$ . La dinamica debolmente non lineare è data dalla propagazione di un pacchetto d'onda avente numero d'onda pari a  $\beta_c$  e che è quindi guidato dal modo marginalmente stabile. L'equazione di Ginzburg–Landau così ricavata è stata utilizzata per predire il comportamento dei vortici di Taylor, nell'ipotesi che il cilindro esterno sia fermo e che il gap tra i cilindri sia piccolo. Si sono infatti trovate quattro differenti tipologie di soluzioni: due stazionarie e due non stazionarie. Per entrambe, si è trovata la soluzione sia quando l'ampiezza si propaga in modo periodico lungo l'asse dei cilindri, sia quando invece si sono imposte opportune condizioni al contorno. In particolare, riguardo quest'ultimo caso, si sono imposte delle condizioni di Dirichlet omogenee ad una determinata lunghezza assiale, in modo da valutare come i vortici si propagano e scompaiano qualora venga messa nel sistema una parete che ripristini la corrente base di Taylor–Couette. Infatti, studiare questa condizione per l'equazione di Ginzburg–Landau, è equivalente a studiare il problema di Navier–Stokes completo

$$\begin{aligned} \nabla \cdot \mathbf{u} &= 0, \\ \partial_t \mathbf{u} + (\mathbf{u} \cdot \nabla) \mathbf{u} + \nabla p - \frac{1}{\mathcal{R}} \nabla^2 \mathbf{u} &= 0, \\ \mathbf{u}|_{S_L} &= \mathbf{u}_{TC}, \\ \mathbf{u}|_{t=0} &= \mathbf{u}_{In}, \end{aligned} \quad (\text{A.5})$$

dove  $S_L$  indica il contorno del dominio fluido tra le pareti poste a  $z = -L$  e  $z = L$ ,  $\mathbf{u}_{TC}$  indica il campo di moto di Taylor–Couette,  $\mathbf{u}_{In}$  indica un opportuno campo di velocità iniziale. La soluzione del problema completo (A.5), è stata quindi comparata con la soluzione approssimata risolvendo il problema di Ginzburg–Landau con condizioni al contorno omogenee e si è potuto osservare come il modello di Ginzburg–Landau predica bene la formazione e la propagazione dei vortici lungo i cilindri, in particolare anche vicino alle pareti. Un esempio di questo risultato è dato in figura A.5. L'equazione di Ginzburg–Landau è stata inoltre studiata con un termine

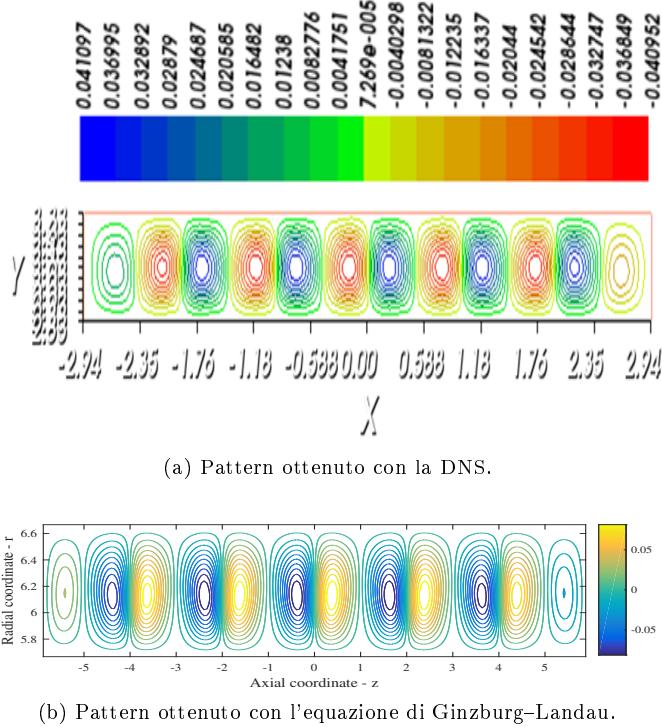


Figure A.5: Comparazione della struttura dei vortici ottenuti con una simulazione DNS A.5a e con il modello di Ginzburg–Landau A.5b.

forzante dipendente in generale dallo spazio e dal tempo. Anche in questo caso, si è riscontrata una buona affidabilità da parte del modello ridotto dell'equazione di Ginzburg–Landau nel descrivere il problema completo simulato con la DNS.

## A.6 Capitolo 6: conclusioni e sviluppi futuri

In questa tesi si è studiata la stabilità fluidodinamica relativa alla corrente di Taylor–Couette, con una maggior enfasi sulla stabilità non lineare. Questo ramo di studio della stabilità è stato reso possibile attraverso la derivazione e l'applicazione dell'equazione di Ginzburg–Landau la quale quindi può essere considerato un buon modello per la descrizione dei vortici di Taylor nell'intorno del punto critico. Inoltre, si è studiata l'evoluzione della soluzione data da questo modello per trarre informazioni sulla sua accuratezza nel descrivere problemi fluidodinamici con condizioni più complesse, come ad esempio l'introduzione di pareti mobili sui cilindri e di forzanti nelle equazioni di governo. Il modello ha dato risposte molto buone per quanto riguarda la visualizzazione dei pattern che si generano e anche quantitativamente per la valutazione della funzione di corrente che li descrivono.

Studiando l'equazione di Ginzburg–Landau si è mostrato come l'ampiezza delle perturbazioni, a causa del termine non lineare, tenda a uno stato stazionario anche per numeri di Reynolds supercritici. Questo fatto non si sarebbe potuto spiegare analizzando la sola stabilità lineare, secondo la quale per numeri di Reynolds superiori a quello critico le perturbazioni crescono esponenzialmente nel tempo portando all'instabilità della corrente base.

Vi sono tuttavia delle limitazioni al lavoro svolto in questa tesi; limitazioni che possono diventare la base per sviluppi futuri riguardo la stabilità non lineare. Innanzitutto, l'equazione di Ginzburg–Landau è stata ricavata permettendo una modulazione dell'ampiezza solo lungo la coordinata assiale; si potrebbe supporre una modulazione anche lungo la coordinata azimutale e vedere come cambiano le soluzioni. In secondo luogo, l'equazione è stata troncata al terzo ordine.

Per ottenere una migliore accuratezza della dinamica nell'intorno del punto critico, termini di ordine superiore (contenenti anche le derivate di  $A$ ) devono essere inclusi. Inoltre, l'equazione di Ginzburg–Landau utilizzata era reale in quanto applicata solo ai vortici di Taylor. Sarebbe interessante studiare l'equazione di G–L riferita ai vortici a spirale, equazione che quindi sarà complessa.

# Bibliography

- [1] Charru, F. (2011), *Hydrodynamic instabilities*, Cambridge, Cambridge University Press.
- [2] Drazin, P.G., Reid, W.H. (2004), *Hydrodynamic stability*, 2nd edn, Cambridge, Cambridge University Press.
- [3] Chossat, P. and Iooss, G. (1994), *The Couette - Taylor problem*, v. 102, New York, Springer - Verlag.
- [4] Chandrasekhar, S. (1961), *Hydrodynamic and hydromagnetic stability*, New York, Dover Publication, Inc.
- [5] Quartapelle, L., Auteri, F. (2013), *Fluidodinamica incomprimibile*, Milano, Casa Editrice Ambrosiana.
- [6] DiPrima, R.C., Eagles, P.M. and Ng B.S. (1984), The effect of radius ratio on the stability of Couette flow and Taylor vortex flow, *Phys. Fluids* **27**.
- [7] Pfister, G., Schmidt, H., Cliffe, K.A. and Mullin, T. (1988), Bifurcation phenomena in Taylor-Couette flow in a very short annulus, *J. Fluid Mech.* **191**.
- [8] Andereck, C.D., Liu, S.S. and Swinney, H.L. (1986), Flow regimes in a circular Couette system with independently rotating cylinders, *J. Fluid Mech.* **164**, pp. 155-183.
- [9] Taylor, G.I. (1923), Stability of a viscous liquid contained between two rotating cylinders, The Royal Society.
- [10] Hoffmann, Ch., Lüke, M. and Pinter, A. (2018), Spiral vortices traveling between two rotating defects in the Taylor-Couette system, *Phys. Rev. E* **72**.
- [11] Antonijoin, J., Marquès, F. and Sánchez, J. (1998), Nonlinear spirals in the Taylor-Couette problem, *Phys. Fluids*.
- [12] Sánchez, J., Crespo, D. and Marquès, F. (1993), Spiral vortices between concentric cylinders, *Applied Scientific Research* **51**, 55-59.
- [13] Lueptow R. (2009), Scholarpedia, 4(11): 6389.
- [14] Fenstermacher, P.R., Swinney, H.L. and Gollub, J.P. (1979), Dynamical instabilities and the transition to chaotic Taylor vortex flow, *J. Fluid Mech.*
- [15] Carini M., Auteri F. and Giannetti F. (2015), Centre-manifold reduction of bifurcating flows, *J. Fluid Mech.*
- [16] Prigent A., Dubrulle B., Dauchot O. and Mutabazi I., The Taylor-Couette flow: the hydrodynamic twin for Rayleigh-Bénard convection.
- [17] Eckhaus W. (1965), Studies in Non-linear stability theory, Springer Tracts in Natural Philosophy 6. Berlin: Springer-Verlag.
- [18] Kolyshkin A.A. and Ghidou M.S. (2002), Stability analysis of shallow wake flows, *J. Fluid Mech.*

- [19] Thorwald H. (1983), On perturbation methods in nonlinear stability theory, *J. Fluid Mech.*
- [20] Eagles P.M. (1971), On stability of Taylor vortices by fifth-order amplitude expansions, *J. Fluid Mech.*
- [21] Jacobsen P.K. (2018), Introduction to the method of multiple scales.
- [22] Tabeling P. (1983), Dynamics of the phase variable in the Taylor vortex system, *J. Phys. Lett.* 44: 665-672.
- [23] Landau L. (1944), On the problem of turbulence, *C. R. Acad. Sci. U.R.S.S.* **44**, 311-314.
- [24] Morse M. and Feshback H. (1954), Methods of Theoretical Physics, American Journal of Physics, **22**, 410.
- [25] Roberts A.J. (1997), Low-dimensional modelling of dynamical systems.
- [26] Roberts A.J. (1997), Low-dimensional modelling of dynamics via computer algebra, *Computer physics comm.*, 100 (1997) 215-230.
- [27] Auteri F. and Quartapelle L. (2006), Algorithms for the spectral solution of 3D elliptic problems in finite cylindrical regions, *Scientific report DIA-SR 06-07*.
- [28] Auteri F. and Parolini N. (2001), Role of the LBB Condition in Weak Spectral Projection Methods, *Journal of Computational Physics* **174**, 405-420.
- [29] Auteri F. and Parolini N. (2002), A Mixed-Basis Spectral Projection Method, *Journal of Computational Physics* **175**, 1-23.
- [30] Billant P. and Gallaire F. (2005), Generalized Rayleigh criterion for non-axisymmetric centrifugal instabilities, *J. Fluid Mech.*, vol 542, pp. 365-379.
- [31] Hecht F., FreeFem ++, Third Edition, version 3.51.
- [32] Hongjun G. and Jinquiao J. (1997), On the initial value problem for the generalized Ginzburg–Landau equation, *J. of Math. analysis and applic.* **216**, 536-548.
- [33] Takanori K. and Mitsuharu Ô. (2018), Local well posedness of the complex Ginzburg–Landau equation in bounded domains, *Nonlinear analysis: real world applications* **45**, 877-894.
- [34] Puzyrev D., Yanchuk S., Vladimirov A.G. and Gurevich S.V. (2014), Stability of plane wave solutions in complex Ginzburg–Landau equation with delayed feedback, *SIAM J. on Applied Dynamical Systems*.
- [35] Zwillinger, D. (1997), *Handbook of Differential Equations third edition*, Academic Press.
- [36] Hinch, E.J. (1991), *Perturbation methods*, Cambridge, Cambridge University Press.
- [37] Nayfeh, A.H. (1973), *Perturbation methods*, John Wiley & Sons.
- [38] Boiko, A.V., Dovgal A.V., Grek G.R. and Kozlov V.V. (2012), *Physics of Transitional Shear Flows*, Springer.
- [39] Schmid, P.J. and Henningson D.S. (2001), *Stability and Transition in Shear Flows*, Springer.
- [40] Quarteroni A. (2009), *Numerical Models for Differential Problems*, Milano, Springer.

# Ringraziamenti

Al termine di questo ciclo di studi, vorrei fare alcuni ringraziamenti.

Il primo va ai miei genitori, Carmen e Luca, per avermi dato la possibilità di arrivare fin qui. Siete sempre stati il mio sostegno in questi cinque anni, incoraggiandomi a dare sempre il massimo e dandomi la serenità per affrontare ogni esame, ogni prova, ogni problema. Non c'è problema che non possa essere risolto. Grazie per tutto quello che avete fatto per me.

Un'enorme grazie va inoltre a mio fratello Elia e a mia cognata Martina, per essermi sempre stati molto vicini, condividendo con me ogni passo in avanti nel raggiungimento di questo traguardo.

Un grazie di cuore alle mie nonne, ai miei zii e a tutti i miei cugini per il loro affetto e per aver mostrato sempre il loro interesse nel proseguo dei miei studi, gioendo con me per gli obiettivi raggiunti.

Ringrazio inoltre i miei amici, che mi hanno sostenuto soprattutto in questo ultimo periodo di tesi. Grazie ai miei compagni di corso, con i quali ho avuto la possibilità di collaborare e di vivere questa esperienza di studio e di amicizia al Politecnico di Milano.

Infine, un sentito ringraziamento al mio relatore, il Prof. Franco Auteri, per aver creduto in me e avermi guidato in questo progetto, rendendosi sempre molto disponibile.

Un particolare ricordo ai miei nonni, Artemio e Cesare,  
ai quali dedico questa mia tesi di laurea.